Deltares

The scientific validation of the hydrographic survey policy of the Netherlands Hydrographic Office, Royal Netherlands Navy

dr. T.A.G.P. van Dijk[1,2]
ir. C. van der Tak[3]
W.P. de Boer, MSc[4]
ir. M.H.P. Kleuskens[1]
drs. P.J. Doornenbal[1]
R.P. Noorlandt, M.Sc[1]
ing V.C. Marges[1]

1201907-000

Deltares

Title
The scientific validation of the hydrographic survey policy of the Netherlands Hydrographic Office, Royal Netherlands Navy

Client	Project	Reference	Pages
Ministry of Defense Defensie Materieel & Organisatie	1201907-000	1201907-000-BGS-0008	165

Address of delivery:
Netherlands hydrographic Office
Royal Netherlands Navy
To: KLTZ J.C.P. Appelman
Van der Burchlaan 31
2597 PC DEN HAAG

Keywords
Hydrography, survey policy, echo sounding, monitoring, morphodynamics, shipping risks, offshore, Netherlands Continental Shelf, North Sea.

Deltares Enabling Delta Life

MARIN

UNIVERSITY OF TWENTE.

Date	Author	Initials	Review	Initials	Approval	Initials
Oct.. 2011	dr. T.A.G.P. van Dijk[1,2]	TvD	dr. A.J.F. van der Spek[1]	ha	dr. R.M. Hoogendoorn[1]	[k]
	ir. C. van der Tak[3]		dr.ir. L.L. Dorst[5]			
	W.P. de Boer, MSc[4,*]		prof. dr. S.J.M.H. Hulscher[2,#]			
	ir. M.H.P. Kleuskens[1]		ir. W.H. van Iperen[3,#]			
	drs. P.J. Doornenbal[1]					
	R.P. Noorlandt, M.Sc[1]					
	ing V.C. Marges[1]					

[1] Dept. of Applied Geology and Geophysics, Deltares
[2] Dept. of Water Engineering and Management, University of Twente (UT-WEM)
[3] Maritime Simulation Centre Netherlands, Maritime Research Institute Netherlands (MARIN)
[4] Dept. of Harbour, Coastal and Offshore Engineering, Deltares
[5] Netherlands Hydrographic Office (NLHO), Royal Netherlands Navy
[*] work conducted when affiliated to the University of Twente
[#] review has been done for merely their institute's contributions

State
final

Deltares

Title
The scientific validation of the hydrographic survey policy of the Netherlands Hydrographic Office, Royal Netherlands Navy

Client	Project	Reference	Pages
Ministry of Defense Defensie Materieel & Organisatie	1201907-000	1201907-000-BGS-0008	165

Address of delivery:
Netherlands hydrographic Office
Royal Netherlands Navy
To: KLTZ J.C.P. Appelman
Van der Burchlaan 31
2597 PC DEN HAAG

Abstract
The Netherlands Hydrographic Office has requested Deltares to validate their re-survey policy for the Netherlands Continental Shelf based on scientific methods. Controlling parameters in the validation are the natural morphodynamics of the North Sea bed and the grounding risks of shipping. Deltares developed an objective method to analyse the seabed morphodynamics from time series of echo sounding data. The quantification of the vertical nodal dynamics of the Netherlands Continental Shelf (on a 25 x 25 m resolution) reveals that regions with rhythmic bedforms are particularly dynamic. Detailed analyses of these dynamic zones provide the growth and migration of individual bedforms. In almost the entire Southern Bight, observed average migration rates are 0 to 5 m/yr, except near Texel, where average migration rates are up to 19 m/yr. The University of Twente performed sand wave modelling to explain the potential impact of environmental conditions on the shape and dynamics of sand waves. In collaboration with MARIN, grounding danger was quantified for the Netherlands Continental Shelf (1 x 1 km resolution). Both the morphodynamics and grounding danger were used in an overlay to validate and optimise the existing re-survey policy of the Netherlands Hydrographic Office.

Contents

Management samenvatting in het Nederlands

De Dienst der Hydrografie (HYD) van de Koninklijke Marine voert hydrografische metingen uit op het Nederlands Continentaal Plat (NCP) om middels karteringen een veilige navigatie voor de scheepvaart te garanderen in de ondiepe Nederlandse wateren van de Noordzee. De nauwkeurigheidseisen voor deze metingen zijn vastgesteld door de International Hydrographic Organisation. Echter, deze eisen bevatten geen aanbevelingen voor de frequentie van heropneming van de waterdiepte in het geval van dynamische zeebodems. Omdat in het ondiepe, zandige deel van de Noordzee dynamische bodemvormen voorkomen, die de waterdiepte en scheepsveiligheid beïnvloeden, is de opnemingsfrequentie zeer relevant voor een betrouwbare kartering. Daarom heeft de HYD een heropnemingsbeleidsplan opgesteld, waarin het NCP is onderverdeeld in gebieden met verschillende frequenties van opneming. De HYD heeft Deltares opdracht gegeven om, in samenwerking met Maritiem Research Instituut Nederland (MARIN) en de Universiteit Twente (UT), dit plan te valideren.

Het doel van dit onderzoek is het wetenschappelijk onderbouwen van het huidige heropnemingsbeleidsplan van de HYD en, indien nodig, het adviseren van mogelijkheden voor de verfijning van het plan. Deltares heeft hiervoor een methode ontwikkeld om de verticale zeebodem dynamiek te kwantificeren op basis van beschikbare data uit het Bathymetric Archive System (BAS) van de HYD. Ter aanvulling zijn gedetailleerde studies uitgevoerd voor een aantal kleine gebieden om de veranderingen (groei en migratie) van individuele bodemvormen te bepalen. MARIN heeft de gevaren voor de scheepvaart gekwantificeerd op basis van de maritieme AIS-database. De Universiteit van Twente heeft een modelleerstudie van zandgolven uitgevoerd ter ondersteuning van de analyse van de morfodynamiek van het NCP.

De kwantificatie van de zeebodemdynamiek heeft geleid tot een kaart van de verticale zeebodem dynamiek van het NCP, die een overzicht geeft van de mate van dynamiek. Uit deze analyse volgt dat de kustzone het meest dynamisch is, vooral de getijdengeulen bij de Wadden en de estuaria. Relatief dynamische gebieden van het Nederlands Continentaal Plat zijn gebieden waar bodemvormen voorkomen. Niet-dynamische gebieden zijn de diepere delen van het NCP (dieper dan 30 m) en enkele ondiepere gebieden ten Noorden van de Wadden, voor de kust van Noord-Holland, Zuid-Holland en Zeeland. In de kwantificatie van de gevaren voor de scheepvaart is onderscheid gemaakt tussen het vastlopen door een beperkte waterdiepte en door het raken van onbekende objecten op de zeebodem. Uit deze schattingen blijkt dat het grootste gevaar op vastlopen voorkomt in de aanvaarroutes naar de havens van Rotterdam en IJmuiden en in de zuidelijke aanvaarroute naar de Westerschelde.

Het vergelijk van deze resultaten en het heropnemingsbeleidsplan van de HYD heeft geleid tot de validatie van het bestaande heropnemingsplan. Hieruit volgt dat het bestaande plan goed overeenkomt met de conclusies in dit rapport. Deze studie bevestigt daarmee, dat voor de gebieden met een lage opnemingsfrequentie inderdaad lage gevaren zijn berekend. Slechts enkele gebieden zijn geïdentificeerd met een significant gevaar voor de scheepvaart die niet worden belicht in het huidige plan. Hieronder vallen een zone met zandbanken in de Diepe Vaarroute Oost en gebieden met bodemvormen ten westen en noorden van Texel en Vlieland. Een andere aanbevelingen voor de verbetering van het huidige plan is het onderverdelen en/of herverdelen van een aantal gebieden, waarvoor een verschillende mate

van gevaar voor de scheepvaart wordt berekend die in het bestaande plan in een één categorie van opnemingsfrequentie vallen. Voor ankergebieden zijn de gevaren als significant berekend, al vereist het verfijnen van de aannames in de uitgevoerde analyse nog verder onderzoek. Gebieden waar de opnemingsfrequentie verlaagd zou kunnen worden, zijn het gebied tussen de diepe vaarroutes ter hoogte van Noord-Holland en de Wadden, en het gebied ten noorden van de vaarroute bij Terschelling, Ameland en Schiermonnikoog.

De methode gepresenteerd in dit rapport biedt de mogelijkheid voor het vaststellen van opnemingsfrequenties voor het ontwerpen van een opnemingsbeleidsplan. Uit analyses volgt dat de opnemingsfrequenties het beste gedifferentieerd kunnen worden in de in dit rapport voorgestelde gebiedsonderverdeling van het NCP.

1 Introduction

1.1 Background and rationale

The Netherlands Hydrographic Office (NLHO) of the Royal Netherlands Navy carries out full coverage hydrographic surveys of the Netherlands Continental Shelf (NCS) for accurate nautical charting, in order to guarantee safe navigation in the shallow Dutch waters of the North Sea. Accuracy requirements of measurements are defined by the International Hydrographic Organisation (IHO) in publication S-44 [*IHO*, 2008]. However, no recommendations are made on the re-survey frequency for a monitoring scheme of dynamic seabeds.

The shallow, sandy part of the North Sea bed is characterised by dynamic bedforms of different spatial scales, such as tidal ridges and sand waves [*Van Alphen and Damoiseaux*, 1989], each changing at different temporal scales. Recent studies of sand waves reveal that both the morphology and morphodynamics of sand waves in the North Sea are highly variable between sites and even within sites [*Dorst et al.*, 2008; *Van Dijk and Egberts*, 2008]. Due to the limited water depths at which these dynamic bedforms occur, these bedforms may interfere with a safe navigation depth in both the offshore and coastal environments. It is therefore important to monitor dynamic sea beds in an appropriate frequency when mapping water depths.

The NLHO designed a re-survey policy for the NCS, based on existing knowledge of water depths and economic interest (e.g. shipping). In this policy, the NCS is divided in different categories of re-survey frequencies (Figure 1.1) with the purpose to carry out hydrographic monitoring that is apt to different areas of the NCS for the production of reliable nautical charts. Since the morphodynamic behaviour of the North Sea bed is largely unknown and the shipping risks were only roughly estimated, these topics need to be investigated in a quantitative way. To date, research on offshore morphodynamics of the NCS is limited to small local case studies (e.g. wind farm sites); large-scaled investigations of national continental shelves have not yet been carried out. The NLHO asked Deltares to quantify the morphodynamics of the seabed and shipping risks for the NCS in order to validate their re-survey policy in a scientific way. This project includes the entire NLHO's survey policy area, which extends from the outer limits of the NCS inwards to the 10-meter isobath.

This research provides new insights in the morphodynamics and shipping risks of the NCS, using state-of-the-art investigations in morphodynamics and up-to-date maritime and hydrographic databases. The validation of NLHO's survey policy will either scientifically support the existing distribution of re-survey categories or lead to adjustment of the policy. Moreover, the optimisation of the policy is expected to increase the efficiency of the policy (lowering the costs of surveying if possible) while keeping the safety at a high level. The refined survey protocol that will result from this investigation may be applied to other continental shelves, firstly those of members of the North Sea Hydrographic Committee (NSHC).

This project is funded by the Netherlands Ministry of Defence (Defensie Materieel en Organisatie) under Purchase Order number 016.09.1013.01.

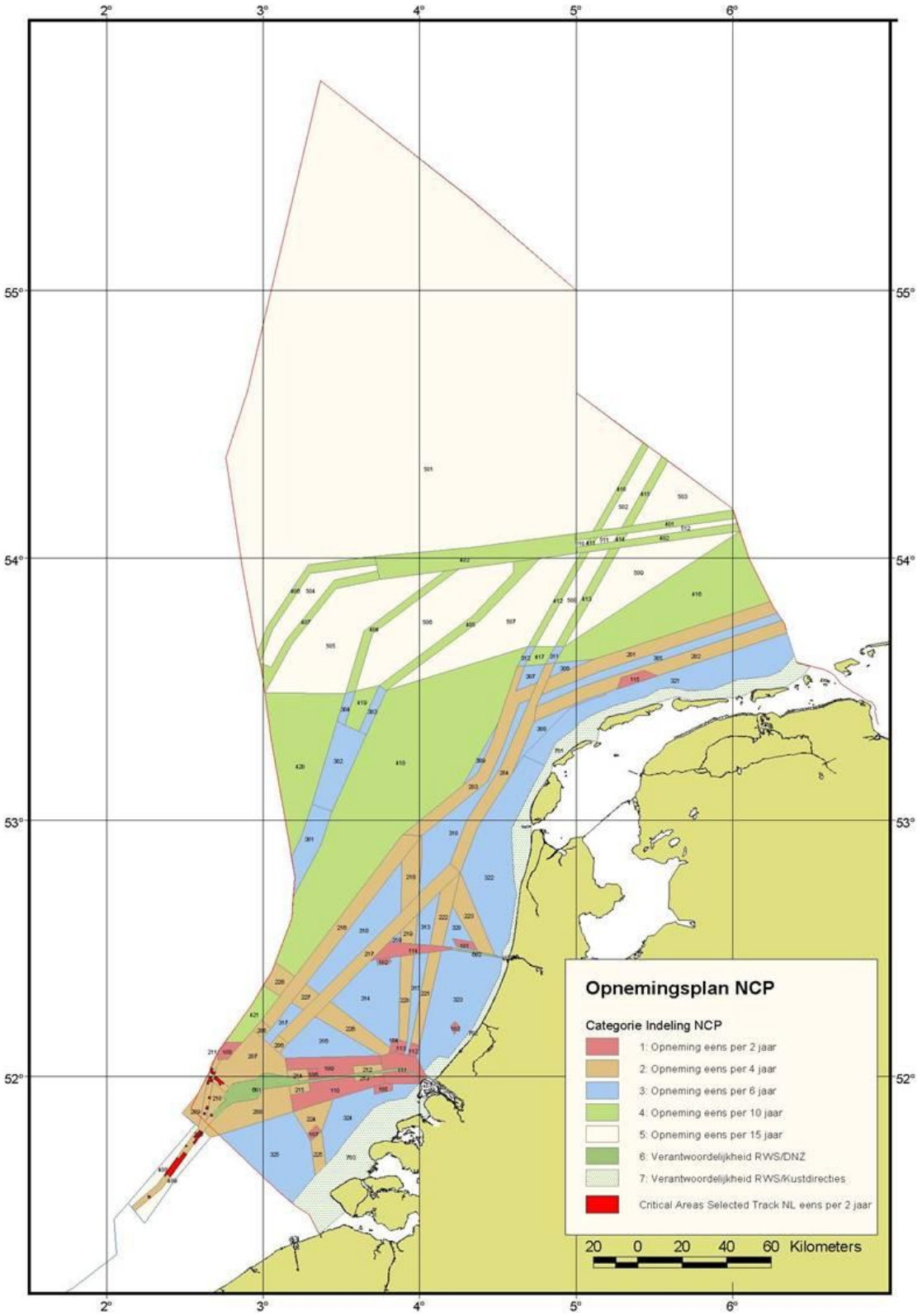

Figure 1.1 *Existing hydrographic re-survey plan of 2007 of the Netherlands Hydrographic Office (NLHO), Royal Netherlands Navy, showing different categories of re-surveying periods*

1.2 Definition of marine bedforms

The morphodynamics of the NCS is influenced by the occurrence of different types of bedforms. The types of marine bedforms subject in this project are defined in Table 1.1 and shown in (Figure 1.2). The largest bedforms are sand banks, or tidal ridges. Sand banks in the North Sea have a wavelength (spacing) of 2 to 10 km, longitudinal lengths of up to several tens of kilometers and may reach few tens of meters in height. Sand banks occur offshore, such as the north-south oriented tidal ridges in the central Southern Bight, parallel to the coast, such as the Zealand ridges, and connected to the coast: shoreface-connected ridges. Offshore tidal sand banks are oriented 0 to 30° anti-clockwise with respect to the main tidal current direction [*Hulscher et al.*, 1993]. Shoreface-connected ridges are observed near the Holland coast (Hoek van Holland to Den Helder) and north of the eastern Wadden Islands and have spacings (wavelengths) of 2 to 5 km and are oriented obliquely to the coast, clockwise with respect to the main tidal current direction [*Van de Meene*, 1994; *Calvete et al.*, 2001]. Offshore sand banks are generated by horizontal flow rectification of oscillating flow [*Huthnance*, 1982], whereas shoreface-connected ridges are generated by storms [*Calvete et al.*, 2001]. The morphodynamic time-scale for the formation of tidal ridges is believed to be hundreds of years. Both offshore and coastal ridges are believed to be relatively stable, i.e. small migration or growth rates.

Table 1.1: Definitions of types of marine bedforms and indication of their morphodynamic time-scales for generation

Bedform	Wavelength (m)	Height (m)	Orientation (degrees to tidal current)	Morphodynamic time scale (order of years)
Offshore sand banks (tidal ridges)	1 000 – 10 000	5 - 50	0 - 30	centuries
Long bed waves	1 000 – 2 000	1 - 10	60	centuries
Sand waves	100 – 1 000	1 – 10	90	years-decades
megaripples	7 – 40	< 1	90	hours

In this report, we define wavelength as the true length between two adjacent trough points, and wave height as the distance from the crest point to the baseline connecting two adjacent trough points normal to that line. These definitions differ from definitions using horizontal equivalents that are also found in the literature.

The second largest bedforms are “long bed waves”, only recently identified by *Knaapen et al.* [2001]. Long bed waves are rhythmic bedforms with a typical wavelength of 1500 m and wave heights up to several meters and are oriented approximately 60° with respect to the main tidal current direction. Long bed waves in the North Sea occur in the south-western part of the Southern Bight and in small patches offshore. The generation of long bed waves can be explained by the same process as the generation of offshore sand banks and the morphodynamic time-scale is hundreds of years [*Blondeaux et al.*, 2009]. Migration rates based on empirical studies are not available in the literature.

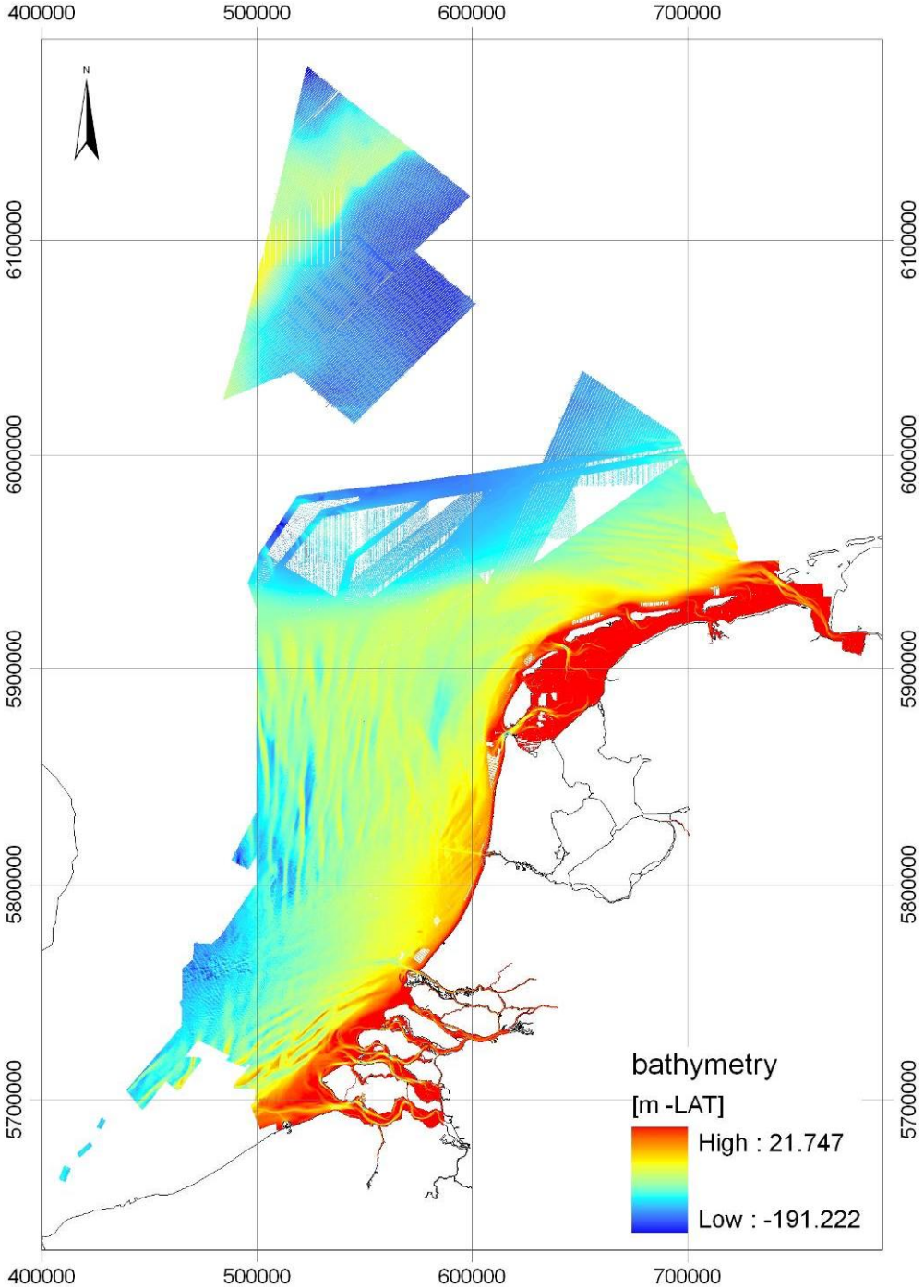

Figure 1.2 Bathymetric map of the Netherlands Continental Shelf (NCS) on 25 m resolution, based on the most recent measurements. The map shows the distribution of different types of marine bedforms in the shallow, sandy southern part of the Dutch North Sea. In the white areas, no digital data are available (see Chapter 2).

Sand waves are the most widespread rhythmic bedforms on the NCS, and are observed in almost the entire Southern Bight in water depths more than 10 or 15 m. Sand waves have wavelengths between 100 and 1000 m, wave heights of several meters and are oriented roughly normal to the main tidal current direction. Their crests may be straight or sinusoidal and may show bifurcation; their cross-sections may be symmetrical or asymmetrical. Sand waves are often superimposed on sand banks, adjusting their orientation on the flanks and

crest of the banks. The only way to model the generation of sand waves is by vertical residual circulation cells, which cause sand at the bed to be transported from troughs upwards to the sand wave crests from both sides, causing growth of the bedform [*Hulscher*, 1996]. Their morphodynamic time-scale is years to decades and observed migration rates on the NCS may vary between 0 to 20 m/yr [e.g. *Van Dijk and Kleinhans*, 2005; *Van Dijk et al.*, 2008; *Dorst*, 2009].

The smallest bedforms observed in multibeam echo sounding images are megaripples. Megaripples have wavelengths of several to tens of meters and heights of less than 1 m. Megaripples may change form and asymmetry within one tidal cycle or during storms. Megaripples are not included in detailed morphodynamic studies in this report, because the resolution of the single beam echo sounding data used in this project is too low to observe megaripples. Therefore, time-series either do not exist or may not cover sufficiently short periods to identify the same megaripples in subsequent datasets with certainty.

Smaller bedforms, such as current ripples, exist but are not subject to this study.

1.3 Overall aims and objectives

The overall aims of this project are:

I. to validate the existing hydrographic re-survey policy of the NLHO in a scientific way, and

II. to formulate recommendations for the refinement of the re-survey policy for the Netherlands Continental Shelf below the 10 m isobath.

The validation will be based on the quantitative risk assessment of vessels running aground due to an elevation of the seabed and unknown objects at the bed, that remain unobserved within the periods between two subsequent surveys. This risk assessment requires *(i)* a quantitative measure of seabed morphodynamics and *(ii)* an estimate of the probability of the running aground of vessels.

To the first topic, morphodynamics: in order to obtain an overview of the variation of morphodynamics on the NCS, a quantification of vertical seabed dynamics (changes in seabed elevation) is essential. This overview allows for the identification of regions of contrasting dynamics, which are then studied in detail with the analysis method developed at Deltares in which the bathymetric signal is separated and semi-automatically analysed [*Van Dijk et al.*, 2008]. The detailed studies have three purposes. Firstly, to specify horizontal migration rates and growth (changes in height) of individual sand waves and sand banks. Secondly, to compare the outcomes of the method used at Deltares to the deformation method presented by Dorst [2009; *Dorst et al.*, 2009]. This comparison provides a handle on the variation between earlier analysis results of work carried out for the NLHO. Thirdly, to analyse sand wave geometry and dynamics at sites of contrasting environmental conditions, such as tidal current velocity and water depth, in order to provide input to and to be able to validate results from sand wave modelling based on physical processes (section 3.2.5). Since large areas of the NCS are covered by merely two datasets in time, the establishment of morphodynamic trends and the prediction of water depths may be surrounded by large uncertainties. The process-based modelling may strengthen these empirical interpretations with physical processes, thereby verifying the (few) observations with a scientific explanation of environmental conditions that control the morphodynamics of sea beds.

To the second point, shipping risks, the risks depend on the dimensions of ships at the NCS in time and local water depth, the presence of unknown objects that are new since the last survey, and the change in water depth since the last survey. It is therefore essential to

investigate the grounding probability and shipping risks for these three variables, taking into account factors such as under-keel clearance, the probability of unknown objects on the seabed (containers, wrecks), shipping intensity and predicted water depths (see section 4.2).

This research uses existing data only. New data are not collected for this project.

In summary, the project objectives and specific objectives are listed below. Project objectives are those investigations that are needed to obtain the overall aims and specific objectives are those studies that are needed to achieve the project objectives.

Objective 1. to analyse the morphodynamics of the seabed at the NCS below the 10 m isobath,
- *1.1.* to quantify vertical morphodynamics of the NCS from existing data,
- *1.2.* to perform detailed (quantitative) analyses on sand wave dynamics (migration, changes in height)
  - *1.2.i.* to specify the dynamics in zones of contrasting dynamics identified in obj. 1.1
  - *1.2.ii.* to compare outcomes of the spectral method used at Deltares [*Van Dijk et al.*, 2008] to the deformation method [*Dorst et al.*, 2009] used at the NLHO
  - *1.2.iii.* to provide morphological input parameters for and to validate the morphodynamic results of sand wave modelling (obj. 1.3.ii)
- *1.3.* to predict water depths and determine temporal variations in water depth
  - *1.3.i.* based on empirical findings
  - *1.3.ii.* to support empirical findings by process-based morphodynamic modelling

Objective 2. to determine the grounding probability and shipping risks, due to:
- *2.1.* limited water depth (regular grounding)
- *2.2.* unknown objects at the bed (object grounding)
- *2.3.* morphodynamics of the seabed

Objective 3. to compare the existing NLHO hydrographic re-survey policy to the morphodynamics and shipping risks established in Objectives 1 and 2, and

Objective 4. to devise a protocol for how to come to a new hydrographic re-survey policy, based on findings of and insights gained in this investigation.

The formulation of these objectives slightly differs from the list of objectives in the original research design [*Deltares*, 2008], for a better structure of reporting on the relevant questions per topic. For example, objectives 2 and 3 in the original project plan have been assembled into Objective 2 in this report and appear as 2.1 and 2.2 (in reverse order). An overview of where the carried out research deviates from the proposal, is given in Appendix 11.1.

1.4 Report structure

The data used in this investigation are described in Chapter 2. Chapters 3 to 5 each deal with one or two of the above listed project objectives (Objectives 1 to 4 in section 1.3). These chapters have a rigid structure, containing an introduction, in which the specific objectives will be recalled, and sections describing the methods and results. The technical part of the modelling (methods) is appended at the end of the report, in order to not interfere with the focus of the main text. Each results chapter has a conclusions section, specifically for the topic of that particular Chapter.
Both the validation and devising of a new re-survey plan are collected in Chapter 5. Chapter 6 is reserved for the assembled overall project conclusions of all themes, including recommendations for a revised re-survey policy.

Furthermore, a list of notation and abbreviations used in the text are provided in Chapters 7 and 8, which are meant to assist the reader.

1.5 Project partners

This project was carried out in collaboration among the following partners:

1. the Netherlands Hydrographic Office of the Royal Netherlands Navy (NLHO),
2. the Department of Applied Geology and Geophysics of Deltares,
3. the Maritime Simulation Centre Netherlands of the Maritime Research Institute of the Netherlands (MARIN-MSCN), and
4. the Department of Water Engineering and Management of the University of Twente (UT-WEM).

Deltares and the NLHO identified research questions. The NLHO provided the available echo soundings, metadata and tools to assist in the processing and analyses of data. Deltares developed tools to carry out and carried out the quantification of the morphodynamics (Chapter 3) and the validation of the existing policy (Chapter 5), formulated a new protocol (Chapter 5) and was responsible for the overall project management, final project report and publication. MARIN focussed on the grounding probability and shipping risks (Chapter 4). The UT contributed the sand wave modelling results (section 3.2.5; full text in Appendix 11.2).

The scientific publication that will result from this project will be a joint effort and is not included in this report.

2 Available data and data processing

The main data used in this project are bathymetric data (i.e. water depths or bed elevation) for the investigation of seabed morphodynamics and grounding risks, and maritime data for the calculation of grounding probabilities and shipping risks. Subsidiary data are environmental data (e.g. sea bed sediments and hydrodynamics) for the physical modelling, and additional data (e.g. sand extraction activities), for the discrimination of natural and anthropogenic changes in sea bed elevation. No side-scan sonar data were used.

2.1 Bathymetric data

The NLHO provided all bathymetric surveys that are stored in the Bathymetric Archive System (BAS), NLHO's digital database [see *Righolt et al.*, 2010]. The BAS-database contains all echo soundings that were collected by both the NLHO (NCS below the 10 m isobath) and RWS (coastal zone, Wadden Sea and approach channels to IJmuiden and Rotterdam) that are digitally available (i.e. surveys since the late 1980s). The data coverage of the NCS is shown in Figure 1.2. Digital data in BAS comprise both single-beam echo soundings (SBES) and multi-beam echo soundings (MBES), that were collected according to the Order 1 standards for hydrographic surveys of the International Hydrographic Organization [*IHO*, 1988; 2008].
Tracks are mostly sailed parallel to the tidal current direction (southwest-northeast) or in a north-south course, therewith crossing marine bedforms of long bed wave scale and sand wave scale normal to their crests. With these courses, tracks are parallel to the offshore tidal ridges in the North Sea.

Multibeam echo sounding data were corrected for tides and ship movements. Single beam data were not corrected, because the beam width is sufficient to compensate for ship movements. Echo sounding data were converted to bathymetric *xyz*-data at the NLHO. All exported data files were supplied as $x\ y\ z\ t_1\ t_2$ files, where x and y are the UTM 31 WGS84 coordinates of Easting and Northing (m), respectively, z is the bed elevation with respect to the vertical reduction level LAT (-m), and t_1 and t_2 are dates that the survey respectively started and ended (in number of days since the year 1900). Although t_1 and t_2 are now tagged to each record (line per data point) in the *xyz*-datasets, all records in one survey have the same start and end dates.

Echo sounding data used in this project include recent surveys, with updates to June 2010.

All maps in this report are presented in UTM zone 31N WGS84 coordinates. Water depths are given in meters with respect to LAT (Lowest Astronomical Tide).

The methods of horizontal positioning, echo sounding, pre-processing and correcting for tides and ship movements have changed for the bathymetric (SBES and MBES) data, so that surveys have different uncertainties and data densities.

In terms of precision, SBES and the vertical soundings of MBES are comparable, in the order of decimetres (< 0.5 m). However, corrections of the two-way travel times with vertical sound velocity profiles in water decreases the precision of the soundings with outer beams of the MBES data, causing 'smiley' or 'droopy' artefacts [*Simons et al.*, 2010]. The older SBES data was often collected with a horizontal positioning system that was less accurate in an absolute sense. In a relative sense, these positioning systems are accurate, so that surveys in time

can be compared well. In the present-day horizontal precision, the effect of horizontal precision on vertical uncertainties is small. For example, for a precision of ± 2 m at a 95% confidence interval and a bed slope of 2 degrees, which would be a steep sand wave of 250 m long and 9 m high, the vertical uncertainty may be increased by 0.14 m. For a horizontal precision of ± 5 m, the vertical uncertainty may become 0.35 m. On the other hand, most marine bed slopes are less than 2 degrees and thus the uncertainties will be much smaller. For a flat bed, the difference in horizontal precision has no effect on the vertical uncertainty.

In terms of data density, the data exports from BAS used in this project are on Level Of Visualisation 2 (LOV2), which means that 1 observation per 3 by 5 meter cell was selected and projected to the centre of the cell. All other data points were removed. Most MBES surveys comprise area-covering datasets with one data point every 3 by 5 m. For SBES data available to this research, the distance between points on track lines has a minimum of 3 to 5 m up to 35 m, but the distance between track lines may be 50 to 1000 meters, depending on the survey. Track line spacing of most SBES surveys is 125 m.

Because large parts of the NCS were not covered by a time series of two (or more) datasets, the NLHO digitised plotted or written fair sheets in order to create hydrographic time series. A list of priority was made by Deltares, based on the inventory of both digital surveys and fair sheets (boundaries were provided by the NLHO as polyline shape-files that were separated per year at Deltares). These fair sheets comprise SBES data that were collected prior to the late 1980's, known as 'historical data'. The data density of historical datasets is much lower than that of digital datasets, because only a small number of data points can be plotted or written on sheets. Therewith, the scale of the fair sheets determines the data density.

When comparing different datasets, three main causes of differences in the data are important: *(i)* the shoal-biased nature of SBES, *(ii)* the tidal reduction, and *(iii)* the selection of shallowest points on fair sheets.
To the first point, most SBES data points are shoal-biased, whereas MBES data points better represent the 'real' water depths. This biasing is caused by the beam width of the vertical beam. SBES measures the first return of the sounding. For example, when megaripples occur, the crest of the megaripple within the beam width determines the measured water depth. For MBES, the separate beams also register the troughs of the megaripples. Thus, comparing shoal-biased SBES and MBES data in a time series results in an underestimation of the deepest points for the SBES; the shallowest points are correct.
To the second point, different methods of tidal reduction result in vertical differences between surveys in time. Before the year 2000, tidal reduction was based on the water level estimations using tide gauges. The mean reduction level (MRL) was estimated on water level measurements during several months. Since 2000, when the use of PREMO had started, echo soundings are reduced to Mean Sea Level (MSL), and uncertainties due to tidal reduction became smaller. The tidal reduction causes the largest vertical differences when comparing surveys in time and is strongly related to surveys. This causes the patchwork, discussed in section 3.2.2. The tool Minimal Detectable Bias (MDB) developed at the NLHO [*Dorst et al.*, 2009], was not applied in this study, since most time series were too short to either establish which of the two is an outlier or to omit one of the surveys.

To the third point, in the plotting of fair sheets, only one plotted value represents many SBES data points. Herein, the shallowest echo soundings are selected, so that water depths in the digitised fair sheets are underestimated.

Although the aim of the project is to analyse the NCS below the 10 m isobath, it was decided not to exclude RWS data files, so that project results also include the coastal zone between 0 and 10 m water depth and the Wadden Sea. Since the analysis is fully automated, including these data did not cost more than a little extra computer calculation time, whilst the results provide valuable insight in the ranges of coastal and offshore morphodynamics and shipping risks.

2.2 Maritime data

2.2.1 Automatic Identification System database

MARIN has access to the Automatic Identification System (AIS) database, collected by the Netherlands Coast Guard, a maritime database in which the tracks of ships larger than 300 GT at sea are stored at all times.

Until recently, ships could not be followed outside the radar coverage from ports. The vessel traffic at sea was composed from vessel movements from port to port, without knowing the exact trajectory over sea, and from observation flights above sea. These observation flights were far from sufficient to achieve an accurate image of the shipping densities and the composition of the traffic. The knowledge about the behaviour of shipping on the North Sea has increased tremendously since the introduction of AIS.

AIS is a system used by ships principally for the identification of vessels at sea. AIS helps to resolve the difficulty of identifying ships when not in sight (e.g. at night, in fog, in radar blind arcs or shadows or at a distance) by providing a means for ships to exchange ID, position, course, speed and other ship data with all other nearby ships and vessel traffic service (VTS-)stations (for abbreviations, see Chapter 8). In case of a potential threat of a collision it will be much easier with AIS to contact the other ship to avoid a collision. AIS works by integrating a standardised VHF-transceiver system with a GPS-receiver and other navigational equipment on board ship (Gyro compass, Rate of turn indicator, etc.).

The international convention of safety of life at sea of the International Maritime Organisation (IMO SOLAS) requires AIS to be fitted aboard all ships above 300 gross tons for international voyages since January 2005. The AIS-transceiver sends the following data every 2 to 10 seconds depending on the vessel’s speed while underway, and every 3 minutes while the vessel is at anchor. This data includes:

- MMSI-number communication equipment – a vessel's unique identification
- Navigational status - "at anchor", "under way using engine(s)", "not under command", etc.
- Rate of turn - right or left
- Speed over ground
- Position accuracy
- Longitude and latitude
- Course over ground
- True heading
- Time stamp.

In addition, the following voyage related data is broadcasted every 6 minutes:

- MMSI-number – the vessel's unique identification
- IMO-number – this number remains unchanged upon transfer of the ship to (an)other flag(s).
- Radio call sign - international radio call sign assigned to a vessel
- Name
- Type of ship/cargo
- Dimensions of ship - to nearest meter
- Location and type of positioning system
- Draught of ship
- Destination - max 20 characters
- ETA (estimated time of arrival) at destination.

The Netherlands Coastguard is responsible for many operational tasks. For these tasks, it is relevant to know where ships are. For this purpose, a network is maintained of AIS base stations, which receive AIS-messages with a range of 30 nautical miles each. All AIS-messages received by the base stations are forwarded to and archived at an operational centre. MARIN receives this valuable data from the Netherlands Coastguard and has permission to use the data for safety studies and to enlarge their insight in the actual sailing patterns on the North Sea.

Within this study, the AIS data of the whole year 2009 is used. The AIS data set of 2009 contains 5800 million AIS messages.

Two points of uncertainty in the AIS data and AIS messages are *(i)* the variation in the AIS-coverage and *(ii)* incorrect draughts.
To the first point, all base station together cover the largest part of the NCS. However, there are some weak spots on the NCS, where the coverage is less. For example, the TSS lanes of North Hinder South (see Figure 2.1), especially in the most southern part, has minor coverage, because this area is located far away from the nearest base station (Westkapelle). Based on counts by *Van Iperen et al.* [2009a], it can be roughly estimated that the amount of received AIS data of North Hinder South in 2008 was only 13% for ships on the south-westward route and 25% for ships on the north-eastward route. A similar analysis was not made for 2009, but the new traffic density results (fading colours in Figure 4.6 in section 4.3.1), imply that the precautionary area west of Maas West Outer TSS (Figure 2.1) and the whole North Hinder South TSS remain large weak spots with respect to the receipt of AIS messages, even though traffic density in these areas is high. The North Hinder South TSS does not belong to the Netherlands Continental Shelf, but the north going traffic lane belongs to the survey area of the NLHO. In the remaining part of the Netherlands Continental Shelf, the coverage varies from nearly 100% along the coast to 80% to 90% along the borders of the NCS. Above 54°N there are some spots with less coverage, but this area is, due to the large water depth and low shipping densities, of minor importance for the re-survey policy.
To the second point of uncertainty in the AIS-data, a number of draughts of ships during the voyage, contained in the AIS-messages, may be incorrect. The draught of the ship is the most important issue for the determination of the grounding probability. The draught of a ship is not always the same, especially not for tankers, that often sail in ballast in one direction and fully loaded in the opposite direction.
Although some items in AIS messages are fed in an automated way by the connection with navigational aids, the draught needs to be filled in manually. As often with manual input, this is not always done, or is done incorrectly, leading to unreliable information. For example, it was seen that many messages, also of ships with draughts smaller than 20 m, contained a

draught of 20 m. These incorrect values require a correction in order to prevent erroneous results in the grounding dangers in this study. Therefore, the AIS draught is compared with the maximum draught from the database with all shipping characteristics. In case the AIS draught of a ship exceeds the maximum draught of that ship, the draught is back scaled to the maximum draught. For ships that were not identified in the shipping database, the maximum draught is based on the ship length.

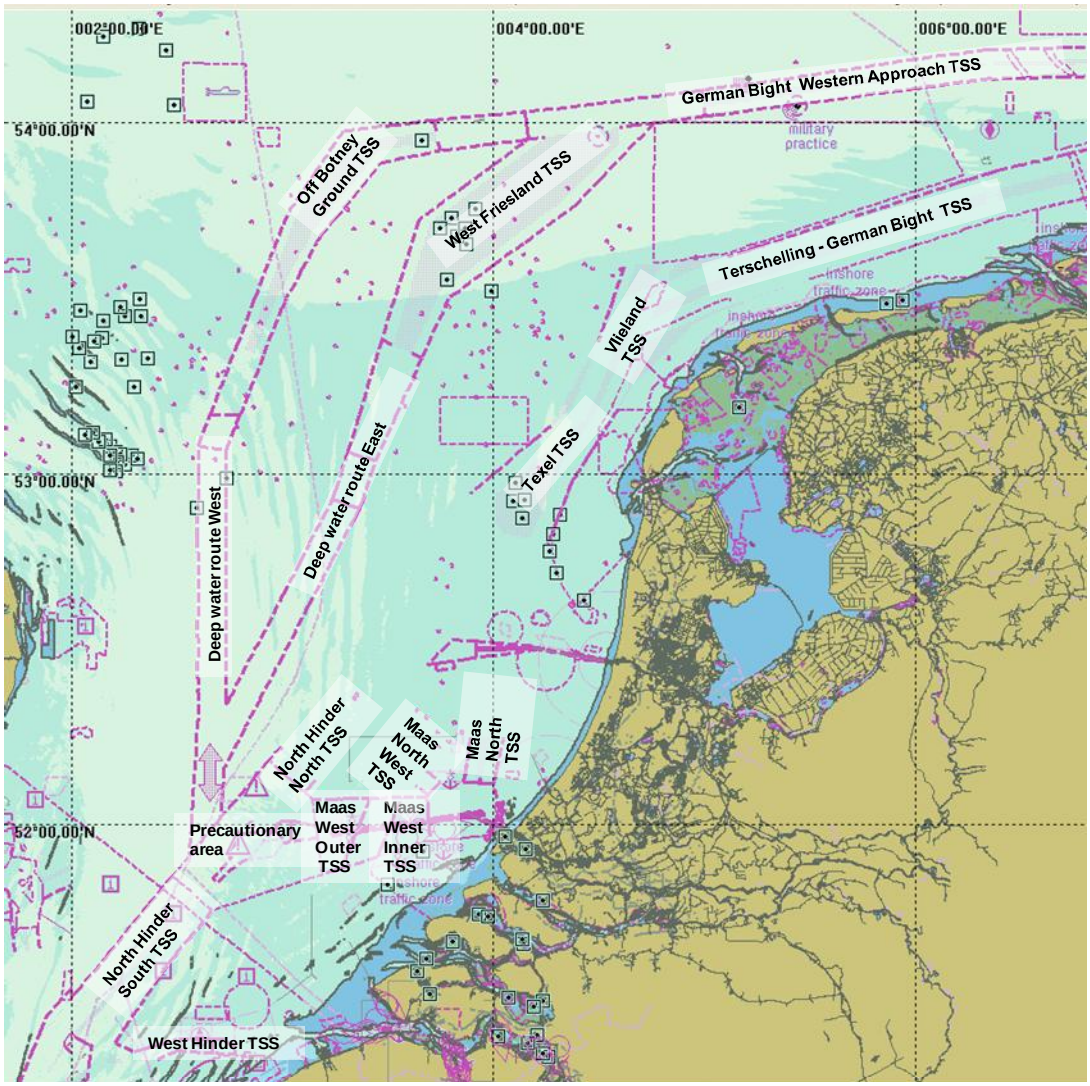

Figure 2.1 Traffic separation schemes in the North Sea

Because the frequency of sending an AIS message for each ship is not always the same, it is not correct to count all AIS messages of 2009. Therefore the positions of each ship are counted with fixed time intervals of 2 minutes. Each time step, all ships at sea are assigned to one of the grid cells based on the last position sent. For each cell, the MMSI number with the draught of the AIS message, cut off in whole meters, is counted. Cutting off in whole meters means that a draught of 5.7 m is cut off to 5 m. Thus a draught of 5 m represents all operational draughts between 5 and 6 meter. A combination of these items is called an AIS hit. The AIS-hits in the database form the basis for grounding calculations.

The records of ships of type ‘drilling’ are removed, because these ships stay on the same location for a long time for exploratory drillings.

2.2.2 Wrecks and obstructions

The NLHO and RWS investigate the occurrence of wrecks and other obstructions at the sea bed and have a created a database of these obstructions. The database contains the discovery date. Each object is labelled with the sounding in case of danger for shipping.

In this project, the point data sets of both RWS and the NLHO were used to estimate the number of newly discovered objects per year and to calculate the grounding danger due to objects (Chapter 4).

2.3 Environmental data

2.3.1 Sea bed sediments

For the sand wave modelling (Objective 1.3.ii; section 3.2.5), the median grain size (D50) of the local sea bed sediment is required. The local median grain size is extracted from a digital map with median grain sizes of the sand fraction (63 – 2000 μm) of the NCS with a spatial resolution of 200 m that was composed by TNO in 2007 (Figure 2.2).

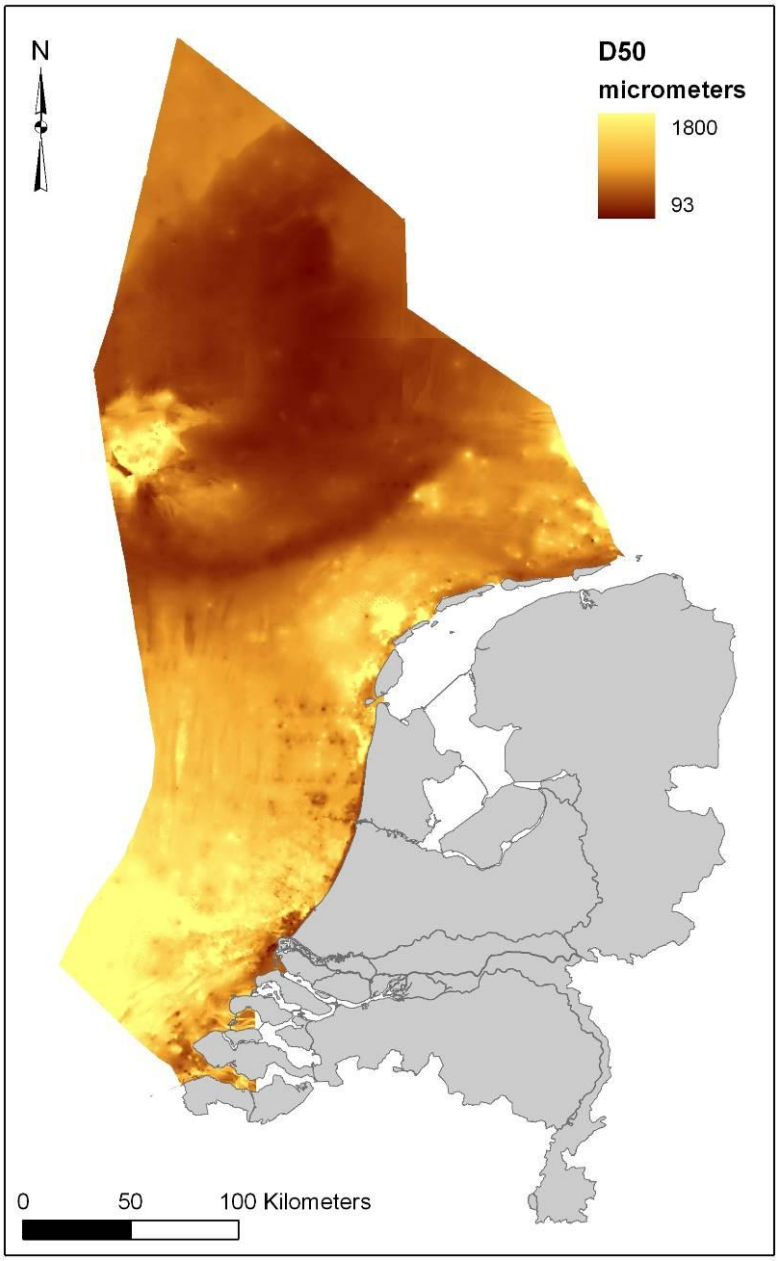

Figure 2.2 *Median grain size (D50) in micrometers of the sand fraction (63 – 2000 µm) of the seabed sediments of the Netherlands Continental Shelf. The digital map has a resolution of 200 m and is available on the internet through Open Earth (http://www.openearth.eu/; http://kml.deltares.nl/kml/tno/ncp/ >Dz50)*

The median grain size per node is based on measured grain size distributions of both bed samples and the top samples of sediment cores in the DINO-database (Data and Information of the Netherlands Subsurface) of TNO. These samples describe the surface of the North Sea bed, not the subsurface. Full grain-size distributions were interpolated in an advanced geo-statistical application (Isatis), that allows for accurate definitions of variograms and an anisotropic Kriging algorithm (Kriging with External Drift) with incorporated pre-existing knowledge, such as the bathymetry [*Maljers and Gunnink*, 2007].

2.3.2 Hydrodynamics

The sand wave modelling (Objective 1.3.ii; section 3.2.5) also requires values for the local tidal current velocity. In this study, realistic tidal current velocities were extracted from the MATROOS-database (Multifunctional Access Tool foR Operational Ocean-data Services), a database that stores modelled (thus not measured) tidal current velocities. Tidal current velocities in the MATROOS-database are modelled using complex, non-linear (engineering) models (based on WAQUA and DELFT3D-FLOW) that solve depth-integrated shallow water equations.

For the offshore sites in the sand wave modelling, results of the hydrodynamic Dutch Continental Shelf Model (CSM8) were used. This model calculates depth-averaged current velocities in the horizontal x- and y-components for the Northwest European continental shelf, based on wind and air pressure fields from KNMI's atmospheric HiRLAM model (updated version at 22 km resolution) [*Verlaan et al.*, 2005, and references therein]. The resolution of the spherical grid is 1/8º by 1/12º, which approximates 8 x 8 km, the highest resolution available for offshore locations. The model includes the effects of wind-driven currents and salinity. The model is tuned with water level measurements at stations along the British and Dutch coasts and on platforms in the North Sea, using the updated automated calibration package WAQAD and Kalman filtering for online data assimilation [*Verlaan et al.*, 2005]. The use of measured water levels is expected to lead to realistic tidal current velocities. The MATROOS database is maintained by Deltares and uses operational data of RWS.

2.4 Additional information

In order to discriminate anthropogenically caused changes in water depth from natural vertical seabed dynamics, Rijkswaterstaat provided a list of sediment extraction and nourishment events since 2002 (updated to week 49 in 2010). Locations of the sand extraction sites were downloaded from Rijkswaterstaats "Noordzeeloket" (http://www.noordzeeloket.nl/) as polyline shape file (ETRS89 coordinates).

The existing hydrographic survey policy (Figure 1.1) was provided by the NLHO as polyline shape file and separated into categories at Deltares.

3 Morphodynamics of the North Sea bed (Objective 1)

3.1 Introduction

Previous empirically-based work on seabed morphodynamics focussed on the analysis of marine bedforms of small sites with specific local conditions [e.g. *Duffy and Hughes-Clarke*, 2005; *Knaapen*, 2005; *Van Dijk and Kleinhans*, 2005; *Winter and Ernstsen*, 2007; *Buijsman and Ridderinkhof*, 2008b; *Van Dijk et al.*, 2008; *Dorst*, 2009]. An overview of the morphodynamics of the NCS does not exist. An NCS-wide overview is achieved by comparing the seabed elevations between surveys in time. However, due to the numerous combinations of overlaps of many different surveys that were all collected in different periods, it is insufficient to use the absolute differences in bed elevation in meters. Instead, the changes in bed elevation need to be expressed in meters per year, so that values are comparable for all locations (i.e. grid nodes) on the NCS. In this report, the term “vertical nodal dynamics map”, or dz/dt-map, refers to the calculated trend in observed (vertical) changes in sea bed elevation in m/yr per grid node of the digital elevation model (see section 3.2).

This chapter describes and discusses the features on the vertical nodal dynamics map (objective 1.1; section 3.3.1) and presents the results of the detailed analyses of growth and migration of individual bedforms (objective 1.2; section 3.3.2). The detailed studies specify the dynamics at zones that were identified on the dz/dt-map (objective 1.2.i), are used as comparison to results by Dorst [2009] (objective 1.2.ii) and serve as input for the sand wave modelling and as validation of model results (objective 1.2.iii). Predictions include the statistical prediction of water depths, based on the calculated dynamic trend and to be used in Chapter 4 (objective 1.3.i; section 3.3.3), and an inventory of the application of sand wave modelling in predicting the behaviour of sand waves under varying local conditions (objective 1.3.ii) in order to support empirical findings.

3.2 Methods

Time series of bathymetric data allow for the analysis of the morphodynamics of the NCS. Hereto, bathymetric data were interpolated into Digital Elevation Models (DEMs). DEMs are not only used for the calculation of the change in bed elevation of the NCS, from which the vertical nodal dynamics trend is calculated, but also serve in the detailed analysis of the mobility and growth of sand banks and sand waves. The morphodynamic modelling of sand waves was used to test whether an idealised model is suitable to support the empirical findings with physical processes.

3.2.1 Digital Elevation Models (DEMs)

Digital Elevation Models (DEMs) are interpolated grids that represent the sea bed as a surface of elevations at regularly spaced *x,y*-locations, or equidistant nodes. The chosen *x,y*-coordinates of the nodes are similar for all bathymetric surveys in the time series and correspond to the maritime grids used in this research, so that calculations of sea bed dynamics and overlays for the validation of the existing survey policy of NLHO (Chapter 5) can be made.

The calculation of DEMs is not applied to all surveys of the entire NCS at once, because the size of the data files would exceed the present-day memory capacity of computers. Besides, many grids would be inefficient in their use, due to large empty parts where no echo

soundings are available. To handle these large amounts of bathymetric data for the NCS, bathymetric datasets were cut into manageable blocks of 5 by 5 km. Blocks include an extra zone surrounding the interpolated nodes, so that all data points within the search radius (partly outside the 5 x 5 km for nodes at the edges) are included and so that edge effects during interpolation of the data are prevented.

Subsequently, DEMs of the NCS were calculated for all blocks per survey, using the Inverse Distance Weighting algorithm in in-house software that was especially developed for handling large datasets. The choice of the interpolation algorithm is supported by comparing precision calculations of both the Kriging and Inverse Distance Weighting interpolations for a small number of test files. Herein, DEMs of both algorithms were resampled to the original data point locations and the differences with the measured data points plotted. Kriging is a linear least squares method that fits a function through all data points with the least error. Kriging calculates the variability of data points in an experimental variogram, which provides a function fitted through the variogram. Inverse Distance Weighting takes the average of the surrounding pixels after weighting them with the reciprocal of the distance. For bathymetric data, which is rather smooth and continuous, the results of both methods are comparable. In our test cases, the inverse distance grid has a slightly smaller difference (smaller interpolation uncertainty) with respect to the original (measured) point data than a Kriged grid. Furthermore, inverse distance weighting is faster and less memory consuming, thus more applicable to the amounts of data that we deal with in this project. Kriging could be a better option if the interpolation would be expanded with prior knowledge, for instance, a preferred direction in the selection of data points included, using directional variograms [e.g. *Goovaerts*, 1997]. In this way, *a priori* knowledge, for example sand wave orientation, can be added to the gridding process. This method is beyond the scope of this research and not necessary at most locations, since the point density is sufficient. Besides, the superposition of bedforms complicates the preferred orientation and tests with a directed interpolation method of RWS and Kriging showed that improvements are small [*Van Halderen*, 2005]. For some of the detailed studies (section 3.2.4) Kriging was used.

In the interpolation, two parameters, grid cell size and search radius, have to be chosen. Here, a grid cell size of 25 x 25 m was used, firstly, because it still provides a sufficiently high resolution on NCS-scale to reveal bedforms of the scale of sand waves, and secondly, because it is a reasonable choice in terms of data density when comparing SBES and MBES data. With this cell size, the use of the high-resolution MBES data is still good and for the data point distribution in track lines for SBES data, interpolation artefacts are kept to a minimum.

The search radius is the maximum distance between an interpolated point (at the node) and a data point. Data points inside the search radius are used to determine the elevation for the node, whereas points outside the search radius are neglected for this particular node. The best choice of the search radius depends on the distance between the track lines of the SBES survey, the scale of morphological features that are of interest and the roughness or smoothness of the grid. The distance between SBES tracks may be 125, 250, 500 or 1000 meters. A search radius of 500 meters would generate a filled grid for all SBES datasets. However, values between the SBES tracks would be the mean of all surrounding points, blurring all interesting features. Since these interpolated points would add a lot of noise to the next processing steps, the radius is chosen to be only 100 meters.

The interpolation precision could be increased when cell size and search radii were determined per survey in a flexible way, depending on the data density differences caused by method (SBES versus MBES) and track distance in case of SBES. However, within the scope of this project, this type of flexible analysis was unfeasible.

Digitised fair sheets have a lower data density (see section 2.1), thereby introducing a larger uncertainty in interpolated grids.

3.2.2 Vertical nodal dynamics of the NCS: analyses of empirical data

The analysis of time series of DEMs allows for the determination of vertical nodal dynamics of the NCS. Initially, the suggested survey-based approach was to compare different overlaps in space and time of all surveys in the database (Figure 3.1a [from Appendix 9.1 in *Deltares*, 2008]) and subtract the nodal elevations of two subsequent grids of known periods to calculate the dynamics in m/yr. However, this would be a quite complicated way of analysing the bathymetric datasets, considering *(i)* the large number of surveys, each with a different extent, overlap and time window of data collection, and *(ii)* that because of arbitrary overlaps in time, not all time windows can be separated as well as is suggested by the example in the research design.

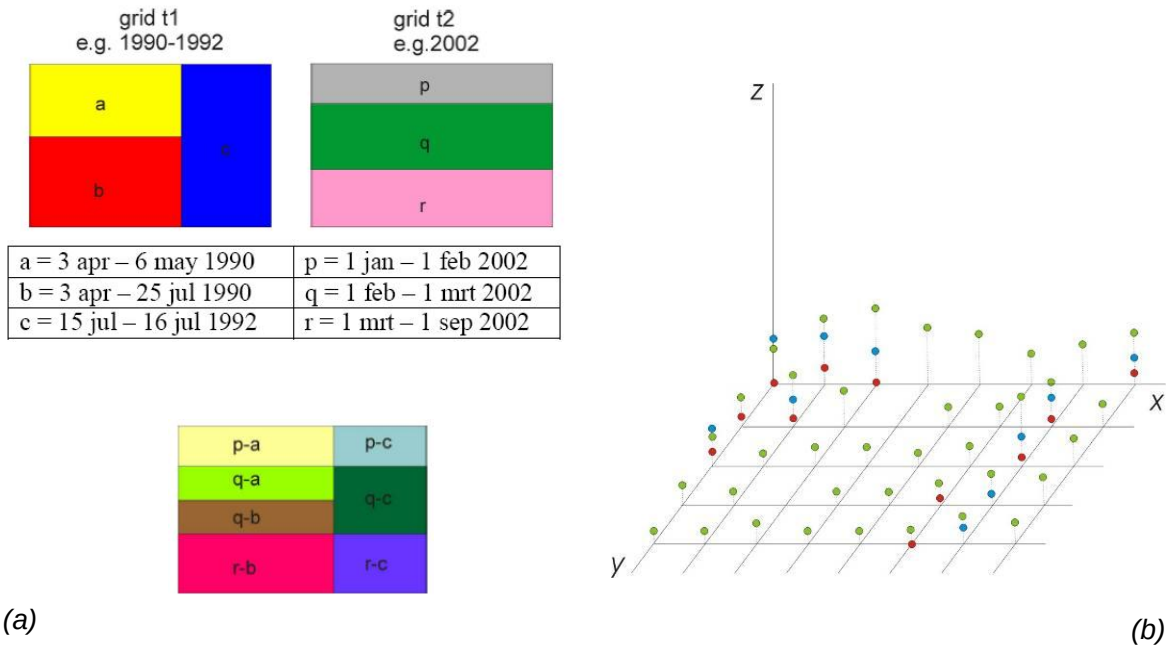

(a) *(b)*

Figure 3.1 *(a) Initial schematic plan to analyse vertical dynamics from DEMs - that may each exist of several surveys - in time series per survey and time-overlap combination (survey-based approach). (b) Revised method to analyse the vertical dynamics per node of the 25 x 25 m DEMs for all datasets in the time series in a fully automated way. This latter method allows for a more three-dimensional approach in which nodes can be labelled not only with a dynamic value but also with the number of surveys used and statistical labels that are an indicative measure of precision.*

Therefore, as opposed to a survey-based approach, the records of all data points were analysed per node as separate points in a three-dimensional dataset within a time series, as illustrated in Figure 3.1b. In this figure, the red and blue dots indicate nodal elevations in SBES datasets, distributed in track lines that do not precisely overlap. The green data points represent an area-covering MBES dataset that overlaps with the data points of the SBES data. In this example, grid nodes may have zero to three (red, blue, green) data points stacked per node in time. The level of the most recent dataset does not necessarily have to systematically overlie or lie underneath the level of the previous survey.

Per DEM block of 5 x 5 km, each vertically stacked series of data points per node in time is evaluated. In this way, the minimum, maximum, mean and median depths are calculated per node. These values provide an impression of the variability in bed elevation in time. Next, the vertical nodal dynamic trend is calculated, using a linear least squares technique. This means

that a best-fit trend is determined with linear regression, based on all elevations in the stacked time series per node (Figure 3.2).

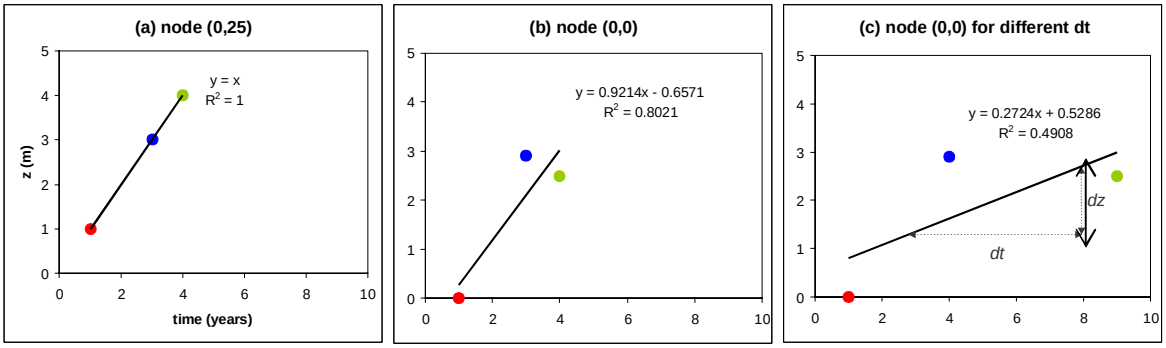

Figure 3.2 *Example of the determination of a vertical dynamic trend (dz/dt) per stacked series of data points per node in time. (a) If the second node (x,y) = (0,25) in Figure 3.1b would show a red dot (T_1) at z = 1 m, a blue dot (T_2) at z = 3 m and a green dot (T_3) at 4 m, and the periods between surveys would be respectively 2 and 1 years, the vertical dynamic trend at this node would be 1 m/yr with a goodness of fit (R^2) of 1 (i.e. perfect fit). (b) For the node (0,0), the trend would be 0.92 m/yr with a goodness of fit of 0.8. (c) For the node (0,0) but with different periods between the surveys, the vertical nodal dynamics would be 0.27 m/yr, with a goodness of fit of 0.49.*

To find the linear function that best fits a set of more than 3 points, the smallest value of the sum of distances between the line and data points is calculated [e.g. *Lawson and Hanson*, 1974].

The uncertainty (goodness of fit) of a linear regression line is affected by the number of surveys and the distribution of the points, which latter represents a variation of the vertical dynamic trend in time. A systematic trend in time results in a R^2 = 1 (see Figure 3.2a), whereas a widely distributed cloud would result in a poor fit (R^2 close to zero). With respect to the number of surveys, for example in Figure 3.2c, if the third survey was not available, the trend would be very different. In extreme cases, a trend could reverse from positive to negative.

Another factor of precision is the length of the period in which the survey is completed. Although the period between the start and end date of a survey may be several months up to one year, in the analyses of morphodynamics we use the middle of the survey period as time reference. A random inspection of the data showed that inaccuracies due to the surveying period do not significantly affect the outcome of the dynamic trend, since survey periods usually are small compared to re-survey frequencies. In order to prevent overlaps at the boundaries of surveys that obscure the pattern in natural dynamics, we did not calculate the vertical dynamic trend for two subsequent surveys of which the period in between the two surveys was less than one year apart.

When performing the analysis described above, the resulting map of vertical nodal dynamics shows a patchwork of contrasting vertical dynamics on the NCS, in which the boundaries correspond exactly to the different surveys, which obscures the natural morphodynamics of the NCS (Figure 3.3). The dominance of data characteristics per survey over the natural morphodynamic values of the NCS (m/yr) that causes this patchwork, may have several reasons. First, the least squares algorithm assumes a constant vertical dynamic trend (*linear* regression). However, if the seabed changes in a non-constant way, for instance in a sinusoidal or stepwise way due to the migration of sand waves or a sudden event, then every combination of time stamps will lead to a different value for the vertical dynamic trend (Figure

3.4). Second, DEMs of low-resolution surveys (SBES) are much smoother than those of high-resolution multi-beam data, since multi-beam data covers more of the morphology. When comparing data in time-series of mixed data types, the effect of resolution and measurement precision may result in locally higher dynamics (e.g. Figure 3.5). Finally, the number of different reference levels used on the NCS makes this calculation prone to errors. The surveys are recorded with respect to the lowest astronomical tide (LAT), mean sea level (MSL), Normaal Amsterdams Peil (NAP) and mean low low-water spring (MLLWS). Some of these reference levels are updated after isostatic adjustment, sea level change or changes in tide. For those surveys of which reduction levels deviated from LAT, DEMs were corrected manually, using two reduction matrices (spatial correction values for the entire NCS with 500 m resolution) provided by the NLHO.

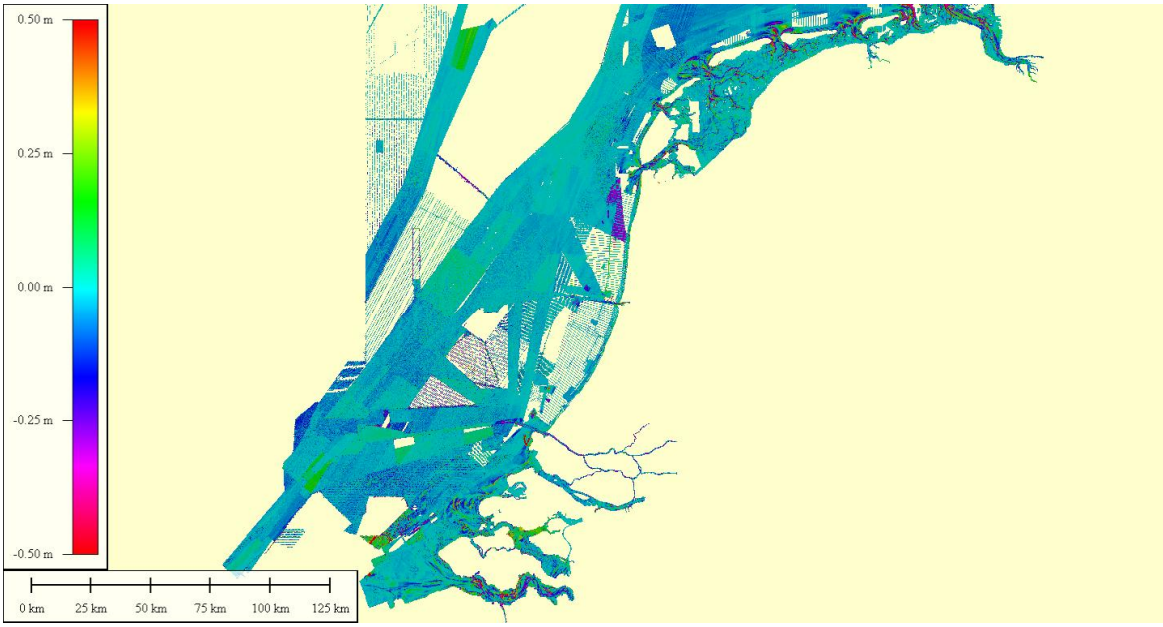

Figure 3.3 *First version of a vertical nodal dynamics map based on the absolute water depths of surveys, showing a patchwork of surveys that obscures the natural morphodynamics of the NCS.*

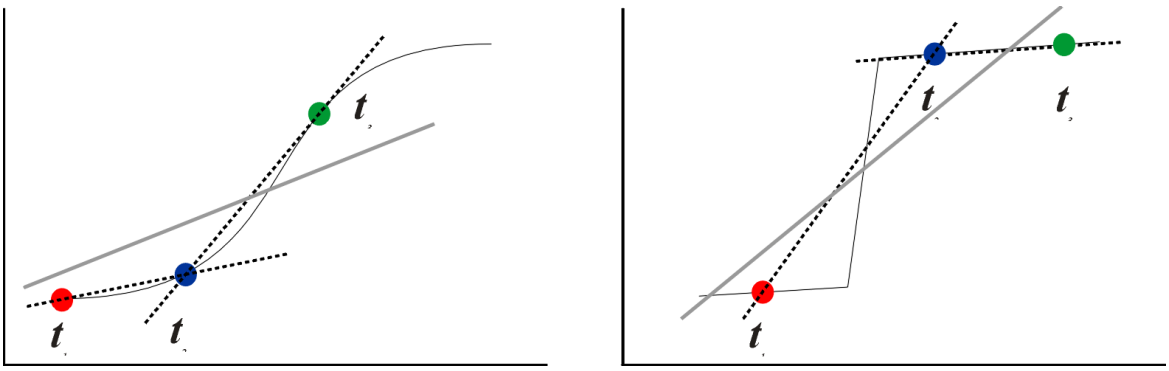

Figure 3.4 *Effect on the vertical dynamic trend between different pairs of subsequent surveys in a time series when the dynamics are (a) sinusoidal and (b) stepwise. The grey trend line represents the vertical dynamics that are calculated in this study.*

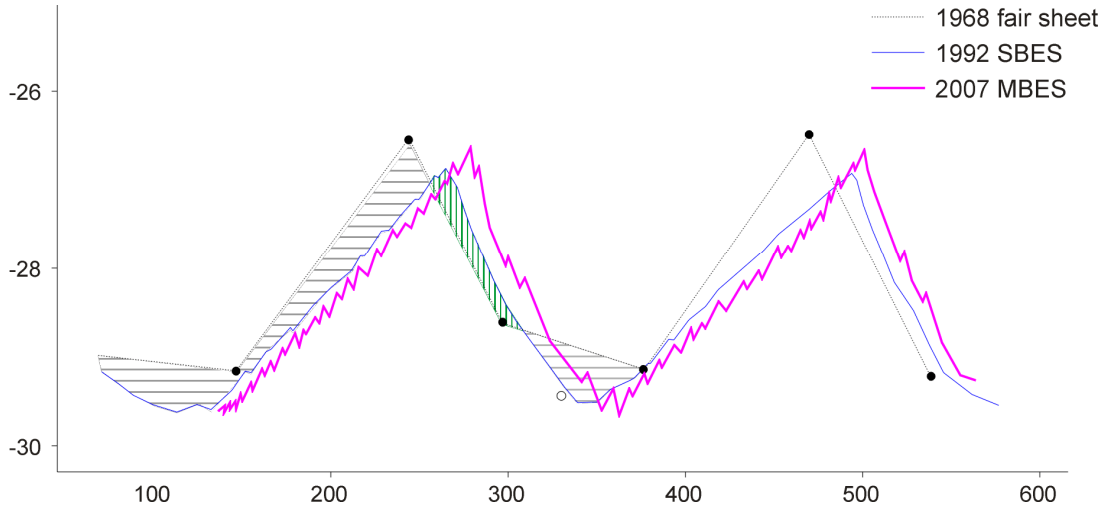

Figure 3.5 *Illustration of the effect of data resolution, measurement accuracy and the selection of shallowest points in the analysis of sea bed morphodynamics from bathymetric time series that comprise different types of data (SBES data from historical fair sheets, and digital SBES and MBES from the BAS-database, see section 2.1).*

In order to obtain the best results in the vertical nodal dynamics map, and at locations where multiple datasets were available in one time series, the datasets that seriously obscured the natural morphodynamics were omitted. If a certain location contained only two datasets, it is impossible to leave out one dataset. In this case, some problems could be solved by changing the reference level of a dataset.

For some areas, these measures (omitting deviating surveys and changing the reference level) were not sufficient to remove the patchwork pattern of surveys in the vertical nodal dynamics map, so that the effect of survey precision remained dominant over the natural morphodynamics. In order to reveal the natural morphodynamics, the effect of survey contrasts was overcome by subtracting the average vertical dynamics for every available stacked combination of surveys from the vertical dynamics at each node (Figure 3.6). In this way, every stacked combination of surveys is corrected in a different way.

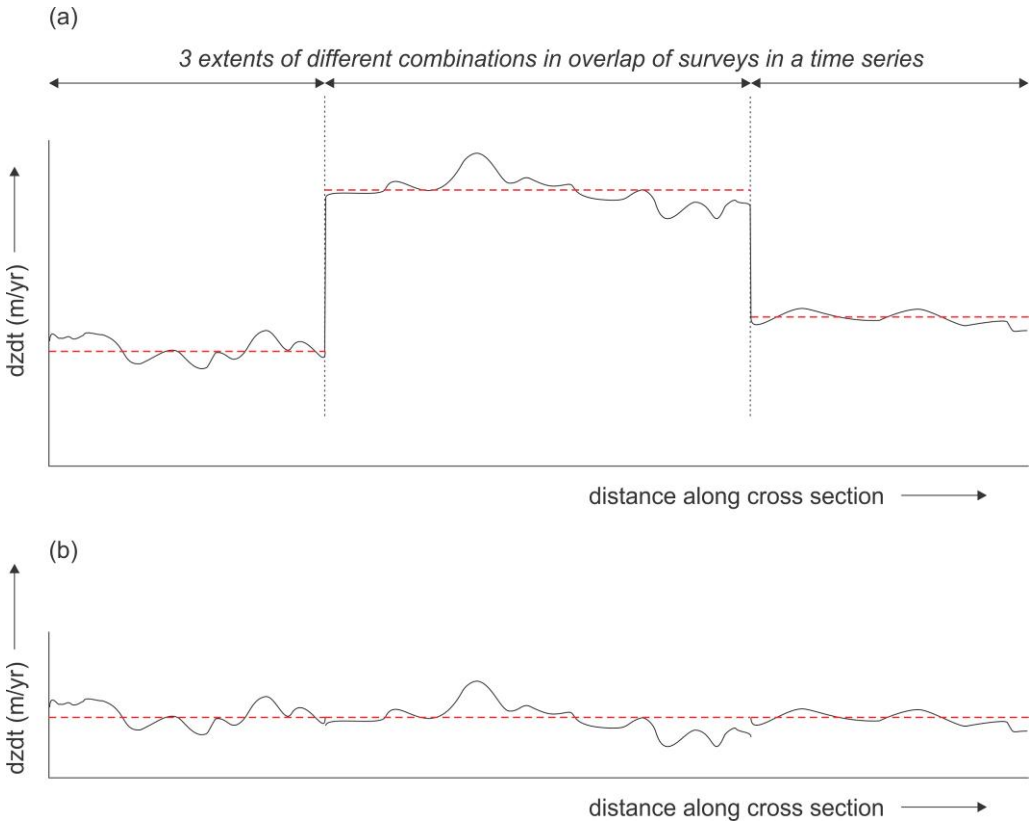

Figure 3.6 *Illustration of the applied correction of the vertical nodal dynamics of the NCS. (a) The calculated dynamics (black solid line)are corrected by subtracting the average dynamics for each combination of survey overlap (red dashed lines) (b) Resulting morphodynamics in which the patchwork is removed and the natural seabed dynamics are revealed.*

The difference between the maximum and minimum water depths at each node in time is a measure for the maximum variation in bed elevation since the first survey (Figure 3.7a). This difference provides the total height of vertical positions covered by the seabed at one point, but does not have a direction (as in Figure 3.7b). In combination with the vertical dynamic trend, the direction can be established. Most time series, however, consist of two surveys only.

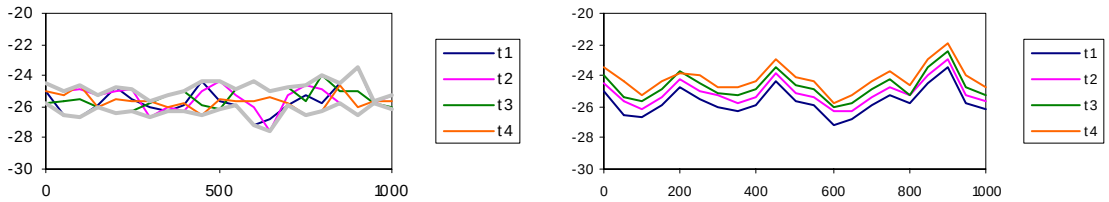

Figure 3.7: Two examples of four synthetic profiles of bed elevation in time, (a) arbitrary, where the area between the grey lines indicates the maximum nodal dynamics, and (b) with a steady trend. For clarity, a profile is used to illustrate the different scenarios; the results will be a map of the maximum variation, presenting the two-dimensional maximum dynamics for the NCS.

3.2.3 Vertical nodal dynamics NCS: prediction

Predictions of vertical nodal dynamics are done in the form of predictions of the water depth at each node by linear extrapolation of the vertical dynamic trend. Although we realise that the dynamic trend may not be linear, time series in this investigation are not long enough to establish a better relation in seabed morphodynamics. For example, 11 surveys are available for the Twin area, which allows for the estimation of changes in the sea bed dynamics. With most time series containing merely 2 or 3 datasets, this is not possible. Moreover, visual inspection of time series demonstrates that the time scale of the prediction is well within the time scale of migration of large bedforms such as sand banks and sand waves, so that sinusoidal trends are not yet an issue. In the time spans for prediction used here, linear extrapolation is justified. When the desired period for extrapolation exceeds the time that is needed for the displacement of sand wave by a quarter of a wavelength, linear extrapolation is not adequate anymore.

The cross correlation technique was not used in this prediction, as proposed in the research design. Using the cross correlation technique in the analysis of the data sets, resulted in unrealistic migration vectors, probably because the cross correlation technique is sensitive to errors in the data sets (unrealistic water depths of over several hundreds of meters are still contained in the data sets).

3.2.4 Detailed analyses of individual bedforms

The morphology and morphodynamics of individual rhythmic bedforms (e.g. migration and growth of sand banks, long bed waves and sand waves) are calculated in detail for specific zones of contrasting dynamics as identified on the vertical nodal dynamics map of the NCS.
Deltares developed a method to quantify the geometry and dynamics of individual rhythmic bedforms from bathymetric datasets, using spectral analyses [*Van Dijk et al.*, 2008]. This spectral method was tested against a geo-statistical method and has shown to perform well [*Van Dijk et al.*, 2008].

For detailed morphological analyses (e.g. geometry of individual bedforms), profiles are sampled from the DEMs in the direction perpendicular to the bedform crests. The orientation of the crests is determined with a spectral analysis (2D Fourier analysis) of each of the DEM's. Since the migration direction is not always normal to the crests, it may be preferred to compile separate profiles for the analysis of migration rates. In this report, most analyses were done on profiles normal to the crest orientation, in order to keep the migration results comparable to previously reported migration rates for comparison (e.g. to methods *Dorst*, 2009 and *Van Dijk et al.*, 2008).

For the morphological and dynamic analyses of individual bedforms, the bathymetric signal is separated into bedform types of different spatial scales by truncating a Fourier approximation at certain frequencies [for details, see *Van Dijk et al.*, 2008]. The locations of crest, trough and inflection points are then determined in a semi-automated way (Figure 3.8b). Semi-automated, because the method allows for manual removal of some undesired points (e.g. the red points in Figure 3.8). This way, the truncation can be as tight as possible, in order to still achieve a good approximation. Subsequently, form these crest and trough points, sand wave parameters, such as length, height, growth rates and migration rates are calculated for individual sand waves.

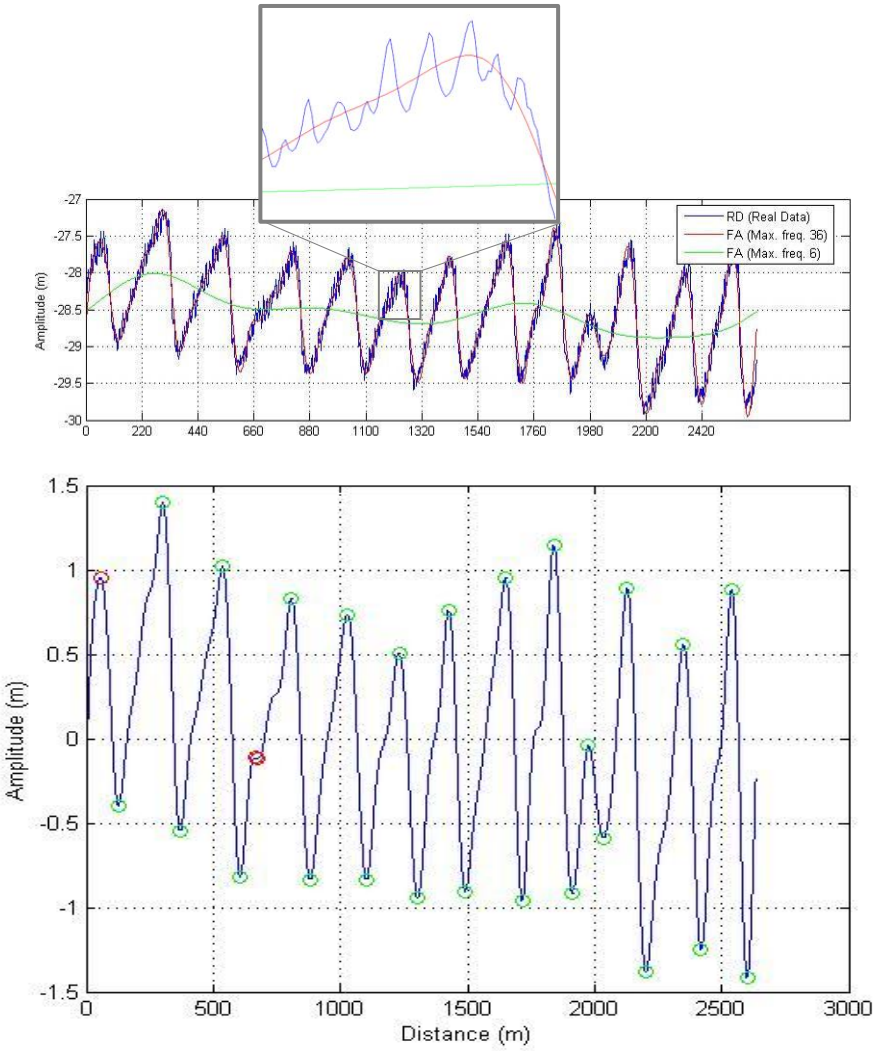

Figure 3.8: Top: Example of a Fourier approximation of an offshore sand wave field (site B in Figure 3.17) from which the sand wave signal (red) is separated from the superimposed megaripples (blue, real data). The underlying large-scaled morphology (green) is indicated. Bottom: semi-automated determination of locations of crest and trough points for individual sand waves from the signal from which megaripples were removed. Red dots were removed and are not included in the analysis, green points are used in the analysis. Inflection points are not shown, since these are not used in this project.

For the detailed study of the north-south oriented tidal ridges in the central Southern Bight, surveys within time series did not allow for a Fourier analysis, since the method requires a number of rhythmic forms and cannot handle a series of less than 2 banks. Their migration rates were therefore quantified manually (read from digital profiles).

3.2.5 Sand wave modelling

A process-based morphodynamic model, developed at the University of Twente, was used to study the impact of environmental conditions, including wind-induced surface waves. Modelling supports the analysed and predicted morphodynamics of the NCS with physical processes and provides insight in the effect on seabed dynamics that cannot be derived from observations, such as the impact of surface waves. A full description of the model, and therewith the methods, is given in Appendix 11.2.

3.3 Results

This section describes and interprets the results of the morphodynamic analysis of the Netherlands Continental Shelf (Objectives 1.1, 1.2 and 1.3).

3.3.1 Quantitative vertical nodal dynamics of the NCS (Objective 1.1)

There are different ways in which seabed morphodynamics may be analysed and visualised. Firstly, the total difference in elevation between the maximum and minimum elevations in the stacked record per node indicates the total height of vertical positions that the seabed has had since the first survey (Figure 3.7), but does not specify a direction of the trend (upward/downward). The interpretation is affected by the total number of surveys and the time intervals at which these surveys were carried out. When the period between two surveys is long, a large elevation difference may be observed, whereas in a location with a short period between surveys, the absolute elevation difference may be small, even though the magnitude of dynamics may be the same in both locations. Maps of the minimum and maximum bed elevation can hardly be distinguished from the bathymetric map in Figure 1.2. Therefore, merely the difference map (maximum minus minimum) of the elevation of the NCS is presented in Appendix 11.3.
To overcome the above shortcomings of the absolute difference in bed elevation (in m), we calculated the vertical nodal dynamics for the NCS as the linear trend of the stacked seabed elevations in time, following the methods described in section 3.2.2. Displaying these values in different ways provides different points of insight. When using a continuous scale of values, both natural patterns of morphodynamics and human-induced changes are revealed (see section 3.3.1). When the vertical dynamics map is displayed in classes of merely high and low dynamics, a simplified map results, which is very useful in identifying areas that may need increased attention in the hydrographic survey plan, but natural patterns may become obscured. The simplified map is presented in Figure 3.10.
A third way to get insight in the morphodynamics, is to calculate the difference between the bathymetry of the most recent measurements and the minimum elevation since the first survey. This provides a more geological insight, in the minimum amount of sediment that has been in motion since the first survey [*Vonhögen et al.*, 2010]. In the case of the dataset for the NCS used in this project, however, the time series are not uniform and in most parts comprise merely one or two periods, so that this approach is less revealing than for instance in the Wadden Sea with long time series (results not shown). With a dataset like of the NCS, the vertical dynamic trend (in m/yr) is the most reliable method.

The quantified vertical nodal dynamic trend of the Netherlands Continental Shelf (Figure 3.9) provides an overview of regions of contrasting dynamics on the NCS. This map needs to be interpreted with care, since the values represent both natural and human-induced seabed morphodynamics and include artefacts due to the quality of the available datasets that interfere with the pattern of natural dynamics.

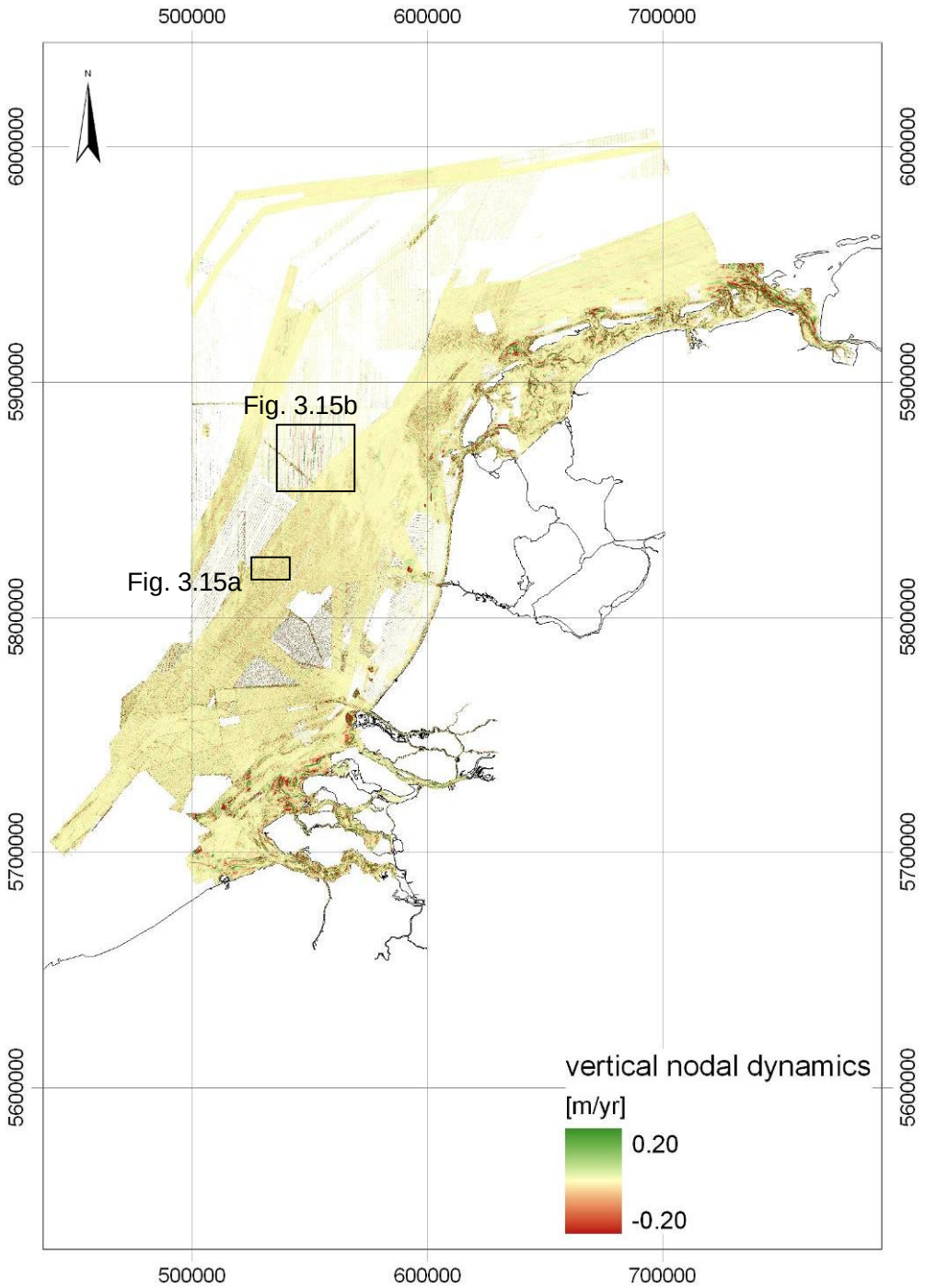

Figure 3.9 *Vertical nodal dynamics of the Netherlands Continental Shelf, presenting the best-fitted trend of the corrected vertical bed elevation in time (dz/dt in m/yr) on a spatial resolution of 25 m. The map reveals areas of contrasting dynamics. Distinct red (degradation) and green (aggradation) indicate highly dynamic areas; light yellow are areas of low dynamics. Offshore areas of high dynamics are the fields where rhythmic bedforms occur. White areas represent parts of the NCS where no time series are available. An enlarged map is included in this report as a separate sheet*

Four main areas of contrasting dynamics may be distinguished on the vertical nodal dynamics map of the NCS. Firstly, the map exhibits that areas of the highest dynamics (common absolute values of 0.1 to 0.35 m/yr with extremes up to 1.5 m/yr) are all coastal areas. Highly dynamic coastal zones include the Wadden Sea, the tidal inlets of the Wadden Sea and their

ebb-tidal deltas, tidal channels near the Zeeland coast, the estuaries Ems-Dollard, Eastern Scheldt and Western Scheldt, as well as anthropogenic areas, such as sand extraction sites. Secondly, areas of moderate vertical dynamics (typically -0.1 to 0.1 m/yr with extremes of 0.3 m/yr in the sand wave fields) occur offshore. Here, the natural vertical nodal dynamics are highest in areas where rhythmic bedforms are present. The appearance of bedform patterns in the vertical dynamics map indicate that the measure of vertical dynamics is controlled by the migration and/or growth of individual bedforms. These zones include a long bed wave field north of Texel and Vlieland, a sand wave field west of Texel, the entire sand wave field in the Southern Bight including tidal ridges, and the tidal ridges 75 km offshore of Texel where sand waves seem absent. Thirdly, areas of low dynamics (around 0 m/yr) occur mostly in parts of the NCS where rhythmic bedforms are absent. Although the dynamics map is scarcely filled in these zone, the larges area of low dynamics occurs in the deeper parts of the NCS, farther offshore and north of de Wadden islands. In addition, areas of low seabed dynamics appear in a zone between the sand wave field west of Texel and the offshore sand banks, and in small patches along the coast offshore Den Haag (although data is scarce), offshore Voorne and the Vlakte van de Raan (ebb-tidal delta of the Western Scheldt). Lastly, areas of high dynamics are observed due to artefacts caused by the data in the time series. These are most prominent in the Deep Water Route East and in the zones of low dynamics north of the Wadden.

The simplified classification map of the vertical dynamic trend (Figure 3.10) confirms the distribution of high and low vertical dynamics on the NCS. The identified dynamic zones are described in more detail in the subsections following below (sections 3.3.1.1 to 3.3.1.4).

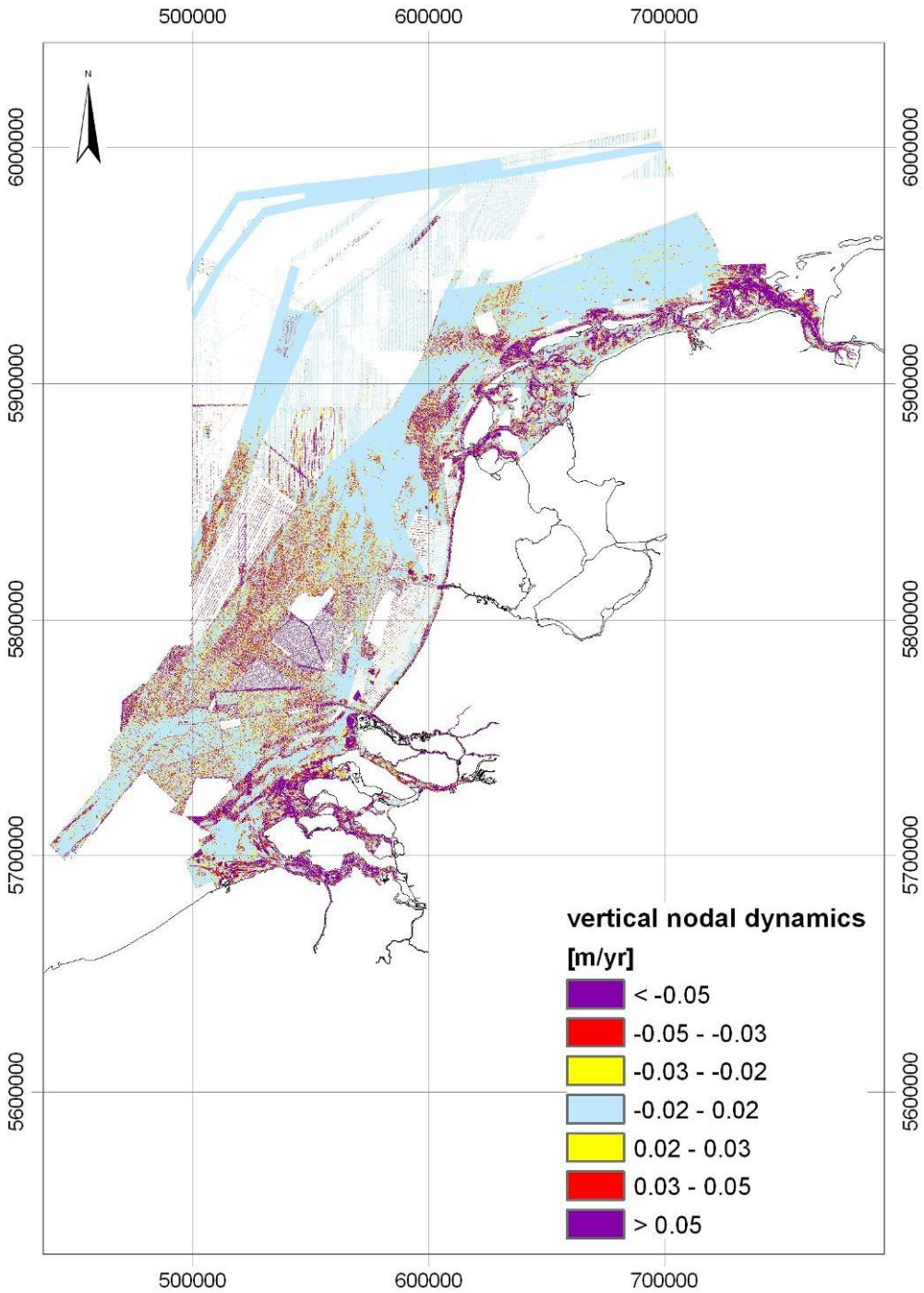

Figure 3.10 *Simplified map of the vertical nodal dynamics map in Figure 3.9 (dz/dt in m/yr), in which colours represent the absolute values of vertical nodal dynamics. This map brings out the areas of high dynamics (red and purple) and low dynamics (light blue) on the Netherlands Continental Shelf.*

When comparing the maximum and minimum elevations at each node in the time series, the resulting elevation difference map (dz in m) (Appendix 11.3) confirms the findings of the vertical dynamic trend.

Additional results, such as maps of the number of surveys per node used in the analysis of the vertical dynamics map and the goodness of fit of the dynamic trends per node (depending on the number of surveys and time intervals between surveys), that serve as background information on the quality of the results, are presented in Appendices 11.4 and 11.5.

3.3.1.1 Coastal zone and Wadden Sea

Eye-catching features on the vertical dynamics map (Figure 3.9) are the tidal inlets of the Wadden Sea, including associated ebb-tidal deltas on the seaward side of the Wadden Islands, the estuaries Ems-Dollard, Eastern and Western Scheldt and the tidal channels along the Zeeland coast. These zones are highly dynamic because of (lateral) channel migration and/or (vertical) deepening or infill of the channels.

For example, the tidal inlet between Vlieland and Terschelling (Figure 3.11a) shows zones of aggradation and degradation with rates up to 0.7 m/yr in the channel. When overlaying the isobaths on the vertical nodal dynamics map, it becomes clear from the combinations of red and green, that some channels have laterally migrated. A multiple combination of green-red-green on the dynamics map may indicate deepening of the channel with aggradation of the adjacent flats. The ebb tidal delta has vertically aggraded in the centre (green), vertically degraded in the western part (red) and seems to reshape its delta slope edge.
The dynamic nature of the tidal inlet and the ebb-tidal delta is also revealed from the elevation difference map (Figure 3.11b), which indicates that total elevation differences on the ebb-tidal delta are 0.2 to 3 m and in the channels these may reach more than 5 m since the first survey (later than 1980s in the time series that we work with). A recent morphological study of the Wadden Sea for a longer time series (since 1926) was carried out at Deltares and confirms these findings [*Vonhögen et al.*, 2010].

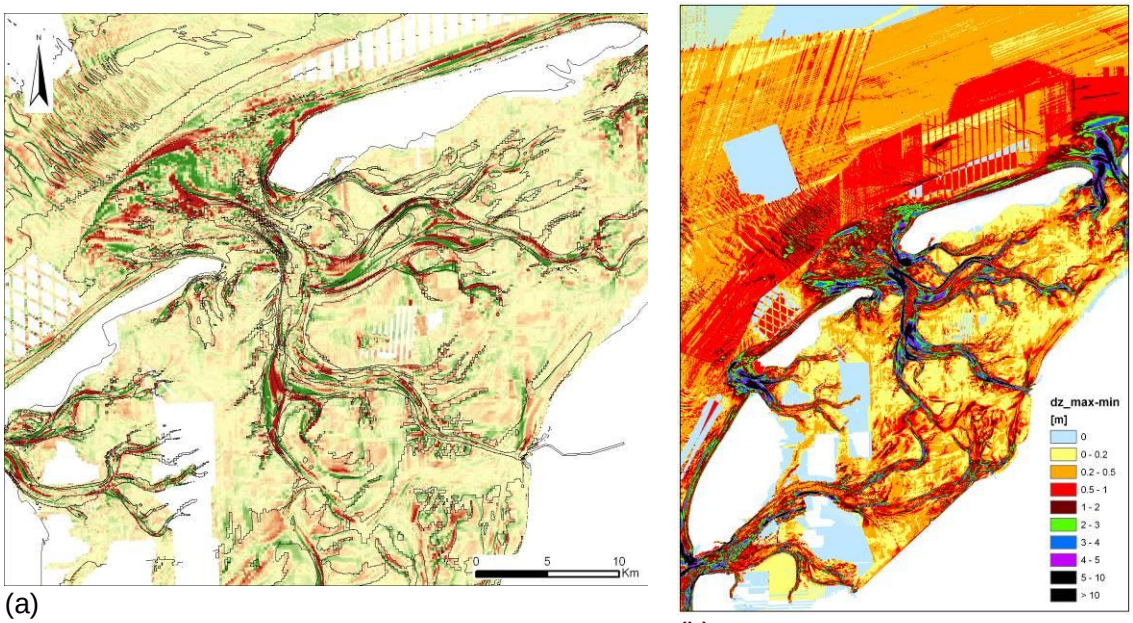

(a) (b)

Figure 3.11 *Tidal inlet between Vlieland and Terschelling. (a) Comparing the vertical dynamic trend to isobaths, it becomes evident that the large dynamics in this area is caused by channel migration. Herein, red represent areas of erosion, green areas of aggradation. (b) Difference between maximum and minimum bed elevations in the time series. The colour scale of (a) is the same as the general dynamics map (-0.2 to +0.2 m/yr).*

The most dynamic parts of the coastal system are the Western Scheldt and the Ems-Dollard estuaries. Again, this is evident on both the dynamic trend and the bed elevation difference, of which the latter is illustrated for the Western Scheldt in Figure 3.12, where the ebb and flood channels have total differences of more than 5 m since the first survey (later than 1980s).

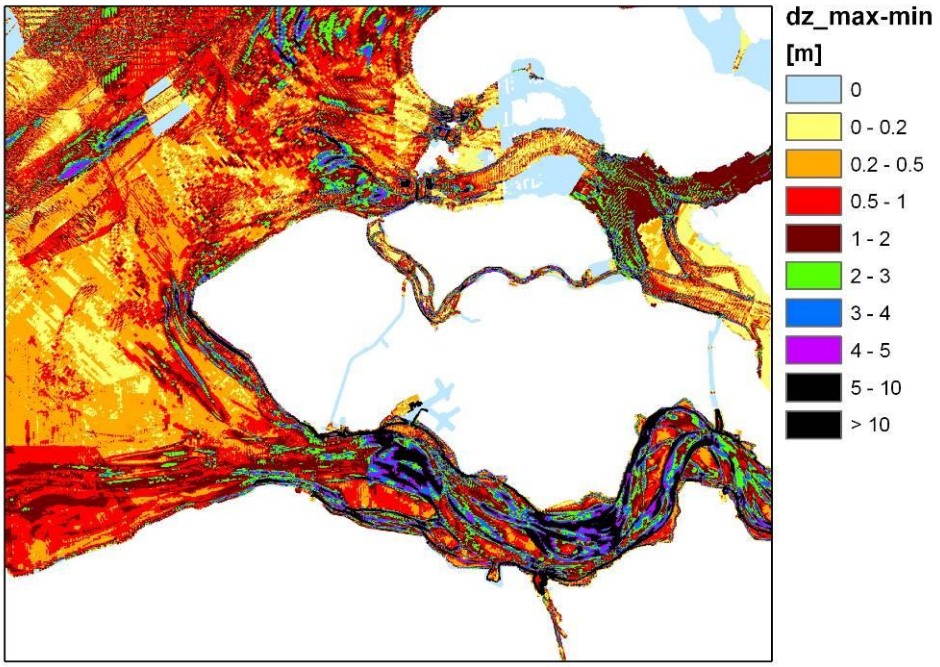

Figure 3.12 *Difference between the maximum and minimum seabed elevation in the stacked record of the Western Scheldt, parts of the Eastern Scheldt and offshore Walcheren. The ebb and flood channels in the Western Scheldt – together with tidal inlets of the Wadden sea – reveal the highest elevation differences of the available data.*

Another coastal feature that emerges to be relatively dynamic are breaker bars, which are longshore sand bars that occur in the zone where surface waves break, close to the beach, at water depths up to 5 m. On the vertical dynamics map (Figure 3.9 and Figure 3.11), these are recognised as red and green pairs, or sometimes multiple pairs, along the coastlines of Noord- and Zuid-Holland and the shorelines north of the Wadden Islands. These bars are expected to be dynamic due to the large impact of breaking waves on the sediment transport at the bed; their dynamic time-scale is much shorter than that of offshore sand banks. The yearly transect measurements at the Dutch coast (Jarkus transects) imply a slow seaward migration of the sand bars with a period of sand-bar pattern repetition of 12 to 15 years for bars at the coast of Noord-Holland and 4 years for those in South-Holland [*Wijnberg*, 1995].
Also, at some locations near the Dutch coast, these zones are used for shoreface nourishments. Effects of such short time-scales cannot be calculated in the vertical nodal dynamics map based on the available time series of bathymetric data. The dynamics in the vertical nodal dynamics map in this report are based on time series of much longer periods than seasons and may thus be not representative for the true natural and/or human-induced dynamics of the breaker bars.

3.3.1.2 Offshore zone (NCS)

The three most prominent zones of highest dynamics of the NCS below the -10 m isobath are the field of long bed waves north of Texel and Vlieland, the sand wave field west of Texel and the main field of both sand waves and tidal ridges (sand banks) in the Southern Bight (Figure 3.9). The pattern of individual bedforms on the dynamics map indicates that the dynamics are natural, which is related to the migration of bedforms.

The long bed waves field north of Texel and Vlieland displays vertical nodal dynamics up to -0.1 to +0.20 m/yr (Figure 3.13). The occurrence of this field of highly dynamic long bed waves is newly identified; no records of this area were found in the existing literature. Therefore, a

detailed analysis is carried out at this site, as part of objective 1.2.i. The long bed waves migrate to the northeast with an average migration rate of 12.4 m/yr. The results of the quantification of the morphodynamics of individual bedforms are described in section 3.3.2.3.

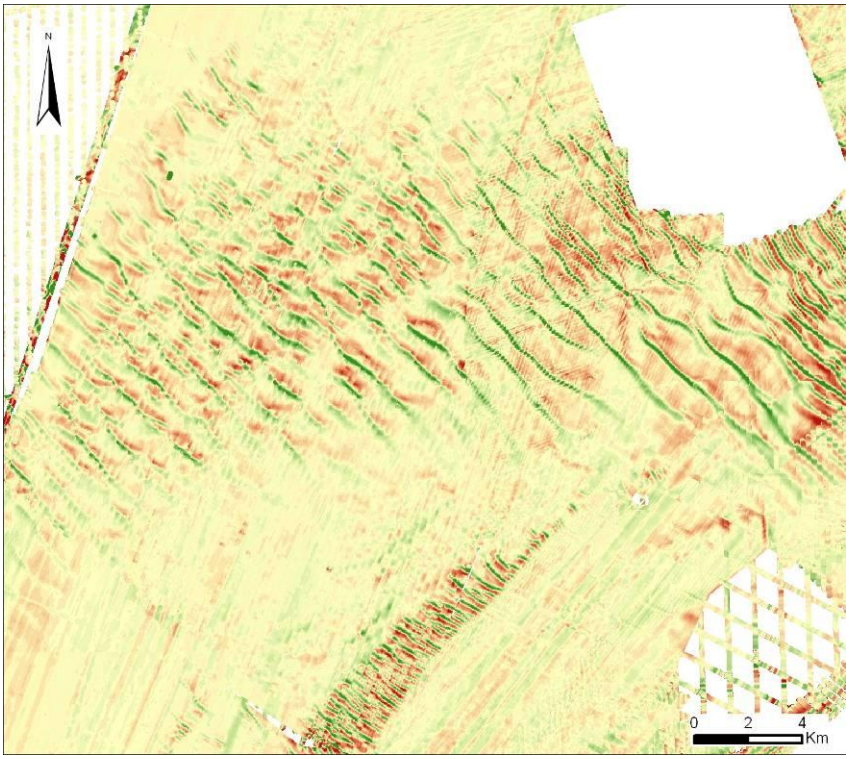

Figure 3.13 *Detail of the vertical nodal dynamics in the long bed wave field north of Texel and Vlieland. Legend is the same as the general dynamics map. The sharp line in the dynamics of sand waves in the bottom of the figure coincides with the sudden absence of sand waves on a shoreface-connected ridge.*

In the sand wave field to the west of Texel, vertical dynamics reach -0.16 to +0.23 m/yr (Figure 3.14). This location was identified as exceptionally dynamic in earlier studies carried out at TNO and Deltares. The field contains two zones of sand waves of different lengths. On the shoreward side, sand waves with wavelengths smaller than 350 m occur, whereas in the offshore part of the field, wavelengths are longer than 350 m. The sand waves have average migration rates of up to 19 m/yr [*Van der Meulen et al.*, 2004; *Van Dijk and Kleinhans*, 2005] and are therewith the most mobile sand waves that are observed on the NCS. Only the sand waves in the Marsdiep (which are shorter and higher in comparison to the sand waves west of Texel) are more mobile with migration rates up to 90 m/yr [*Buijsman and Ridderinkhof*, 2008a; 2008b].

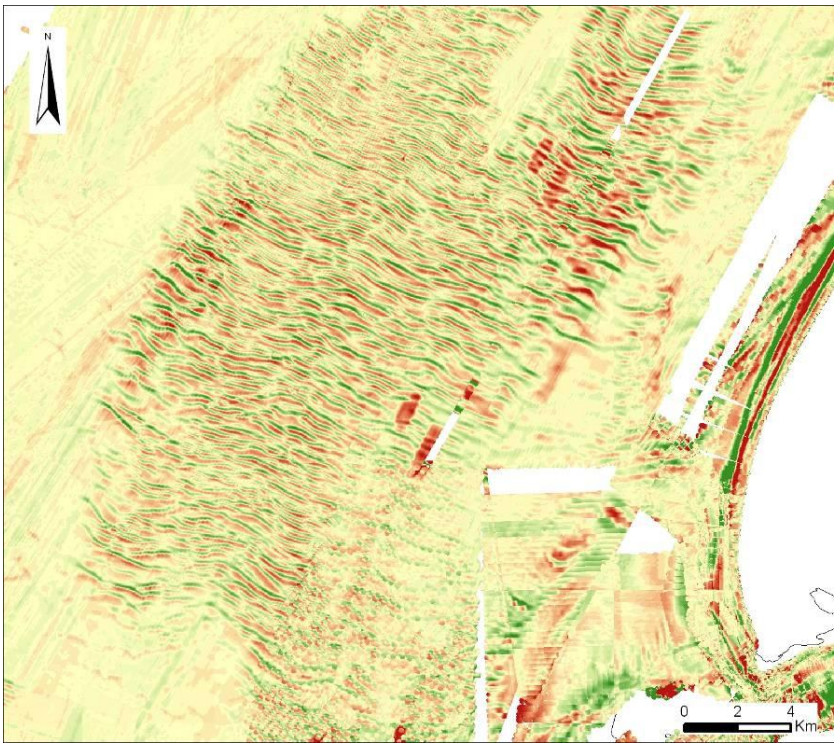

Figure 3.14 *Detail of the vertical nodal dynamics in the sand wave field west of Texel. The legend is the same as in the general dynamics map. The stripy red parts are artefacts in the data. The longshore sand bars are also nicely visible.*

The main field of high dynamics observed in the Southern Bight is also related to the migration of marine bedforms. This field comprises combined occurrences of offshore tidal ridges with superimposed sand waves in the central part, long bed waves and sand waves in the south-west corner, and mainly sand waves in the rest of this field.
Based on previous knowledge, sand banks in the Southern Bight are assumed to be approximately stable over periods in the order of decades. This study shows that the vertical nodal dynamic trend is mostly due to sand wave dynamics in the southern part and possibly due to migration of the sand banks themselves in the northern part (Figure 3.15).

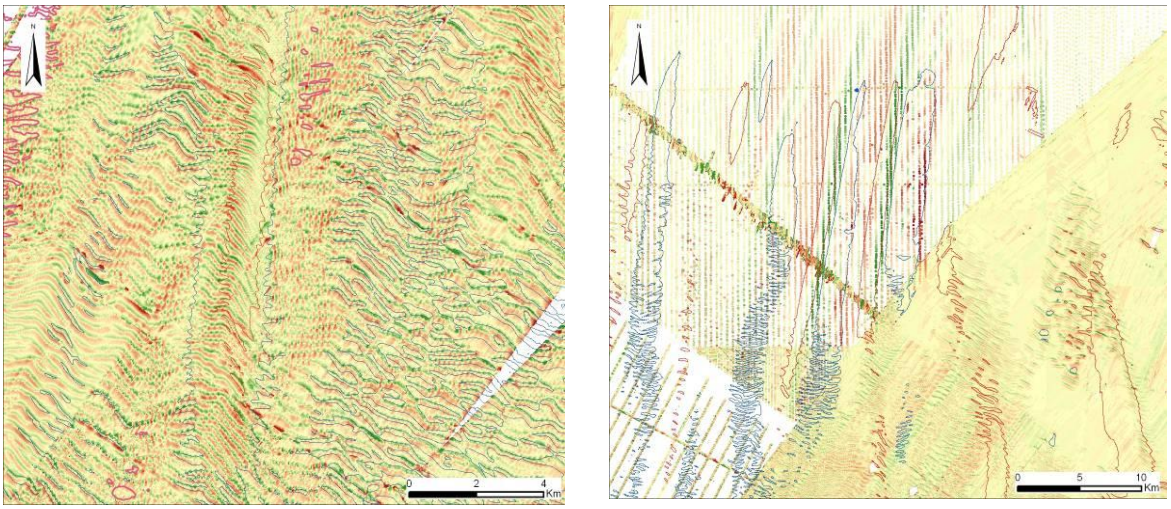

(a) (b)

Figure 3.15 *Details of (a) the first offshore sand bank to the east of the Brown Ridge, and (b) the northern ends of sand banks 75 km offshore of Texel in a time series with low-resolution fair sheets of 1976. Interval of isobaths is 5m (blue is -30m; red is -25m). For location of these zooms, see Figure 3.9).*

When overlaying the morphodynamic and bathymetry maps, the southern ends of the Brown Ridge and the surrounding banks (Figure 3.15a) show the highest dynamics on the ridges, whereas the dynamics in the adjacent, deep troughs is almost zero. Dynamics on the banks are mainly due to dynamics of sand waves. This contrast could be explained by the high tidal current velocities over the crests of ridges and the low velocities in the deep troughs of these ridges. The two banks to the east of the Brown Ridge display that sand wave dynamics on the west flanks is high, but the east flanks remain almost unchanged. This would agree with a flood-dominated tide. Details of the (manually) quantified morphodynamics of these banks are described in section 3.3.2.5.
For banks to the north-east, 40 km offshore Alkmaar, geomorphology-related patterns differ. These banks show no dynamics of their west flanks and crests, but large sand wave dynamics (mainly aggradation) on their east flanks. This may mean that either sand waves do not occur on the west flanks or that sand waves do neither grow nor migrate. Higher dynamics on the east flanks would suggest dominant ebb currents.

To the north, 75 km offshore of Texel, these banks seem more dynamic (Figure 3.15b). This, however, may be partly caused by the data resolution in the time series (affecting the magnitude of values). On the other hand, since the pattern does not relate to the survey boundaries and the dynamic trend varies with the geomorphology of the banks within the track lines of the survey, the changes may in part display natural migration of the banks. These banks show a sharp and repetitive contrast between lowering (red, down to -0.1 m/yr) on the west sides and elevation (green; up to 0.3 m/yr) on the east sides of the banks, indicating a migration of sand banks towards the east (landward). In addition, the troughs between the banks are much lowered (some troughs with rates of -0.2 m/yr and the crests of the banks are subtly rising, which indicates growth of these banks. This is a new observation because this time series was newly created by digitising fair sheets from 1976 (SBES) that now overlap with 2003 MBES data. Despite this, the contrast between west and east flanks is more distinct then in other zones of the offshore tidal ridges in the Southern Bight, which strongly suggests the effect illustrated in Figure 3.5. Furthermore, on these northern parts of the banks, superimposed sand waves seem to be absent. This is not an implication of the lower resolution in Figure 3.15b, because this observation was made on the high resolution banthymetric map.
In this case, when the time series consists of merely two datasets, the total elevation difference does not add much to the interpretation of the vertical dynamics. However, it may be interesting to know the total elevation differences in the period between 1976 and 2003 (27 years) (for map see Appendix 11.3). On the present-day crests, total differences of 0 - 2 m are calculated. Total differences in the troughs are 0.5 – 3 m for the western trough, which increases up to 1 - 7 m in the eastern trough. Highest values occur on the east flank of one bank (7.3 m). In combination with the dynamic trend, we know that troughs and west flanks erode and that crests and east flanks vertically aggrade. The map also shows a variation in the north-south direction, with maximum differences in depressions in the troughs and fading out to the north (also seen on the dz/dt map).
This site would be interesting for detailed analyses, however these data were received during the later phases of the project, and were time-wise not included in the detailed analysis.

Lastly, in the zone of long bed waves in the south-west corner of the NCS, contrasts in vertical dynamics to the rest of this main offshore field of high dynamics, were not observed.

3.3.1.3 Areas of high anthropogenic sea bed dynamics

The vertical nodal dynamics map displays small areas of abrupt and extremely high values (up to 1 m/yr) in shapes that are unrelated to natural processes. An overlay of the locations of marine aggregate sites of RWS demonstrates that all of these features are either sand extraction or dumping sites (Figure 3.16). For example, the hat-shaped site offshore IJmuiden, north of the approach channel (site Q8F), is a sand extraction site. Although no mining has been recorded since 2002, vertical nodal dynamic trends of -0.1 to -0.25 m/yr were calculated. This area is covered by a surveys from January 2001 and 2002, in which no depression is observed, and August 2008 and May 2009, in which the depression is observed. If the mining records are correct, this suggests that sand extractions have a large impact on the local vertical dynamics over periods at least of several years. Other examples are two sites offshore Schagen (Q5G and Q5F), which are sand extraction sites for beach nourishments. These sites show values on the vertical nodal dynamics map down to -0.35 m/yr. More than 1 and 4 million m^3 was extracted in 2008 and approximately 0.5 million m^3 in 2009 over respective surface areas of 120 and 266 ha, which would result in a lowering of up to 1.6 m for the largest mining action, if evenly distributed over the area (corresponding to a dz/dt-trend of 0.23 m/yr between 2001 and 2008). A calculated dynamic trend that exceeds the estimated lowering, based on volumes and size of the area, suggests that little vertical dynamics is compensated in time. Furthermore, the maintenance of e.g. the Maasgeul is distinguished (site P18PW2). Vertical dynamic values range between -0.35 and +0.37 m/yr, due to almost yearly dredging and dumping of sea bed sediments. Another site in front of IJmuiden is not explained with the locations of RWS's mining sites, but is interpreted to be an anthropogenic dumping site.

The vertical dynamics map also exhibits that in locations where merely Jarkus transects are available, sand extraction sites may still be identified, such as seen offshore Noordwijk.

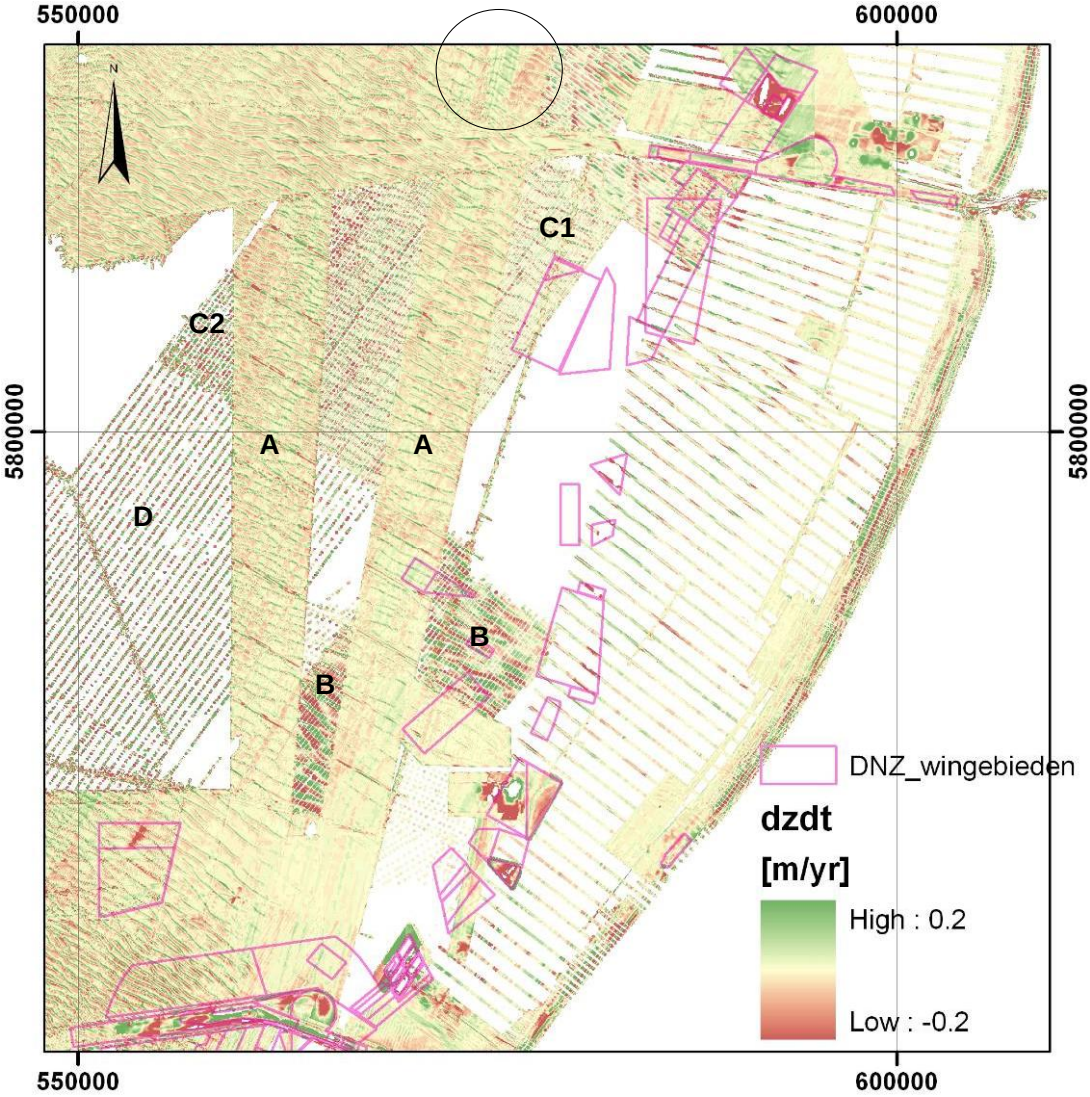

Figure 3.16 *Detail of the vertical dynamics map offshore Den Haag to IJmuiden, with an overlay of RWS sand extraction sites (pink polygons). This map also shows the contrasts in dynamics related to differences in data quality in the time series of varying types of data (e.g. fair sheets, low-resolution SBES and high-resolution MBES; letters A t/m D and the circle are clarified in section 3.3.1.4).*

3.3.1.4 Other dynamic locations identified

Other locations that show high vertical dynamic values on the dz/dt-map are caused by artefacts due to survey overlaps, differences in data density and/or the use of different echo sounding methods in one time series and due to precision of echo soundings, the tidal reduction and interpolation into DEMs. In terms of overlap, the narrow bands where surveys overlap are visible in the southern part of the NCS, far offshore Zeeland (Figure 3.9) and in Figure 3.15b, where the red and green is clearly more intense in the overlap. Even though it was attempted to remove this artefact by eliminating those nodes for which the period between two subsequent surveys was less than one year, these overlaps remain in the vertical dynamics map. The same effect occurs where tracks that were sailed perpendicular to the survey track lines in order to check the echo soundings ('*controleslagen*') overlap with the survey tracks (Figure 3.16). The artefact due to overlap may be caused by the measuring

precision and tidal corrections. This artefact does not obliterate the pattern of natural morphodynamics.

The second type of artefact occurs where low-resolution single beam surveys are overlain with high-resolution multi-beam surveys, or where digitised fair sheet data are overlain with digital data, which also results in zones of high dynamics (illustrated in Figure 3.5; this effect is especially clear in the simplified vertical dynamics map in Appendix 11.1, where the some areas in which time series were created with digitised fair sheets show up as purple). A good example of deviating results due to the survey data is the offshore zone from Den Haag to IJmuiden (Figure 3.16). Here, different combinations of surveys result in zones of contrasting dynamics, four of which (A t/m D in Figure 3.16) will be described below.

(A) Firstly, two lanes of high-resolution data (1999-2001 and 2007 time series) reveal mainly a low dynamic zone (yellowish) with a sand wave pattern in vague red and fine green lines, where the direction normal to the crests is to the northeast (ignoring the perpendicular tracks).
(B) The seemingly underlying survey offshore Den Haag also displays a sand wave pattern, but the range of the dynamic values differs. Although the sand waves correspond in both orientation and wavelength, the pattern of full red and green bands suggests the occurrence of highly dynamic and larger bedforms. Since the deviating values are limited to the extent of one survey, it seems reasonable to interpret that this contrast is caused by either the dissimilarity in resolution or tidal reduction precision (the time series consists of 1984 and 1999-2001 data).
(C) The seemingly underlying survey offshore Zandvoort (1984 and 1999 SBES data) has a slightly lower resolution than the high-resolution lanes, but the same sand wave pattern is still recognisable (C1). Towards the southwest of this survey, however, the magnitude of dynamics slightly increases. West of the lanes, the southwest corner (also 1984 and 1999 data) shows even higher vertical dynamic values in a lower resolution (C2), in which the sand wave pattern is largely obscured, although an overall orientation may still be made out.
(D) To the southwest of this survey (D), a low resolution zone in the dynamics map displays the highest dz/dt-values of this region, probably due to low-precision and shoal-biased data of digitised fair sheets. The time series comprises 1985 and 1999-2000 data, but only overlap on the lines shown in the map). No sand wave pattern is recognisable, because the gaps between the data are larger than the spatial scale of the bedforms.

The last type of artefact is the along-track contrasts within surveys. These are observed on the vertical nodal dynamics map north of the Wadden, in the Deep Water Route East (both near the UK border and at the latitude of the long bed wave field north of Texel and Vlieland) and in the zone of low dynamics between sand wave field west of Texel and the main bedform field in the Southern Bight (also visible in Figure 3.16 at the top edge within the circle). This artefact may be caused by the vertical precision of echo sounding and/or tidal reduction. Since the artefact shows wide bands of multiple tracks, the most probable cause is tidal reduction precision. For multibeam data specifically, an extra along-track artefact may occur due to the differential vertical precision of the multibeam echo soundings themselves (i.e. the increase in uncertainty towards the outer beams), as discussed by *Righolt et al.* [2010] and *Simons et al.* [2010]. However, these do not occur in wide bands and may not be observed on the scale of the entire NCS as presented in this report. The interpolation of data points distributed in tracks of large distance into DEMs also shows an interpolation artefact, but given the multiple-track width of the bands, this artefact does not seem to be such an interpolation artefact. The along-track striping dominates in areas of low dynamics, such as north of de Wadden. Here, the pattern of natural dynamics may not be observed because of this overruling artefact. For example, the subtle dynamics of the shoreface-connected ridges north of Ameland and Schiermonnikoog has become in part indistinctive. In opposition, the

natural pattern is not obliterated when dynamics are high enough. For example, the tidal ridges in the Deep Water Route East on the latitude of Petten fully overcome this artefact. Also, in the southwest corner of the NCS, the along-track bands are vaguely present in surveys of low dynamics and subordinate in areas of high dynamics.

3.3.2 Detailed bedform dynamics: the quantification of migration and growth rates of individual bedforms (Objective 1.2)

Based on the zones of contrasting morphodynamics, as identified on the vertical nodal dynamics map (Figure 3.9), a selection of sites was made at which the detailed quantification of morphodynamics of individual bedforms was performed (Obj. 1.2). These sites were selected to include all types of bedforms, from sand banks to sand waves.
Firstly, since sand waves are known to vary in their morphology and morphodynamics [*Van Dijk and Egberts*, 2008], and three purposes were formulated having to be served with the sand wave analyses (see objectives in Chapter 1), a number of sand wave fields was selected for detailed study. The areas are indicated in Figure 3.17.

(a) Areas Texel, B and C are sand wave fields with variable dynamics on the vertical morphodynamics map, thereby serving specific objective 1.2.i.
(b) Sites West of IJmuiden (WIJ12), West or Rotterdam (WR1) and the TWIN area were analysed in order to compare migration rates to those found in Dorst [2009] (i.e. obj. 1.2.ii).
(c) The other sand wave areas, numbered 1 to 5, were analysed to provide input to the sand wave modelling and validate the results (obj. 1.2.iii). These areas were selected so that the differences among environmental conditions (e.g. water depth, tidal current velocity) were the largest.

Secondly, to the north of Wadden islands Texel and Vlieland, the vertical morphodynamics map reveals an area of highly dynamic bedforms with long wavelengths (long bed waves), of which its dynamics were not yet known. To date, there are no records of the dynamics of long bed waves in the international literature. This area is thus relevant for a detailed study.
Thirdly, a series of shoreface-connected ridges is observed to the north of Wadden islands Ameland and Schiermonnikoog. Even though the morphodynamic map does not indicate these to be dynamic, the present-day knowledge on migration rates and vertical morphodynamics of shoreface-connected ridges on the NCS is limited. Shoreface-connected ridges near the island Spiekeroog, Germany, were found to migrate at maximum rates of 100 - 200 m/yr [*Antia*, 1996]. The site north of Ameland and Schiermonnikoog is thus selected to be relevant for a detailed investigation.
Lastly, the north-south oriented offshore tidal ridges in the central Southern Bight appear to be more dynamic on the vertical nodal dynamics map than was to be expected based on the general knowledge of morphodynamic time-scales of sand banks. Since these banks reach up to less than 20 m of water depth, located far offshore, they form a potential hazard to shipping. Therefore, three of these banks are selected for a detailed study.

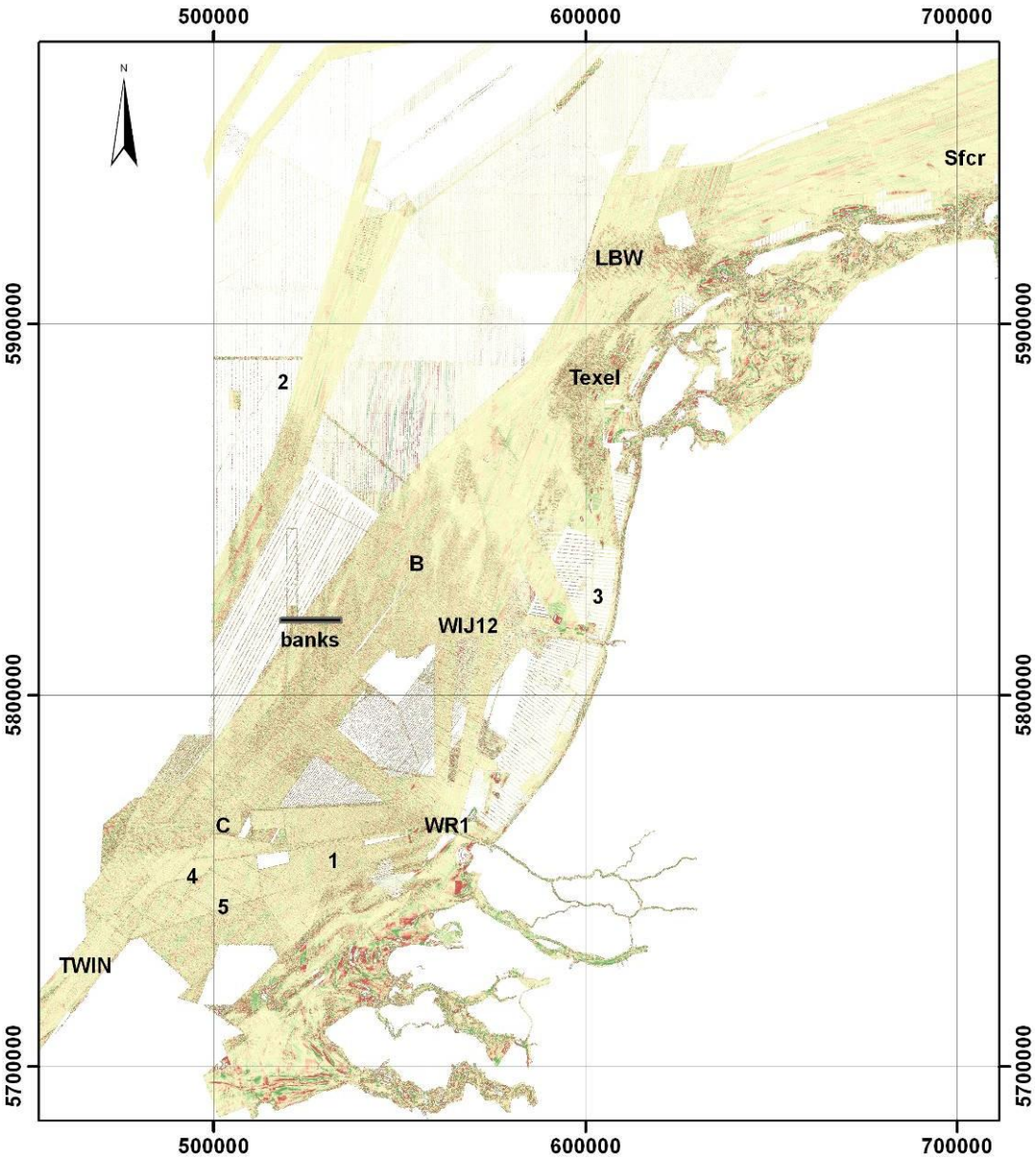

Figure 3.17 *Selected locations of the detailed studies in order to quantify the dynamics of individual bedforms*

3.3.2.1 Quantitative migration rates of sand waves on the NCS (obj. 1.2.i)

This section focuses on the detailed studies of sand waves that were analysed either to specify the identified high dynamics on the map of the NCS (objective 1.2.i) or to serve the sand wave modelling (objective 1.2.iii). Since a large number of detailed studies of sand wave dynamics on the NCS was performed, merely site 1 (in block S2; Figure 3.17) serves as an example of what observations can be made at detailed studied sites. The other sites are not described in detail, but are only given as summarised quantitative results in this section. Bedforms longer than sand waves are described separately in sections 3.3.2.3 to 3.3.2.5. A full table in which all quantified results of morphodynamics of all bedforms are collected is given in Appendix 11.6.

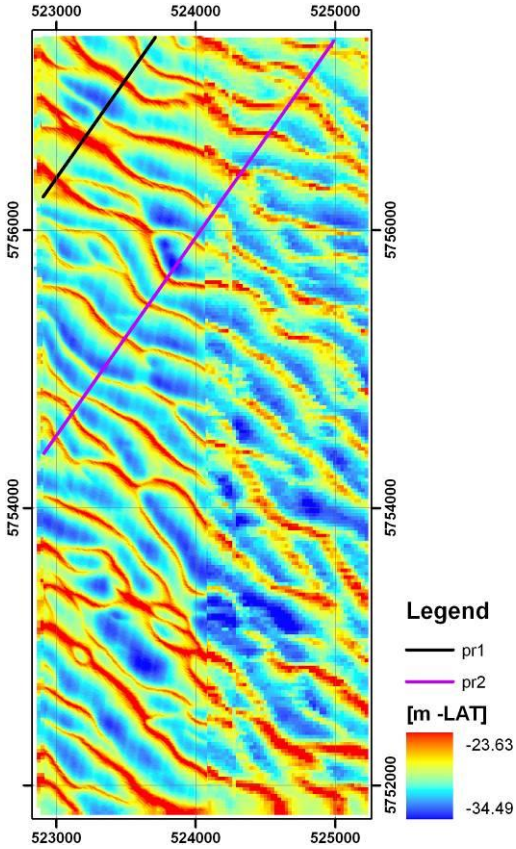

Figure 3.18 *Site 1: bathymetry and location of profiles analysed. For location see Figure 3.17*

Site 1 (Figure 3.18) is covered with a time series of 1999, 2002 and 2007 data. Two profiles, with in total 13 sand waves, were analysed. The sand waves in profile 1 (Figure 3.19a) are symmetric (i.e. symmetry indices are approximately 1), whereas in profile 2 (Figure 3.19b), they are more asymmetric with their steep sides facing northeast. The range in sand wave lengths of both profiles and all surveys is from 141 to 361 m, with an average of 249 m. The range in height of both profiles and all surveys is 2.0 to 5.9 m with an average of 3.7 m. Migration is variable, with an average migration rate of all crest and trough points of 1.9 m/yr to the northeast between 1999 and 2002 (3.54 yrs), and 7.3 m/yr to the southwest between 2002 and 2007 (4.45 yrs). The net migration rate (1999 - 2007) is 3.2 m/yr to the southwest. Figure 3.20 displays the quantified results for all crest and trough points.

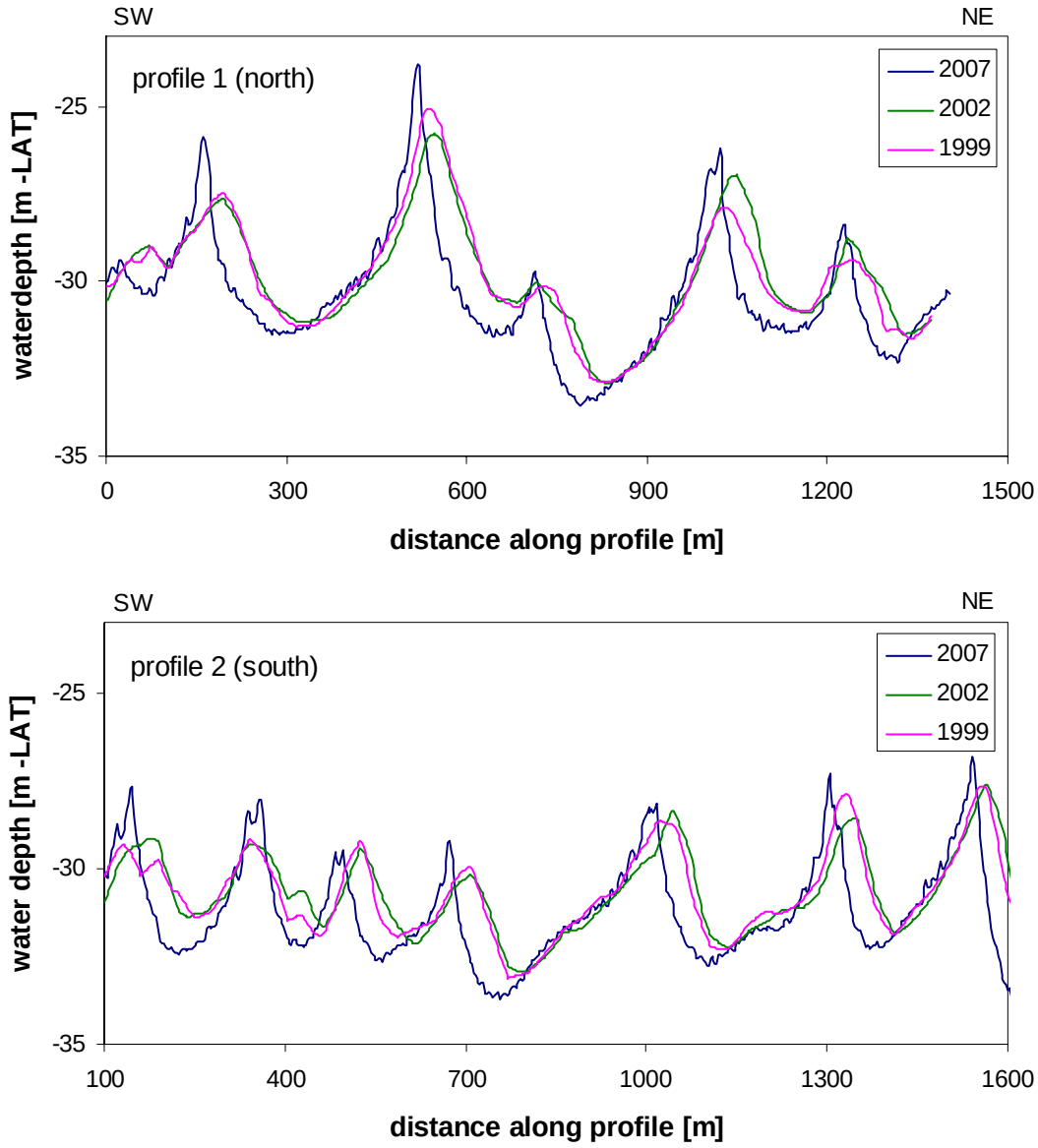

Figure 3.19 *Time series of two profiles studied at site 1 (from left to right is from southwest to northeast), displaying sand wave migration to the southwest. The horizontal and vertical scales are the same for both profile 1 and the detail of profile 2.*

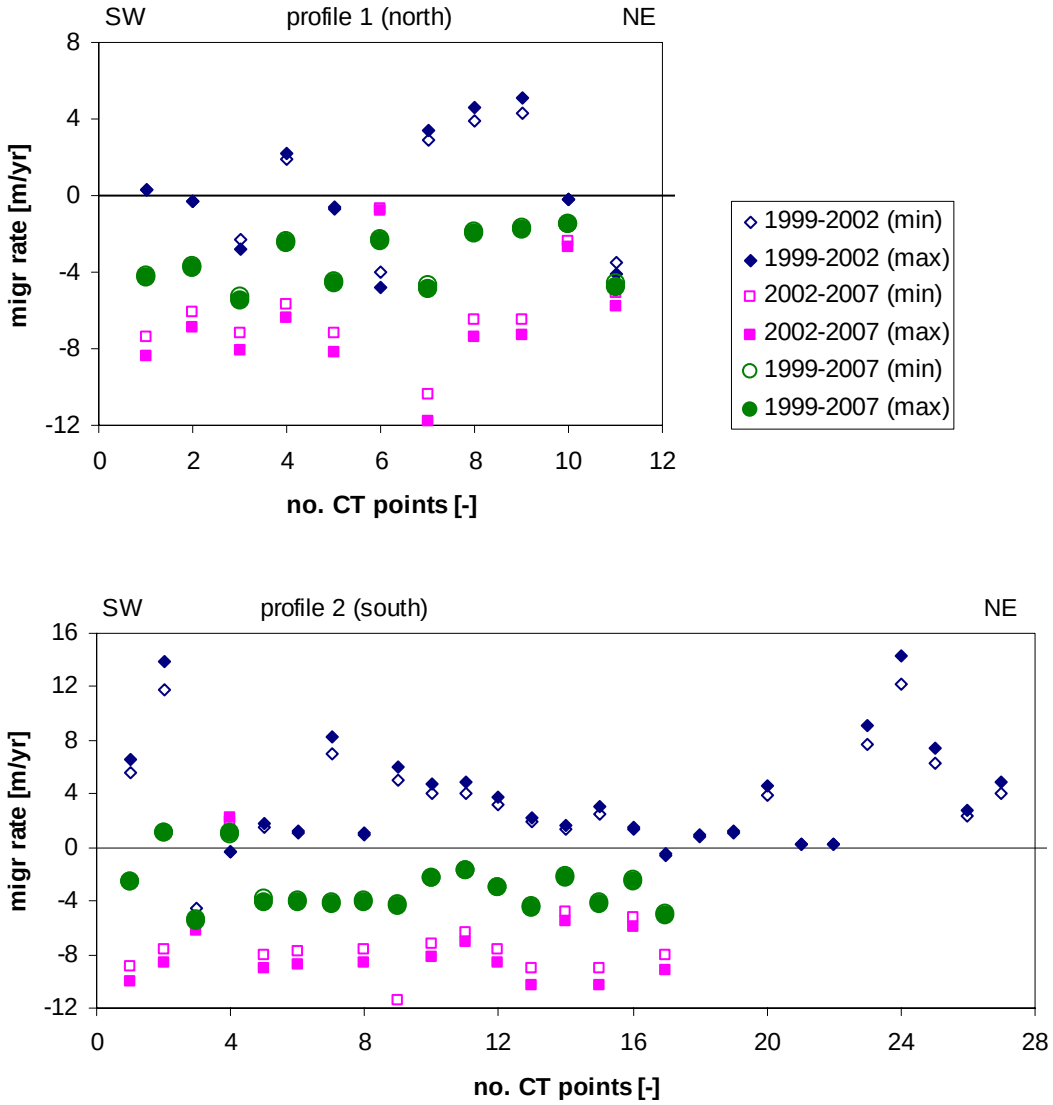

Figure 3.20 Quantified migration rates of crest and trough points at Site 1 of (a) profile 1 and (b) profile 2. Profiles run from southwest to northeast. Blue and pink points represent migration rates in the separate periods; green points represent the net migration rates between 1999 and 2007. The minimum and maximum values refer to the minimum and maximum periods between two subsequent surveys, which is here specified (in contrast to the middle of periods in the vertical dynamics map)

The time series of the profiles (Figure 3.19) show that lateral displacement (dx in m) of the sand waves to the northeast between 1999 and 2002 (3.54 years; both SBES) is – relatively – smaller than southwest-directed displacement between 2002 and 2007 (~5 years; MBES). This may be due to natural processes (to the southwest may be the preferred migration direction; to the northeast may be an exception due to e.g. temporary local conditions), or may be due to a difference in methods of both echo sounding and horizontal positioning (before and after 2000, different methods were applied at the NLHO).
Although not for all sand waves, most crests were lowered between 1999 and 2002. Between 2002 and 2007, on the other hand, crests were elevated and troughs were lowered, thus indicating sand wave growth. (*N.B.* The troughs were deepened down to 1 m in individual cases, which exceeds the error introduced by the difference between shoal-biased SBES

data and mean depths of the MBES data.) The change in sand wave length is -1.1 m and 1.1 m for the two periods, and -1.8 m (shorter) between 1999 and 2007, although the change in sand wave length is less directly relevant to the safety of ships at sea. The average wave height is indeed decreased in the period 1999-2002, as observed in the profiles in Figure 3.19, and increased in the period 2002-2007. The average net growth of the sand waves at site 1 is 1.3 m per 8 years (Table 3.1), which corresponds to 0.1625 m/yr

Table 3.1 Changes in sand wave length, dL [m], for separate periods between 1999-2002 and 2002-2007, and the net change in length, DL [m], between 1999 and 2007 (in bold). Similar results for the change in sand wave height, dH [m], per period, and the net change in height, DH [m]. Values are based on both profiles with in total 13 sand waves, i.e. 27 CT-points.

	dL99-02	**dL02-07**	**DL99-07**		**dH99-02**	**dH02-07**	**DH99-07**
MIN	-39	-22	**-23**		-0.85	0.47	**0.17**
MAX	29	24	**24**		0.93	2.3	**2.1**
AV.	-1.1	1.1	**-1.8**		-0.14	1.4	**1.3**

Similar analyses were performed at the sites indicated in Figure 3.17, of which the results are summarised in the table below.

Table 3.2 Averaged quantitative dimensions and dynamics for all sites, based on characteristics of individual sand waves. Columns contain minimum, average and maximum values of the sand wave length, L, sand wave height, H, and the migration rate and the number of sand waves included in the analysis of L and H (number of CT-points used in the migration is 2n+1).

Site	**L [m]**			**H [m]**			**Migr [m/yr]**			**n**
	min	**av**	**max**	**min**	**av**	**max**	**min**	**av**	**max**	
1	141	249	361	1.95	3.65	5.98	-5.4	-3.2	1.2	13
2		1000			0.4		.	.	.	
3		730			1.1		.	.	.	
4	127	203	415	1.3	3.3	5.6	-1.6	0.66	4.0	13
5	149	299	445	2.24	5.12	9.66	0.64	3.35	5.74	10
Texel 1	100	345	800	0.3	1.4	3.2	5	16-19	34	>20
Texel 2							12	16-19	37	10
B	171	239	337	1.67	1.99	2.46		1.98		9
C	72	159	288	1.69	3.92	6.85		0.396		8
WIJ12	172	398	688	1.1	2.9	5.8	-2.9	2.2	6	28
TWIN	140	274	382	2.5	4.8	7.3	-4.5	-1.5	0.064	8
WR1A1	136	263	639	1.2	3.2	5.4	-0.09	4.7	8.5	17
WR1A2	121	229	496	0.07	0.88	1.8	.	.	.	37
Wr1N	149	322	434	1.1	3.38	4.6	0.2	3.7	15	19

3.3.2.2 Comparison to migration rates found by Dorst (2009) (obj.1.2.ii)

The spectral method for the quantification of sand wave dynamics developed at Deltares was previously compared to a geostatistical method developed at the TU Delft and demonstrated to perform well [*Van Dijk et al.*, 2008]. In order to establish how comparable the results are to those calculated with the deformation method described in *Dorst* [2009] and *Dorst et al.* [submitted], three sites similar to those of *Dorst* were also investigated in this study (see Table 3.3). The same surveys in time series were used in the analysis as much as possible.

*Table 3.3 Quantified sand wave characteristics of Dorst [2009] and this study for sites West of IJmuiden (WIJ12), West of Rotterdam (WR1) and TWIN, specifying the wavelength, L, wave height, H, and the migration rate. Negative migration rates indicate migration to the southwest; positive values to the northeast. The number of sand waves studied per site, n, is given per site (total number of analysed crest and trough points = 2*n + 1). Dots indicate a lack of results.*

	L [m]			*H* [m]			Migr. rate [m/yr]		
	min	***av***	***max***	***min***	***av***	***max***	***min***	***av***	***max***
Site WIJ12-pr1									
Dorst (2009)	200	400[#]	900	▫	▫	▫	-3	▫	7
this study (*n=28*)	170	400	690	1.1	2.9	5.8	-2.9	2.2	6*
Site WR1									
Dorst (2009) (A-F)	208	▫	360	▫	▫	▫	0.6[+]	3.7[+]	7.6[+]
this study (*n=17*)	140	260	640	1.2	3.2	5.4	-0.09	4.7	8.5
Site TWIN									
Dorst (2009)	150	▫	300	▫	▫	▫	▫	▫	▫
this study (*n*=8)	140	270	380	2.5	4.8	7.3	-4.5	-1.5	0.064

[#] Dominant wavelength reported in Dorst [submitted].

** Migration rate WIJ12: all CT points range between -3 to 6 m/yr when the outlier of 18 m/yr is ignored.*

[+] calculated from Table 4.1 in Dorst [2009] , sites A t/m F.

Although algorithms and exact locations at which sand waves were analysed are different, the results of both methods agree very well. The ranges of wavelengths for sites WIJ12 and TWIN are slightly larger in this study than those found by *Dorst*, except for the maximum wavelength at WIJ12. Average wavelengths were not reported by *Dorst* [2009]; for WIJ12 the dominant wavelength was retrieved from *Dorst et al.* [submitted]. Heights were not specified by *Dorst*, but are mentioned here because these are of interest.
Wavelengths were rounded to 50 meters by *Dorst* so that the accuracy was not suggested to be higher than the method allows for. The spectral method may achieve slightly more accurate values, because *(i)* the DEMs – that are at the basis of the analyses – are of higher resolution, *(ii)* the spectral method approximates the data better than the modelling of idealised sand waves and *(iii)* the stepwise calculation of migration rates allows for back-and-forth migration in time. Therefore, values in Table 3.3 are rounded to tens of metres for wavelengths and to 0.1 m for wave heights.

In terms of migration rate, the ranges of the migration rates calculated by *Dorst* for WIJ12 and WR1 agree well with the findings in this study. The calculated average rate for site WR1 is 1 m/yr higher compared to *Dorst*, which may be explained by analysing different parts of these sand waves, the use of different time series and/or uncertainties of both methods. Migration rates at the site TWIN were either zero or not detected with the deformation method. The spectral method provides reliable results of an average net migration rate (1991 to 2006) of 1.5 m to the southwest, from a time series with 11 data sets. Herein, although migration was back and forth, the behaviour was systematic for the majority of the sand waves in this profile (Figure 3.2.1).

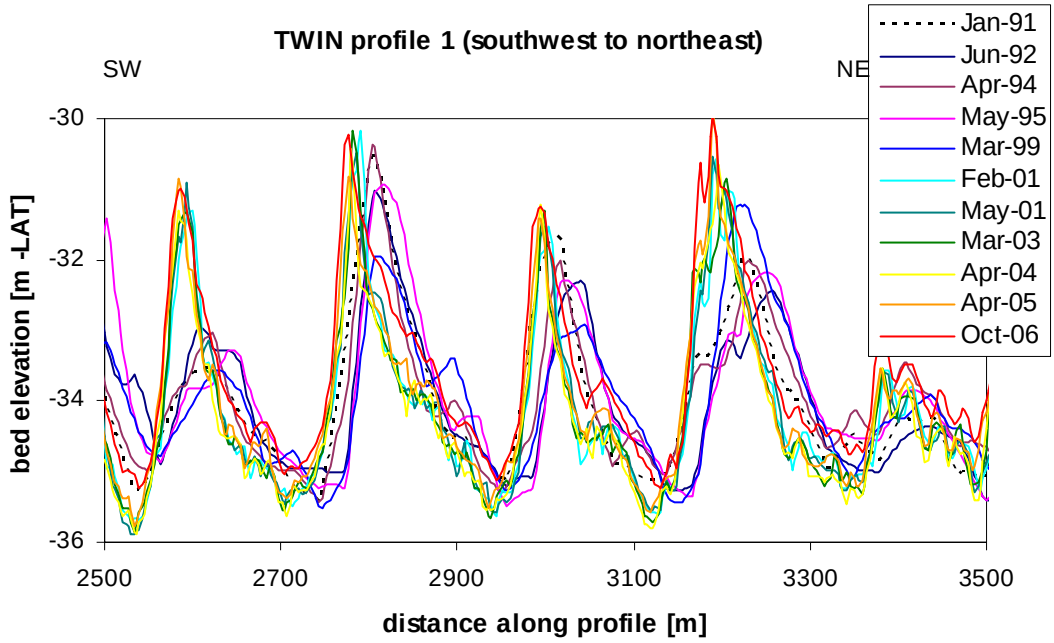

Figure 3.21 *Detail of the profiles analysed at the site TWIN (left to right is southwest to northeast). The time series show a back-and-forth migration in time and a net migration to the southwest. Also, in the profile shown, crests are elevated and sand waves have grown*

3.3.2.3 Long bed waves north of Texel and Vlieland

The quantification of the geometry of individual long bed waves north of Texel and Vlieland results in an average wavelength of 1125 m and an average wave height of 3.4 m. The changes in the average wavelength and average wave height of the bedforms are both negligible, with differences in the range of 3 m in length and 0.15 m in height between the three surveys in the time series. Net migration rates between 1990 and 2009 range from 10.5 to 18.4 m/yr, with an average of 12.4 m/yr, and are based on 5 long bed waves (11 crest and trough points) of which 3 surveys exist (Figure 3.22). The migration rates in the period 1990 to 2003 are three times the rates in the period between 2003 and 2009, possibly due to methods of horizontal positioning. The migration direction is for all crest and trough points in both periods to the northeast. Elevation differences of the crest and trough points are insignificant, with values ranging between -0.01 and 0.03 m/yr (net displacement between -0.27 and 0.50 m in 19 years).

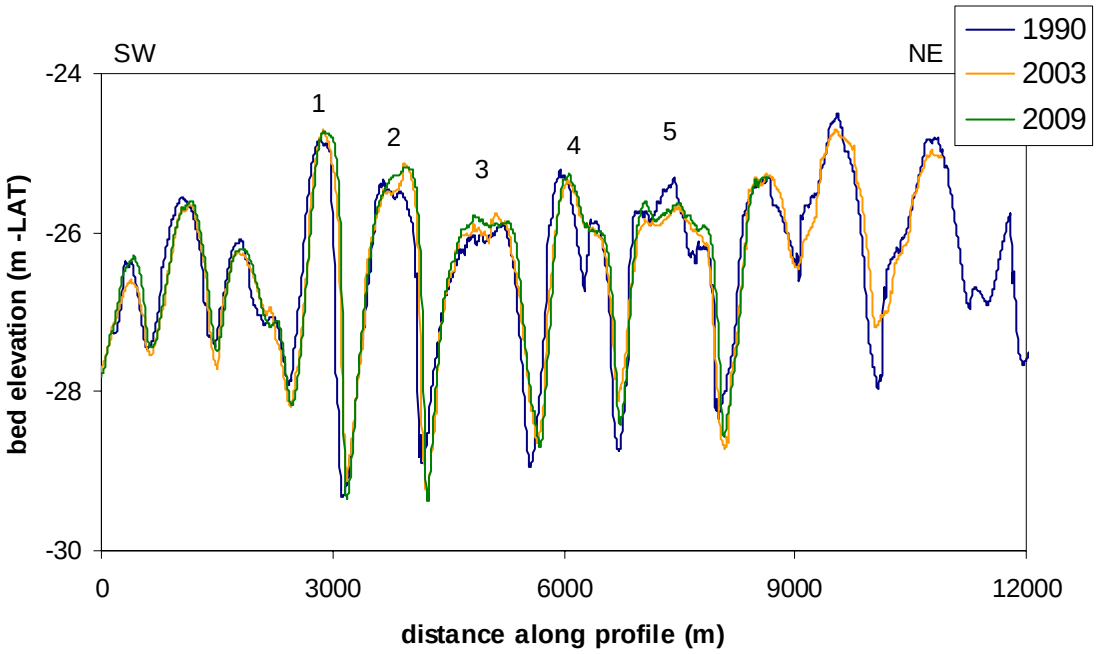

Figure 3.22 *Time series of profiles normal to the crests of long bed waves, which were identified on the morphodynamics map to be highly dynamic (Figure 3.17). Profiles run from southwest to northeast.*

3.3.2.4 Shoreface-connected ridges north of Ameland and Schiermonnikoog

The shoreface-connected ridges north of Ameland and Schiermonnikoog occur at water depths of 10 to 30 m (Figure 1.2). A detailed study of a profile perpendicular to the crests of these ridges, including 3 ridges, established that the average wavelength of the ridges is 4614 m and that the average height is 4.3 m. A comparison of the 1997/1998 and 2006 profiles (Figure 3.23) reveals that the bedforms neither change in shape nor migrate much in time. The calculated average increase in wavelength was 13 m (i.e. 1.6 m/yr on a wavelength of 4614 m) and the growth in height is 1.4 cm (i.e. 1.6 mm/yr). These values are much smaller than the measurement errors and are thus meaningless. The average migration rate of crest and trough points is 1.0 m/yr to the southwest.
In comparison, shoreface-connected ridges at the north coast of Spiekeroog, one of the German Wadden islands, also migrate landwards, but are much more dynamic [*Antia*, 1996]. The maximum migration rate of 100-200 m/yr is a factor 4 to 40 times more than rates reported from ridges in North-America, which range from nearly stable to 6 m/yr [*Antia,* 1996, and references therein]. Although the environment and physiology of the banks at Spiekeroog seem similar to the shoreface-connected ridges at Ameland and Schiermonnikoog, the dimensions of the banks are different (Table 3.4). The migration of ridges at Spiekeroog are found to be storm-induced [*Antia*, 1996].

Table 3.4 Comparison of shoreface-connected ridge characteristics at Ameland/Schiermonnikoog (this study) and Spiekeroog (Antia, 1996).

	WD [m]*	**L [m]**	**H [m]**	**Migr [m/yr]**
Ameland/Schier (this study)	10 - 30	4614	4.3	1.0 landward
Spiekeroog (Antia, 1996)	8 - 25	1000 - 2000	3 - 5	100 – 200 landward

* *water depths in this study in m below LAT, in Antia not specified*

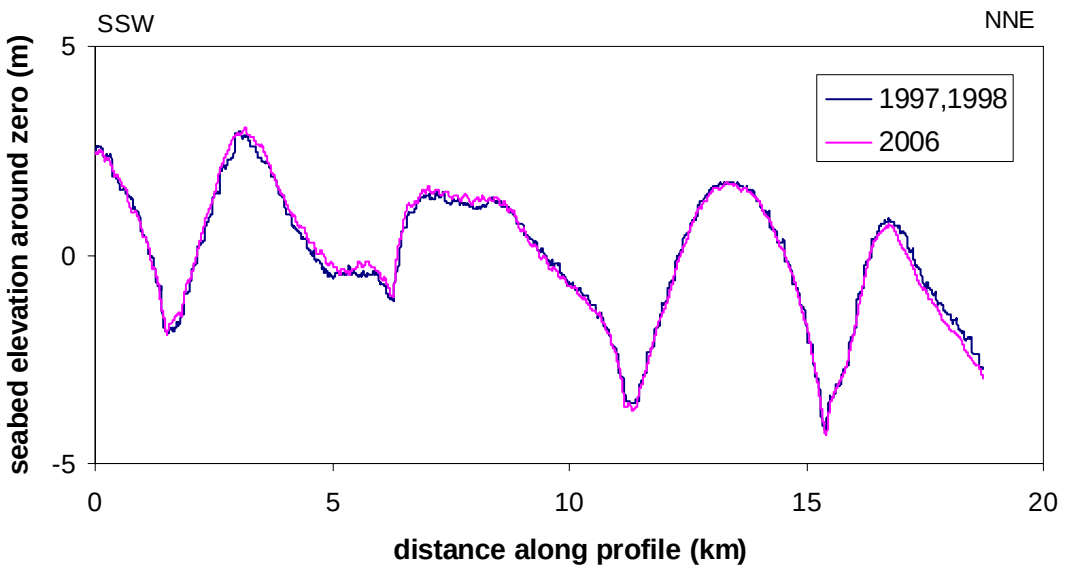

Figure 3.23 Profiles across shoreface-connected ridges north of Ameland and Schiermonnikoog (SSW-NNE) of 1997/1998 and 2006 surveys. Seabed elevations are plotted around zero (subtraction of average water depth at this site from the local water depths), because both surveys have a systematic offset due to erroneous corrections in the data. Location is indicated in Figure 3.17.

3.3.2.5 Offshore tidal ridges in the central Southern Bight

In the detailed analysis of the tidal ridges in the central part of the Southern Bight, three profiles were analysed crossing the north-south oriented Brown Ridge and two ridges to its east (Figure 3.24). Time series show that the sand banks maintain their general cross-sectional shapes in time, however, superimposed sand waves are responsible for changes in the morphology of the banks.

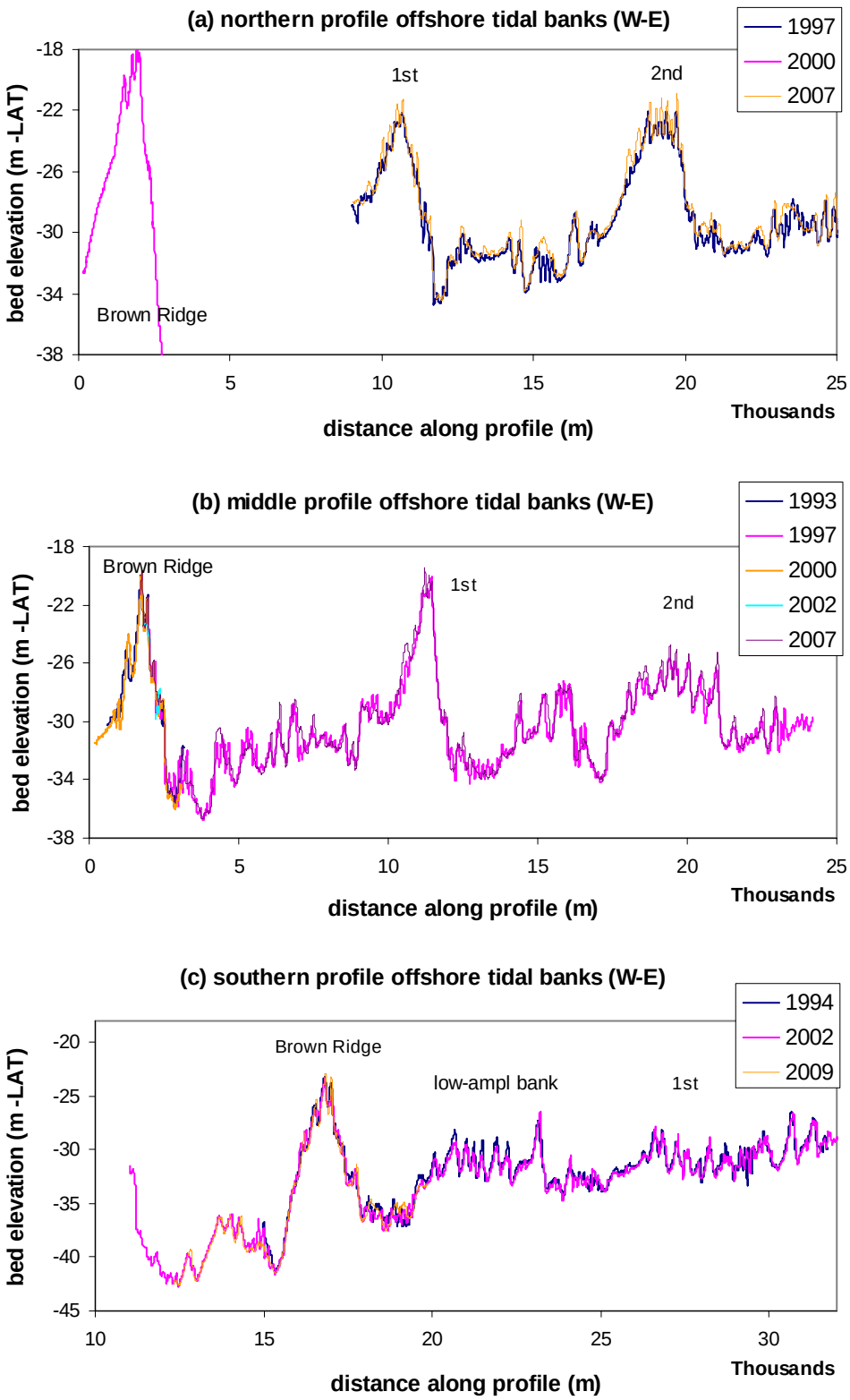

Figure 3.24 *Three profiles across three offshore tidal ridges in the central part of the Southern Bight reveal that crests of banks elevate mainly due to the growth of superimposed sand waves and due to the migration of sand waves towards the crest of the bank (see text). The profiles run from west to east. The northern profile is located 9570 m to the north with respect to the middle profile, and the latter is located 10630 m to the north of the southern profile. For location of the profiles, see Figure 3.17. The Brown Ridge is the most western bank on the left, and the two banks to the east are in the text referred to as 'the first bank' and 'the second bank to the east'.*

The wavelength (spacing between the crests) of the ridges is 9 km. The banks are up to 30 m high in the Southern Bight, but at the location of the profiles, which were sampled there where the best time series are available, the banks are lower.

The Brown Ridge (on the left in Figure 3.24) has a height of 23.4 m in the northern profile, which reduces to the south to 15 m in the southern profile. The net elevation of the crest of the Brown Ridge increases only 0.5 m per 10 years and 0.1 m per 15 years, based on merely the highest points on the two southernmost profiles. The superimposed sand waves on the Brown Ridge are observed to increase in height and to migrate onto the bank from both sides with rates of 0.4 m/yr in the middle profile (n=5) and a net migration rate of 0.8 m/yr mostly in an eastern direction but moving back and forth and weakly towards the crest of the bank (n=3) in the southern profile.

The first ridge to the east of the Brown Ridge, in the centre of the northern and middle profiles, has a height of 12.5 m and 14 m in the respective profiles. The southern profile runs at the southern end of this bank. In this profile, the first bank would be located at 27 km on the x-axis, but has almost disappeared. The northern and middle profiles (Figure 3.24a and b) show a net increase of the crest elevation of 1 m and 0.6 m, respectively, in a period of 10 years (i.e. 6 to 10 cm/y), thereby decreasing the water depth with the same amount. Although the individual sand waves that are superimposed on the first bank are difficult to identify in the subsequent surveys, visual inspection of their shapes reveals that the sand waves grow both in length and height on both flanks of the sand bank. As at the Brown Ridge, here too, sand waves on the flanks migrate onto the bank towards the crest. This was also reported in earlier Deltares studies (internal reports).

The second bank to the east of the Brown Ridge (on the right in Figure 3.24a and b) is 10 m high in the northern profile. The middle profile runs across the southern end of the second bank, where its height is only 6.5 m, which is comparable to the low-amplitude banks between the prominent banks. The elevation of the highest crest point shows a net increase of 0.7 m and 0.9 m in the northern and middle profiles, respectively, in the period of 10 years. Although the time series consists of merely two data sets (1997 and 2007), the data imply convincingly that the increase in elevation of the bank is caused by the increase in height of the superimposed sand waves. On this bank, sand waves migrate towards the east, with a rate of 5.25 m in the northern profile (n=9) and 4.8 m/yr in the middle profile (n=10).

Especially for the two banks to the east of the Brown Ridge show the same features in dynamic behaviour. The following two features are most evident at the second bank in the northern profile and the first bank in the middle profile. Firstly, the gain in cross-sectional sand wave ‘volume’ is largest on the western flanks of the banks. Here, two sand banks merge into one large sand wave and heights more than double. Secondly, the eastern flank is almost entirely unchanged. For the Brown Ridge, both the east and west flanks change equally and in moderate amounts.

These findings confirm the changes that are presented in the vertical dynamics map.

3.3.3 The prediction of water depth based on vertical nodal dynamics NCS (Obj. 1.3.i)

The linear extrapolation of the calculated vertical dynamic trend for each node to 2011, 2015 and 2020, result in three maps of predicted nodal water depths. Because the predicted water depths are hardly distinguishable from the bathymetry map (Figure 1.2), we here present the differences between the predicted water depths. The difference for the prediction for 2011 with an earlier bathymetry map is arbitrary, since the most recent data collected may vary

between the early 1990s and 2010. The differences in predicted water depth of 2011 to 2015 and 2011 to 2020 are shown in Figure 3.25 and Figure 3.26, respectively.

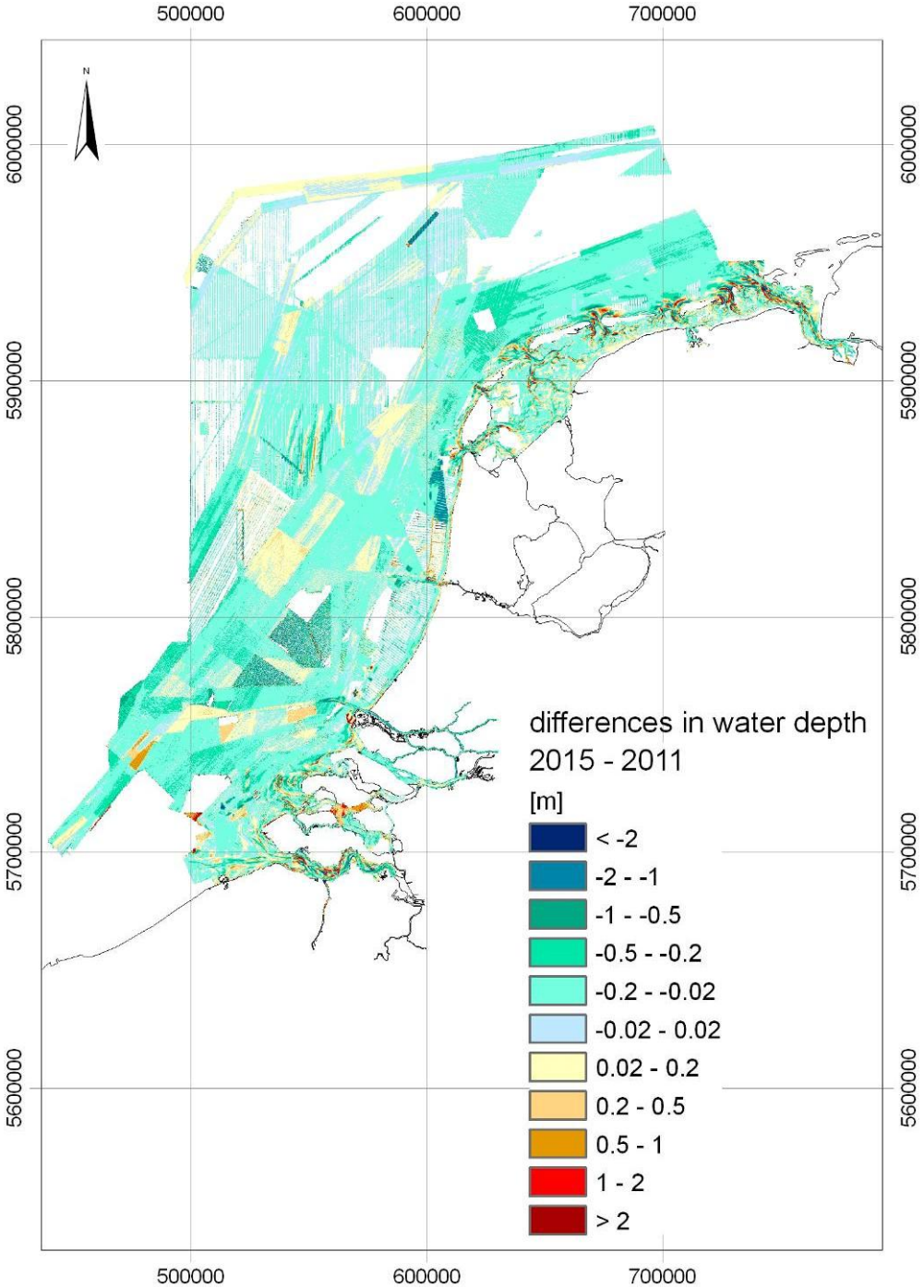

Figure 3.25 *Difference in predicted water depth between 2011 and 2015. A negative value (scales of blue) indicates lowering of bed elevation, and therewith an increase in water depth; a positive value (scales of red) indicates an increase in bed elevation and thus an decrease in water depth. Light blue indicates nearly no vertical change in bed elevation.*

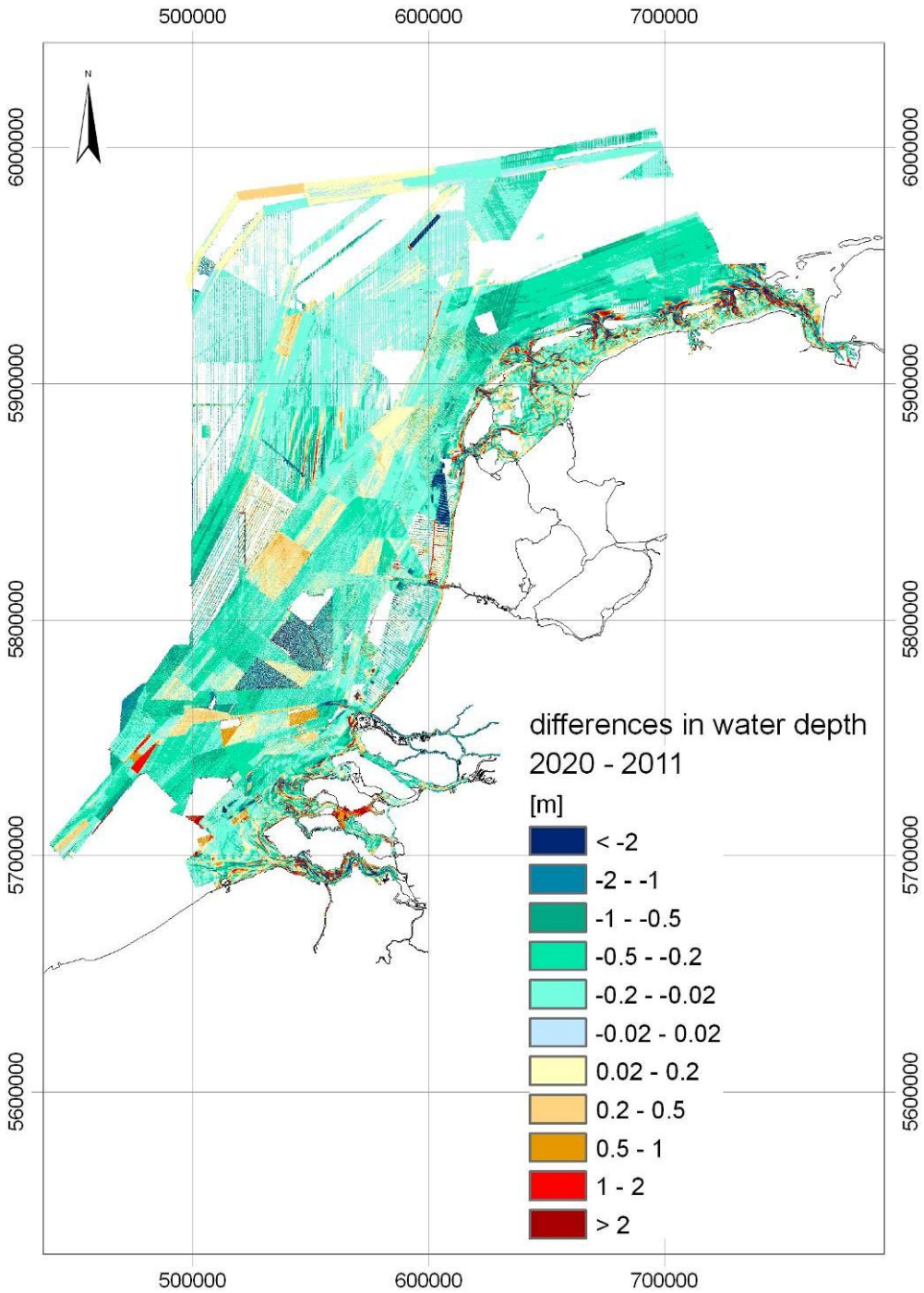

Figure 3.26 *Difference in predicted water depth between 2015 and 2020. A negative value (scales of blue) indicates lowering of bed elevation, and therewith an increase in water depth; a positive value (scales of red) indicates an increase in bed elevation and thus an decrease in water depth. Light blue indicates nearly no vertical change in bed elevation*

The predicted water depths mainly serve the grounding danger calculations based on dynamic water depths (section 4.2.3) that are used in the overlays for the validation and optimisation of the re-survey policy of the NLHO (Chapter 5).

3.3.4 Modelled sand wave evolution (Obj 1.3.ii)

Process-based models aim to describe the important physical processes of water and sediment motion, which are expressed in differential equations and solved using mathematical techniques. Therefore, process-based sand wave models are able to simulate the effects of physical parameters on the sand wave characteristics and, moreover, the effects of storm events or human interventions. This way, process-based sand wave models may provide an estimation of the sand wave characteristics, especially in those areas where time series of observations are lacking.

The University of Twente developed an idealized, process-based, non-linear sand wave model, called the Sand Wave Code (SWC), specifically designed to describe sand wave dynamics [*Németh et al.*, 2006; *Van den Berg and Van Damme*, 2006; *Sterlini*, 2009]. Whereas most available sand wave models are linear [e.g. *Hulscher*, 1996; *Besio et al.*, 2003; 2004] and, hence, only suitable for studying the initial stage of sand wave evolution, the SWC is a non-linear model, which allows for the analysis of sand wave characteristics in all stages of sand wave evolution [*Sterlini*, 2009]. So far, the SWC has shown promising results in estimating the characteristics of the Golden Gate sand wave field [*Sterlini*, 2009]. In this section we explore what role the SWC can play in predicting sand wave dynamics in the North Sea. To this end, we investigate how well model results compare to field observations at several locations in the North Sea. In addition, we investigate the effect of surface waves on the sand wave characteristics, by varying surface wave height, period and angle. With sensitivity tests, factors controlling the sand wave dynamics may be identified.

This section describes the model results. The description of the model, assumptions, input parameters and the sensitivity tests can be found in Appendix 11.2 (full text including the results).

3.3.4.1 Selection of field locations

One time series of the Netherlands Hydrographic Office of the Royal Netherlands Navy, was provided as a test data set and will be referred to as “Site 1” in the remainder of this section, is one of the selected areas to be studied. This area is also investigated in parallel studies, which allows for comparisons between the studies in a later stage of the project. Furthermore, we use the interpolated sand wave data of Van Santen [2009], containing information of about 30 different locations. From these locations we select four sites, based on the local water depth and tidal current. To cover the range of water depths and tidal currents we took extreme ends of the water depths and tidal currents. The characteristics of the selected field locations are presented in Table 3.5. Sites 2, 3, 4 and 5 refer to the areas 135, 180, 213 and 222 in Van Santen [2009].

Table 3.5. Overview of the characteristics of the selected field locations.

Site	x* (m)	y* (m)	H (m)	D_{50} (µm)	U_0 (ms^{-1})	U_{res} (ms^{-1})
1	524142	5754800	30.5	300	0.66	0.02
2	525671	5890409	26.34	269.77	0.46	0.05
3	592918	5823315	17.16	236.35	0.52	0.02
4	489951	5766250	36.87	249.07	0.70	0.03
5	501468	5748168	34.63	343.45	0.69	0.03

* Centre point, in the coordinate system ED50 UTM 31N

3.3.4.2 Model results and comparison with field data

The SWC results for the wavelengths L_s, corresponding to the fastest growing modes (FGMs) for the five selected locations, are listed in Table 3.6. Figure 3.27 shows an example of the growth rates for different wavelengths for Site 1. The wavelength corresponding to the maximum growth rate corresponds to the FGM (in this case L_s = 200 m). Figure 3.28 shows the results of the long-term calculations for site 1. The upper panel shows the growth of the sand wave crest and trough in time towards their final height H_s and the lower panel shows a side view of the final sand wave shape. In this example the sand waves grow to a more or less stable, saturated state, as expected. However, there are also model runs in which the final sand wave shape is unreliable, as the sand wave does not reach a stable, saturated state (see Figure 3.29 and Figure 3.30).

For both stable and unstable runs the sand wave height H_s is determined by averaging the sand wave height over the last 100 time steps (each time step is 10 weeks), to average possible instabilities. The migration rate M_s is calculated over the last 10-50 time steps of the simulation. In case of stable results, the lengths of these calculation periods do not affect the sand wave height or migration rate (as long as the sand wave has reached its saturated state at the start of the calculation period). However, in case of unstable results, the sand wave height and, especially, the migration rates can be very sensitive to the length of this period. Therefore, the migration rates are checked qualitatively by means of animations of the model results, in order to check whether the directions as well as the magnitudes of the migration are reliable relative to the other (stable) model results. The thus obtained modelled sand wave characteristics are summarized in Table 3.6 and compared to empirical results for all selected field locations.

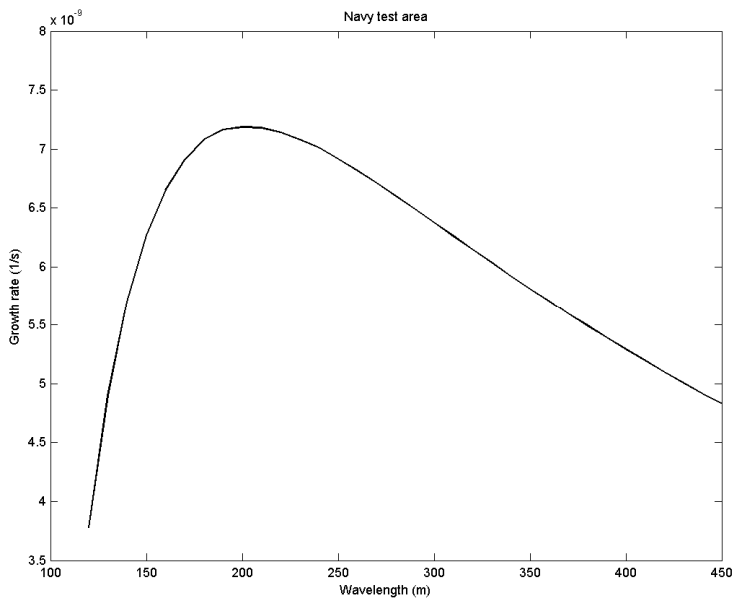

Figure 3.27. Prediction of the FGM for the Site 1. The largest growth rate, corresponding to the FGM, is obtained by a wavelength of 200 m.

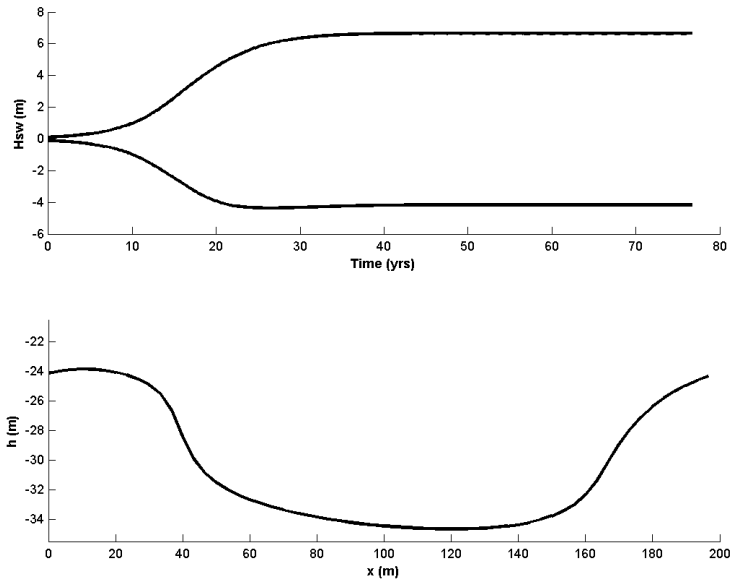

Figure 3.28. Upper panel: growth of the sand wave crest and trough in time for the FGM for Site 1. Lower panel: predicted final bedform shape (crest to crest).

The results in Table 3.6 show that the modelled sand wave lengths match the measured wavelengths well for the locations 1, 4 and 5. However, at the other locations the wavelengths are not in agreement with the data. For the locations 2 and 3, the large difference between the observed and modelled sand wave lengths may partly be explained by the relatively lower U_0, implying that the velocities are relatively closer to the critical velocity for the initiation of motion. Therefore, at these locations it may not be valid to neglect the critical shear stress in the sediment transport calculations. For the locations with relatively higher U_0 the agreement between modelled and observed wavelengths is much better.

Table 3.6. Overview of observed and modelled sand wave characteristics for all selected field locations.

	h_0 (m)	U_0 (ms^{-1})	U_{res} (ms^{-1})	L_s (m) [min;mean;max]	H_s (m) [min;mean;max]	M_s (my^{-1}) [min;mean;max]
Site 1						
Data	30.50	0.66	-	141; 249; 361	1.95; 3.65; 5.89	-5.4; -3.2; 1.2 *(1999-2007)*
Model	30.50	0.66	0.02	200	10.8	2.1
Site 2						
Data	26.34	0.45*	-	1000	0.4	-
Model	26.34	0.46	0.05	150	7.2	5.7
Site 3						
Data	17.16	0.57*	-	730	1.1	-
Model	17.16	0.52	0.02	150	8.4	2.1
Site 4						
Data	36.87	0.76*	-	127; 203; 415	1.3; 3.3; 5.6	-1.6; 0.66; 4.0 *(1995-2003)*
Model	36.87	0.70	0.03	230	7.9#	0.7#
Site 5						
Data	34.63	0.73*	-	149; 299; 445	2.24; 5.12; 9.66	0.64; 3.35; 5.74 *(1990-2003)*
Model	34.63	0.69	0.03	210	9.2#	0.9#

*Note that the tidal currents used in the model differ from the data of Van Santen [2009], because we used a longer dataset

#Unstable model results (see also Figure 3.29 and Figure 3.30), but qualitatively tested

The sand wave height is considerably overestimated for all locations. Although the observations may be hampered by the presence of other bed forms, making it difficult to estimate the sand wave height, the differences between observed and modelled sand wave heights are (unrealistically) large. This suggests that other processes, which are not accounted for in the SWC, may play a role in the sand wave development, such as grain size sorting or suspended sediments, or the above mentioned negligence of the critical shear stress. Additional research is necessary to tackle this problem. Since sand wave height is not affecting the model results for sand wave migration [*Németh et al.*, 2007], the model result for migration are trustworthy.

Migration rates of sites 4 and 5 are in best agreement with values estimated from empirical analysis (Table 3.6). However, these two areas show unstable results and, therefore, may be unreliable. To improve the reliability of the model results, we increased the number of (numerical) steps in x-direction Nx from 60 to 120. Figure 3.29 and Figure 3.30 show that the stability does not necessarily improve with a larger Nx, although a positive effect is found for other areas. A disadvantage of increasing Nx is the considerable increase in computation time.
The modelled migration rate at site 1 is in opposite direction than in the field; for sties 2 and 3 no migration rates were determined from empirical data.

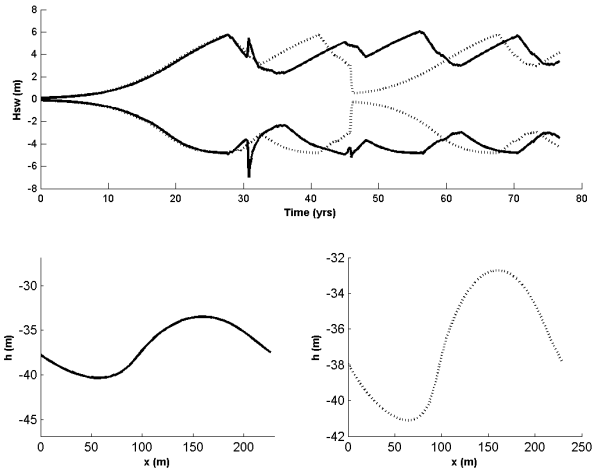

Figure 3.29. Same as Figure 3.28, but now for area 4. The solid black lines indicate the model results for Nx = 60 and the dotted black lines for Nx = 120.

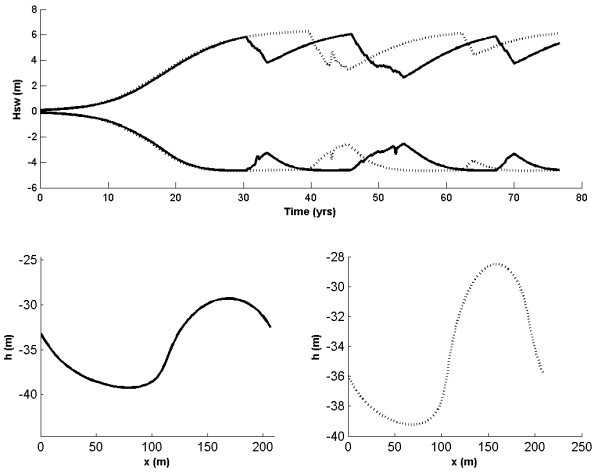

Figure 3.30. Same as Figure 3.28, but now for area 5. The solid black lines indicate the model results for Nx = 60 and the dotted black lines for Nx = 120

3.3.4.3 Effects of surface waves

The surface waves hardly affect the lengths of sand waves, as is also indicated by Sterlini [2009]. Therefore, the wavelengths found without surface waves are maintained. The simulation results for the effects of surface waves under variable angle with the currents (φ = 0-180°) on the sand wave heights and migration rates are presented in Figure 3.31 and Figure 3.32, respectively. Note that these figures are partly based on unstable simulation results. Simulations that crashed are omitted from the analysis. Therefore, one should be cautious while interpreting the results quantitatively. Nevertheless, the figures can be useful to compare the sand wave characteristics at the different locations in a qualitative way.

Figure 3.31 shows that the (average) sand wave height generally decreases with increasing surface wave height for the areas 1, 3, 4 and 5. This is in agreement with the findings of Sterlini [2009]. However, for area 2, the sand wave height tends to increase with an increasing surface wave height. It is not exactly clear what explains this

behaviour, because there is no clear alternative relation between the sand wave characteristics and the conditions in terms of water depth and tidal currents at this location. Furthermore, we observe that for the locations 4 and 5 the wave angle has a considerable impact on the sand wave heights for smaller surface wave heights relative to the other locations. Since these locations have large water depths, and thus the impact of surface waves is expected to be relatively small, this large impact is probably caused by the severe instabilities in the model results for these locations. Finally, we note that the ranges in sand wave heights due to surface waves under different angles are considerably larger for the locations 1, 4 and 5 compared to the other locations (also for stable model results). This could indicate that the former locations are more sensitive to changes in surface wave characteristics than the latter ones. The locations 1, 4 and 5 have in common that (1) the water depths (h_0) are relatively large, which seems to be counter-intuitive as one expects surface waves to have less impact in deeper water, and (2) the tidal currents (U_0) are relatively strong (also found by [*Sterlini*, 2009]).

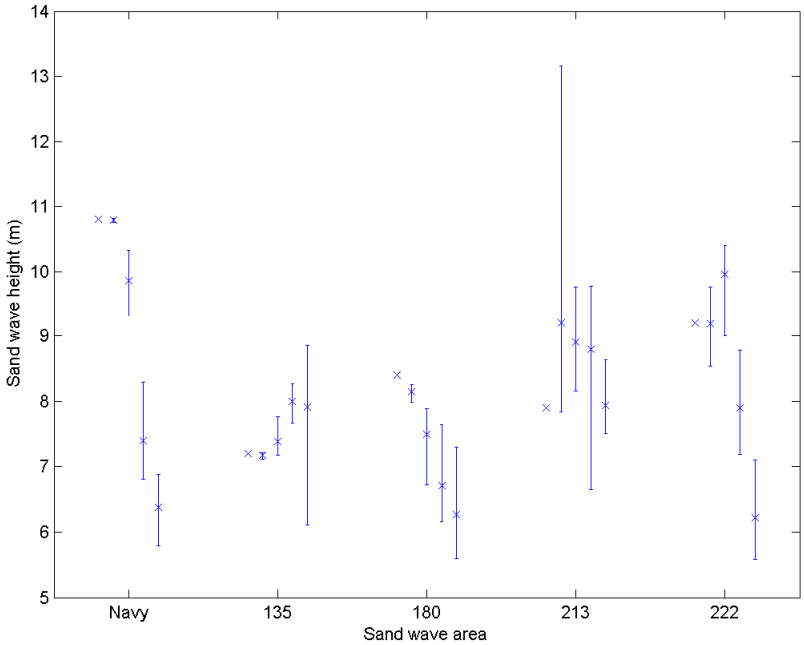

Figure 3.31. Overview of the effects of surface waves on the sand wave height. For each location the results without surface waves are indicated with the most left cross. Then, from left to right the results of increasing surface wave heights (see Table 3.5) are shown. For each type of surface waves the angle with respect to the tidal curent is varied between 0° and 180° resulting in a range of sand wave heights (indicated by the bar). The crosses indicate the mean sand wave height for each type of surface waves.

Figure 3.32 shows that both the average migration rate and the range in the migration rates increase for increasing surface waves under different angles with the currents, as one would expect. In addition, we observe that the locations 2 and 3 generally have larger (absolute) migration rates than the other areas, which may suggest that in these areas the sand waves are (slightly) more dynamic than in the other areas. What these locations have in common is a relatively smaller water depth than the other locations. Although the water depth at location 2 is larger than at location 3, a larger residual current at 2 is probably the cause of the larger (absolute) migration rates at this location. Finally, note that, although we consider rather extreme (continuous) surface wave scenarios, the migration rates are comparable to empirical values. This is rather

remarkable, as one would expect much larger migration rates compared to milder storm conditions in the field.

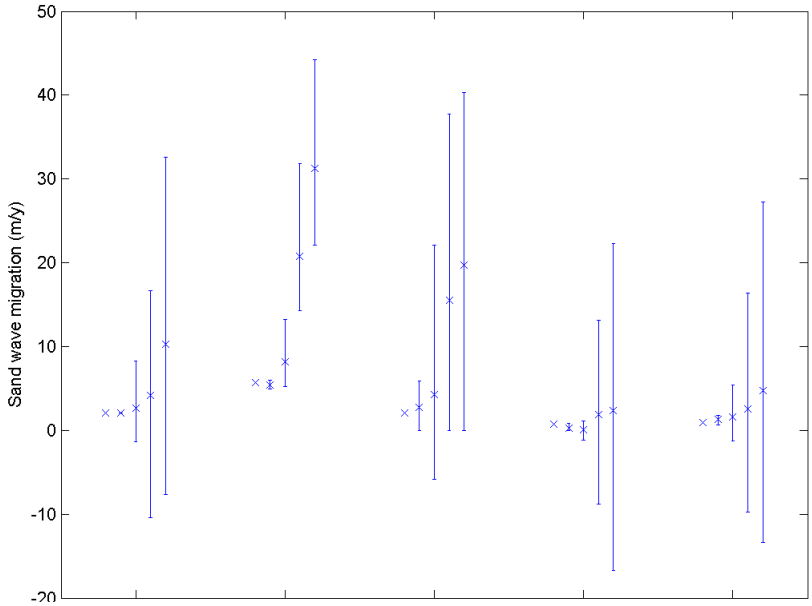

Figure 3.32. Overview of the effects of surface waves on the sand wave migration rates. For each location the results without surface waves are indicated with the most left cross. Then, from left to right the results of increasing surface wave heights (see Table 3.5) are shown. For each type of surface waves the angle with respect to the tidal current is varied between 0° and 180° resulting in a range of migration rates (indicated by the bar). The crosses indicate the mean sand wave migration rate for each type of surface waves.

3.3.4.4 Modelling conclusions

In this study, we find that for some locations in the North Sea the sand wave lengths are modelled reasonably well, but for other locations the sand wave lengths are considerably underestimated compared to field observations. Sensitivity tests, in which we vary the eddy viscosity, slip parameter, slope factors and residual current, show that the model results can be quite sensitive to parameter variability, but cannot explain the differences between the sand wave lengths predicted by the SWC and those observed in the field. Especially the locations with small tidal currents show an underestimation of the sand wave length. This suggests that the exclusion of the critical bed shear stress for initiation of motion may play a role here, i.e. where the currents are small, the critical shear stress is relatively more important for the sediment transport. Furthermore, it is noteworthy that we especially modelled locations with either an extreme value for the water depth h_0 or for the oscillating tidal current U_0. The model seems to give more reasonable sand wavelengths for intermediate conditions, i.e. for site 1, although this has not been tested extensively.

The sand wave heights modelled by the SWC are overestimated for all the selected field locations, independent of the local conditions in terms of water depth and tidal currents. This suggests that other processes, not included in the model, may play a role here, such as grain size sorting (or the presence of a fixed or armoured layer) or interaction between bed load and suspended load sediment transport. Additional research is necessary to tackle this problem. Therefore, in its current form, the SWC is not able to provide (reliable) quantitative information on the sand wave height. Since the sand wave height

does not affect the modelled migration rates, the migration results may still be trustworthy.

The present version of the SWC simulates sand wave migration speeds of realistic magnitudes, but – of the few compared sites – magnitudes or directions do not always agree with field observations. The migration rate results of unstable simulations are less reliable.

Although the SWC may not provide reliable quantitative information on the sand wave heights, it can still be useful to investigate the effects of physical parameters (water depth, residual currents, surface waves) on the sand wave height in a qualitative way [see *Sterlini*, 2009]. This is not possible with a linear stability analysis, as it only provides information about the initial stage of sand wave evolution. Furthermore, the SWC allows for a qualitative investigation of the effects of surface waves on the sand wave characteristics. This is an advantage compared to data-based models, which are only capable of investigating these effects after a storm. Qualitative model investigations of the sand wave characteristics may identify areas that are more or less dynamic or more or less sensitive to storms, and therewith are a valuable addition to this research.

The model results for five selected locations in the North Sea show that the sand wave height generally decreases for increasing surface wave height. The ranges in the sand wave heights due to variable angles between the surface waves and currents differ among different locations. The average migration rates as well as the ranges in the migration rates increase for increasing surface wave heights for all locations. However, the absolute migration rates differ among areas. The ranges in the sand wave heights and migration rates may be a measure for the potential sand wave dynamics at the different locations.

3.4 Conclusions

Vertical nodal dynamic trends were calculated from hydrographic survey data on a 25 m resolution for the Netherlands Continental Shelf and coastal zone. Highest vertical dynamics are found in the coastal zone, including *(i)* the Wadden Sea, *(ii)* tidal inlets to the Wadden Sea and associated ebb-tidal deltas on the seaward ends, *(iii)* breaker bars parallel to the North Sea beaches, *(iv)* the Ems-Dollard, Eastern and Western Scheldt estuaries, and *(v)* the tidal channels in front of Zeeland. The seabed of the Netherlands Continental Shelf is less dynamic. The majority of the vertical nodal dynamics of the NCS is up to 0.1 m/yr (both erosion and aggradation).

Highly dynamic areas of the shelf:
Even though the different types of data that are available to this study cause contrasts in dynamics that are not real, areas of high and low natural sea bed dynamics were identified on the NCS. The highest vertical nodal dynamics in the offshore region are caused by the migration of tidal bedforms, such as sand banks and sand waves. Vertical nodal dynamics due to sand wave migration may be up to 0.2 m/yr, either degradation or aggradation. Three main areas were identified to be dynamic: (1) a field of long bed waves north of Texel and Vlieland, (2) a sand wave field west of Texel and (3) a major field of combined sand banks and sand waves in the Southern Bight. At these sites, detailed studies were carried out in order to specify the dynamic behaviour of individual bedforms (growth and migration). West of Texel, sand wave migration rates are the highest, with average rates of up to 19 m/yr.

The north-south oriented sand banks in the central southern Bight are more dynamic than expected, mainly due to sand wave migration on their flanks. The actual migration rate of the banks was not established.

Areas of high vertical dynamic trends also showed the highest bedform migration rates. These bedform fields often occur in critical water depths for shipping. Predictions of water depths indicate that these areas also are more prone to changes. Furthermore, the impact of surface waves on bedform height and migration at these water depths is expected to be large. The modelling showed that, in general, sand wave migration increases with increasing surface wave height. This effect is larger for shallow areas with high tidal current velocities.

Low-dynamics areas of the shelf:
The vertical nodal dynamics map also reveals areas of low dynamics (i.e. less than absolute values of 0.02 m/yr). The majority of these areas occurs in the deeper parts of the outer shelf, where tidal current velocities are low, wave impact is small and, consequently, sediment grain sizes are small. Smaller low dynamic patches occur offshore Noord-Holland and near the coast of Zuid-Holland and Zeeland and coincide with fine-grained seabeds where sand waves are absent. For some of these areas, time series involve digitised fair sheets, thus covering long periods. Even though the use of historical data may overestimate the vertical dynamics due to a resolution problem in the time series (section 3.2.2), low dynamics were calculated. The prediction of water depths, based on linear extrapolation of dynamic trend, shows that water depths do not differ more than an absolute 0.2 m in the periods 2001 to 2015 and 2015 to 2020. From process-based modelling it is known that at large water depths, the impact on bed evolution is small. With these factors, it seems confirmed that low dynamics in these areas is a reliable conclusion. An example of a site where dynamics were found to be low in shallower water (20-30 m) and with the presence of bedforms is the shoreface-connected ridge area north of Ameland and Schiermonnikoog.

Digitised fair sheets:
For some time series that were created with digitised fair sheets, the data resolution appeared too low for the identification of bedforms of a spatial scale smaller than the resolution (e.g. sand waves in zone offshore Noordwijk, Figure 3.16). However, long time series have demonstrated to be very useful where bedforms are large-scale or absent (low relief sea bed). For example, the tidal ridges 75 km offshore Texel exhibit very good results, which otherwise would remained unidentified. Also, the zones between Off Botney Ground TSS, West Friesland TSS and Vlieland TSS, the created time series reveal low dynamics, despite the long time series and the expected overestimation when comparing low precision and low resolution data with modern data.

4 Grounding probability and grounding danger (Objective 2)

4.1 Introduction

The probability calculation of grounding risks requires a quantitative measure of seabed dynamics (Chapter 3) and a quantitative estimate of the probability of vessels running aground, taking into account factors such as under-keel clearance, the probability of unknown objects on the seabed and shipping intensity. The objectives for this chapter are *(1)* to estimate the probability of unknown objects on the seabed and *(2)* to assess the grounding danger for shipping at the Netherlands North Sea. All calculations on grounding probability and grounding danger were performed by MARIN, based on minimum, maximum and average water depths, water depths above objects and predicted water depths as presented in the earlier chapters of this report.

4.2 Methods

In order to formulate a more risk-driven survey policy than the present survey policy, a more detailed probability calculation is required, based on a thorough knowledge of the shipping traffic, the water depth and obstructions. When taking into account these three topics, the probability calculation is based on ship movements, whereas the existing survey policy follows a more static approach, based on the maximum size of ships and some water depth levels, such as indicated in NLHO [2003] and illustrated in Figure 1.1.

Risk can be described as the probability of an undesired event multiplied by the consequence of such an event (e.g. damage (in Euros), number of casualties). Consequences of the events are difficult to quantify. In case of a grounding, the consequences will be limited, because the seabed consists of sediment (*versus* more solid beds). However, in case of a contact with an obstruction the consequence may be a penetration of the hull of a ship, causing the foundering of the ship. The focus in this study is the probability element of the risk, thus assuming more or less that the average consequences are the same for each incident. Therefore, we use the term grounding danger rather than risk.

From analyses of casualty databases, it can be extracted that there are two main causes for grounding, namely:

1. A navigational error that is not corrected before the grounding occurs, due to
    1. Incorrect position,
    2. Inaccurate nautical chart,
    3. Human induced navigational error.
2. A technical failure due to which the ship is partly or completely not under control and finally grounds, when
    1. the failure was not repaired in time,
    2. the ship could not anchor,
    3. and external assistance was not in time.

The second cause of grounding is less related to the water depth. There is a small relation because the ship will ground earlier when it is closer to the critical isobath, but a higher survey frequency will not prevent this type of grounding. Therefore, this type of grounding is not dealt with in this report.

We focus on the first cause of grounding, a navigational error due to an inaccurate nautical chart, which in turn might be caused by seabed morphodynamics or an unknown object on the seabed. These two groundings – regular grounding and object grounding – are the subject of this study because these are influenced by the re-survey policy of the NLHO.

In the grounding danger calculations, only the NCS below the 10 m isobath is included.

4.2.1 Regular grounding probability

The regular grounding probability is the probability of running aground due to a (locally) limited water depth at time of passing of a vessel, and therewith depends on the draught of the ship and the water depth.

In this study, the critical water depth, WD_c, for ships on the Netherlands Continental Shelf is defined as

$$WD_c = dg + UKC + 2 \tag{4.1}$$

where dg is the draught of a ship (m) and UKC is the Under Keel Clearance (m), a safety margin which is set to 20% of the operational draught. The constant is an extra safety margin of 2 m. This definition is the criterion used by the NLHO; other definitions may be more appropriate in other locations, such as coastal approaches to ports.

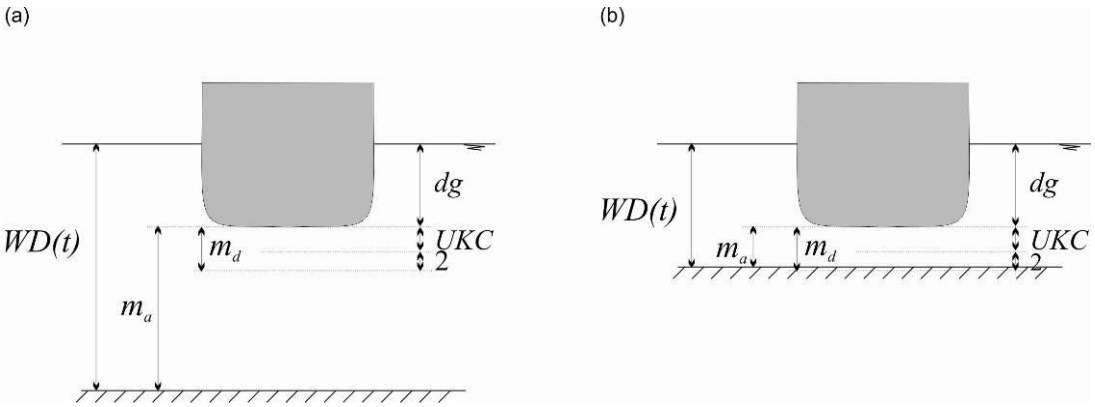

Figure 4.1 Schematic overview of parameters used in the formulation of the grounding probability: actual water depth at a point in time, $WD(t)$, draught of a ship, dg, Under Keel Clearance, UKC, the actual grounding margin, m_a, and the desired margin, m_d. Examples represent (a) a non-critical situation and (b) a critical situation.

Figure 4.1 illustrates the parameters used in the probability calculations. When the actual margin $m_a < 0$, i.e. the draught exceeds the actual water depth, $WD(t)$, the grounding probability is 1, i.e. the ship surely grounds. When the actual margin is larger than the desired margin, m_d, i.e. the actual water depth exceeds the critical water depth, the regular grounding probability is 0 (Figure 4.1a). In cases where the actual margin is smaller than the desired margin and $m_a > 0$, there is a grounding danger (Figure 4.1b).

In the quantification of the grounding danger, the regular grounding probability $P_{g,reg}$, is calculated for each AIS hit, which is the location of a ship at a specific moment as captured by the AIS system, by:

$$P_{g,reg} = P\{m_a < m_d\} \tag{4.2}$$

in which the actual grounding margin for regular grounding, $m_{a,\,reg,}$ is defined as:

$$m_{a,reg} = WD(t) - dg \tag{4.3}$$

and the desired margin, $m_{d,}$ is defined as:

$$m_d = UKC + 2\,. \tag{4.4}$$

The dynamic water depth, $WD(t)$, in eq. (4.3) is:

$$WD(t) = WD_0 + \frac{dWD}{dt} \tag{4.5}$$

where WD_0 is the measured water depth (constant, (m)) and dWD/dt is the change in water depth since the last survey (m/yr).

In this study, the regular grounding danger will first be calculated assuming a constant water depth, so that eq. (4.3) becomes

$$m_{a,reg} = WD_0 - dg \tag{4.6}$$

The dynamic water depth will be discussed in section 4.2.3, based on predicted water depths (presented in section 3.3.3).

As described earlier in this section, grounding may occur when the actual margin is smaller than the desired margin and $m_a > 0$. The probability density function for an actual regular grounding margin between 0 and m_d is unknown. For example, it depends on the extra water depth at the time of passing. Furthermore, since we used a grid cell size of 1 by 1 km, within which the water depth is variable, the real grounding probability also depends on where the ships have sailed exactly within this area. All these aspects could not be included in this study.

With N_{AIS} is the number of AIS hits within a grid cell in one year, the regular grounding danger $D_{g.reg}$ for that grid cell is defined as the sum of the regular grounding probabilities of all AIS hits:

$$D_{g,reg}(x,y) = \sum_{i=1}^{N_{AIS}} (P_{g,reg,i}) \tag{4.7}$$

where (x,y) is the south-west corner of a 1 by 1 km grid cell.

The input data for the calculations of the regular grounding danger are described in sections 4.3.1 and 4.3.2.

4.2.2 Object grounding probability

The object grounding probability, $P_{g,obj}$, is the probability of running aground due to the presence of objects at the seabed, and therewith depends on the draught of the ship, the water depth to the seabed and the height of the object.
The object grounding probability of an AIS hit for object *j* is:

$$P_{g,obj,j} = P\{m_{a,obj,j} < m_d\}P_{obj} \tag{4.8}$$

in which P_{obj} the probability of the existence of an object at a location and the actual margin, m_a, is now alternatively defined as the actual margin above object *j*:

$$m_{a,obj,j} = WD(t) - dg - H_{obj,j}(t) \tag{4.9}$$

for an object with actual height $H_{obj,j}(t)$.

The effect of a dynamic water depth $WD(t)$ is calculated in section 4.2.3. First, when we assume a constant water depth, the actual margin above object *j* is simplified to

$$m_{a,obj,j} = WD_0 - dg - H_{obj,j} \tag{4.10}$$

In calculating the object grounding probability, we assume that the probability of hitting a properly charted (i.e. *known*) object is zero. The probability of hitting an *unknown* object follows a distribution function dependent on object height: $P_{g,obj} = P_{g,obj,j}(H_{obj,j})$. The distribution function for $H_{obj,j}$ will be derived in sections 4.3.3 and 4.3.4, based on the object observation results of surveys in three periods of one year.

This gives a probability of hitting any unknown object within a cell of 1 x 1 km for one year of

$$P_{g,obj} = \sum_{j=1}^{N_{obj}} (P_{g,obj,j}) \tag{4.11}$$

where N_{obj} is the number of object classes in the distribution function.

The object grounding danger $D_{g,obj}$ in a grid cell is

$$D_{g,obj} = \sum_{i=1}^{N_{AIS}} (P_{g,obj}) \tag{4.12}$$

for all AIS hits N_{AIS} within a grid cell.

The probability $P_{g,obj}$ of hitting an unknown object in eq. (4.12) has to be written in more detail. The object is only hit when the ship crosses the unknown object. This probability can be approximated by specifying the travelled path, ship breadth (B_{ship}) times the speed (v) and the time the ship is at that location.

$$P_{g,obj,j,i} = P_{obj}(t)\frac{B_{ship,i}v_i t_i}{A} \tag{4.13}$$

in which

t	= the time passed after the last survey
$P_{obj}(t)$	= probability of an object present after time t
$B_{ship,i}$	= the breadth of the observed ship i (AIS hit)
v_i	= speed of ship i
t_i	= time of ship i in grid cell
A	= surface of a grid cell

Each AIS hit represents the presence of that ship for the time between two successive observations.

The probability of an unknown object at a location increases with the time passed after the last survey for that location. The object grounding danger is calculated for each location (grid cell) for the case that exactly one year has been passed since the last survey. The probability of an unknown object at that location depends on the shipping density at that location, because the object is originated by a ship. In this study distinction is made between the ship types on a certain location.

$$P_{obj} = P(unknown\ object \mid ship)\frac{N_{AIS}(t)}{t} \tag{4.14}$$

in which $P(unknown\ object \mid ship)$ is the probability of an object caused by 1 ship per year and $N_{AIS}(t)/t$ is the average number of ships at that location.
The probability $P(unknown\ object \mid ship)$ is derived in section 4.3.4.

4.2.3 Effect of morphodynamics on grounding probability

Morphodynamics cause changes in seabed elevation and therewith the water depth. A changing water depth affects the grounding probability. This impact is modelled for the regular grounding probability and the object grounding probability for a case that the area is not surveyed during a period of t years

4.2.3.1 Regular grounding probability

The effect of morphodynamics on the regular grounding after t years without a survey means that the water depth changes, whereas the distribution of draughts of ships remains unchanged. The regular grounding danger is calculated with eq. (4.5) multiplied by the number of years, t. In the calculations in this study, we use the predicted water depths as provided in section 3.3.3.

4.2.3.2 Object grounding probability

The effect of morphodynamics on the object grounding probability is more complex than on the regular grounding probability, because the actual water column above an unknown object depends on when the object is fallen. Figure 4.2a shows a rising seabed. This means that the object will be covered by sediment. In case of a seabed going down (Figure 4.2b), it is assumed that the object will not go down with the sea bed (neglecting processes of self-burial by concentrating currents around the object). This means that the objects will be relatively less high in case of a rising seabed than in case of a seabed going down. However, the water column above the object **remains unchanged**. This means that water column at the moment that the object is fallen determines the grounding probability.

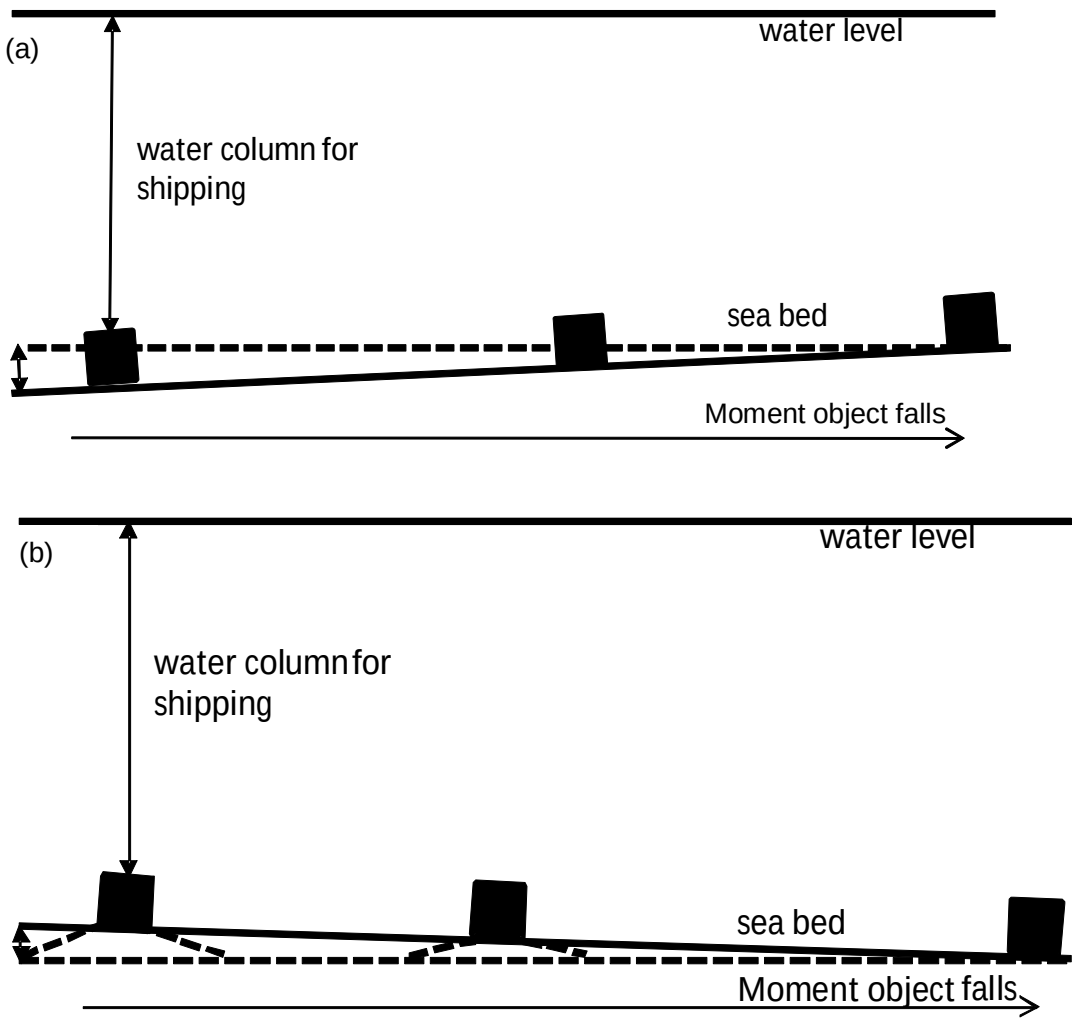

Figure 4.2 *(a) Objects on a rising sea bed. (b) Objects on a subsiding sea bed. The objects shown are three different objects; the time on the x-axis thereby indicates both the moment of falling of new objects and time in which the sea bed is going down.*

Using equations (4.8) and (4.9) and the distribution that is derived in sections 4.3.3 and 4.3.4, the actual margin for a certain object *j* with height $H_{obj,j}$ can now be defined as:

$$m_{a,obj,j} = WD_0 + t\frac{dz}{dt} - dg - H_{obj,j} \tag{4.15}$$

where WD_0 is the most recently measured water depth (i.e. the last survey) and t is the number of years that remain unobserved since the last survey. In this period [0, t] there are four cases:

1. There is always sufficient water above the object, positive margin ($m_a > m_d$; P_g=0);
2. There is never sufficient water above the object, negative margin ($m_a < 0$; P_g=1);

3. The margin is 0 at time t_1 and a rising seabed (t_1 is the time at which an object falls onto the bed). All objects of these heights that have fallen onto the bed in the period [t_1, t] are taken into account;
4. The margin is 0 at time t_1 and a lowering seabed. All objects of these heights that have fallen onto the bed in the period [0, t_1] are taken into account.

Thus, there is only an effect of morphodynamics in the case that the critical margin $m_{a,\ obj,j}$ = m_d is reached within the preceding period of t years without survey. Otherwise, the object contributes always or never to the object grounding probability. The object grounding probability for a certain height of an object is linearly related to the duration of the margin less than 0.

The object grounding probability is determined for a one year period after t years without being surveyed, based on the predicted water depths for 2011, 2015 and 2020 (section 3.3.3).

4.2.4 Effect of grid size

The grid size plays a role in the calculation of the danger on regular grounding and object grounding, because the water depth is an important variable and this water depth is kept unchanged within one grid cell. In order to keep the difference between the minimum and maximum water depth in a grid cell as small as possible, the grid cell has to be as small as possible.

From the AIS it is known where ships sail and with which draught. This is therefore a good base for the calculation of the regular and object grounding danger. In this calculation, the relation between the draught of the ship and the water depth is important. It is not possible to follow the trajectory of each individual ship and to determine the grounding probability during the whole voyage given the draught, the water depth, the external conditions and the real distance to obstructions. A simplification is absolutely necessary. The approach followed is to count the number of visits of ships for each grid cell (AIS hits) divided in draught classes. A fine grid increases the accuracy, but too fine means that the amount of data becomes unmanageable. After some trials, a grid size of 1 by 1 km was chosen.

The limitation due to grid size is just one of the limitations of the present implementation of the method. Its merits and restrictions are discussed in section 4.4.

4.3 Results

4.3.1 Shipping from AIS

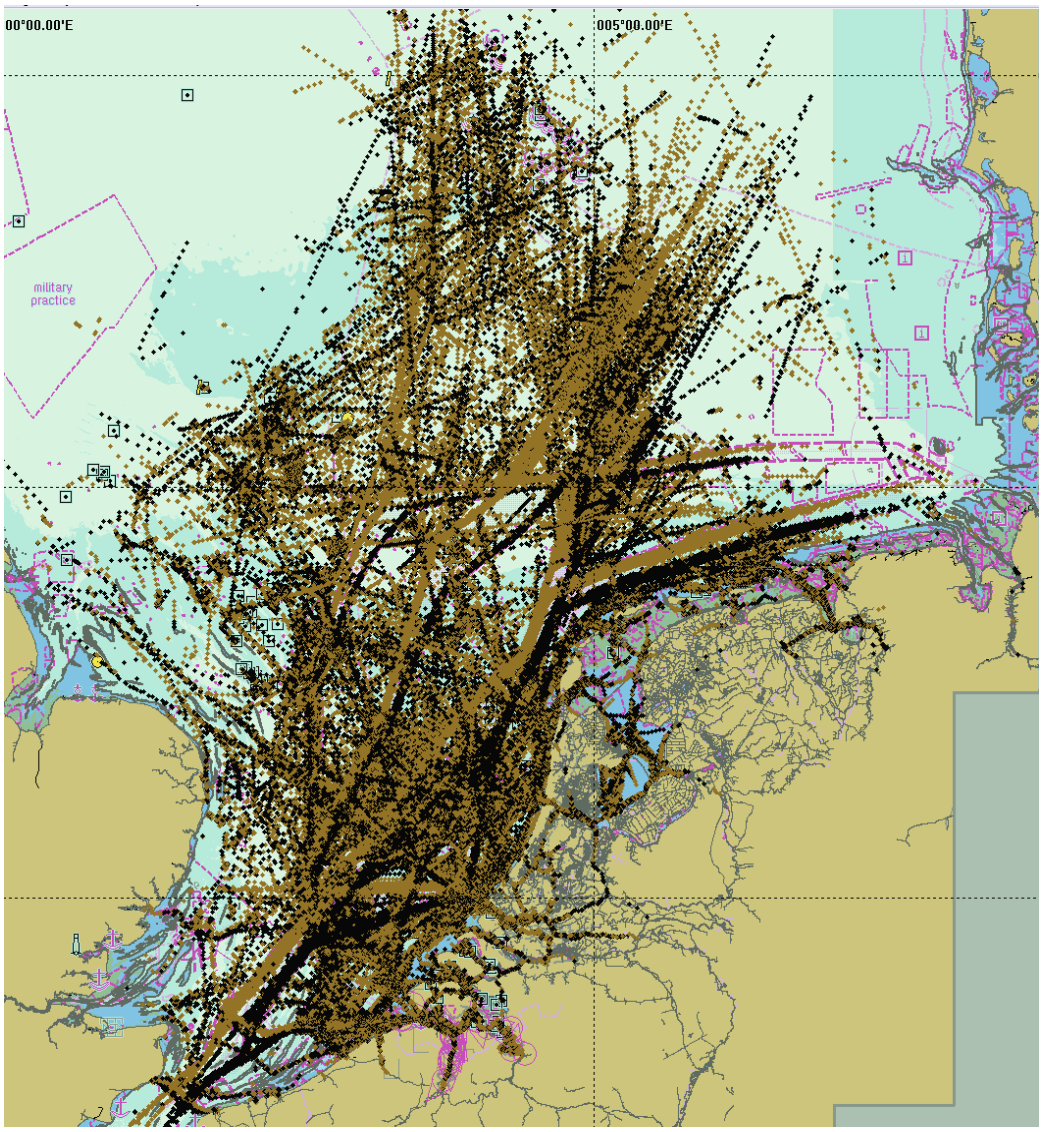

Figure 4.3 *AIS of one week in July 2009. Black dots represents ships going eastwards; brown dots ships going westwards*

Figure 4.3 shows the positions of all ships of one week of AIS. The positions of each ship are plotted each 10 minutes with a brown or a black dot, depending on the direction of the ship. A black dot is used for a ship moving eastwards (course over ground between 0° and 180°) and a brown dot for a ship moving westwards (180° to 360°). Figure 4.3 shows also that the coverage of AIS decreases with the distance to the Dutch coast. Areas with lower coverage typically show incomplete ship tracks, for example tracks of a ship sailing at constant speed (recognizable by a straight line of equidistant dots) that ends at open sea and continues farther up ahead.

Figure 4.4 contains the same information as Figure 4.3, but zoomed in for the approach of Rotterdam. On this scale the figure shows more detail, for example the ships at anchor in the anchorage areas (yellow circles). These ships turn around the anchor during their stay in the anchorage area, as a result of which the tracks of these ships form a more or less circular clustering of dots.

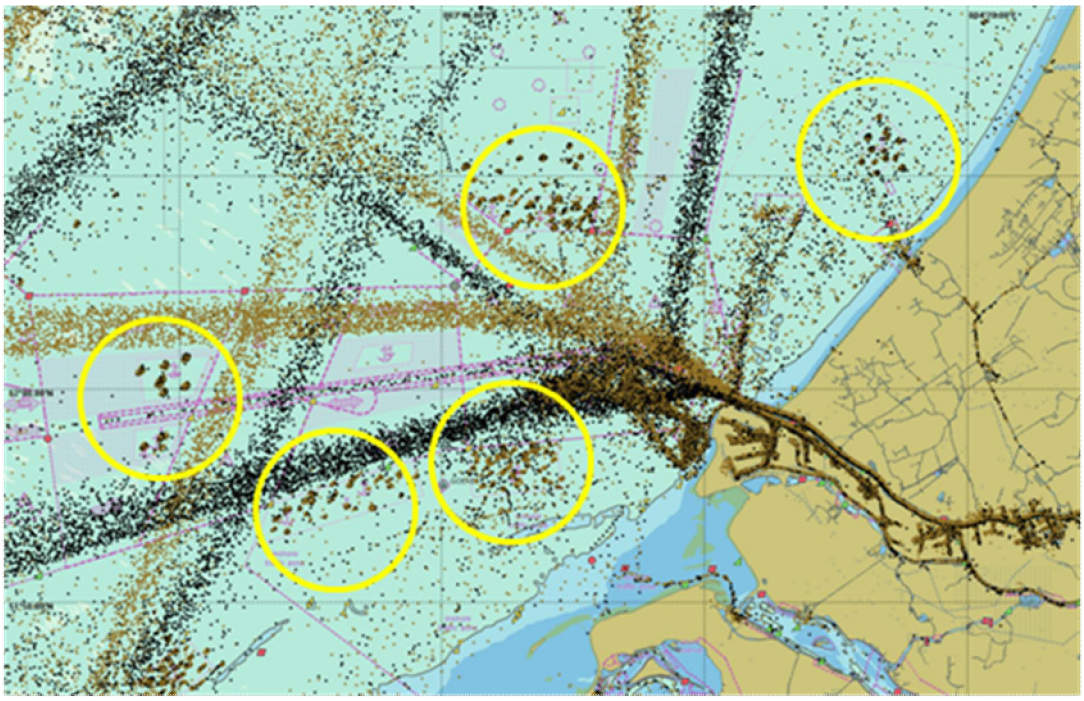

Figure 4.4 AIS of one week in July 2009 near Rotterdam. Yellow circles indicate anchorage areas

The density charts based on AIS are the successors of the well known posters “Vessel traffic on the North Sea”, based on the VONOVI flights, published by Ministry of Transport and NLHO (last one in 2004, given in Figure 4.5). Thereafter, new charts of the densities of shipping on the North Sea have been made based on AIS for 2006, 2007 and 2008 [in *Van Iperen and Koldenhof*, 2008; *Van Iperen et al.*, 2009b; 2009a, respectively]. These network evaluation studies have been performed for RWS Noordzee Directorate. In this study, we compiled a new density chart for all ships with AIS, based on the data of 2009 (Figure 4.6). The same legend is used through the years to keep the charts comparable with each other (number of ships per 1000 km^2). A density of 15 ships per 1000 km^2 in Figure 4.6 corresponds to an average of 0.015 ships per km^2 (i.e. the grid cell size in this study). With counts each two minutes, this corresponds with 0.015*365*24*30 = 3942 AIS hits per year.

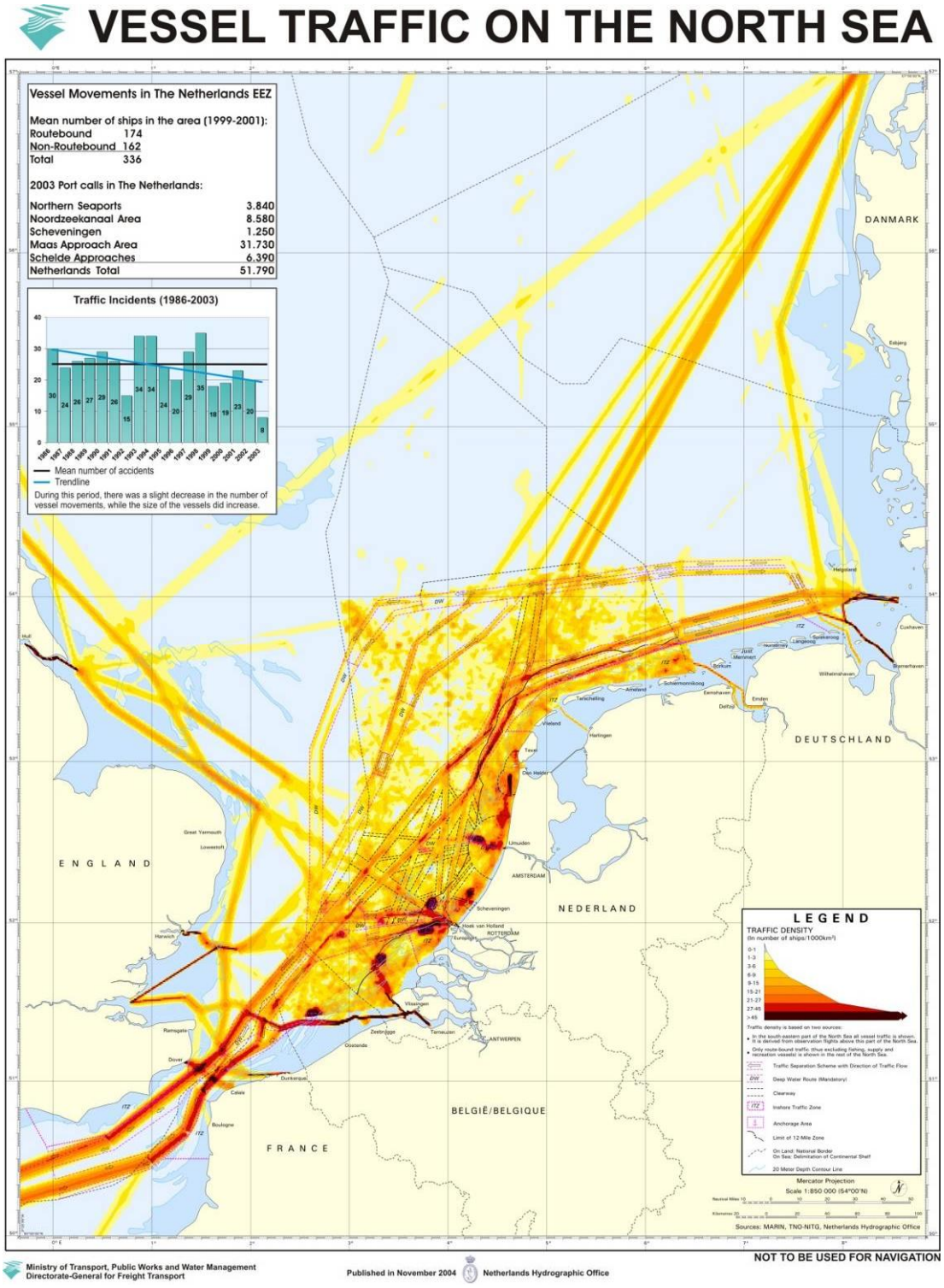

Figure 4.5 Classic vessel traffic density at the North Sea (2004).

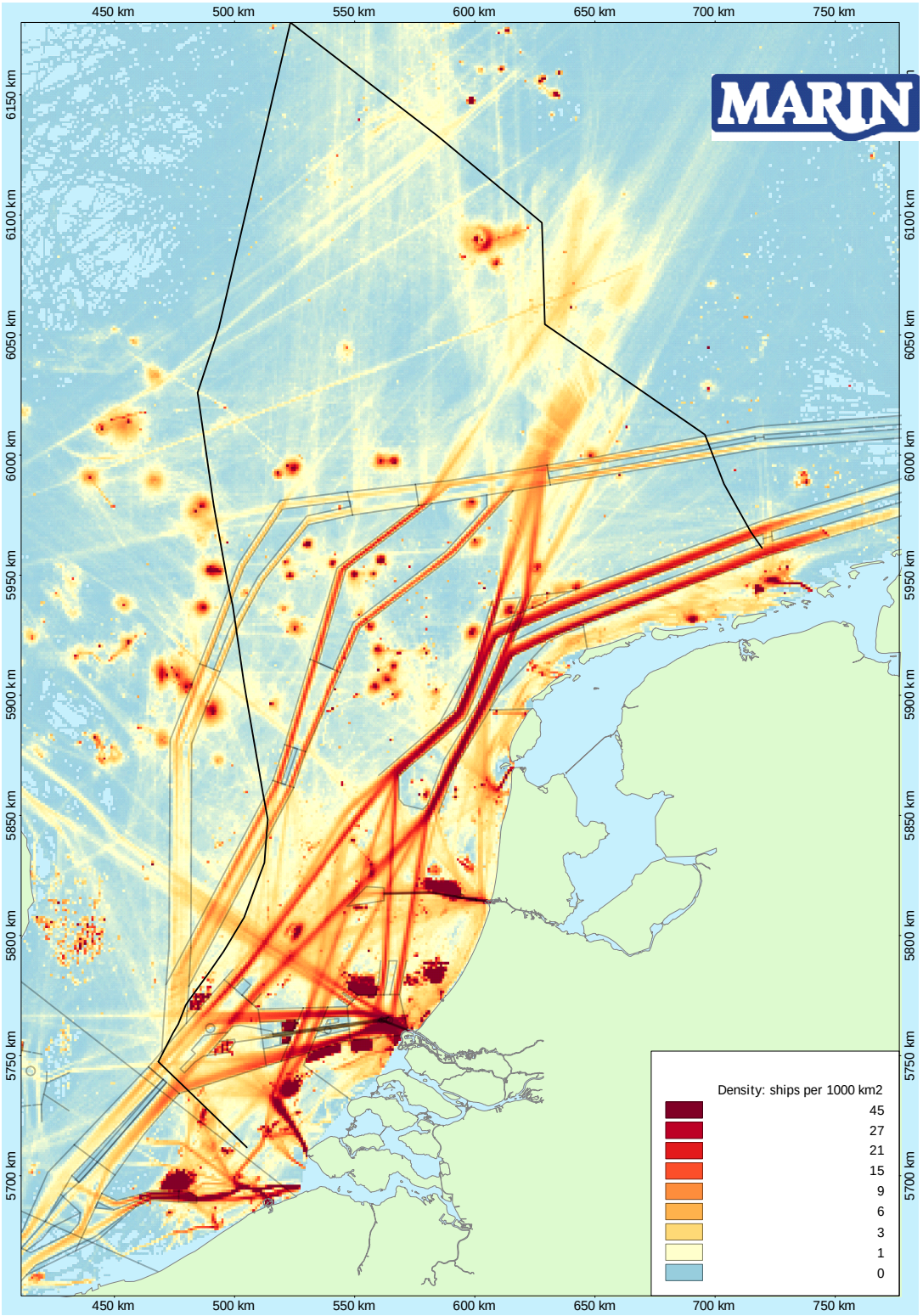

Figure 4.6 New traffic density map of all ships at the Dutch North Sea with AIS for 2009

Figure 4.6 shows a variation of densities within the same traffic lane, indicating that the coverage of the AIS-network is not equally well in the whole area, as discussed in section 2.2. These variations in coverage will affect the grounding danger results in this study.

4.3.2 Water depth

In the assessment of the grounding probability, water depths were used on the same grid nodes as the shipping counts. Herein, the most recently measured water depth and the water depth at locations of obstructions, as documented in the obstruction database of NLHO, were used. In the zones where water depths are not available (see Chapter 2), grounding probabilities could not be calculated.

The water depth varies within the grid cells of 1 x 1km. In order to determine the effect of this variation on the probability calculation, three water depths were used, namely the minimum, mean and maximum water depths from the DEM's (Chapter 3), reduced to grid cells of 1 x 1 km.

The used water depth is shown in Figure 1.2. The possible effect on the probability calculation is the difference between the maximum water depth and minimum water depth per grid cell of 1x1km (illustrated in Appendix 11.3). It shows that the difference is considerable to the west of Rotterdam and Zeeland.

The calculated grounding probability is large when the water depth in the analysis model is less than in reality. In that case, the calculation results will predict more groundings than can be expected. This happens more often in cells with large differences between the minimum and maximum water depth.
Also the extra water column that will exist in reality due to tide is not taken into account. Therefore, ships that can only enter Rotterdam/Amsterdam and the Western Scheldt will have a high grounding probability. This will be visible when presenting the grounding results (section 4.3.5).

The water depth on the location of the obstruction, each time that this location is surveyed, is used to estimate the size of the obstruction and is dealt with in section 4.3.3.

4.3.3 Known obstructions

Objects on the seabed can be a danger for the passing shipping. These objects are further referred to as obstructions, because this is the name used in the database of the NLHO to indicate objects, wrecks and natural dangerous points (rocks). The charted obstructions are points where the water depth above the obstruction is less than in the vicinity. The water depth above the obstruction, or sounding, is indicated in the chart. Ships will avoid sailing over these points when the draught approaches the water depth. Often these obstructions will be passed on a sufficient distance of a few hundred meters, thus within the same grid cell, but without any probability of grounding. Therefore the calculated grounding probability remains a rough indication, based on the assumption that the grounding probability will increase when more ships have to deviate from their track to avoid crossing over the obstruction. Because this behaviour is not available on a grid level of 1 x 1 km this grounding (or contact) probability is not further quantified in this study.
Another more dangerous situation will occur in case of an obstruction that is not charted because the obstruction was created after the last hydrographic survey. In this case the shipping is not aware of the obstruction and does not deviate when it would have been necessary. This is dealt with in next chapter.

Assuming that obstructions have a fixed known geographical location, the water depth from surveys could be determined. The last measured water depth is compared with the sounding above the obstruction, also extracted from the last survey. The height of the obstruction follows from the water depth minus the sounding of the obstruction. The result is given in Table 4.1.

Table 4.1 Height of obstructions

Height of obstruction		Number of obstructions	Fraction above lower limit
Lower limit [m]	Upper limit [m]		
0	1	85	1.0000
1	2	129	0.8752
2	3	114	0.6858
3	4	87	0.5184
4	5	65	0.3906
5	6	53	0.2952
6	7	40	0.2173
7	8	26	0.1586
8	9	25	0.1204
9	10	20	0.0837
10	11	10	0.0543
11	12	12	0.0396
12	13	8	0.0220
13	14	5	0.0103
14	15	0	0.0029
15	16	0	0.0029
16	17	1	0.0029
17	18	1	0.0015
18	19	1	0.0015
0	19	681	1.0000

Table 4.1 shows that 87 obstructions are surveyed in class 4, thus with a height between 3 and 4 meter. The exceedance probability of 3 m (the lower limit) is 0.5184, thus roughly 50% of the obstructions are higher than 3 m. The exceedance probability function is given in Figure 4.7. This function can be taken as probability distribution function for the height of obstructions.

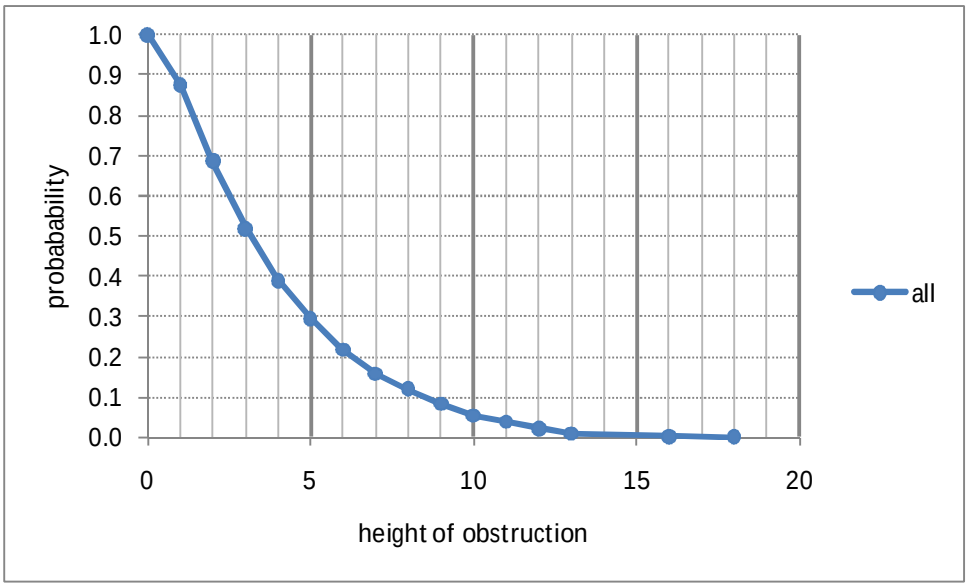

Figure 4.7 The probability that an obstruction at sea is higher than a certain value

4.3.4 Unknown obstructions

With the time that an area is not surveyed, the probability increases that new obstructions will occur in the area. In order to get an indication of how often a new obstruction will occur, the NLHO has, for three time periods of one year from 1 May 2007 to 1 May 2010, delivered the data of the obstructions with an indication of whether it was an old, new, deleted or changed obstruction. The height of all new obstructions in the period of three years are dealt with in the same way as in the previous chapter. The result is given in Table 4.2.

Table 4.2 Height of new obstructions

Height of obstruction		Number of obstructions			Fraction above lower limit
Lower limit [m]	Upper limit [m]	recovered	novel	total	
0	1	5	7	12	1.0000
1	2	3	12	15	0.8286
2	3	4	3	7	0.6143
3	4	5	4	9	0.5143
4	5	4	2	6	0.3857
5	6	4	2	6	0.3000
6	7	3		3	0.2143
7	8	4	2	6	0.1714
8	9	1		1	0.0857
10	11	1		1	0.0714
11	12	2		2	0.0571
12	13	1		1	0.0286
13	14				0.0143
14	15				0.0143
15	16				0.0143
16	17		1	1	0.0143
0	17	37	33	70	1.0000

In Table 4.2, a distinction is made between “recovered” and “novel” obstructions. Recovered means that an old obstruction, not observed in the previous survey, is found again and added to the database.
The last column contains the exceedance probability of a certain height. This column is plotted in Figure 4.8 together with the height of all obstructions of Chapter 4.3.3. It shows that the two distributions are very similar. Because there is no indication that the size of the obstructions is changing, the size distribution of the whole database is used. The number of new obstructions in three years gives an indication of the probability that a new obstruction will occur.
Assuming that shipping intensity remained the same, the number of 70 new obstructions found in the last three years, includes implicitly the effect of improved sensors and improved position technique. This means that it is possible that new obstructions are found that were already there during former observations. Therefore the number of new obstructions will be less. On the other hand it is expected that the probability of large obstructions will be in the right order of magnitude, because the probability that they are covered is larger than for small obstructions.

Furthermore, the probability of large objects is presumably less than is assumed, because in case that large objects, as containers, fall over board, the incident is reported to the Netherlands Coastguard, after which the reported incident is investigated by RWS and the NLHO. This means that the time of existence of those reported obstructions before surveyed is less than the average time of being present. Because it is not known which obstructions are found after a report to the Coastguard, this distinction could not be made in this study.

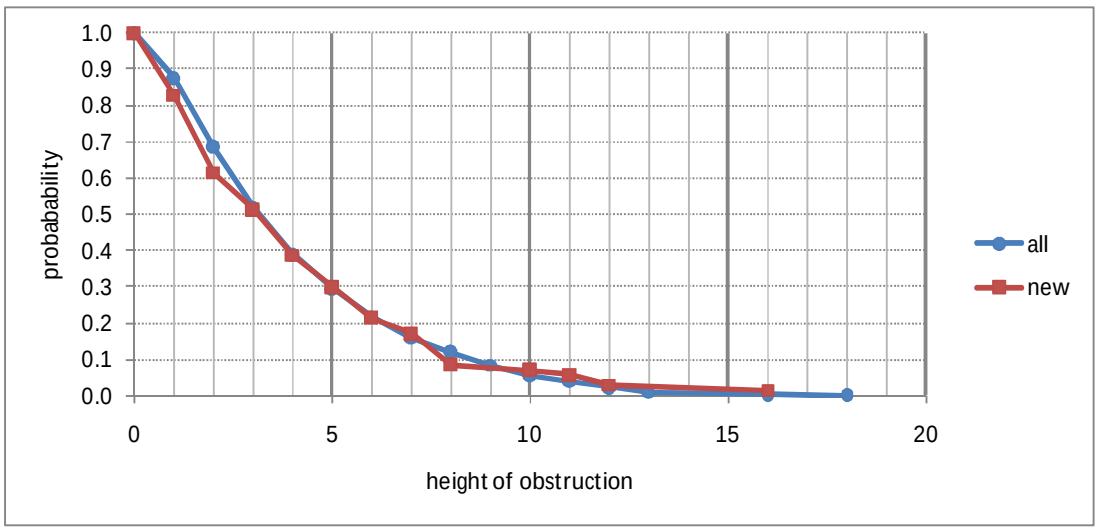

Figure 4.8 The probability that an obstruction at sea is higher than a certain value

The number of new unknown obstructions in one year, equals roughly 17.5 (70 obstructions divided by an assumed average of 4 years past a previous survey). It is assumed that the probability of an obstruction is related to the number of ships. There are on average 268 ships in the study area in water depth > 10 meter. Thus the number of new unknown objects is 0.065 (=17.5/268) per ship per year. This is $P(unknown\ object \mid ship)$ after one year, equation (4.13) in section 4.2.

4.3.5 Grounding Probability

4.3.5.1 Regular grounding probability

Figure 4.9 shows the number of ships counted in each cell with a negative margin for the mean water depth, thus the regular grounding danger formulated in equation (4.7) in section 4.2. A classification was applied to all ships that were assigned to a cell after steps of 2 minutes, and each cell is observed 30 * 24 * 365 = 262,800 times per year. Thus the highest scale level of 10,000 in Figure 4.9, means that on average once in the 26.28 times that the cell is observed, a ship was found with a negative margin. This does not mean that the ship will actually ground, because of the safety margin of 2 meters, the safe upper value for the draught (cut off value +1), the UKC of 20%, the additional water column of the tide and by using the LAT and finally because the water depth varies over the cell.
Unless all these uncertainties it is plausible that the cells with high counts will have high grounding probabilities. The highest values are found when approaching the ports. Also there are a few spots in the traffic lanes with relatively high grounding probability. For example, the four spots offshore in the Deep Water Route East are caused by the combination of the occurrence of sand banks (small water depths; Figure 1.2), the occurrence of relatively large ships and a relatively high shipping intensity (Figure 4.6).

Maps similar to Figure 4.9 were constructed for ships with a negative margin between -4 and 0 m, for -8 and -4 m and for -8 m, thus a relatively small shortage of water and therefore a relatively lower grounding probability. The interval -4 to 0 is arbitrary chosen. It is roughly the sum 2 meter extra water, 20% under keel clearance for ships with a draught of 10 m is already 2 m. A negative margin between -8 and -4 m is closer to real groundings. These respective figures show the grounding probabilities on the same locations, but with much lower counts. These maps are presented in Appendices 11.7, 11.8 and 11.9.

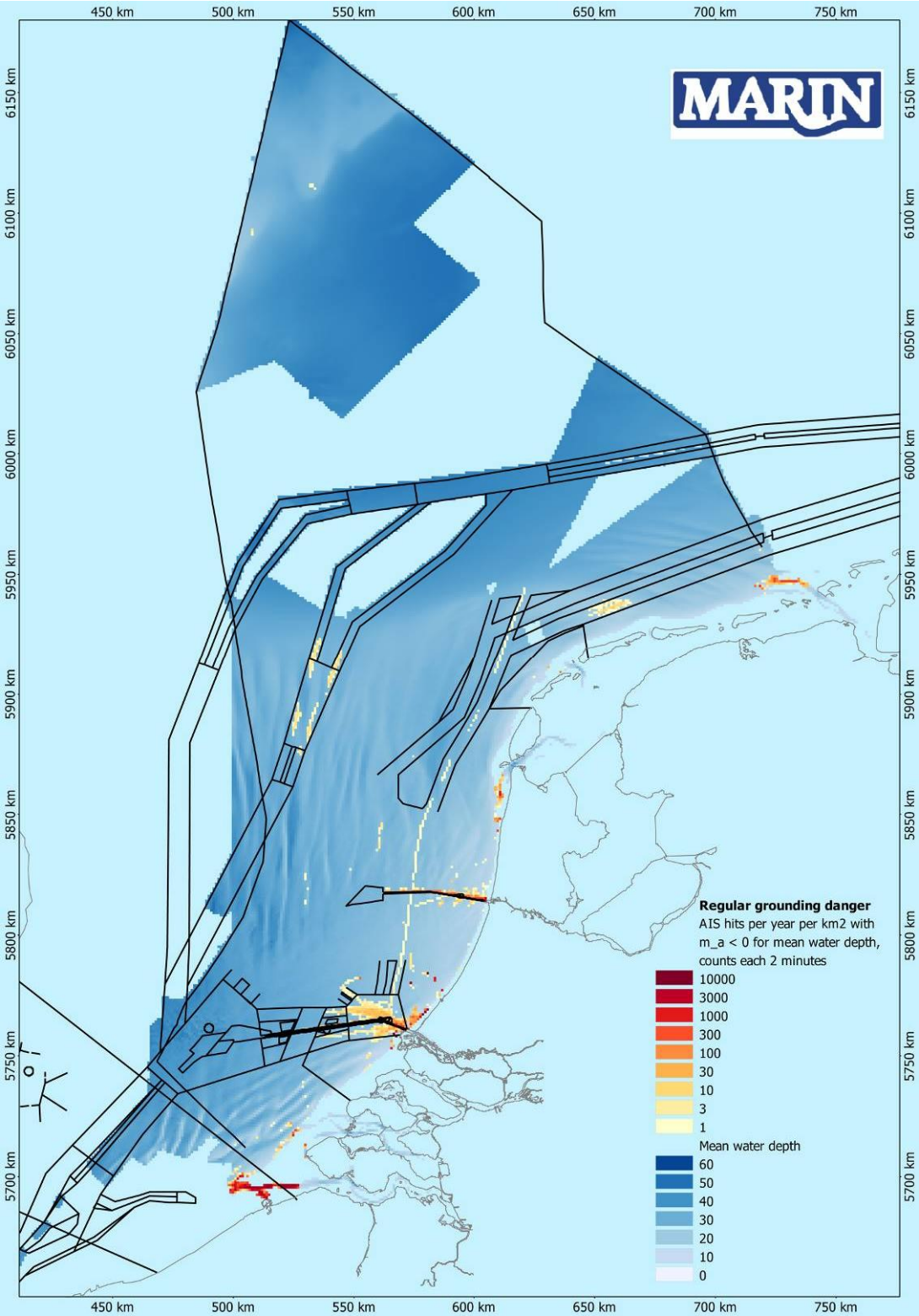

Figure 4.9 *Regular grounding danger of all ships (thus with actual margin < 0) for mean water depth as calculated with eq. (4.7). In all areas where water depths (shades of blue) are visible, the grounding danger is zero.*

4.3.5.2 Contact with an unknown obstruction

The object grounding danger is given in equation (4.12) in section 4.2. In section 4.3.4 it was found that the height distribution of new obstructions is similar to that of existing obstructions. Because the collection of existing obstructions is larger, this collection is used for the distribution function for the height of unknown obstructions in the calculations. This distribution in height and the related exceedance probability is given in Table 4.1 and in Figure 4.7.

The contact probability has been calculated for the situation in which the whole North Sea is not surveyed during a period of one year. For this situation the probability of unknown obstructions is known for each grid cell based on the observed AIS hits in that cell. The number of new unknown objects per ship is 0.065 (=17.5/268) (see section 4.3.4) per year.

The average speed of all moving ships in the North Sea amounts 11 knots. The speed of small merchant ships is relatively very low. The average speed of ships above 5000 GT amounts 14 knots, based on observations that were analysed for the AIS data of 2008. Because the probability of grounding or contacting an unobserved object is much larger for larger ships, this speed of 14 knots is used in the calculations. This speed is too high in the anchorage areas. In these areas the ships will turn with a few tenths of a knot around the anchor by the wind and current. Therefore the area that these anchoring ships travel during their stay in a grid cell is much lower than calculated, which means that the probability of a contact with an unknown obstruction is overestimated. On the other hand, there will be relatively more obstructions in anchorage areas, because anchors are mainly lost in these areas. It is difficult to indicate the overestimations in anchorage areas, but even in case of a factor ten, being a one colour scale step, the probability of a contact in an anchorage area is relatively high. Furthermore, the anchorages areas belong already to category 1 of the survey policy.

The resulting object grounding danger with an unknown obstruction in each grid cell is presented based on the minimum water depth in Figure 4.10. In fact, no real contact probabilities are presented but a type of danger that is strongly related with the probability of a contact with an obstruction, as calculated in eq. (4.12). In the figure, a value of 0.1 means that an average of 0.1 ship (AIS hit) per grid cell (1 km^2) per year may ground due to an unknown object (point). Similar maps for object grounding danger for the mean water depth and the maximum water depth are presented in Appendices 11.10 and 11.11, respectively. The three figures look similar, thus suggesting that the variation in water depth within one cell plays a minor role with respect to the height of the objects.

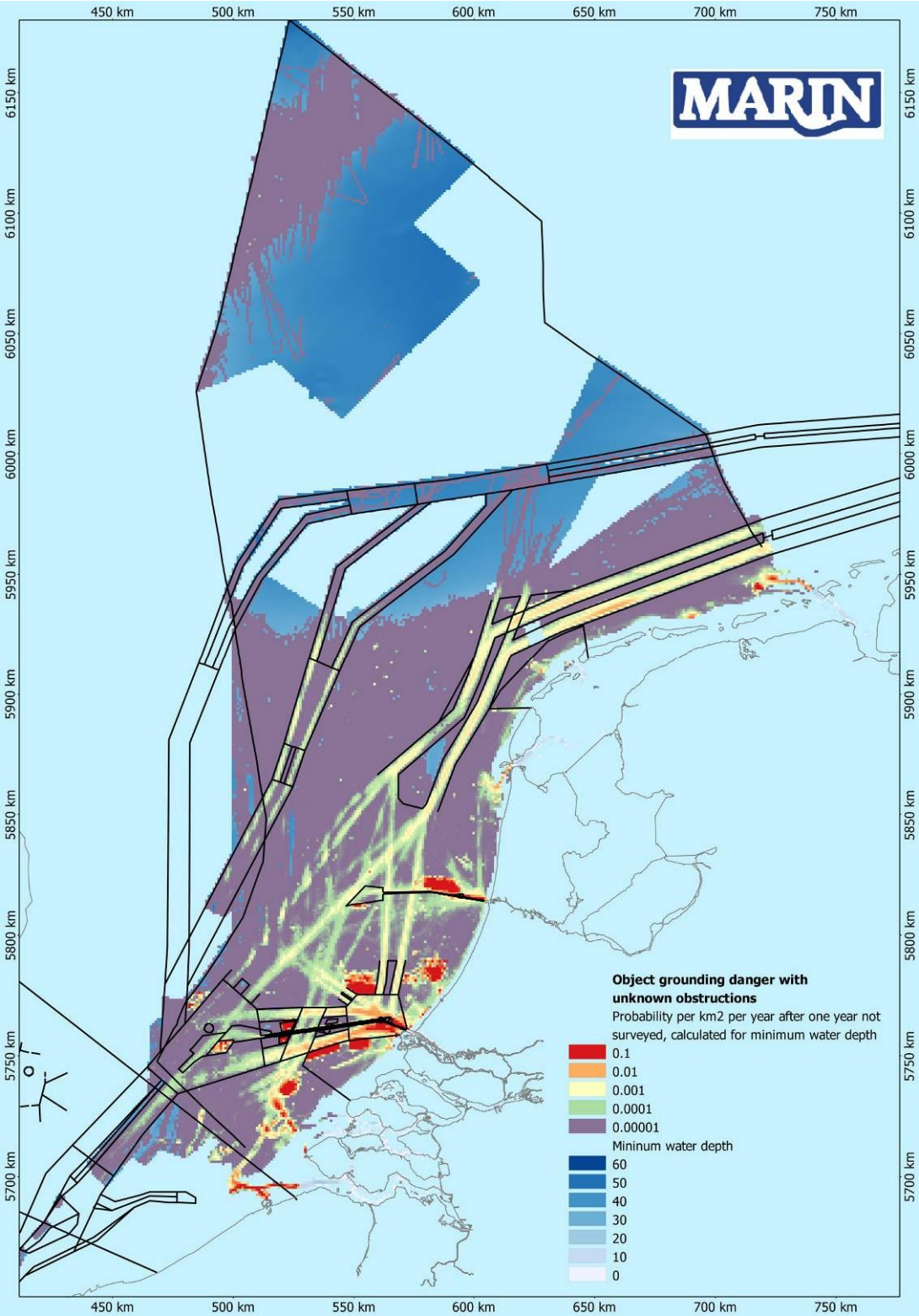

Figure 4.10 Object grounding danger with unknown obstructions for minimum water depth

Sensitivity analysis

The sensitivity for the variation in water depth is further investigated by assuming 3 meter extra water in Figure 4.11. This figure is rather similar to Figure 4.10 and Appendices 11.10 and 11.11. Figure 4.12 shows the result for the situation in which the height of the new unknown obstructions is 0 meter. As expected, it looks similar to Figure 4.9, because an object height of 0 meter means it is equal to the seabed elevation, thus the same grid cells will contain a danger. The presented values are different, however, because Figure 4.9 presents the grounding danger, i.e. all AIS hits of ships that may ground, whereas Figure 4.12, presents the same ships (AIS hits) multiplied by the probability of an object in the grid cell and the probability that the object (a point) is touched by the observed ships (eq. (4.13)). In Figure 4.12 the probability of grounding due to an unknown obstruction disappears nearly completely.

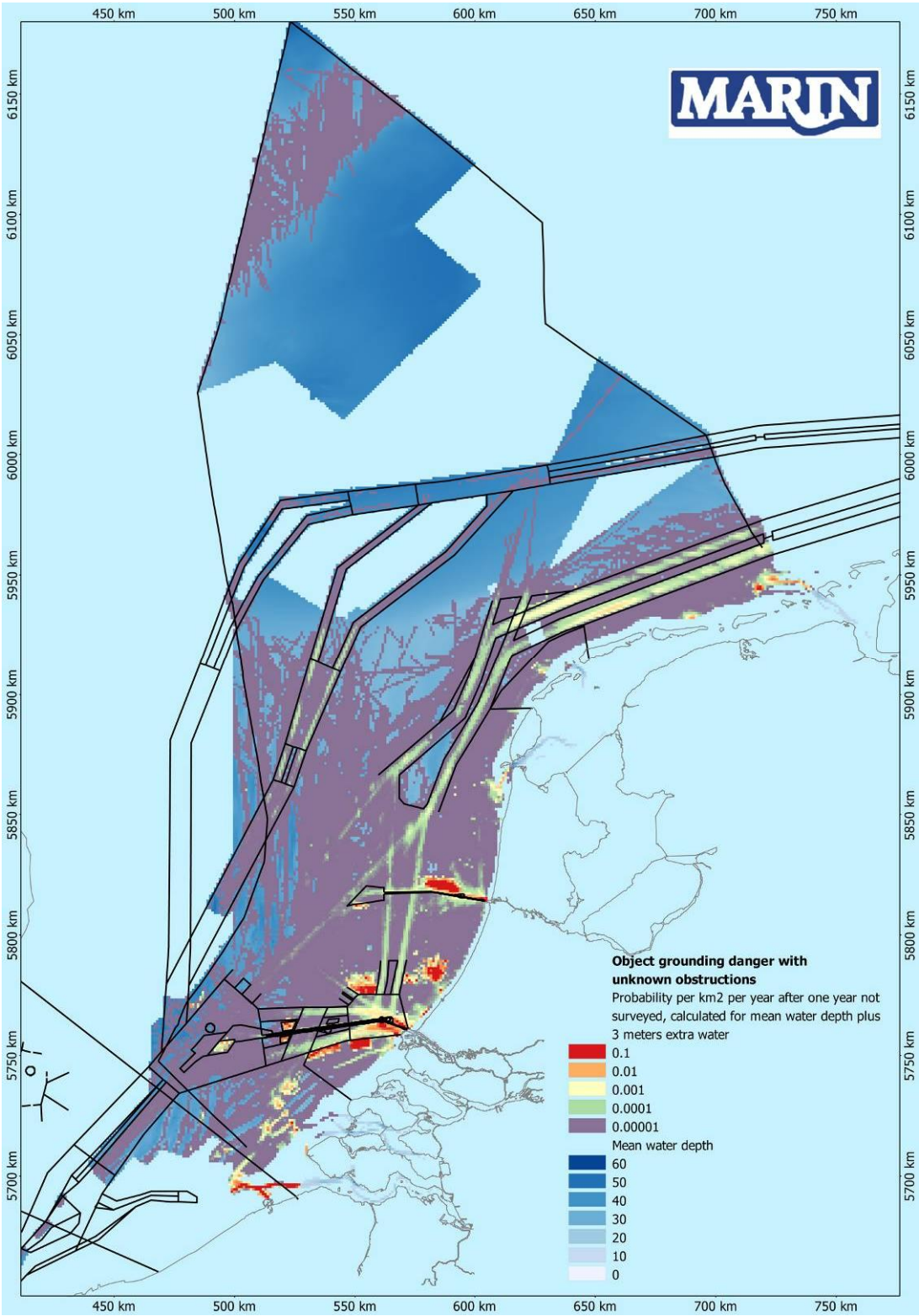

Figure 4.11 Ship contacts with unknown obstructions for mean water depth plus 3 extra meters water

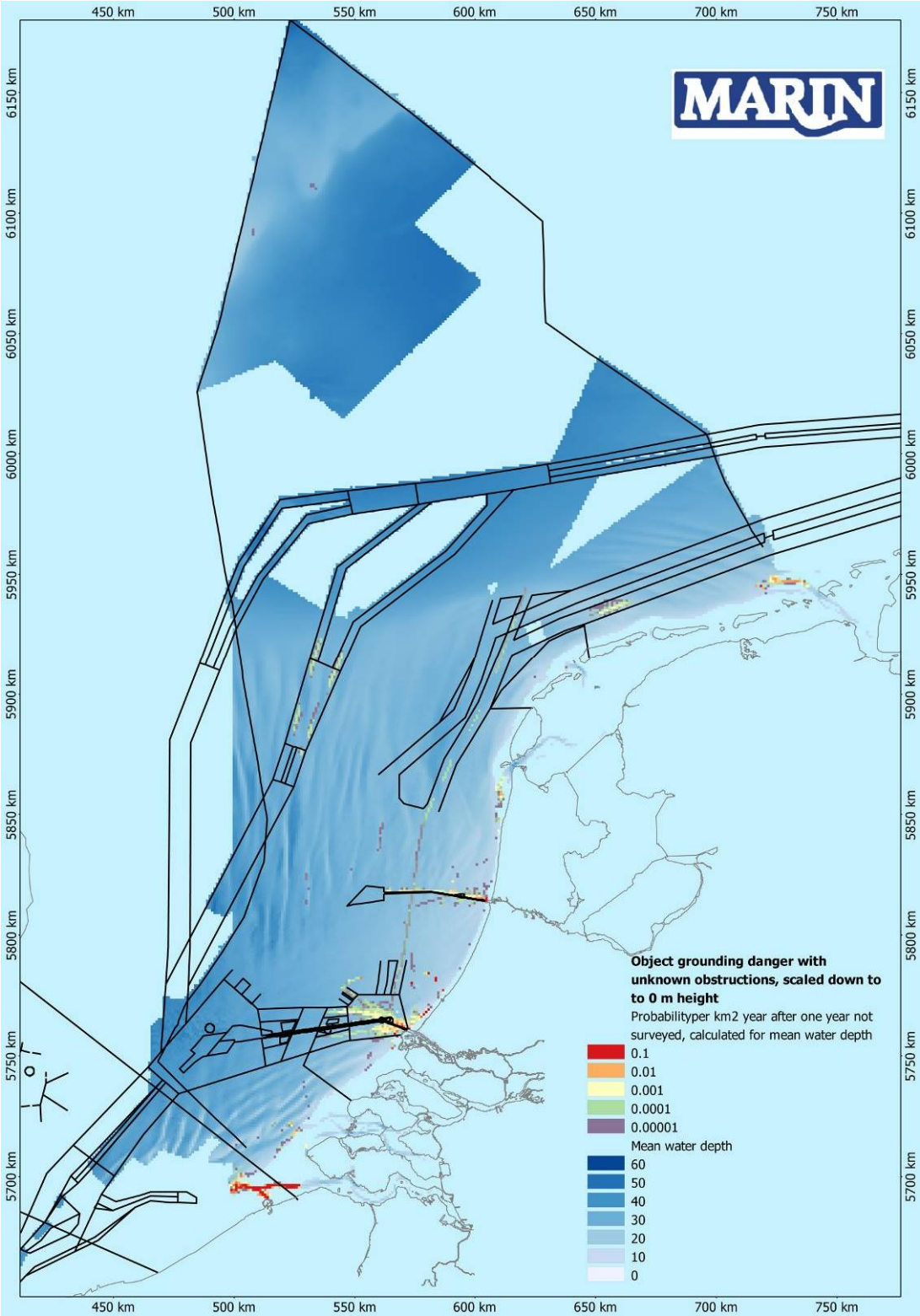

Figure 4.12 Object grounding risk for mean water depth with unknown obstructions with a height of 0 m.

4.3.5.3 Grounding danger for dynamic water depths

In order to assess the impact of morphodynamics on the grounding danger, grounding danger was determined for the predicted water depths for

- 2011, without a survey in the past year,
- 2015, without a survey in the past 4 years, and
- 2020, without a survey in the past 9 years.

Figure 4.13 and Figure 4.14 show the regular and object grounding dangers for the predicted water depth for 2011, respectively. The other maps are provided in Appendices 11.12 to and including 11.15. These maps reveal that the same distributions were found as in the grounding dangers for constant water depth (Figure 4.9; Figure 4.10), but with increasing counts for increasing periods between surveys.

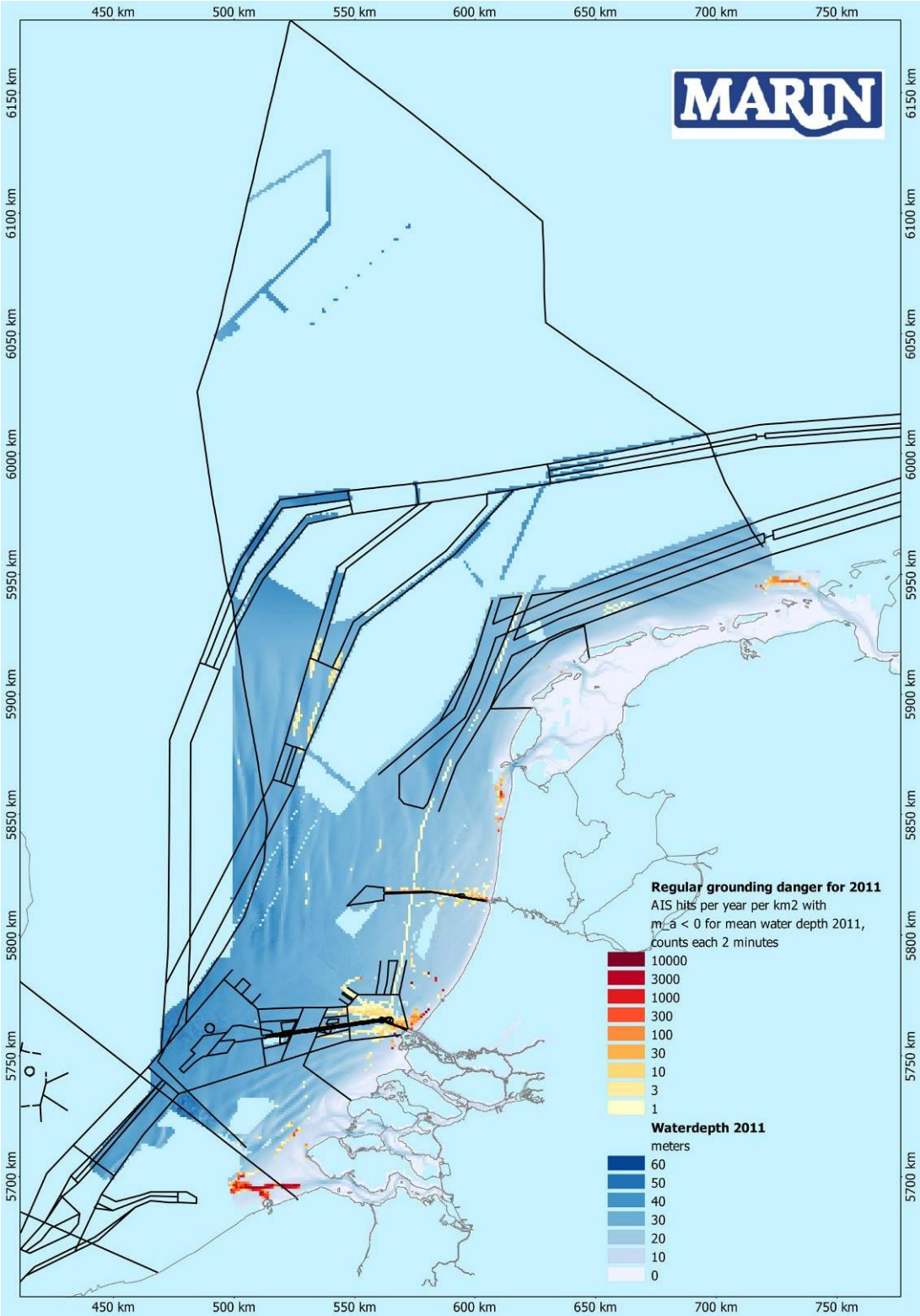

Figure 4.13 Regular grounding danger for the predicted water depth for 2011

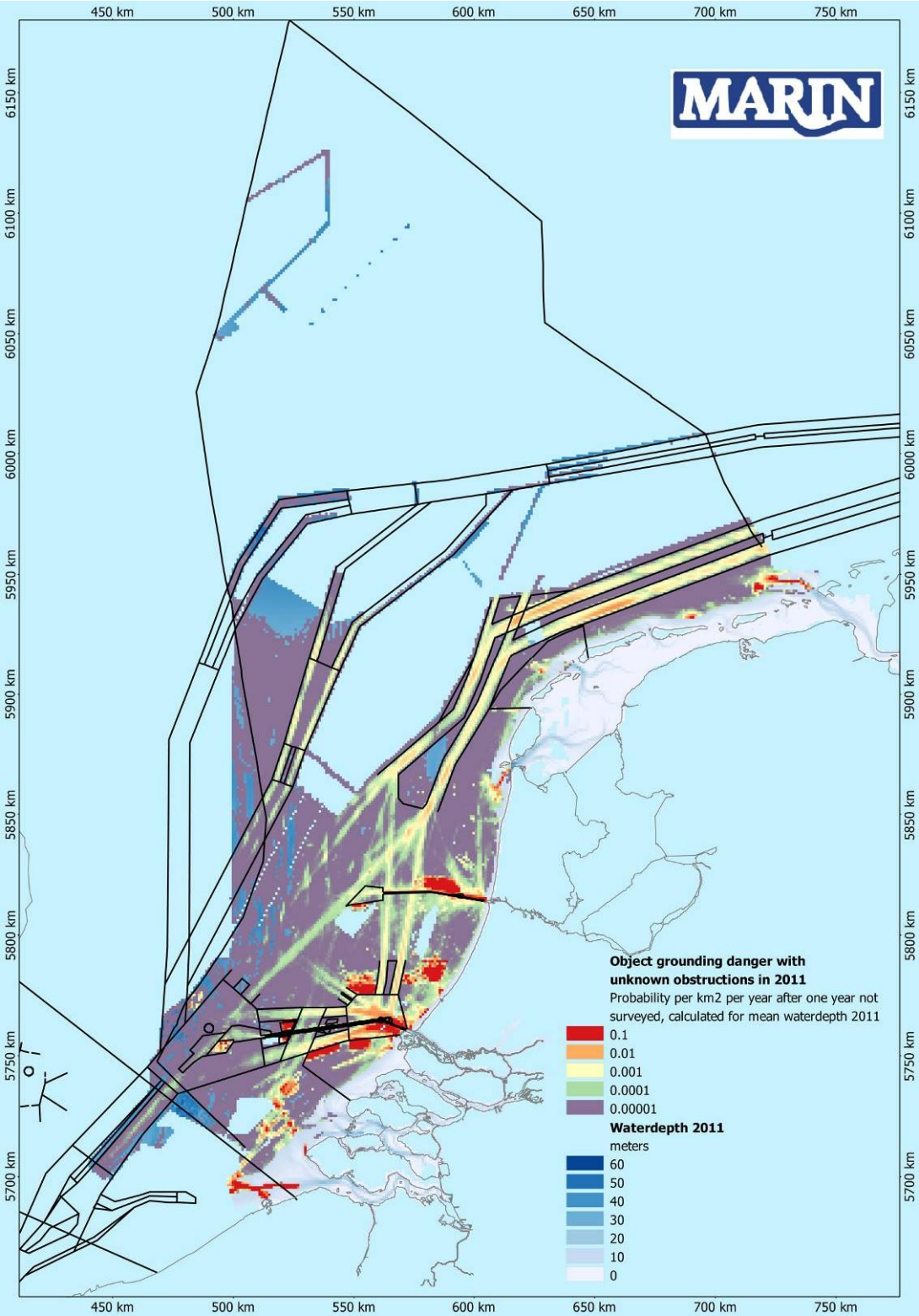

Figure 4.14 Object grounding danger for the predicted water depth for 2011

4.4 Conclusions

The largest grounding danger occurs in the approaches to the ports and the Western Scheldt. Because ships are familiar with the tide bounded entry to these areas they will only enter when it is possible with respect to their operational draught. This means that the groundings calculated for these areas will not occur in reality. The fact that these areas give the highest probabilities of groundings means that ships have to sail carefully.

The additional water column in reality above the water depth is not taken into account because this requires a much larger study. The objective of this study is to indicate the areas that require a more frequently survey than others. Thus it is sufficient to indicate the relative grounding danger for various areas.

In case an area is not surveyed during a certain period, unknown obstructions, thus not charted, will be caused by objects falling from ships. It is plausible that these obstructions will be located where ships sail. For this reason the probability of unknown obstructions is related to the densities of ships.

The average height of an obstruction is 3.9 meter. The height distribution of obstructions is used to calculate the probability of a contact with an unknown obstruction. The contact probability is related with the area travelled in a grid cell, divided by the dimensions. Further, it is assumed that each ship has a speed of 14 knots. That is not the case in the anchorage areas. Therefore the contact probability in the anchorage areas is overestimated, but taken into account that anchors are lost mostly in anchorage areas, it is estimated that the overestimation of contact probability is only a factor 10 (one colour scale step). Even considering this, the figures with the contact probability show relatively high probability in the anchorage areas. Further, the contact probability for unknown obstructions for the mean water depth per grid cell is given in 11.10. It shows that the high contact probability in the anchorages areas is also still present with a lower scale colour.
When comparing the contact probability with the survey policy of the NLHO, it shows that the intensity of surveying is high in the areas with the highest contact probability. In general the survey plan is confirmed by this contact probability calculation. Only some fine tuning can be performed. For example the deep draught route off Brown Ridge tends to need more attention, certainly when taken into account that the coverage is presumably less in this area far from the coast. Also in the other traffic lanes are some attention movements possible.

The grounding and contact probability in the North Hinder South TSS is higher than is presented, because it is known that the AIS coverage is bad in this area.

Recommendation MARIN Grounding
The present results have to be considered as a first step in a new development. Some aspects require additional research in case they are sensitive for the overall result. These are:

- The distribution of unknown obstructions;

  An improvement is possible when more data can be collected about this distribution.

- The AIS coverage in the areas further away of the coast;

  There are some white spots in the Dutch Continental Shelf with respect to the reception of AIS messages, because these areas are too far from the coast and base stations on offshore platforms. For example, white spots are the precautionary area west of Maas West Outer TSS and the whole North Hinder South TSS. The North Hinder South TSS does not belong to the Dutch Continental Shelf but the north going traffic lane does

belong to the survey area of the NLHO. The Netherlands Coast Guard was asked to investigate why the coverage in this area is so bad. The working of this AIS base station is included in this investigation. Furthermore, the outer west and northern part of the Dutch Continental Shelf are covered for less than 90%. The real coverage in these areas varies.

- To include the real speed of the ships in the grid cells.

This is more a refinement of the results than absolutely necessary.

5 Validation of the existing re-survey policy (Objective 3) and steps towards a formulation of a new re-survey policy (Objective 4)

5.1 Introduction

In the existing re-survey policy, the NLHO defined five categories of re-survey frequencies for the Netherlands Continental Shelf below the 10 m isobath (Figure 1.1). Two categories are applied in the coastal zone (Category 7) and the approach channels to the ports of Rotterdam and IJmuiden (Category 6), which are the responsibility of RWS. The division into re-survey categories is partially based on an in-house developed application at the NLHO that is based on geo-statistics and the deformation analysis. This implies that the application is valid for areas that have been surveyed at least 3 times. In addition, national and international experience was used in the re-survey categories [*NLHO*, 2003].

The categories are [*NLHO*, 2003]:

CAT 1: At least once every two years
This category includes *(i)* traffic lanes where the critical water depth in equation (4.1) is larger than the measured water depth when reduced to LAT, and *(ii)* anchorage areas.

CAT 2: At least once every four years
Traffic lanes that are not included in CAT 1 but that are of importance to shipping on this route.

CAT 3: At least every six years
Areas within this category include *(i)* areas bounded by the 10 m isobath along the coast in the east and the traffic lanes of category 2, where water depths are less than 30 m, *(ii)* the Deep Water Route from the Brown Ridge to the 30 m isobath, and *(iii)* the route towards the Skagerrak to the 30 m isobath.

CAT 4: At least every 10 years
Category 4 includes *(i)* areas that are not included in categories 1 to 3, where water depths are less than 30 m, *(ii)* the Deep Water Route, where water depths are more than 30 m, and *(iii)* the route towards the Skagerrak, where water depths are more than 30 m.

CAT 5: At least every 15 years
All other areas that are deeper than 30 m.

CAT 6: Once per year to once every 4 years, depending on the area
Areas that fall under the responsibility of RWS (Noordzee Directorate), including the IJ-channel, the approach zone to the Euro-channel, the Euro-channel and the Maas-channel (Maas West Outer and Maas East Inner TSS).

CAT 7: Once per year to once every 6 years, depending on the area.
Areas that fall under the responsibility of RWS coastal Directorates, including the coastal zone, estuaries, the Wadden Sea and the IJsselmeer.

For a map of the categories, see Figure 1.1.

The existing re-survey policy will be scientifically validated by testing the effectiveness of the existing re-survey categories in capturing the change in water depth due to both morphodynamics and new obstructions on the seabed in periods between two subsequent surveys (Objective 3). By coupling the re-survey frequencies to a combined grounding danger map, areas of contrasting danger within categories are identified and new areas of dissimilar danger may be revealed, resulting in an optimised re-survey policy. Similarly, combined grounding danger maps for the years 2011, 2015 and 2020, based on predicted water depths, establish the future danger development in the periods between two surveys within the relevant category. This way, it is possible to place temporal labels to the potential grounding areas and to verify areas where the potential grounding danger is found to be low. The identification of these areas leads to a revised re-survey policy (Objective 4)

5.2 Methods

In the validation of the existing re-survey policy of the NLHO, we used a GIS-overlay method. An overlay method combines two or more maps on a cell-by-cell basis (Figure 5.1). The result of this coupling is a new map, in which a new, unique class is created for each possible combination of classes of the underlying layers. For example, overlaying the two grounding danger maps presented in Chapter 4, each of which contain 9 classes as defined by MARIN, creates an overlay map of potentially 9 * 9 = 81 classes. The large number of classes in the overlay map often impedes the interpretation of the new map. In order to keep the number of classes manageable, a re-classification of the underlying maps is needed [*Doornenbal et al.*, 2006].

Figure 5.1 *Example of an overlay map, where the marine landscape approach couples different layers on a cell-by-cell basis [from Doornenbal et al., 2006].*

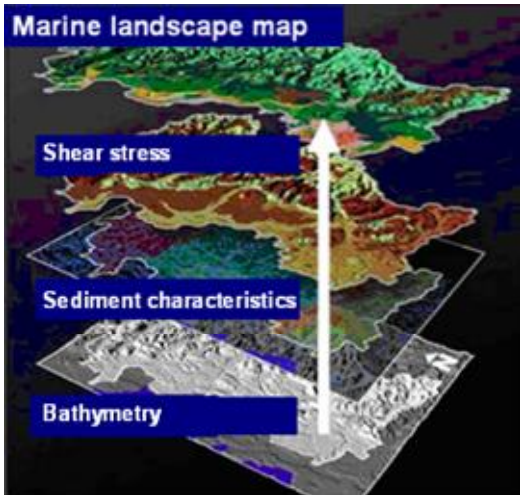

5.2.1 Re-classification and combined grounding danger

In the first overlay, we combined the map of regular grounding danger of all ships for the mean water depth (Figure 4.9) and the map of object grounding danger of unknown obstructions for the minimum water depths (Figure 4.10). Because the extents of the separate grounding maps were cropped to the limits of grounding-danger values >0, and hence did not cover the extent of the NCS, we assigned the empty nodes with value 0 (Figure 5.2; steps a → c and b → d).

The reduction of classes needs to be done in a meaningful way. We re-classified each of the two input maps into 4 classes that still represent the danger classes defined by MARIN (Table 5.1; columns 3 and 4 for the respective object grounding and regular grounding). The number

of new classes in the overlay map is herewith reduced to a maximum of 16, although, in this case, only 12 classes exist (Table 5.1, column 2; Figure 5.2e). For example, the new class in the overlay map of 32 indicates the combination of a re-classified value of 30 for the object grounding danger and a re-classified value of 2 for the regular grounding danger. The re-classified value of 30 represents a high object grounding danger of 0.01 to 10 in Figure 4.9 and the re-classified value of 2 represents a moderate regular grounding danger of 447 to 932 in Figure 4.10.

Table 5.1 Classifications of regular grounding danger and object grounding danger used in and resulting from the GIS overlay method. Columns 3 and 4 define the re-classification for the respective object grounding danger (0, 10, 20, 30) and regular grounding danger (0, 1, 2, 3). The second column displays the new classes in the overlay map (for explanation see text). The first column displays the choice of 5 colour categories used in Figure 5.5 (section 5.3.1).

Colour class	Combination class	Object re-class	Regular re-class	Object Grounding		Regular Grounding	
				from	to	from	to
0	0	0	0	0	0.0000001	0	1
low	1	0	1	0	0.0000001	1	447
	10	10	0	1E-07	0.0001	0	1
moderately low	11	10	1	1E-07	0.0001	1	447
	20	20	0	0.0001	0.01	0	1
moderate	21	20	1	0.0001	0.01	1	447
	22	20	2	0.0001	0.01	447	932
high	23	20	3	0.0001	0.01	932	17658
moderate	30	30	0	0.01	10	0	1
high	31	30	1	0.01	10	1	447
	32	30	2	0.01	10	447	932
	33	30	3	0.01	10	932	17658

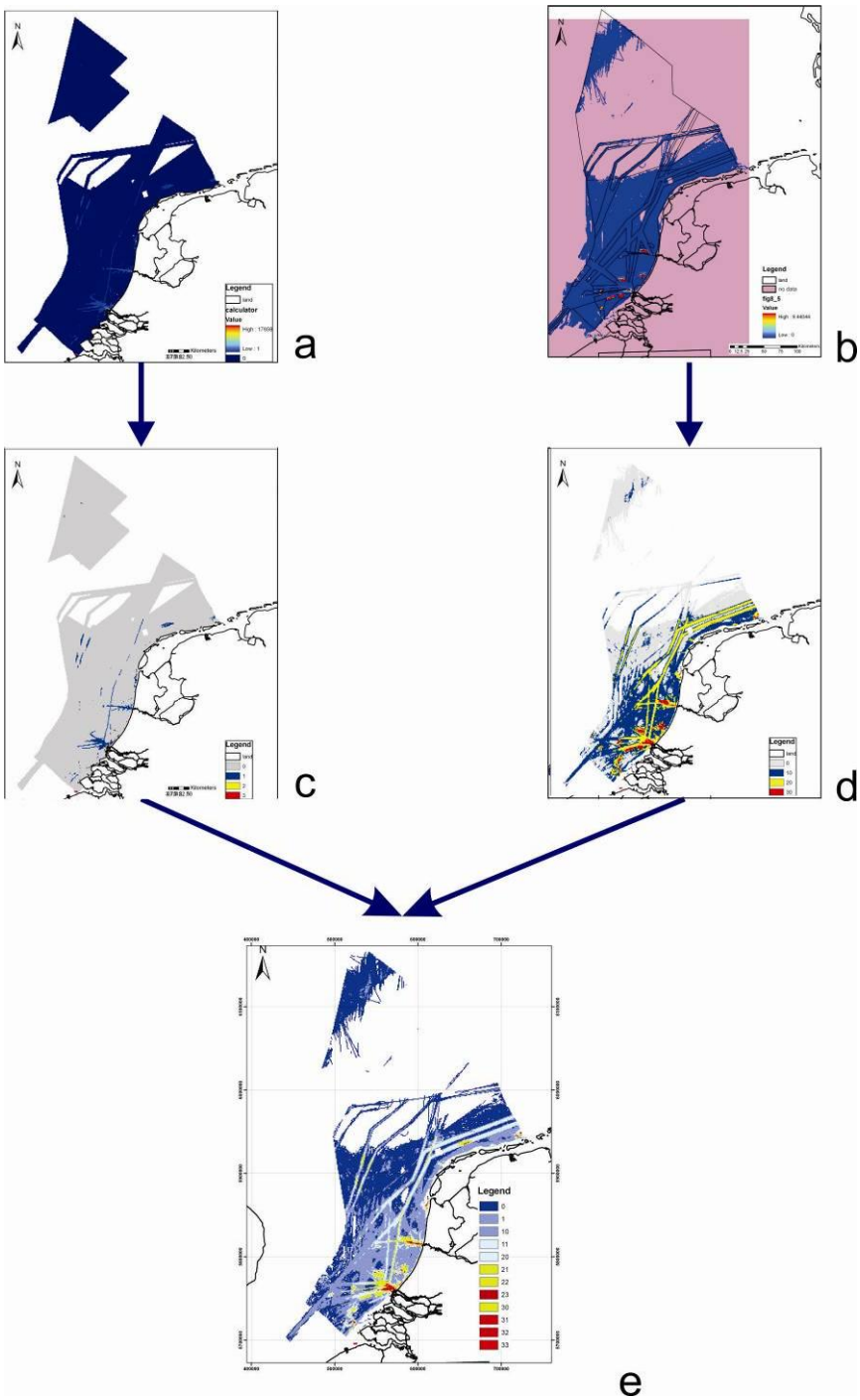

Figure 5.2 *Visualisation of the processing of the grounding danger maps into extents that cover the NCS and the combination of both grounding danger maps in the overlay method. (a) grid of regular grounding danger for mean water depth, (b) grid of object grounding danger, (c) re-classified regular grounding danger into 4 classes, (d) re-classified object grounding danger into 4 classes, and (e) overlay map of the combined grounding danger (12 classes), re-coloured for increased illustrative purposes, where blue represents low grounding danger and red high grounding danger. For illustrative purposes of the overlay method only.*

Two critical notes on combining both dangers are:

(1) Regular grounding danger and object grounding danger are not comparable when it comes to the impact of both types of grounding danger. Also, the anticipation of navigators is dissimilar: water depth is known and measured on board, thus may be anticipated. A navigator cannot anticipate in its course around unknown objects. Thus, despite equal probabilities for both types of grounding danger, object grounding forms a larger risk than regular grounding. When a risk assessment would be made (considering the consequences of grounding danger), these two dangers cannot be combined.

(2) The classification could be done later in the procedure. However, to come to a validation and a preliminary proposed re-survey policy, the classification is necessary.

5.2.2 Validation

To validate the representation of the established combined grounding danger by areas of the existing re-survey policy, the occurrence of combined grounding danger classes (Figure 5.2e) were analysed within each re-survey category for the NCS. A large range in classes of grounding danger within one category suggests that the extent of the category may be reconsidered, whereas the occurrence of merely one class of combined grounding danger indicates that the re-survey category is efficient. Obviously, identified areas of high grounding danger should be captured in a category with a high re-survey frequency and areas of low grounding danger in a category with a low re-survey frequency.

5.2.3 Prediction of grounding danger development

In the overlay for the prediction of the combined grounding danger development, we used the maps of regular grounding for mean water depth and object grounding for minimum water depth for the most recent water depths and the predicted water depths in 2011, 2015 and 2020 (Figure 4.9, Figure 4.10, Figure 4.13, Figure 4.14 and appendices 11.12 to 11.15). The same re-classification (Table 5.1) is applied to these input maps to create simplified overlay maps for the combined grounding danger for 2011, 2015 and 2020.

To reveal the change in grounding danger, the four maps in time were subtracted (Figure 5.3). This way, it is possible to define areas where the change in combined grounding danger is small (and remains in the same class), or where it shows a decrease or an increase between two subsequent surveys.

Subsequently, the combined grounding danger maps for 2011, 2015 and 2020 are compared with that of the most recent water depths in the following way:

- a comparison of the combined grounding danger map of the most recent water depths with those of 2011, 2015 and 2020 (Figure 5.3; step a, b → c),
- a re-classification of grounding danger that remains in the same class (small change), a decrease and an increase in grounding danger (Figure 5.3, step c → d), and
- an overlay of the combined grounding danger map of the most recent water depths and the maps with grounding danger increase/decrease for 2011, 2015 and 2020 (Figure 5.4, a, b → c).

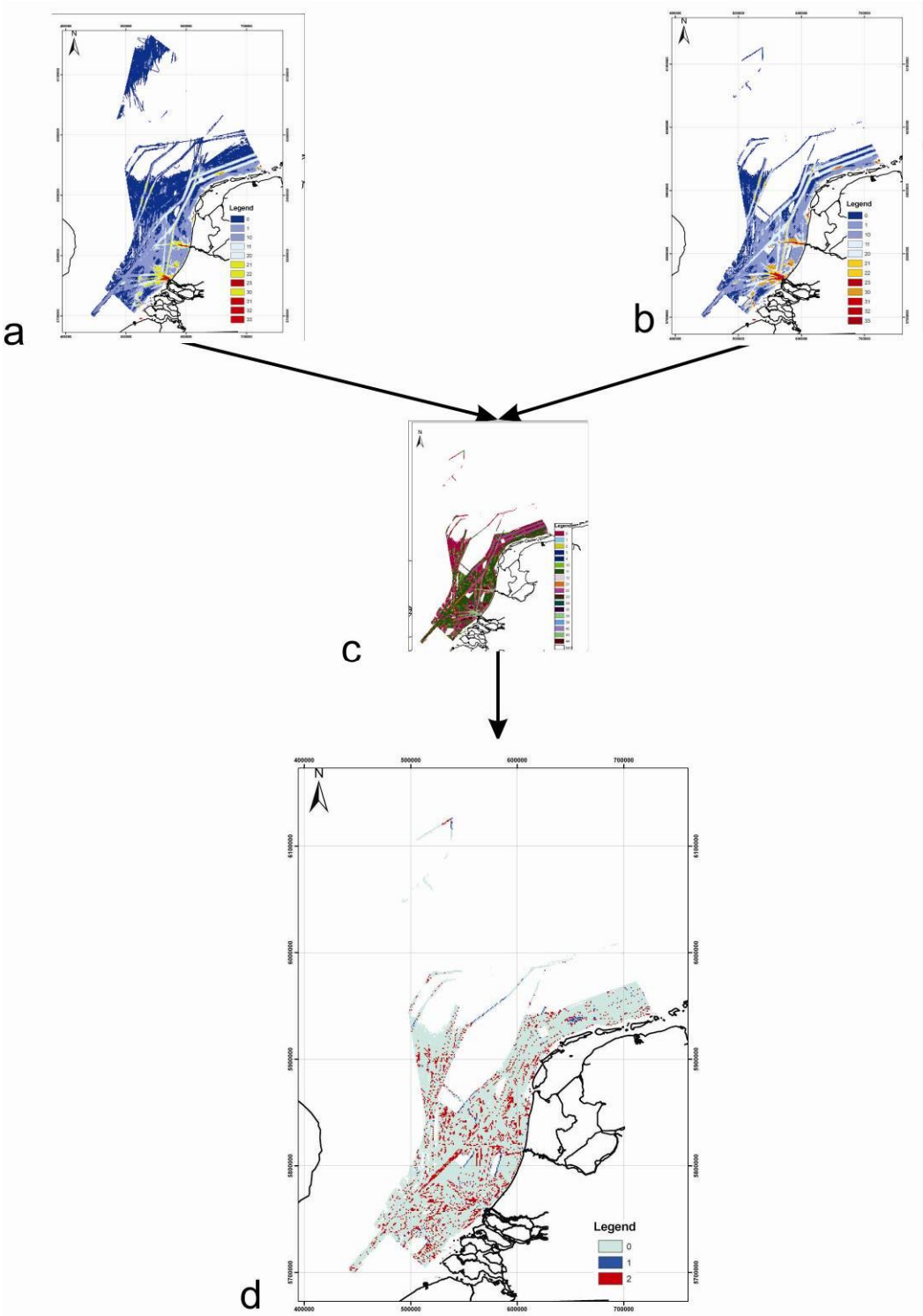

Figure 5.3 *Visualisation of the calculation of the difference in grounding danger maps of (a) combined grounding danger for most recent bathymetry, (b) combined grounding danger in 2011, (c) change in combined grounding danger between the most recent water depths and predicted water depths of 2011, and (d) a simplified version of map c. For illustrative purposes of the overlay method only*

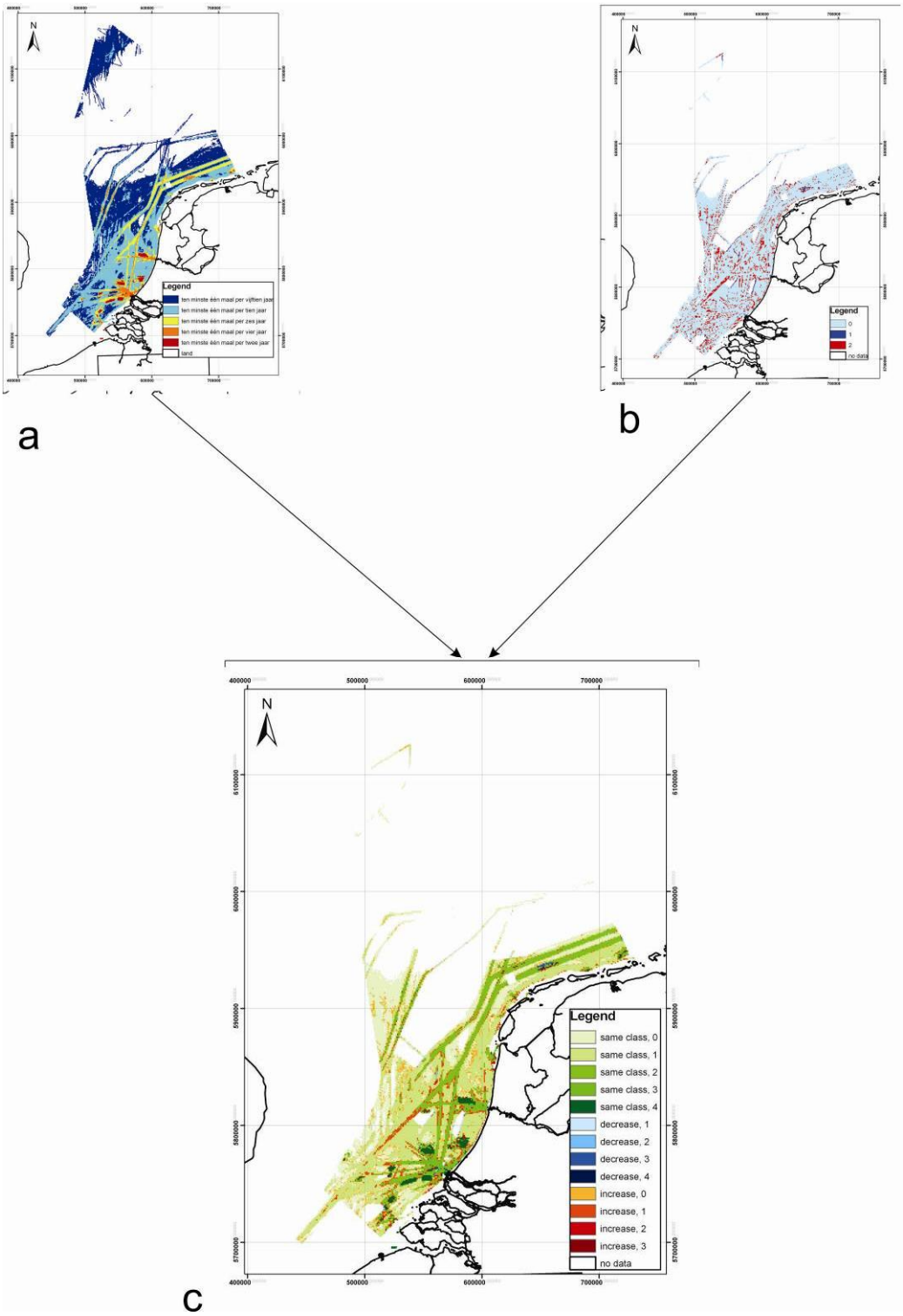

Figure 5.4 *Visualisation of the overlay of (a) grounding danger based on the most recent mean water depth and (b) the change in grounding danger between the recent water depth and predicted water depths for 2011, resulting in the overlay map (c) grounding danger development with respect to the most recent bathymetry, where green indicates that danger remains in the same class, shades of blue indicate a decrease in grounding danger and shades of red indicate an increase in grounding danger. For illustrative purposes of the overlay method only.*

5.3 Results

5.3.1 Combined grounding danger

The combined grounding danger on the NCS for the most recent water depths is presented in Figure 5.5. Combining the two re-classified maps resulted in 12 unique classes. The classes are categorised into five categories (colour codes in the legend) so that a comparison can be made with the categories of the existing hydrographic re-survey policy. A choice is made herein. For example, we give the same weight (all yellow) to the combined classes 30 (i.e. high object grounding danger, class 30, and zero regular grounding danger, class 0 in Table 5.1), 21 (moderate object grounding danger, class 20, and low regular grounding danger, class 1 in Table 5.1) and 22 (moderate object grounding danger, class 20, and moderate regular grounding danger, class 2 in Table 5.1). Decisions with regard to the choice of how to divide these classes are not final. The outcomes are therefore preliminary and may change, when acceptable dangers are established to be different from the choices made here.

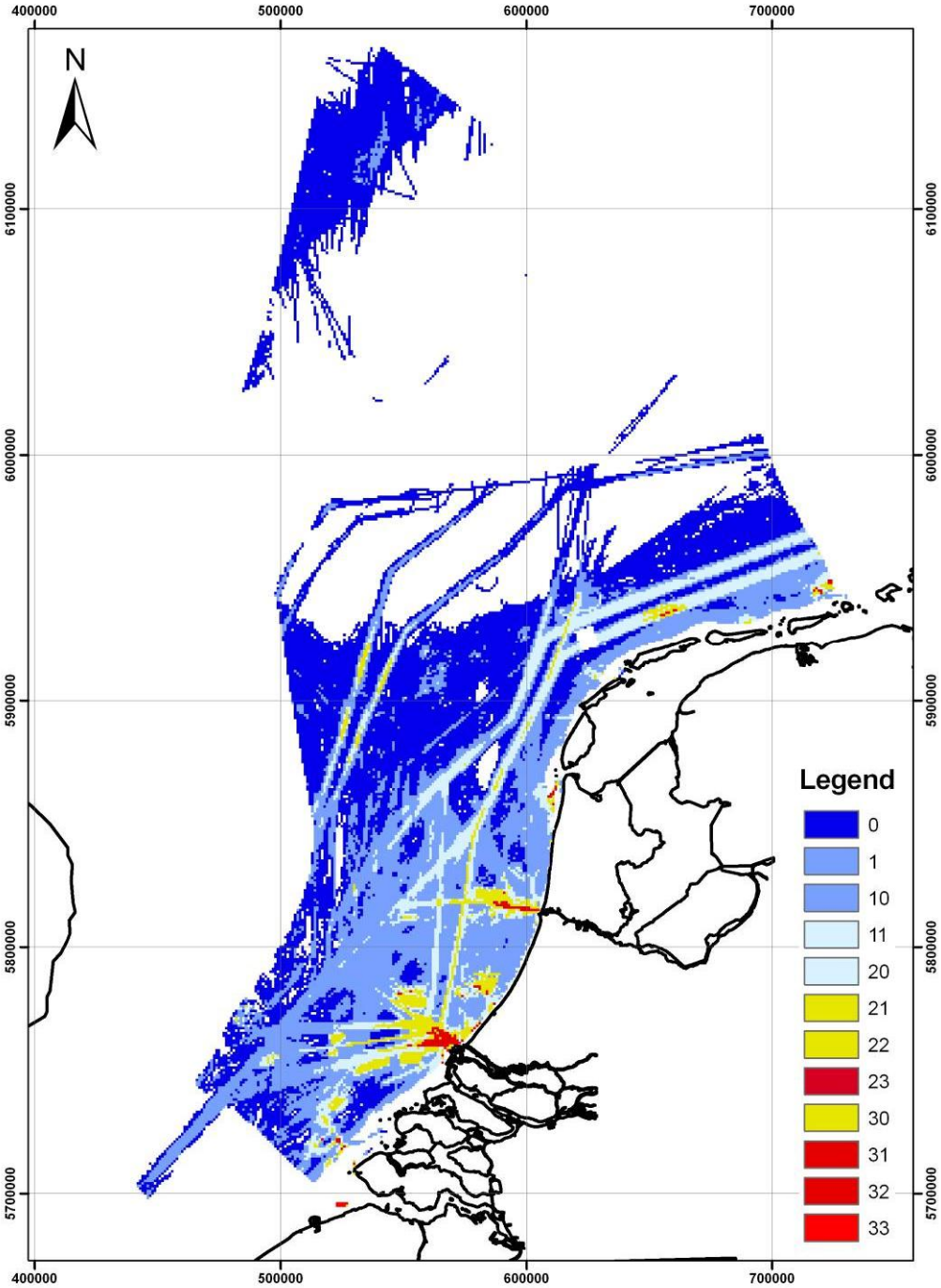

Figure 5.5 *Distribution of the combined grounding danger classes that resulted from the overlay of the regular grounding for mean water depths and the object grounding for minimum water depths. Dark blue represents a combined grounding danger of zero, shades of lighter blue represent low grounding danger, yellow represents moderate danger and shades of red represent high grounding danger. The white areas offshore indicate areas where data is absent, and near the coast where the water depth is less 10 m. These labels remain qualitative until acceptable values of grounding danger are decided upon (see text).*

On the combined grounding danger map, class 0 (no danger; dark blue in Figure 5.5) makes up 49% of the total area and is therewith largest class on the NCS. This class mostly covers the central to northern parts of the NCS, where water depths are high and shipping intensity is low, and in small zones between the north-south oriented tidal ridges (in the deep troughs). In these zones of zero grounding danger, the shipping lanes stand out with slightly higher but still low danger (light blue colour). The northward (eastern) shipping lane from Maas North TSS to Texel TSS (easting 570000, northing 5760000 to 5840000) reveals a moderate grounding danger (yellow) due to shallow water. Isolated patches of moderate grounding danger (yellow) in other parts of the traffic lanes are also due to shallow water. Closer to the ports, combined grounding danger is high (red).

The approach channels to the ports of IJmuiden and Rotterdam are recognised by moderate and high combined grounding dangers. The approach zone (the western parts) have a lower danger, mainly due to larger depths. Closer to the ports the grounding danger increases mainly due to regular grounding danger caused by shallower water depths.

The anchorage areas are also distinct with a moderate grounding danger due to objects. As explained in Chapter 4, the object grounding danger in these areas may be overestimated.

The tidal ridges in the centre of the NCS are pronounced on the combined grounding danger map due to smaller water depths compared to the surrounding area.

5.3.2 Validation of the existing re-survey policy

The comparison of the existing re-survey policy with the combined grounding danger map (Figure 5.5) reveals that the combined grounding danger classes vary within single categories. It attracts attention that, in general, the occurrence of regular grounding danger classes is smaller than the object grounding danger classes. This is indicated in the bar graphs in this section by low percentages for the classes ending on 1, 2 and 3 (see also Table 5.1).

<u>Category 1: at least once every 2 year</u>
This category includes the navigation routes where the reduced water depth is smaller than the critical water depth in equation (4.1). Figure 5.6 shows that within this category the occurrence of object grounding danger classes is high (class numbers 20 and 30 in total make up 42% of the area). The occurrence of regular grounding danger classes (ending on 1, 2 and 3) in this category is higher than in other categories (total 25%).

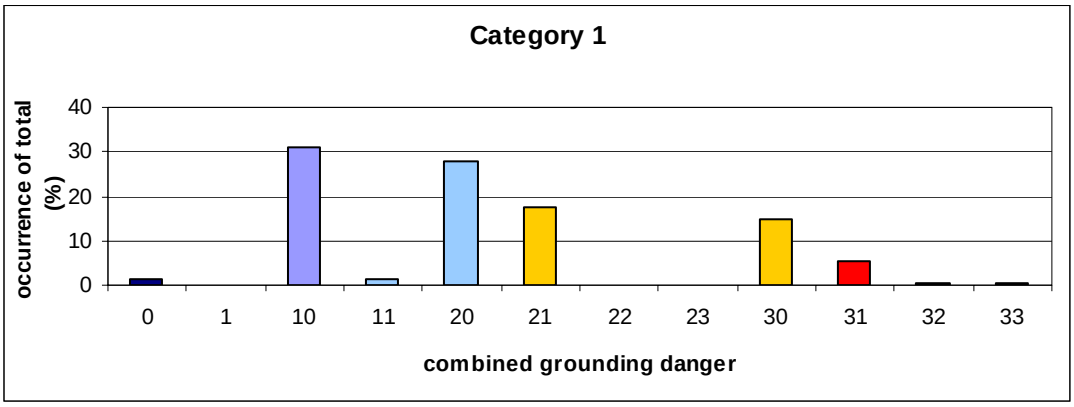

Figure 5.6 Presentation of the variation of danger classes that fall within re-surveying category 1.

The occurrence of classes of moderate and high grounding dangers and the near absence of the no-danger class (only 1% of class 0) corroborates that a high re-survey frequency is necessary. However, this category also contains a considerable amount (31%) of class 10, indicating a relatively low grounding danger. On the combined grounding danger map, these areas of low danger occur in between the traffic lanes. This category also includes anchorage areas, which show moderate grounding dangers on the combined danger map. Although the grounding danger in anchorage areas may be overestimated, a better estimate is presently not available.

Category 2: at least once every 4 years

This category includes shipping lanes that are not included in category 1, but are of importance for navigation. The main difference is that the water depths are deeper than the critical water depth. This becomes evident in Figure 5.7, where a regular grounding danger is almost absent (merely a few percent in the classes 11 an 21). Moderate grounding dangers are caused mainly by objects (33% of the cell values belong to class 20). 49% Of the cells in this category represent the combined low object grounding danger and no regular grounding danger (class 10). Category 2 also contains 14% of the class 0 (no grounding danger).

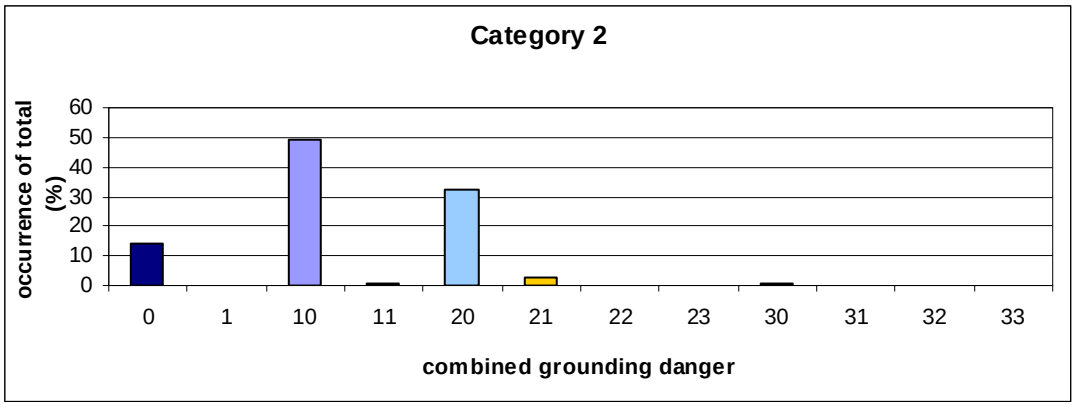

Figure 5.7 *Presentation of the variation of danger classes that fall within re-surveying category 2. Note that the scale on the y-axis is different from Figure 5.6*

The range of classes that represent no danger, low danger en moderate danger within one category suggests that the extent of this category may be optimised.

Category 3: at least once every 6 years

This category comprises areas with water depths between 10 and 30 meter with no navigation routes except the DW-route and the route towards Skagerrak. The dangers in this category are low. Class 10 (i.e. low object grounding/no regular grounding danger) occurs in 60% of the area of this category. Class 0 (no danger) occurs in 28% of the area.

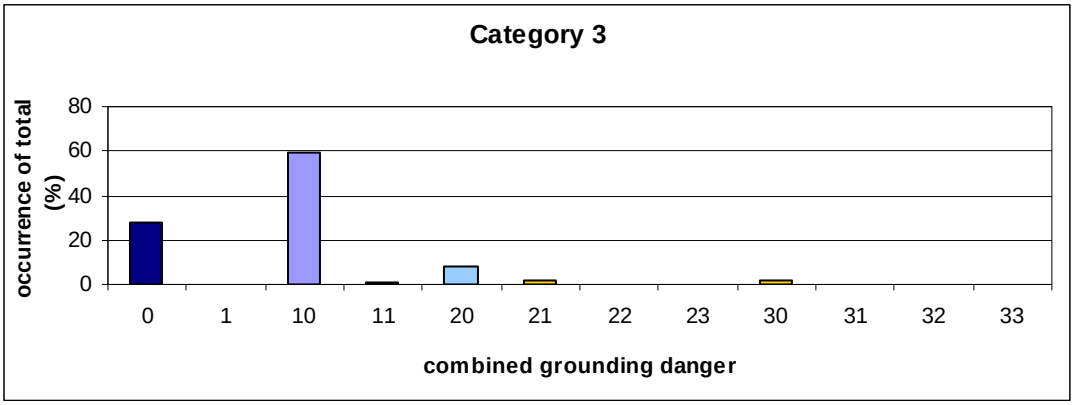

Figure 5.8 Presentation of the variation of danger classes that fall within re-surveying category 3. Note that the scale of the y-axis is different to the previous bar graphs.

The occurrence of classes within this category shows a range of no danger to moderate grounding danger, like category 2, but with more weight to the low danger end. It is thus verified that a lower re-survey frequency suffices, but ideally, areas of no danger would fall in a category of a lower re-survey frequency.
The areas that account for the moderate grounding danger in this category include the four spots in the Deep Water Route East due to the occurrence of offshore sand banks, where water depth are less than 30 m. These sand banks are presently not accounted for in the re-survey policy.

<u>Category 4: at least once every 10 years</u>
This category comprises areas shallower than 30 meter and not included in categories 1 to 3, as well as the parts of the DW-route and the route to Skagerrak that are deeper than 30 meters. In this category, 83% of the cell values indicate no grounding danger (Figure 5.9). 16% Indicates a low object grounding danger. Moderate and high grounding dangers do not occur.

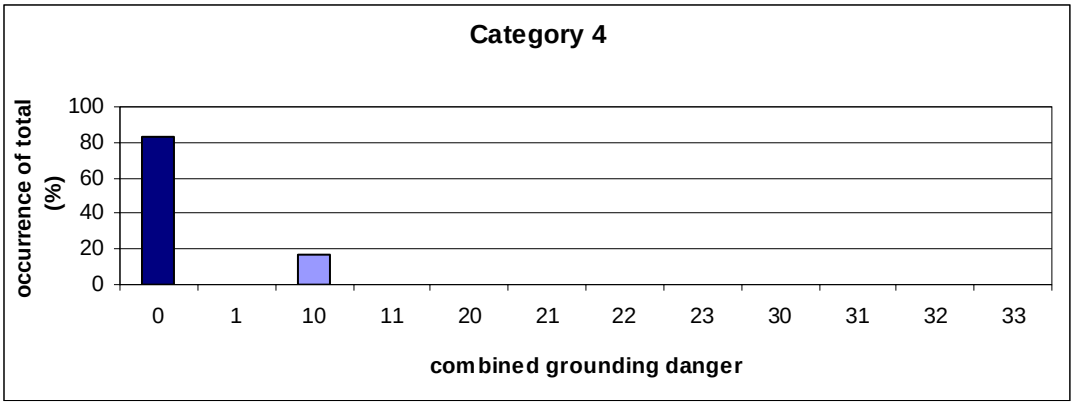

Figure 5.9 Presentation of the variation of danger classes that fall within re-surveying category 4.

This occurrence of dominantly no danger, an occurrence of 16% in low object danger and the absence of moderate and high grounding dangers imply that a category with a low re-survey frequency is indeed adequate. More, the areas of class 0 ideally fall in a category with the lowest-possible frequency.

The areas within category 4 that fall in class 10 are concentrated between the Deep Water Route East (UTM 530000, 5900000) and the North Hinder North TSS (UTM 520000, 5780000). The recognition of the north-south oriented sand banks may be surprising, since class 10 is related to object grounding danger and not regular grounding danger, but indeed Figure 4.10 exhibits a pattern that coincides with the sand banks.

Category 5: once every 15 years

This category comprises areas with water depths deeper than 30 m and no navigation routes. It corresponds nearly entirely to areas of no grounding danger (95% in class 0).

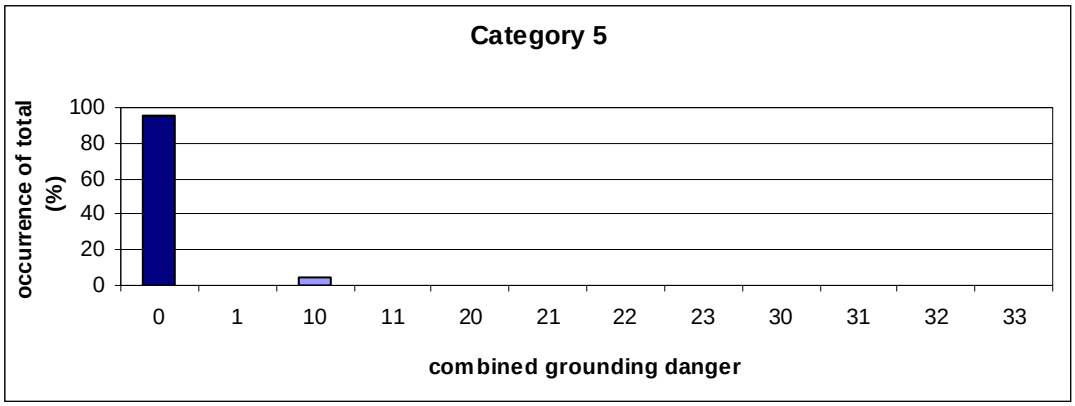

Figure 5.10 Presentation of the variation of danger classes that fall within re-surveying category 5.

It seems confirmed that a very low re-survey frequency is sufficient. Categories 4 and 5 seem alike and a distinction between surveying once in 10 or 15 years is not yet examined in this stage.

Category 6: dependent on the area, once every year to once every 4 years

Areas in this category are the responsibility of RWS Noordzee Directorate. The area covers the IJ-channel, the approach zone to the Euro-channel, the Euro-channel and the Maas-channel. Water depths are shallower here in comparison to the other categories, which results in higher regular grounding danger (higher values for classes 21 and 31 in Figure 5.11). The variations in the occurring grounding danger classes may correspond with the variations in re-survey frequencies (once per 1 – 4 years), but specifying these falls outside the scope of this research.

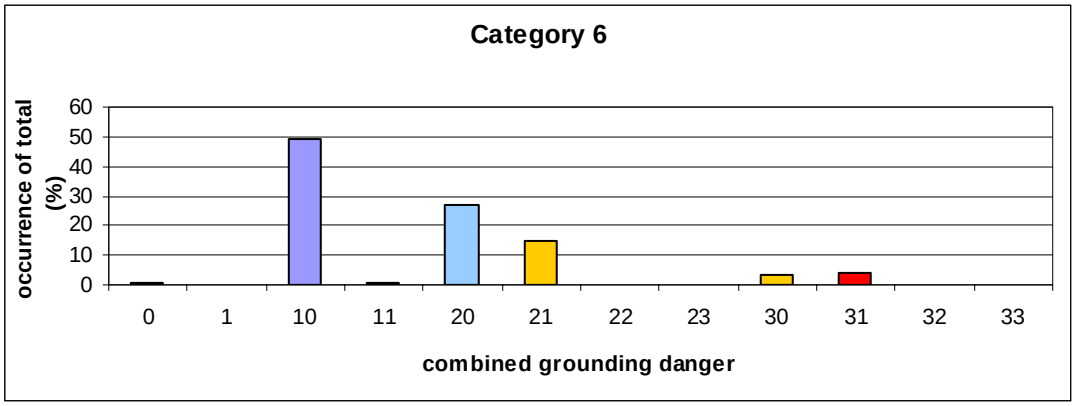

Figure 5.11 Presentation of the variation of danger classes that fall within re-surveying category 6.

Category 7: dependent on area, once every year to once every 6 years
This area covers the seabed in the coastal zone and is also the responsibility of RWS Directorates. Due to low shipping intensity in the AIS 2009 data (ships > 300GT), most grounding dangers in this area are low (class 10 = 57 %), but classes of moderate danger occur.

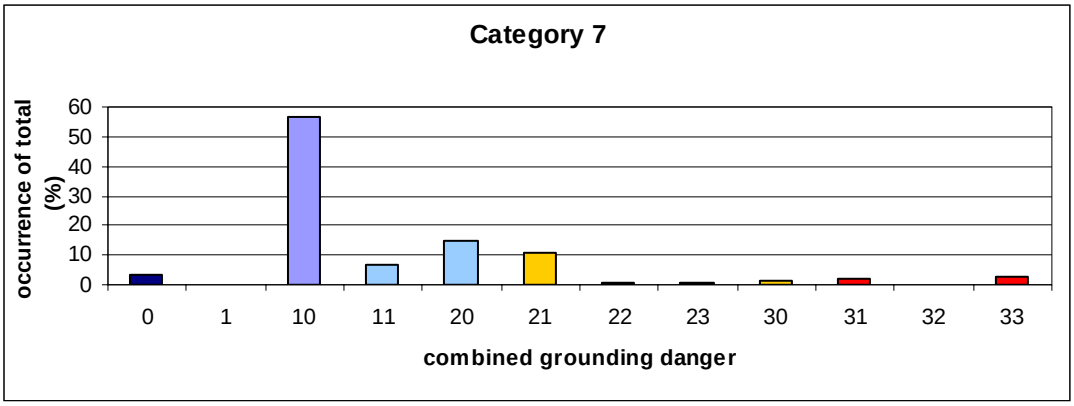

Figure 5.12 Presentation of the variation of danger classes that fall within re-surveying category 7.

The occurrence of classes in category 7 are most alike the occurrence of classes in offshore categories 3. The lowest re-survey frequency of category 7 corresponds to that of category 3. It must be noted that, although shipping intensity may be low in this area, the coastal zone is the most dynamic environment (Chapter 3). Therefore, for accurately capturing changes in water depth, frequent monitoring may be essential. Similar to category 6, specifying whether the occurrence of the classes agrees with the different re-survey frequencies that are associated to this category is not within the scope of this study.

5.3.3 Towards a refined re-survey policy

The new map of combined grounding danger for the most recent water depths exhibits distinct areas of contrasting grounding dangers (Figure 5.5). This map does not only serve the validation of the existing re-survey policy, it may also suggest refinement of the existing policy. When the 5 preliminary classes of the established combined grounding danger on the NCS (colours in Figure 5.5) are coupled to the areas of re-survey categories of the existing policy, a preliminary proposed new re-survey policy is the result (Figure 5.13). Herein, absolute re-survey frequencies have not yet been associated to the categories. A way to associate the categories to re-survey frequencies is proposed in section 5.3.4.

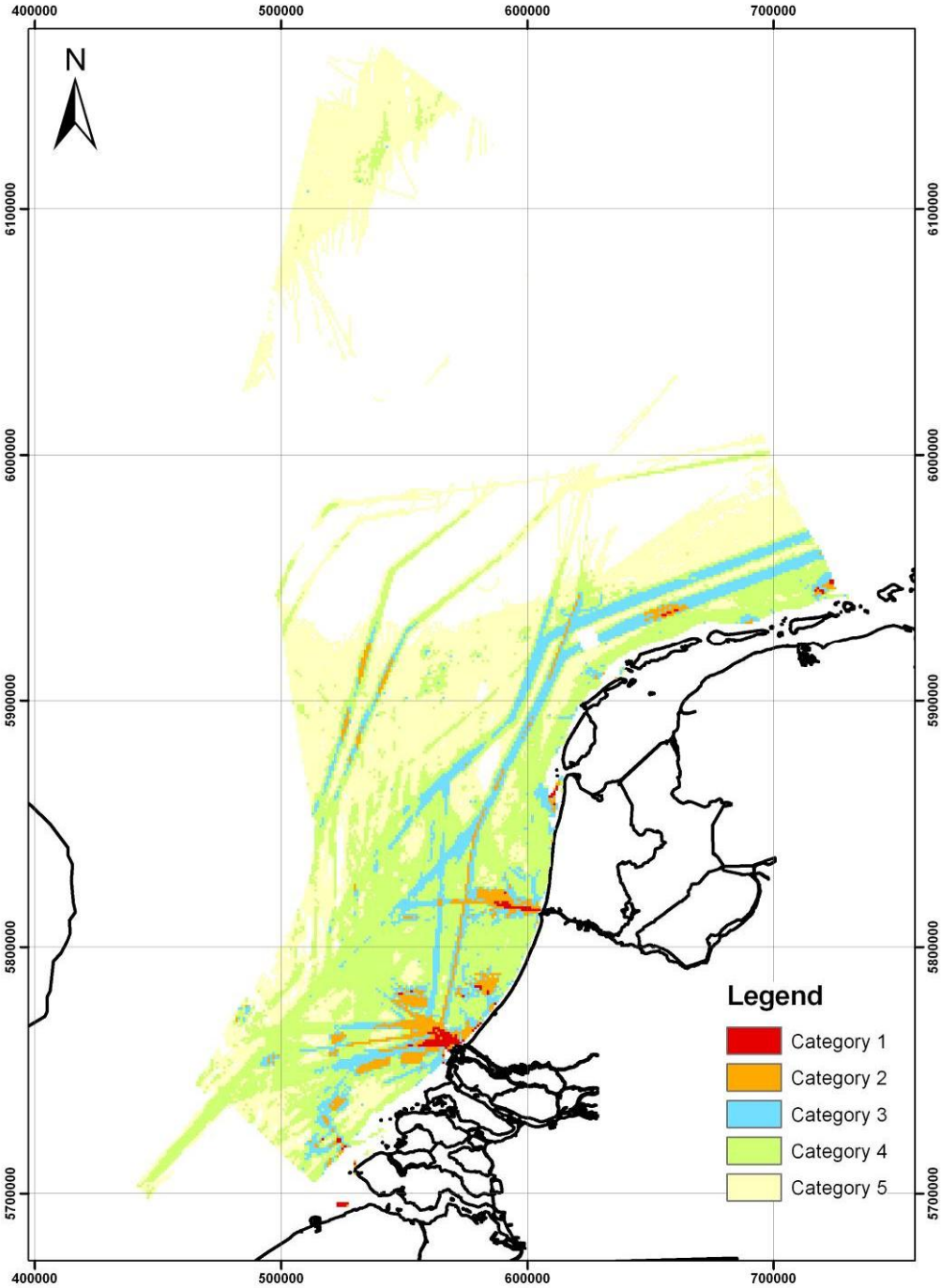

Figure 5.13 *Preliminary proposed new re-survey policy, based on the combined grounding danger on the NCS. Colours correspond to the existing policy in Figure 1.1. The 5 categories are based on the choices of low, moderate and high danger categories in Figure 5.5 that were preliminary made (see also Table 5.1). When different decisions are made on what absolute levels of grounding danger are acceptable, the outcome of this new policy may change. A way to associate the categories to absolute re-survey frequencies is proposed in the following section.*

Firstly, it should be pointed out that the areas may have received a different category compared to the existing policy. For instance, areas in CAT 2 in the existing policy are now in CAT 3, and areas in CAT 3 in existing policy are now in CAT 4. This is a consequence of the choices of the categorisation of the 12 classes; if this were chosen differently, categories would be labelled differently.

A first observation of the preliminary new re-survey map is that is shows good agreement with the existing policy. The existing policy has categories that correspond very well to the distribution of quantified combined dangers in this research. Examples are the discrimination of shipping lanes, approach channels to ports and the distinction between zones of 10 - 30 m water depth and >30 m depth. Also, the small patch of category 1 north of Terschelling in the existing policy is identified on the combined grounding danger map as moderate to high danger (surrounded by low-danger areas).

A second observation is that also some differences are revealed. Main differences with the existing survey policy are:
- 4 spots in the Deep Water Route East appear in this new map, suggesting that here re-survey frequencies should be increased.
- The northward lane from Maas North TSS to Texel TSS should be in a category with a higher frequency than the southward lane.
- The combined grounding danger in the North Hinder North TSS fades out into deeper water (towards southwest). In the existing policy, the entire TSS falls within category 2 (once per 4 years). The new grounding danger map suggests that at this TSS may be divided into categories.

Minor differences are not all described.

5.3.4 Predicted grounding danger development

In the previous sections, ‘static’ comparisons were made between the combined grounding dangers based on regular grounding for mean water depths and object grounding for minimal water depths on the one hand, and the existing re-survey policy on the other hand. Also, the existing categories with associated frequencies were used as a basis. The validation of the categories with occurrences of danger classes is therefore not yet labelled with a temporal component (e.g. every four years, every 6 years or why not every five or eight years). In this section, we compare the predicted grounding dangers for the scenarios that the NCS is not being surveyed for periods of 1, 5 and 10 years.

The predicted grounding danger development is presented in Figure 5.14, Figure 5.15 and Figure 5.16. Herein, areas are visible where for the years 2011, 2015 and 2020 an increase, decrease or equal danger is calculated with respect to the grounding danger calculated for 2010. Although the water depths were predicted using a linear extrapolation of the vertical dynamic trend (Chapter 3), the grounding danger development is not linear. Namely, firstly for regular grounding, for as long as the actual water depth is larger than the critical water depth (equation (4.1)), the grounding probability is zero. However, when the water depth becomes less than the critical water depth, the probability may increase steeply and suddenly. Secondly, the used relation for object grounding due to new obstructions was given in Chapter 4. By knowing this future development, one can determine what temporal label (i.e. re-survey frequency) could be given to the established categories.

Seven areas of prominent changes, or absence of changes, are described in the text below the three maps and are indicated in Figure 5.16.

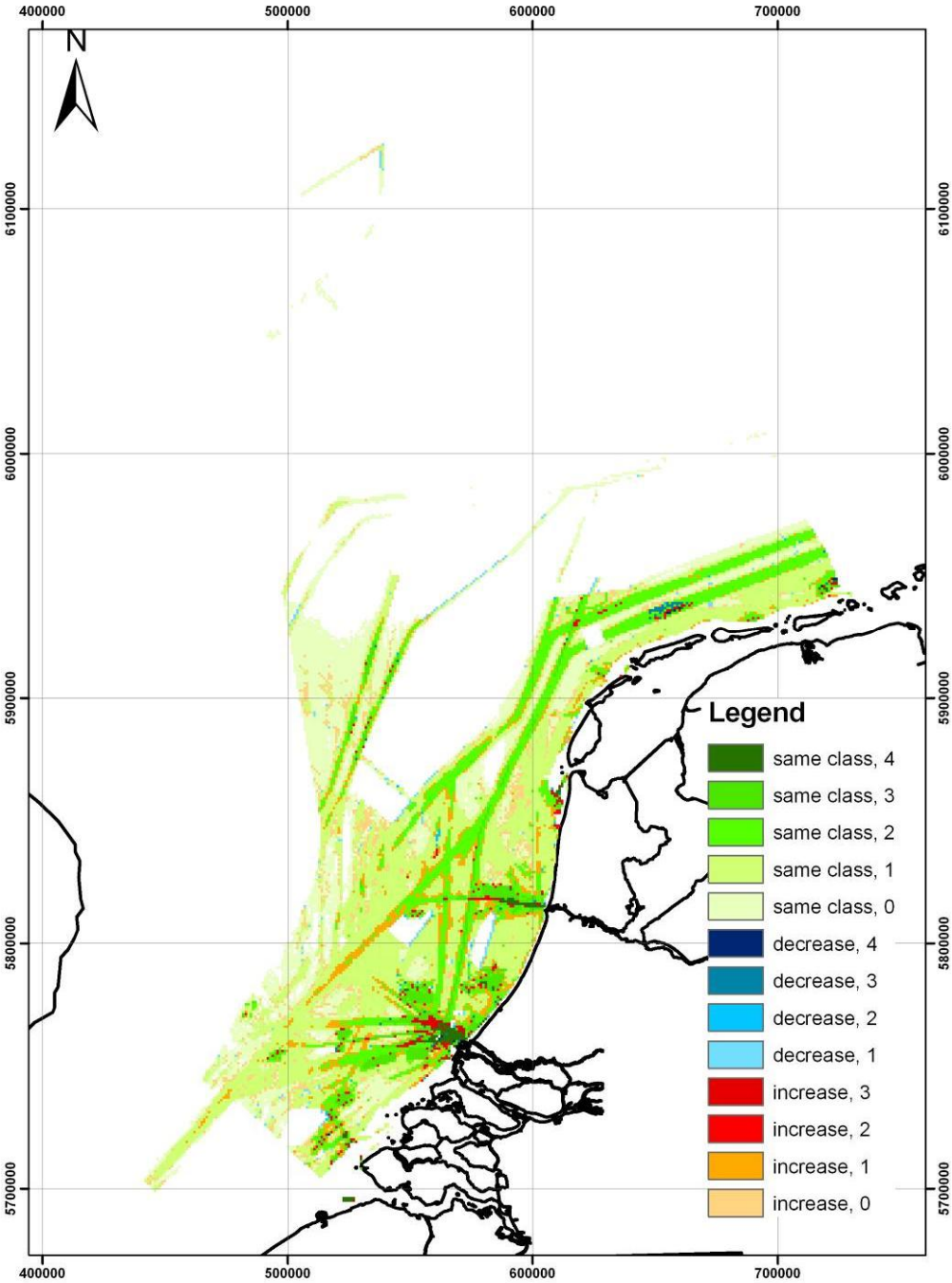

Figure 5.14 *Changes in combined grounding danger between those calculated for 2010 and the predicted grounding danger for 2011. Shades of green indicate that the grounding danger remains in the same class, shades of blue indicate a decrease in danger, and the shades of red indicate in increase in danger. The numbers in the legend are an indication of the danger level for the most recent water depths (0 is no danger; 4 is a high danger).Decreases in grounding danger are uncommon (see text).*

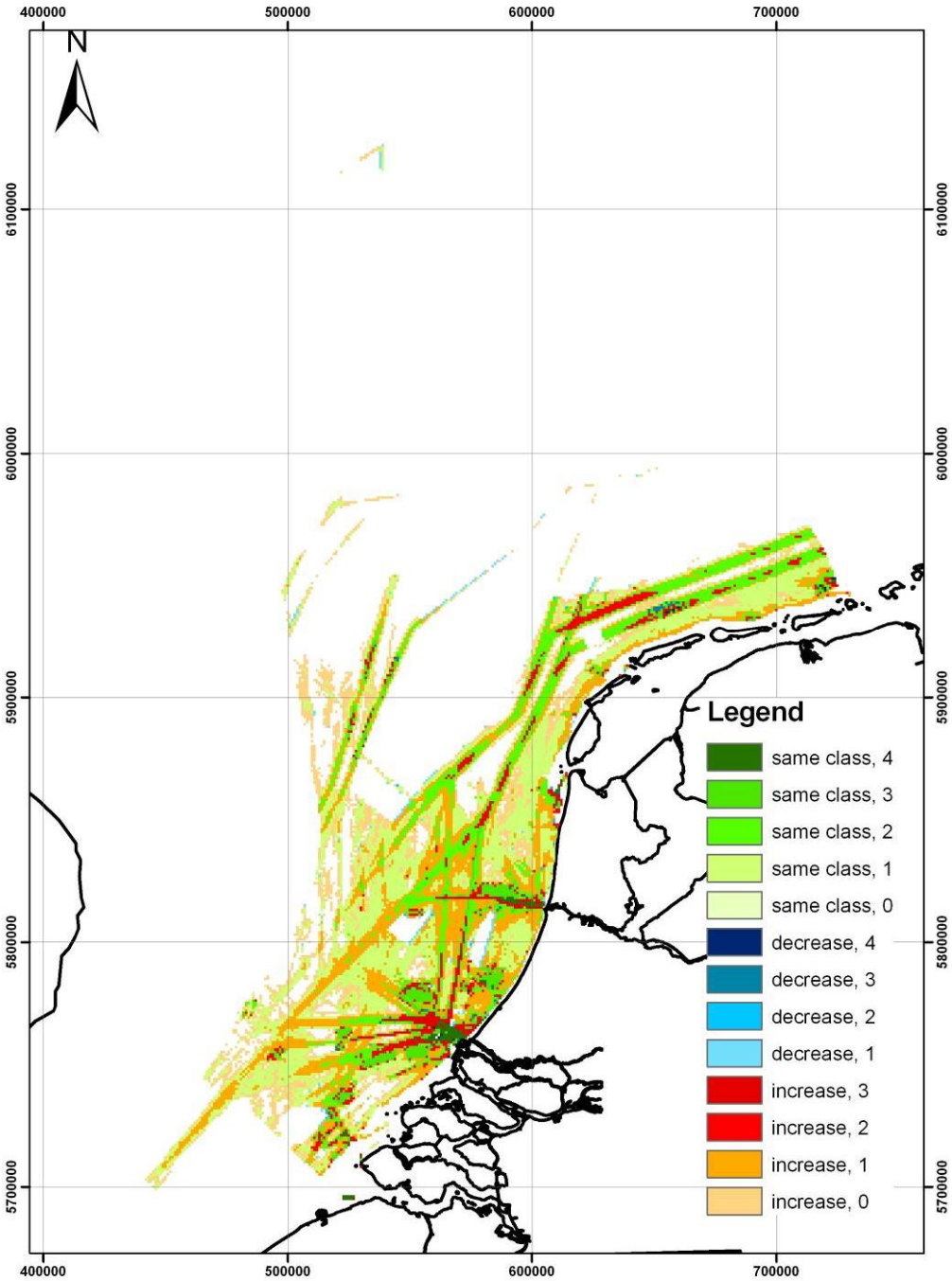

Figure 5.15 *Changes in combined grounding danger between those calculated for 2010 and the predicted grounding danger for 2015. Shades of green indicate that the grounding danger remains in the same class, shades of blue indicate a decrease in danger, and the shades of red indicate in increase in danger. The numbers in the legend are an indication of the danger level for the most recent water depths (0 is no danger; 4 is a high danger). Decreases in grounding danger are uncommon (see text).*

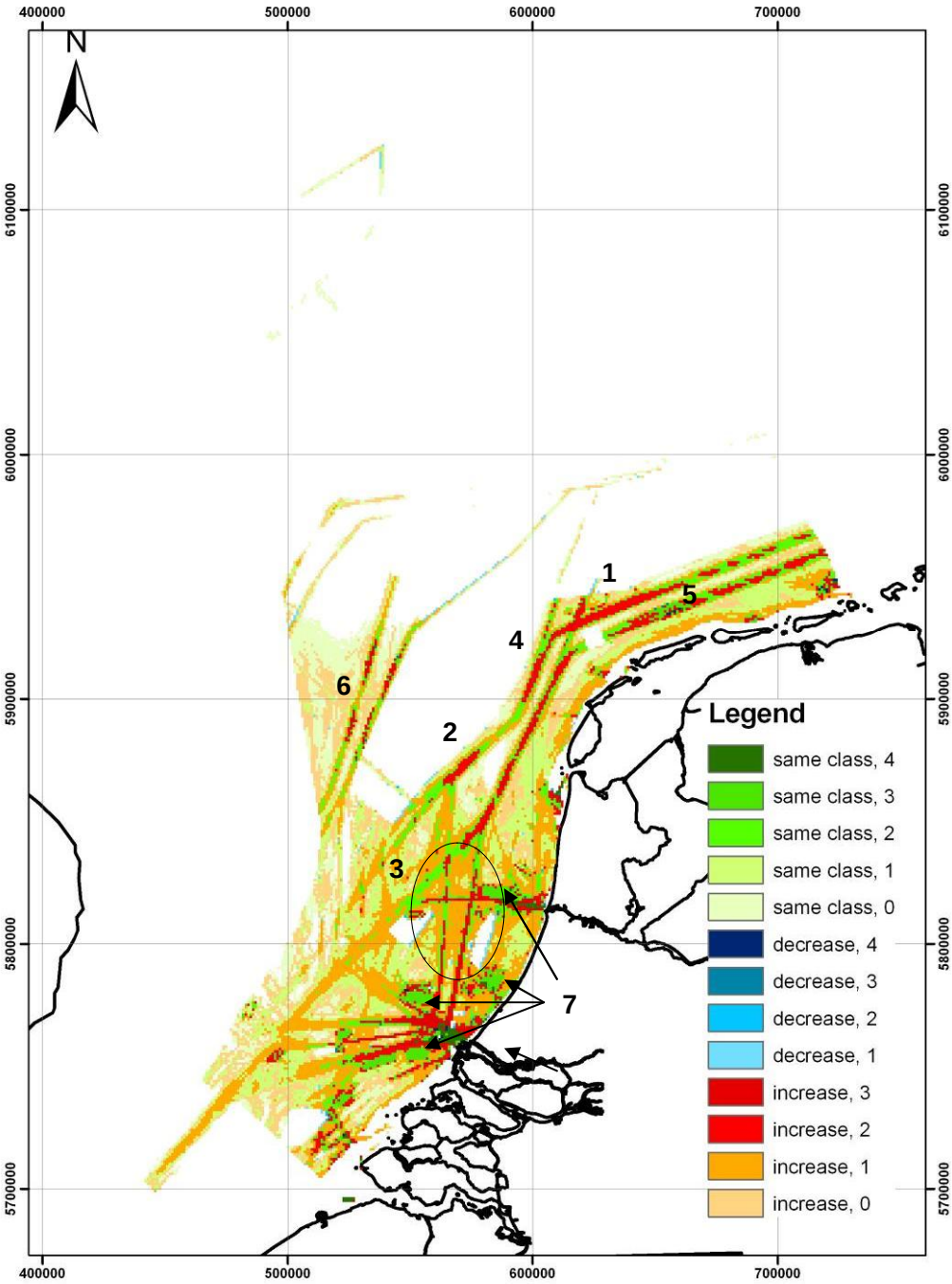

Figure 5.16 *Changes in combined grounding danger between those calculated for 2010 and the predicted grounding danger for 2020. Shades of green indicate that the grounding danger remains in the same class, shades of blue indicate a decrease in danger, and the shades of red indicate in increase in danger. The numbers in the legend are an indication of the danger level for the most recent water depths (0 is no danger; 4 is a high danger). Decreases in grounding danger are uncommon (see text). The numbers in the map indicate areas discussed in the text.*

In the grounding danger development until 2011, changes between the combined grounding danger calculated for 2010 and the predicted grounding danger for 2011, are small.
In general, decreases in grounding danger are uncommon, because object grounding danger always increases in time (the probability of new objects increases). At the sites where a decrease occurs, this is explained when the increase in depth sufficiently reduces the regular grounding danger to also lower the combined danger. Since the predicted grounding dangers are based on water depth predictions by linear extrapolation of the vertical dynamic trend, these predictions cannot be used for the estimation of grounding danger indefinitely (see section 3.2.3).

Between 2011 and 2015, the predicted moderate grounding danger in area 1 (north of Vlieland/Terschelling) has increased. This is also the case for areas 2, north-east of 3, 4 and in the approach channels to Rotterdam. The shipping lane from Rotterdam to IJmuiden shows an increase in danger. Area 5 of moderate to high grounding danger first shows a decrease until 2011, due to an increase in depth, followed by an increase between 2011 and 2015, when object grounding has increased. Area 3 also shows an increase (larger parts become orange), but is relatively less urgent. Remarkably, area 6, in which 4 spots of moderate grounding danger were identified that were not accounted for in the existing survey policy, does not significantly increase in the grounding danger development to 2015. This is because the predicted change in water depth is small (see Figure 3.25 and Figure 3.26).

Between 2015 and 2020, areas 1, 2, north-east of 3, 4, 5 and the approach channels to ports all show an increase in grounding danger. Area 3 steadily increases. The shipping lane from Rotterdam to IJmuiden shows an increase in grounding danger. The four spots in area 6 have increased by 2020. The anchorage areas (areas 7) remain in the same grounding danger class until 2020.

Temporal labels, associated with the new categories and presented here, are neither exact (e.g. distinction with 1 year accuracy) nor final. This is because *(i)* the exact decrease or increase in grounding danger is not displayed in the generalised classes (i.e. small changes may remain within one danger class, whereas even smaller changes may be sufficient to become a higher danger class and thus result in an increase in Figure 3.16), *(ii)* the prediction is only performed for 3 selected periods (1, 5, and 10 years), and *(iii)* absolute levels by which classes of the combined grounding danger map were defined, are not definite. Refining the prediction of grounding danger development is described in the recommendations in Chapter 6.

The development in grounding danger may be spotlighted per category of the existing re-survey policy of the NLHO. For example, the grounding danger development between 2010 and 2011 is of importance for the resurveying frequency of category 1 (once every two years). Similarly, changes in grounding danger between 2010 and 2015 are relevant for the categories 2 (once every 4 years) and 3 (once every six years). Lastly, changes in danger between 2010 and 2020 are relevant the categories once every 10 years and once every 15 years. Figure 5.17 displays the results for the example of category 4, once every 10 years. These results give a clear view in the future development in grounding danger per category and can be used in the design protocol of a new re-survey policy.

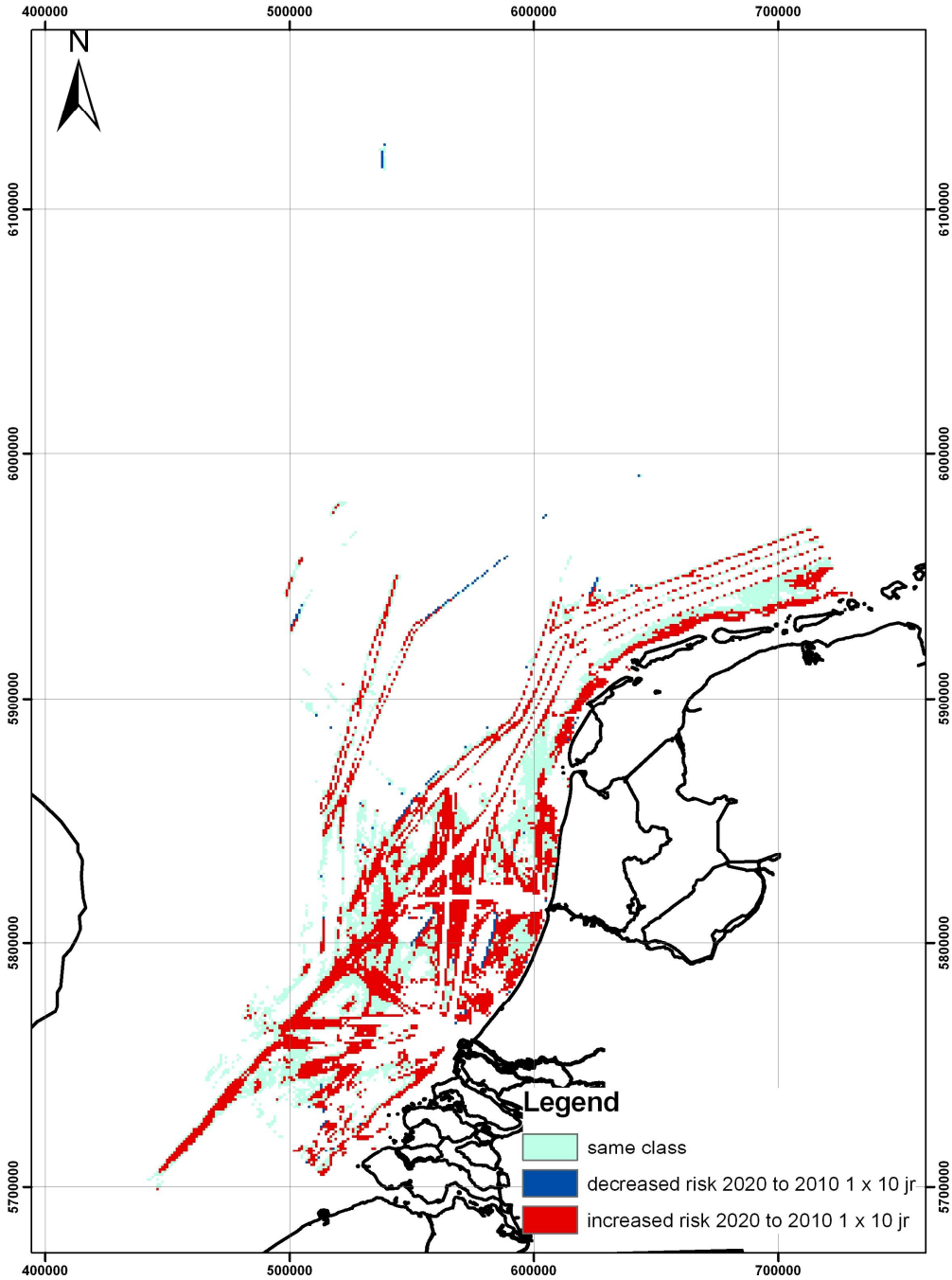

Figure 5.17 *Changes in grounding danger for the predicted water depths for 2020 with respect to those of the most recent measurements for the category once every 10 years (i.e. in the new survey policy of Figure 5.13). White indicates other categories. Areas with small changes (light blue), a decrease (blue) and an increase (red) are visible.*

5.4 Conclusions

The new overlay-map of the quantitative combined grounding danger reveals the variation in levels of grounding danger for the NCS due to both water depth and the occurrence of unknown obstructions at the seabed. Coupling this map to the existing categories of the re-survey policy of the NLHO, which was designed to cover the levels of combined grounding danger on the NCS, shows a remarkable agreement between the extent of the categories and the distribution of the grounding danger.

The validation of the existing categories brings out the inconsistent grouping of areas with a variable combined grounding danger. This analysis also identifies areas where grounding danger is moderate to high that are presently not accounted for in the re-survey policy. Moreover, the validation confirms areas of low grounding danger.
The occurrence of grounding danger classes per category shows that categories 1, 2 and 3 contain a large variation of grounding danger levels, and thus could be optimised by sub-dividing categories or by re-arrangement of the extents of the categories. It is confirmed that categories 4 and 5 contain a low to zero variation in danger levels. Categories 6 and 7 both show a larger variation, which corresponds to differences in re-surveying frequencies defined in these categories. These two latter categories fall outside the aims of this study.

The presentation of the variation in rounding danger classes within one category is quantitative in the way that the percentages of cells of the NCS-grid are given, but remains qualitative in the validation of the re-survey frequencies associated to existing categories. The predicted grounding danger development on the NCS when not being surveyed for periods of 1, 5 and 10 years since the last survey, allows for the labelling of a temporal component to the new categories.
An area of relatively high danger that may deserve extra attention (based on the combined danger map for the most recent survey) comprises the four spots in the Deep Water Route East, where sand banks occur. Based on the grounding danger development until 2020, dangers in the Texel TSS and Vlieland TSS have increased before 2015 north of Vlieland and Terschelling and by the year 2020 also west of Den Helder.

Areas of low danger are confirmed and may be expanded in the zones *(a)* between the Deep Water Route East and the TSS North Hinder North to Texel TSS and north of 53ºN latitude (based on Figure 5.5 only), and *(b)* west of the Deep Water Route East and north of the 53ºN latitude.

It must be stated that this chapter mostly presents the validation and steps towards a protocol of how to optimise the existing re-survey policy. The results presented here are not final results, because the classification of the combined grounding danger map remains preliminary. A digital environment for the optimisation of a re-survey policy was developed in this project, so that adjusting the classifications will be a relatively quick action.

6 Overall conclusions

In order to validate and optimise the existing re-survey policy of the Netherlands Hydrographic Office (NLHO), Royal Netherlands Navy, the quantification of seabed morphodynamics and the calculation of grounding dangers due to water depth variations and the occurrence of unknown objects at the seabed are essential. These two factors are combined in an overlay method and compared to the existing categories in the re-survey policy of the NLHO for the validation of the policy. The new map of combined grounding danger and the occurrence of the variation of danger classes per category, present possibilities for refining and optimising the existing policy. Predicted grounding danger for 1, 5 and 10 years without surveying, allow for the labelling of categories with a temporal component.

6.1 Quantitative seabed morphodynamics (Objective 1)

For the analysis of sea bed morphodynamics, all data that is contained in the NLHO's Bathymetric Archive System (BAS) were used, including digitised fair sheets. In this research, Deltares developed a method for the quantification of the vertical seabed dynamics (in meters per year) on nodes of a grid with a resolution of 25 x 25 m for the entire Netherlands Continental Shelf. The vertical nodal dynamics map (Figure 3.9) is the main result of this part of the project. This map provides the first overview of seabed dynamics of the Netherlands Continental Shelf. It shows that the coastal zone is particularly dynamic, with common absolute rates of bathymetric change of 0.1 to 0.35 m/yr and with extremes up to 1.5 m/yr. Offshore, vertical sea bed dynamics are lower. Here, absolute values typically range from 0 to 0.1 m/yr, with extremes of 0.3 m/yr in the sand wave fields. Three offshore zones of high dynamics were identified: *(i)* a field of long bed waves north of Texel and Vlieland due to bedform migration, *(ii)* a sand wave field west of Texel due to bedform migration and *(iii)* the main part of the Southern Bight where mobile bedforms occur.

Detailed studies at selected sites were carried out, using a spectral method previously developed at Deltares. These local studies specify the changes in length and height and the migration rates of sand waves and other rhythmic bedforms in the North Sea. It was revealed that *(i)* the increase in sand wave height, and thereby decrease in water depth, are significant in several of the selected research sites (North Hinder South TSS, offshore Rotterdam and on sand banks) and were observed to be up to 2 m in several years, and *(ii)* average migration rates of offshore sand waves commonly range between 0 – 5 m/yr, except in the more dynamic field west of Texel, where an average migration rate of 19 m/yr occurs. The average migration rate of the long bed waves north of Texel and Vlieland is 12.4 m/yr. The increase in the height of sand waves and their migration onto sand banks elevates the crests of these sand banks.

Areas of low seabed dynamics are *(i)* the deep water routes north of 53ºN, *(ii)* north of the Wadden island of Terschelling, Ameland and Schiermonnikoog, *(iii)* a northwest-southeast oriented zone offshore Noord-Holland, and *(iv)* small patches offshore Zuid-Holland and Zeeland, see Figure 3.9.

Factors such as the impact of storms remain an uncertain aspect in seabed morphodynamics. The sand wave modelling presented in this report, uses an idealised, process-based morphodynamic model, that relates the sand wave growth and migration to environmental conditions, such as water depth, tidal current velocity and grain size. The model also calculates the effect of the height of wind-induced surface waves on the sand wave

behaviour. The sand wave modelling shows that an increase in the height of wind-induced surface waves lowers the sand wave height and increases their migration rate. It was also shown that surface wave direction can alter the migration direction. Of 5 selected sites, those sites deeper than 30 m – as to be expected – were found to be less affected by surface waves. Except for one site far offshore, sand wave heights decrease with increasing surface wave height. This suggests that the impact of storms will not endanger shipping safety. In all 5 locations, sand wave migration rates increased with increasing surface wave height. In the modelling results, the largest increases were found at the sites in the north of the Southern Bight and smaller increases in the south. The current version of the model overestimates sand wave heights, so that the outcomes of the model may be used merely in a qualitative way.

6.2 Quantitative grounding danger (Objective 2)

Grounding probabilities were calculated on a resolution of 1 x 1 km for two types of grounding: (1) regular grounding, due to limited water depth, and (2) object grounding, due to unknown obstructions at the seabed. In the latter case, the probability of unknown obstructions is based on the occurrence of known obstructions, using NLHO's database.

(1) Regular grounding danger is highest in the approaches of the ports of IJmuiden and Rotterdam and the southern approach to the Western Scheldt. The grounding danger in these areas may reach the level at which 10000 ships during 262800 observations per year per grid cell have a grounding danger. It does not mean that these ships will ground, because this value is a *maximum* estimate, taking into account the under keel clearance, an extra safety margin of 2 m, the safe upper value for the draught (cut off value +1), using the LAT reduction level and ignoring the additional water column of the tide. Also, the variation in water depth within a 1 by 1 km cell overvalues the danger near the edges of shipping lanes that are deeper than their surroundings. A more realistic grounding danger is calculated by leaving out the under keel clearance and extra safety margin, resulting in 30 to 300 ships per year that have a grounding danger. Some localised offshore areas have moderate grounding dangers (100 ships per cell per year). Unexpected areas of moderate grounding danger were identified in this study in the Deep Water Route East, due to locally shallow water above sand banks, the occurrence of relatively large ships and a high shipping density.

(2) Object grounding danger is more related to the traffic density, thus the danger map displays moderate to high dangers in the traffic lanes. Levels reach 0.0001 to 0.01 ships per year with a grounding danger in the offshore traffic lanes, with higher levels in the approach channels to the ports, of up to 0.1 ships per year. The highest object grounding danger occurs in the anchorage areas (up to 10 ships per cell per year), but with the assumptions we had to make in this study, the absolute levels of danger in anchorage areas are uncertain.

Regular grounding danger was calculated to be zero in the largest part of the Netherlands Continental Shelf, except for those areas mentioned. Object grounding danger is only zero in the deep parts of Dutch North Sea where traffic densities are low and where the water depth always exceeds the critical water depth above unknown obstructions.

Predictions of the future development of grounding dangers facilitate the design of a new re-survey policy (sections 6.3 and 6.4). These predictions of grounding danger, both regular grounding and object grounding, were based on predicted water depths for 2011, 2015 and 2020, which were calculated by linear extrapolation of the vertical dynamic trend (Chapter 3). These predictions of grounding danger show the same distribution of grounding danger as described in the two points above, but with an increase in time, because object grounding danger always increases due to a higher probable number of new objects in time.

6.3 Validation and optimisation of the existing re-survey policy of the NLHO (Objective 3)

For the validation of the existing re-survey policy of the NLHO, we combined the distributions of regular grounding danger and object grounding danger. For the comparison of the combined grounding danger to the areas of re-survey categories of the existing re-survey policy, it was necessary to generalise the grounding dangers into classes. The occurrence of different grounding danger classes per re-survey category on the NCS (bar graphs in section 5.3.2) brings out the inconsistent grouping of areas with a variable combined grounding danger. From this, suggestions for the refinement and optimisation of the existing policy are made. The predicted grounding danger development for different periods without surveying allows for the labelling of a temporal component to the new categories.

The existing policy for the parts of the Netherlands Continental Shelf deeper than the 10 m isobath (categories 1 - 5) shows a remarkable agreement between the extent of the categories and the distribution of the combined grounding danger. Merely a few locations of moderate to high grounding danger were found in this study that are presently not accounted for in the existing policy. Categories with high re-survey frequencies (categories 1, 2 and 3) contain a large variation of grounding danger levels, and thus could be optimised by sub-dividing categories or by re-arrangement of the extents of the categories. Moreover, the validation confirms areas of low grounding danger at the NCS and that categories 4 and 5 contain a low variation in danger levels.

Areas deeper than the 10 m isobath that are identified in this study to be of moderate to high danger and that are not covered by frequent surveying in the existing policy, are:

- The four unexpected spots in the Deep Water Route East, where sand banks occur. The development of danger in these spots, is not rapid, due to low vertical dynamics in this area, but does show an increase of the danger by 2020. The sand wave modelling at a site in the vicinity of these spots, suggests that, in exception to other sites, both sand wave heights and migration rates may increase when surface wave heights increase. Thus storms may be an unpredictable factor at this location.
- The long bed wave area north of Texel and Vlieland and the sand wave field west of Texel show high vertical seabed dynamics and high migration rates of bedforms. These sites were not included in the sand wave modelling. The combined danger map reveals low dangers at these sites. However, based on the grounding danger development until 2020, dangers in the Texel TSS and Vlieland TSS north of Vlieland and Terschelling will increase before 2015 and locally west of Den Helder by the year 2020.
- Detailed studies based on observations of sand waves revealed the growth of sand waves, resulting in crest elevation and thus in decreasing water depths (e.g. North Hinder South TSS, offshore Rotterdam and on some offshore sand banks). These areas were not distinct on the vertical nodal dynamics map. These findings at selected, local sites suggest that, presently, other sites of sand wave growth and/or crest elevation may have remained unidentified. The grounding danger development predicts a danger increase in the approach channel to Rotterdam (southern lane of the Maas West Inner TSS) in 2015 and 2020 (Figure 5.15 and Figure 5.16, respectively).
- All anchorage areas exhibit a moderate combined grounding danger, based on the analysis of past observations, and remain moderate in the predictions. Apart from the possible overestimation due to assumptions made in this study, the extents of the danger areas are larger in this study than those in the existing re-survey policy of 2007. The change in the anchorage area locations in 2008 has not been implemented.

Apart from the areas of low danger that already existed in the re-survey policy of the NLHO, additional zones of low grounding danger were identified in this study. In these zones, the re-survey categories associated to low re-survey frequencies may be expanded, based on the

preliminary danger classes awaiting redefinition of absolute acceptable levels of danger. These zones are:

- The zone between the Deep Water Route East and the TSS North Hinder North to Texel TSS and north of 53ºN latitude. Here, the combined grounding danger, based on surveys in the past, is low (Figure 5.5). The predicted grounding danger development does not cover this area. The vertical nodal dynamics map revealed that the north-south oriented sand banks in this area (75 km offshore Texel) are dynamic. This finding, however, is based on a time series of merely 2 data sets, of which one comprises digitised fair sheets. Neither sand wave analyses nor sand wave modelling were carried out in this zone. An additional detailed study at this site is necessary to verify whether this area may be categorised in a lower re-survey frequency.
- The zone north of the Terschelling – German Bight TSS. The combined grounding danger map displays no dangers and the predicted danger development outside the shipping lanes remains in the same class until 2020. A detailed study of the shoreface-connected ridges north of Ameland and Schiermonnikoog, that extend into this area, shows that these ridges are stable (though based on merely 2 datasets in time).

Moreover, the zone west of the Deep Water Route East and north of the 53ºN latitude shows a low grounding danger, and the grounding danger development predicts a modest increase in danger in 2015.

6.4 Advised protocol for devising a re-survey policy (Objective 4)

The present research results in a proposed protocol that optimises the existing re-survey policy of the NLHO. Morphodynamics and grounding dangers due to both water depth and unknown obstructions at the seabed were found to be good factors to use as a basis for designing a re-survey policy. The protocol comprises the following steps:

1. Quantifying the vertical seabed morphodynamics based on updated empirical data *(a)* to provide for a general overview of the contrasts of dynamics in the area to be surveyed (in this case the NCS) and *(b)* to provide the dynamic trend for the predictions of water depths. Performing detailed studies on bedform growth and migration to support and verify the vertical dynamics.
2. Quantifying the regular and object grounding dangers on the NCS.
3. Combining both types of grounding danger into one map of total grounding danger, leading to the extents of re-survey categories. If grounding risks (consequences of grounding) are included in the decisions, combining of both dangers is not appropriate.
4. Analysing the occurrence of variation within the new categories in order to verify whether the categories are consistent in the grouping of grounding dangers on the NCS.
5. Predicting water depths based on the vertical nodal dynamic trend, established in point 1, in order to predict the grounding danger development in future years. These predictions allow to associate absolute re-survey frequencies to the categories.

6.5 Recommendations

This study presents a validation and optimisation of the existing re-survey policy of the NLHO, as well as a protocol for the design of a new re-survey policy. This study made use of all available hydrographic data contained in NLHO's BAS database and the AIS database. However, assumptions were made in the quantifications of morphodynamics and grounding dangers. For further improvement, we recommend the following.

1. Optimising the re-survey policy

A decision on absolute levels of acceptable grounding dangers is required for finalising the advised new policy for re-survey frequencies. The results presented in this report are based on preliminary choices of classes and will alter when classes are redefined. This way, the policy can be adjusted to more efficient yet effective classes.

2. Grounding dangers

In the calculations of grounding danger for ships, the assumptions may be refined in order to provide for a good representation of the present-day shipping. For example, neglecting water depth fluctuations due to tides results in an overestimation of the grounding danger. Approaches of ports nowadays work with tide-windows. The variation in water depth within one cell of 1 by 1 km also affects the grounding dangers, especially near the edges of shipping lanes that are deeper than their surroundings. Refining the assumptions by including tides and the use of smaller grid cells will result in more realistic estimates of grounding dangers on the NCS. Including the actual speed of ships would improve the estimates of grounding dangers, particularly in anchorage areas. In this study we assumed one speed for all ships, thereby overestimating the danger in anchorage areas.

By making the grounding danger calculations more flexible would further improve the predictions of grounding dangers. The change of traffic density and ship size in time is now not included in grounding danger predictions. Also, when expanding the assessment to grounding *risks*, the grain size of sea bed sediments are relevant to include.

The effect of morphodynamics on the grounding danger development is now only predicted for 3 periods (1, 5 and 10 years) in the future. This could be expanded to a yearly prediction, thereby refining the re-survey frequencies linked to the categories in the policy.

3. Morphodynamics

The analysis of morphodynamics at the NCS, and thereby predictions of water depth, would improve by extended time series of bathymetric data. Bathymetric time series in most locations of the NCS are short (2 datasets, sometimes 3, but time series of more than 3 surveys are scarce), which results in an uncertainty of the dynamic trends calculated in this research. An update of the morphodynamic quantification, as soon as new surveys become available, helps in making the calculation of the dynamic trend more accurate. Extending time series with perhaps commercial datasets, or oil & gas 3D seismics – of which water depths can be extracted in an automated way – may significantly increase the validity of the calculated dynamic trends. For example, a recommended extension of a time series following from this research is the sand bank area 75 km offshore Texel. Moreover, time series with multiple surveys allow for establishing a temporal variation in vertical dynamics at a location (in the case of such a variation, linear extrapolation is no longer justified).

Furthermore, expanding the number of detailed studies would make it more certain that the local growth of sand waves, or other marine bedforms, is not being overlooked. Examples of desired detailed studies that directly follow from the present work are the sand banks 75 km offshore Texel and those in the Deep Water Route East. A wider implication of more detailed studies would be a better spatial insight in the pattern of sand wave growth in the North Sea, so that our understanding of the behaviour of sand waves on the NCS would improve.

The protocol presented in this report is not yet fully developed into a tool that is ready for use, but a digital environment for the optimisation of a re-survey policy is created, so that adjusting the classifications will be a relatively quick action. Devising a decision support system tool (computer programme) based on the steps in the protocol and the recommendations of making calculations more flexible, and linked to information on tides and shipping, would help to come to an operational re-survey policy. Such a tool should also facilitate the updates of the re-survey policy when parameters in morphodynamics, shipping or management

decisions change. An adjustable survey policy based on flexible parameters leads to adequate and efficient hydrographic mapping of the Netherlands Continental Shelf. With these new developments, the NLHO may serve as an international example for a accurate performance of reliable hydrographic mapping.

7 List of used notation

D50	Median grain size of the sand fraction (0.063 - 2 mm)
$D_{g,reg}$	Regular grounding danger
$D_{g,obj,j}$	Object grounding danger for object j
dg	operational draught of the shipping expected in the area [m]
dz/dt	vertical dynamic trend per node [m/yr]
H_{obj}	Height of object [m]
m_a	actual grounding margin [m]
$m_{a,reg}$	actual margin for regular grounding [m]
$m_{a,obj,j}$	actual margin above object j [m]
m_d	desired safety margin [m]
$P_{g,reg}$	Regular grounding probability [-]
$P_{g,obj,j}$	Object grounding probability for object j [-]
P_{obj}	Probability of existence of an unknown object [-]
U_0	Tidal current velocity [m/s]
U_{res}	Residual tidal current [m/s]
UKC	Under Keel Clearance (20% of dg) [m]
WD_0, h_0	(Measured) water depth [m, reduced to LAT]
WD_c	Critical water depth [m, reduced to LAT]
WD(t)	Dynamic water depth [m, reduced to LAT]
z_{min}	minimum elevation of the seabed [m below LAT]
z_{av}	average elevation of the seabed [m below LAT]
z_{max}	maximum elevation of the seabed [m below LAT]

8 List of abbreviations

AIS	Automatic Identification System
AIS-hit	An observation of a ship at a specific moment, as captured by the AIS
BAS	Bathymetric Archive System, the digital database of the NLHO
DINO	Data en Informatie van de Nederlandse Ondergrond, geological database of the deep and shallow subsurface of the Netherlands, available from the Geological Survey of the Netherlands of TNO.
GIS	Geographical Information System
GPS	Global Positioning System
IHO	International Hydrographic Organisation
IMO	International Maritime Organization
LAT	Lowest Astronomical Tide
LOV	Level of Visualisation
MATROOS	Multifunctional Access Tool foR Operational Ocean-data Services, Deltares' database that uses RWS data
MMSI	Maritime Mobile Service Identity is a unique number to call a ship. The number is added to each AIS message.
NCS	Netherlands Continental Shelf
NLHO	Netherlands Hydrographic Office of the Royal Netherlands Navy
RWS	Rijkswaterstaat of the Ministry of Infrastructure and the Environment
SAMSON	Safety Assessment Model for Shipping and Offshore on the North Sea
SOLAS	international convention for the Safety Of Life At Sea
TSS	Traffic Separation Scheme
VHF	Very High Frequency, the frequency range from 30 MHz to 300 MHz, in which the frequency range used for Marine VHF radio communication (156 – 174 MHz) falls.
VTS	Vessel Traffic Service. A VTS-station guides shipping traffic safely and efficiently though a certain area on the therefore appointed radio channel(s).

9 Acknowledgements

The data used in this report were made available by the Netherlands Hydrographic Office of the Royal Netherlands Navy (Ministry of Defence) and Rijkswaterstaat (Ministry of Infrastructure and the Environment). Employees of the Netherlands Hydrographic office are thanked for providing the necessary data and metadata. Pieter Roos (University of Twente) valuable contributed in the discussions on the sand wave modelling. Roel Savert of the graphics department of Deltares assisted in finalising the figures in this report.

10 References

Antia, E. E. (1996). Rates and patterns of migration of shoreface-connected ridges along the sourthern North Sea coast. *Journal of Coastal Research*, 12 (1), p. 38-46.

Besio, G., Blondeaux, P. and Frisina, P. (2003). A note on tidally generated sand waves. *Journal of Fluid Mechanics*, 485, p. 171-190, doi: 10.1017/S0022112003004415.

Besio, G., Blondeaux, P., Brochinni, M. and Vittori, G. (2004). On the modeling of sand wave migration. *Journal of Geophysical Research*, 109 (C04018), doi: 10.1029/2002JC001622.

Blondeaux, P., De Swart, H. E. and Vittori, G. (2009). Long bed waves in tidal seas: an idealized model. *Journal of Fluid Mechanics*, 636, p. 485-495.

Buijsman, M. C. and Ridderinkhof, H. (2008a). Long term evolution of sand waves in the Marsdiep inlet, I: high-resolution observations. *Continental Shelf Research*, 28 (9), p. 1190-1201.

Buijsman, M. C. and Ridderinkhof, H. (2008b). Long-term evolution of sand waves in the Marsdiep inlet, II: relation to hydrodynamics. *Continental Shelf Research*, 28 (9), p. 1202-1215.

Calvete, D., Falqués, A., De Swart, H. E. and Walgreen, M. (2001). Modelling the formation of shoreface-connected sand ridges on storm-dominated inner shelves. *Journal of Fluid Mechanics*, 441, p. 169-193.

Deltares (2008). Research design for the scientific validation of the hydrographic survey policy of the Hydrographic Office of the Royal Netherlands Navy. Unpublished document.

Doornenbal, P. J., Schokker, J., Maljers, D., Van der Wal, J. T. and Van Heteren, S. (2006). Marine-Landscape Map of the Dutch Continental Shelf. http://searchmesh.net/pdf/Imares_Dutch_Marine_landscape_Map.pdf.

Dorst, L. L. (2009). *Estimating sea floor dynamics in the southern North Sea to improve bathymetric survey planning*. Published Ph.D. thesis, University of Twente, Enschede, Netherlands, 218 pp.

Dorst, L. L., Roos, P. C. and Hulscher, S. J. M. H. (submitted). Spatial differences in sand wave dynamics between the Amsterdam and the Rotterdam region in the Southern North Sea. *Continental Shelf Research*.

Dorst, L. L., Roos, P. C., Van der Meer, F. M. and Hulscher, S. J. M. H. (2008). Sand wave migration in an anchorage area in the southern North Sea. *In: D. Parsons, T. Garlan and J. Best (Eds.)*: *3rd International Workshop on Marine and river dune dynamics (MARID2008)*, University of Leeds, Leeds, UK, 87-96.

Dorst, L. L., Roos, P. C., Hulscher, S. J. M. H. and Lindenbergh, R. C. (2009). The estimation of sea floor dynamics from bathymetric surveys of a sand wave area. *Journal of Applied Geodesy*, 3 (2), p. 97-120.

Duffy, G. P. and Hughes-Clarke, J. E. (2005). Application of spatial cross correlation to detection of migration of submarine sand dunes. *Journal of Geophysical Research*, 110 (F04S12), doi: 10.1029/2004JF000192.

Goovaerts, P. (1997). *Geostatistics for Natural Resources Evaluation*, Oxford University Press, Oxford, UK.

Hulscher, S. J. M. H. (1996). Tidal-induced large-scale regular bed form patterns in a three-dimensional shallow water model. *Journal of Geophysical Research*, 101 (C9), p. 20,727-20,744.

Hulscher, S. J. M. H., de Swart, H. E. and de Vriend, H. J. (1993). The generation of offshore tidal sand banks and sand waves. *Continental Shelf Research*, 13 (11), p. 1183-1204.

Huthnance, J. M. (1982). On one mechanism forming linear sand banks. *Estuarine, Coastal and Shelf Science*, 14, p. 79-99.

IHO (1988). *IHO Standards for Hydrographic Surveys*. 4th ed., International Hydrographic Bureau, Monaco.

IHO (2008). IHO Standards for Hydrographic Surveys. Special publication No. 44. International Hydrographic Bureau, Monaco.

Knaapen, M. A. F. (2005). Sandwave migration predictor based on shape information *Journal of Geophysical Research*, 110 (F04S11), doi: 10.1029/2004JF000195.

Knaapen, M. A. F., Hulscher, S. J. M. H., de Vriend, H. J. and Stolk, A. (2001). A new type of sea bed waves. *Geophysical Research Letters*, 28, p. 1323-1326.

Lawson, C. L. and Hanson, R. J. (1974). *Solving least squares problems.*, Prentice Hall, Englewood Cliffs, NJ.

Maljers, D. and Gunnink, J. (2007). Interpolation of measured grain-size fractions. http://searchmesh.net/pdf/lmares_Interpolation%20of%20measured%20grain-size%20fractions.pdf.

Németh, A. A., Hulscher, S. J. M. H. and Van Damme, R. M. J. (2006). Simulating offshore sand waves. *Coastal Engineering*, 53, p. 265-275.

Németh, A. A., Hulscher, S. J. M. H. and Van Damme, R. M. J. (2007). Modelling offshore sand wave evolution. *Continental Shelf Research*, 27 (5), p. 713-728.

NLHO (2003). Beleidsplan van de Dienst de Hydrografie. Netherlands Hydrographic Office, Royal Netherlands Navy.

Righolt, R. H., Schaap, J., Dorst, L. L. and Vos, E. M. (2010). Needle in a haystack. *In: P. J. M. Van Oosterom, M. G. Vosselman, T. A. G. P. Van Dijk and M. Uitentuis (Eds.)*: *Management of massive point cloud data: wet and dry*. Nederlandse Commissie voor Geodesie, Delft, 49; p. 104.

Simons, D. G., Amiri-Simkooei, A., Siemes, K. and Snellen, M. (2010). Recent developments in multi-beam echo-sounder processing – The multi-beam potential for sediment classification and water column sound speed estimation. *In: P. J. M. Van Oosterom, M. G. Vosselman, T. A. G. P. Van Dijk and M. Uitentuis (Eds.)*: *Management of massive point cloud data: wet and dry*. Netherlands Geodetic Commission, Delft, 49; p. 33-44.

Sterlini, F. M. (2009). *Modelling sand wave variation*. Published Ph.D. thesis, University of Twente, Netherlands, Enschede.

Van Alphen, J. S. L. J. and Damoiseaux, M. A. (1989). A geomorphological map of the Dutch shoreface and adjacent part of the continental shelf. *Geologie en Mijnbouw*, 68 (4), p. 433-443.

Van de Meene, J. W. H. (1994). *The shoreface-connected ridges along the central Dutch coast*. Published Ph.D. thesis, University of Utrecht, Utrecht, Netherlands.

Van den Berg, J. and Van Damme, R. M. J. (2006). Sand wave simulations on large domains. *In: G. Parker and M. H. Garcia (Eds.)*: *River, Coastal and Estuarine Morphodynamics (RCEM2005)*, Urbana, Illenois, USA. Taylor and Francis Group, 991-997.

Van der Meulen, M. J., Van Gessel, S. F., Tiemersma, J. J. and Van Dijk, T. A. G. P. (2004). Grind en stenen voor de kust van Texel en de winbare voorraad suppletiezand. 25. Netherlands Institute of Applied Geosciences (TNO-NITG), Utrecht, NITG 04-236-B1299.

Van Dijk, T. A. G. P. and Kleinhans, M. G. (2005). Processes controlling the dynamics of compound sand waves in the North Sea, Netherlands. *Journal of Geophysical Research*, 110 (F04S10), doi: 10.1029/2004JF000173.

Van Dijk, T. A. G. P. and Egberts, P. J. P. (2008). The variability of sand wave migration in the North Sea. *In: D. Parsons, T. Garlan and J. Best (Eds.)*: *3rd International Workshop on Marine and river dune dynamics (MARID2008)*, University of Leeds, Leeds, UK, 63-68.

Van Dijk, T. A. G. P., Lindenbergh, R. C. and Egberts, P. J. P. (2008). Separating bathymetric data representing multi-scale rhythmic bedforms: a geostatistical and spectral method compared. *Journal of Geophysical Research*, 113 (F04017), doi: 10.1029/2007JF000950.

Van Halderen, L. (2005). Vergelijking tussen de interpolatiemethodes DIGIPOL, SURFIS en KRIGING. 100.

Van Iperen, W. H. and Koldenhof, Y. (2008). Netwerkevaluatie Noordzee 2006. MARIN.

Van Iperen, W. H., Koldenhof, Y., Saladas, J. and Van der Tak, C. (2009a). Netwerkevaluatie Noordzee 2008. MARIN.

Van Iperen, W. H., Koldenhof, Y., Saladas, J. and Van der Tak, C. (2009b). Netwerkevaluatie Noordzee 2007. MARIN.

Van Santen, R. B. (2009). *Tidal sand waves in the North Sea: data analusis and modelling*. Unpublished MSc dissertation, University of Utrecht, Utrecht, Netherlands.

Verlaan, M., Zijderveld, A., De Vries, H. and Kroos, J. (2005). Operational storm surge forecasting in the Netherlands: developments in the last decade. *Philosophical Transactions fo the Royal Society A*, 363, p. 1441-1453, doi: 10.1098/rsta.2005.1578.

Vonhögen, L. M., Van Heteren, S., Marges, V. C., Wiersma, A. P. and De Kleine, M. P. E. (2010). Comparison between the internal dynamics of the Dutch Wadden Sea and the volumes involved by subsidence areas. *In*: *NCK days 2010*, West-Kapelle, Netherlands, 1 pp.

Wijnberg, K. M. (1995). *Morphologic behaviour of a barred coast over a period of decades*. Published Ph.D. thesis, University of Utrecht 245 pp.

Winter, C. and Ernstsen, V. B. (2007). Spectral analysis of compound dunes. *In: C. M. Dohmen-Janssen and S. J. M. H. Hulscher (Eds.)*: *5th IAHR Symposium on River, Coastal and Estuarine Morphodynamics (RCEM 2007)*, University of Twente, Enschede, The Netherlands Taylor & Francis, 2, 907-911.

11 Appendices

11.1 Deviation in carried out research from project proposal

In carrying out the research and handling the data, some methods of analysis were adjusted and expanded. For example, the quantifications of morphodynamics were never done on this scale in previous studies, and increased insight resulted in an adjustment of methods. These changes were discussed with project partners and the NLHO and are documented in the project progress reports. This appendix provides an overview of where the research deviates from the proposal.

Research proposal	Carried out	Elucidation
5 objectives	Combined objectives 2 and 3 into one (Objective 2)	Both objectives comprise grounding probability and it was clearer to report on the results by combining these into one.
Survey-based analysis approach	Separate data point approach	Using stacked data points per node in a three-dimensional space allows for the analysis of vertical nodal dynamics without having to deal with the different overlaps and periods of surveys.
Vertical dynamic trend calculated from the differences in bed level of subsequent surveys	Extended with a correction	Because the straight forward calculation of the vertical nodal dynamics resulted in a patchwork map, in which survey-related contrasts dominated the natural morphodynamics (mainly due to tidal reduction differences), an additional correction had to be done in order to remove the survey-related contrasts and to bring out the pattern of natural morphodynamics.
Cross correlation technique	Was tested, but gave unreliable results	Due to errors in the data, unrealistic migration vectors resulted from the cross correlation analysis. Working with corrected data files may make this analysis possible.
Minimum Detectable Bias tool	Not used	Most time series are too short to identify outliers or omit surveys

11.2 Sand Wave Modelling (University of Twente)

This appendix contains the full text of the sand wave modelling carried out by the University of Twente. In the appendix, the original names of sites are maintained, whereas these were adjusted in Chapter 3.

Prediction of Sand Wave Dynamics in the North Sea with the Sand Wave Code - Explorative study on the suitability of the Sand Wave Code for the Netherlands Hydrographic Office of the Royal Netherlands Navy

W.P. de Boer,
Department of Water Engineering and Management, University of Twente

Table of Contents

1 Introduction

Understanding of the dynamics of tidal sand waves is important for many human activities, such as navigation and the infrastructure of cables and pipelines. The Netherlands Hydrographic Office of the Royal Netherlands Navy is responsible for the generation of navigation maps of the North Sea and, therefore, interested in sand wave dynamics, as it may alter the local navigation depths. Currently, the navigation maps are mainly based on bathymetrical surveys of the North Sea in combination with statistical methods (sometimes also referred to as data-based models). However, at some locations, time series of the bathymetry are either (too) short or even lacking. At these locations (geo-)statistics are not adequate to estimate the navigation depths sufficiently accurately. In addition, statistics are less suitable for predicting the effects of events, such as storms, or human interventions on the sand wave characteristics. Therefore, the Netherlands Hydrographic Office would like to explore the possibilities of using process-based models for predicting sand wave dynamics. Process-based models aim to describe the important physical processes of water and sediment motion, which are expressed in differential equations and solved using mathematical techniques. Therefore, process-based sand wave models are able to simulate the effects of physical parameters on the sand wave characteristics and, moreover, the effects of storm events or human interventions. This way, process-based sand wave models may provide an estimation of the sand wave characteristics, especially in those areas where time series are lacking.

The University of Twente developed an idealized, process-based, non-linear sand wave model, called the Sand Wave Code (SWC), specifically designed to describe sand wave dynamics (Németh et al., 2006; Van de Berg and Van Damme, 2006; Sterlini, 2009). Whereas most available sand wave models are linear (a.o. Hulscher, 1996; Besio et al., 2003,2004) and, hence, only suitable for studying the initial stage of sand wave evolution, the SWC is a non-linear model, which allows for the analysis of sand wave characteristics in all stages of sand wave evolution (Sterlini, 2009). So far, the SWC has shown promising results in estimating the characteristics of the Golden Gate sand wave field (Sterlini et al., 2009). In this report we explore what role the SWC can play in predicting sand wave dynamics in the North Sea. To this end, we investigate how well model results compare to field observations at several locations in the North Sea. In addition, we investigate the effect of surface waves on the sand wave characteristics, by varying surface wave height, period and angle. With sensitivity tests, factors controlling the sand wave dynamics may be identified.

The outline of this report is as follows. Firstly, we examine the model description, in which we discuss the model set-up, potential benefits, assumptions and extensions of the SWC (Chapter 2). Then, we discuss the model input for the SWC, focusing on data collection and data analysis (Chapter 3). In Chapter 4 we present the model results for different locations in the North Sea and compare them to field data. Moreover, the effects of surface waves on the sand wave characteristics are investigated. Chapter 5 examines the sensitivities of the SWC. Finally, in Chapter 6 the conclusions and recommendations are discussed.

2 Model Description

This Chapter gives a brief description of the Sand Wave Code (SWC). Firstly, section 2.1 describes the model set-up of the (basic) SWC. Secondly, the potential benefits of the SWC compared to other types of models are discussed in section 2.2. The model assumptions are examined in section 2.3. Finally, section 2.4 describes possible model extensions of the SWC.

2.1 Model set-up

In the class of process-based models, two model approaches exist: *idealized* and *full* ("engineering") process-based models. *Full* process-based models (such as Delft 3D) contain geometric details and state-of-the-art formulations of the physical processes and, as a consequence, require complicated numerical solution techniques. So far, no *full* process-based model has proven to be capable of describing the formation and long-term evolution of sand waves (Sterlini, 2009). The SWC is an *idealized* process-based model, implying that the model domain and physical mechanisms are simplified, while retaining the essential elements. Therefore, calculations with *idealized* models are rather quick.

Most of the idealized sand wave models that have been developed so far are based on linear stability analysis (e.g. Hulscher, 1996; Besio et al., 2003; 2004). These models are only capable of describing the initial stage of sand wave development, providing information on the sand-wave lengths and migration rates. However, information on the final shape of the sand waves, i.e. height and asymmetry, cannot be obtained from linear stability analysis. In contrast, the SWC is a non-linear idealized process-based model and, therefore, capable of modelling all stages of sand wave evolution, also providing information about the (final) sand wave height and shape (Sterlini, 2009).

The SWC is based on the so-called morphodynamic loop (
Figure 68), which describes the interactions between the water motion (hydrodynamics), sediment transport and bottom evolution. (1) Starting from an initial flat bed with a small bottom perturbation, (2) the hydrodynamics are solved by means of the 2DV shallow water equations, describing the water motion in terms of conservation of momentum and mass in the vertical direction. (3) The hydrodynamics are input for the sediment transport calculation, which is based on a Meyer-Peter-Müller type of bed-load formula (Komarova and Hulscher, 2000), taking into account that sand is transported more easily downhill than uphill (which is crucial for the formation of sand waves). (4) The sediment balance couples the hydrodynamics and the sediment transport and determines the change in bed level. The change in bed level from step (4) determines the new bathymetry in step (1) for the next time step (feedback mechanism), for which the same procedure can be repeated. For the mathematical description of the model, we refer to Sterlini (2009).

When the bed is stable, all bed perturbations will be damped. However, when the bed is unstable, certain bed perturbations will grow and the sea bed is changed. In this case, the flow field is changed such that, averaged over a tidal cycle, vertical residual recirculation cells occur. These cells cause small net transport of sediment towards the crests of the perturbations, thereby causing growth. The fastest growing mode (FGM) is the perturbation that triggers the fastest initial growth. A limitation of the SWC is that we first need to determine the wavelength of the FGM and then fix the model domain to this wavelength (Sterlini, 2009). In doing so, we only model one sand wave of a fixed wavelength and, hence, we omit (non-linear) wavelength evolution in time and interaction between sand waves of different wavelengths. However, when the model domain is not fixed to the wavelength of the FGM, the simulations finally evolve to one large bed form with a wavelength equal to the

length of the domain (Sterlini, 2009). This behavior is caused by the fact that the large wavelengths are not totally damped, but have small, positive growth rates.

For the SWC simulations we calculate the initial growth rates for perturbations of different wave lengths (steps of 10 m) and determine the perturbation with the fastest growth rate (FGM). Consequently, the long term calculations provide information on the sand wave evolution in time and the sand wave height and shape in its fully grown (or saturated) state. In its fully grown state the sand wave is in equilibrium and will not change in time anymore.

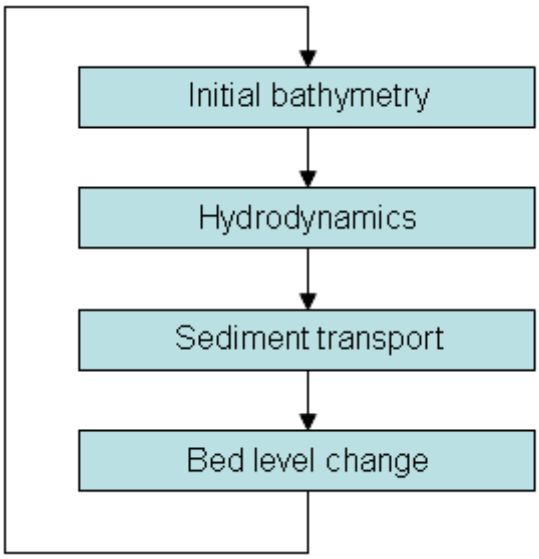

Figure 68. The morphodynamic loop.

2.2 Potential benefits of the SWC compared to other types of models

So far the SWC is the only available sand wave model capable of describing all stages of sand wave evolution (Sterlini, 2009). Therefore, it provides not only information about the sand-wave lengths and migration rates in the initial stage of the development (such as models based on linear stability analysis), but also about the final shape of the sand waves, i.e. height and asymmetry. Since the SWC is an idealized process-based model, it allows for insight in the physical mechanisms underlying sand wave formation by systematic variation of (controlling) parameters. Therefore, the SWC may provide information on sand wave characteristics where no data is available (for example because of changing environmental conditions or human interventions) in contrast to data-based (statistical) methods. Because of its idealized character, the SWC has relatively short computation times, allowing for a quick sensitivity analysis of the sand wave characteristics under different conditions.

2.3 Model assumptions

In the basic SWC (without extensions such as surface waves, suspended sediment transport and grain size distributions) the following simplifications are made:

Hydrodynamics:

- Effects of the Coriolis force are not taken into account (believed to be of minor importance).
- Assumes a simplified turbulence model with a constant vertical eddy viscosity A_v and a partial slip parameter S (choice of A_v and S is difficult). By means of a partial slip condition, one can model the shear stress at the bottom without including explicitly the complicated processes in the thin bottom boundary layer (Hulscher, 1996).

- Assumes the sand wave crests to be perpendicular to the principal tidal current. This is fair for bed evolution purposes, but less for sand wave migration.
- The tidal forcing consists of the principal tidal constituent and a residual current, higher harmonics are not taken into account. This is fair when the principal tidal constituent accounts for the major part of the tidal current, which is true for a large part of the North Sea. However, at some locations at sea higher constituents may play a significant role.

Sediment transport:

- Only bed load transport is taken into account, which is assumed to be dominant in tidal offshore regimes. Suspended sediment transport is not taken into account. However, Sterlini (2009) showed that suspended sediment transport may be important for the sand wave characteristics.
- The choice of a bed-load formula and corresponding parameters is difficult, no single generally accepted formula exists. The chosen bed-load formula is a Meyer-Peter-Müller type of formula which takes into account slope effects (Komarova and Hulscher, 2000). The formula does not account for a critical shear stress corresponding to the initiation of motion. This is fair in areas where the tidal currents are relatively high (exceeding the critical flow velocity/shear stress), but may lead to overestimations of the bed load transport in areas with relatively low tidal currents (especially when the critical flow velocity/shear stress is not exceeded).
- The chosen bed-load formula is based on the mean grain size and, therefore, may be more appropriate in areas where sediments are well-sorted than where sediments are poorly-sorted. Sand waves and sand banks consist typically of fairly well-sorted sediments, but this is not true for the entire North Sea. Roos et al. (2007) explored the incorporation of non-uniform sediments in a model for sand wave evolution, but not yet without problems.

Sand wave simulation:

- Since the model is numerical, the growth rates and migration rates of the sand wave modes cannot be derived analytically as in linear stability analyses.
- As noted in section 2.1, the long domain simulations finally tend to evolve to one large bed form, with a wavelength equal to the length of the domain (Sterlini, 2009). Therefore, the length of the domain is fixed to the wavelength of the fastest growing mode (FGM). However, in doing so, we omit (non-linear) wavelength evolution in time and interaction between sand waves of different wavelengths. Nevertheless, Van den Berg (2007) suggests that for the first 25 years of sand wave evolution, also simulations with a larger domain than the wavelength of the FGM may still be valid as the FGM is still the dominating mode within this period.
- No flow separation is taken into account. This is fair as long as the lee slopes are not steeper than the 14 degrees that is needed for flow separation (Paarlberg et al., 2006; Best et al., 2004), which is the case for most marine bed slopes. Typical slopes of sand waves in the North Sea are 2 degrees (H = 5 m; 0.5L = 150 m) and relatively steep slopes (H = 8 m; L_{lee} = 50 m) do not exceed 9 degrees.
- Sand wave migration can only be determined in the direction of the tidal current (or under an angle of 180 degrees, e.g. exactly opposing the tidal current). However, in practice the dominant migration direction may differ from the direction of the (residual) tidal current (e.g. Buijsman and Ridderinkhof, 2008; Van Dijk et al., 2008), especially when surface wave effects are taken into account.
- Biological influences may play a role in determining the sand wave characteristics (Borsje et al., 2009a; b; c), but are believed to be of minor importance and not taken into account.

2.4 Extensions of the SWC

Sterlini (2009) suggests some extensions of the SWC to account (separately) for the effects of surface waves, suspended sediment transport and non-uniform sediment. In the current configuration the SWC is only capable of dealing with these extensions separately. In a combination of these processes, the interactions between the individual processes also become important and further model extensions are necessary. Here, we focus on the effects of surface waves, since Sterlini (2009) found that surface waves can considerably affect the sand wave characteristics and improve model predictions compared to field observations, especially in shallow water. Moreover, surface waves may (partly) explain the temporal variability in the sand wave characteristics, implying they can be of importance in predicting the sand wave characteristics where no (long) datasets are available. The main assumptions for the inclusion of surface wave effects are discussed in 2.4.1. Furthermore, we extend the model to account for surface waves under different angles with the tidal current in 2.4.2.

2.4.1 Model assumptions for inclusion of surface wave effects by Sterlini (2009)

For the implementation of surface waves in the SWC, the following assumptions/ simplifications are made:

- The surface waves are not expected to break, since sand waves occur in relatively deep water. Therefore, wave breaking is excluded.
- The implementation of surface wave effects is based on linear wave theory and takes into account the Doppler effect (to take into account the effects of the water velocity on the sand waves).
- Currents are assumed to influence the wave characteristics, whilst the waves do not influence the currents (Mei, 1999).
- Waves and currents are assumed to be collinear (i.e. in parallel directions).
- The absolute frequency of the surface waves is assumed to be constant.

The bed load sediment transport is based on the same formula as without surface waves, but now accounting for the effects of both current and wave shear stresses on the sediment transport. As before, the critical shear stress for the initiation of motion is not taken into account.

2.4.2. Surface waves under different angles with the tidal current

As indicated in the previous sub-section, Sterlini (2009) assumes that currents and waves are collinear, i.e. the angle between currents and waves φ = 0°. However, in practice currents and waves are often under an angle. IJzer (2010, personal communication) proposes a way to include surface waves under different angles φ with the tidal current and his initial tests suggest that wave direction may play an important role in sand wave development. The flow components u (parallel to the flow) and v (perpendicular to the flow) may be expressed as follows (see Figure 69):

$$u = u_f + u_w * \sin \sigma t * \cos \varphi ,$$
$$v = u_w * \sin \sigma t * \sin \varphi ,$$

where σ is the angular wave frequency of the surface waves and u_f and u_w are the tidal and the wave-induced currents, respectively. The sediment transport rate q_b is proportional to the velocity to the power three. Averaged over one tidal period and restricting ourselves to the sediment transport in x-direction this becomes:

$$\left\langle u_x^3 \right\rangle = \left\langle \left|\vec{U}\right|^2 * u \right\rangle = \left\langle \left(u^2 + v^2\right) u \right\rangle = \left\langle u_f^3 + \left[1 + 2\cos^2 \varphi\right] \sin^2 (\sigma t) u_w^2 u_f \right\rangle = u_f^3 + \gamma u_w^2 u_f ,$$

with:

$$\gamma = \left[\frac{1}{2} + \cos^2 \varphi\right].$$

The parameter γ = 1.5 for φ = 0. However, in Sterlini (2009) it is assumed that γ = 1.0 implying that φ = 45°. According to Mei (1999) this also has consequences for Doppler's effect in the expression of the wave frequency, which now becomes:

$$\omega = Uk\cos\varphi + \sqrt{gk\tanh(kh)}\ ,$$

instead of equation 3.1 in Sterlini (2009). With this new formulation for the wave frequency, the model allows us to simulate the sand wave characteristics for surface waves under different angles.

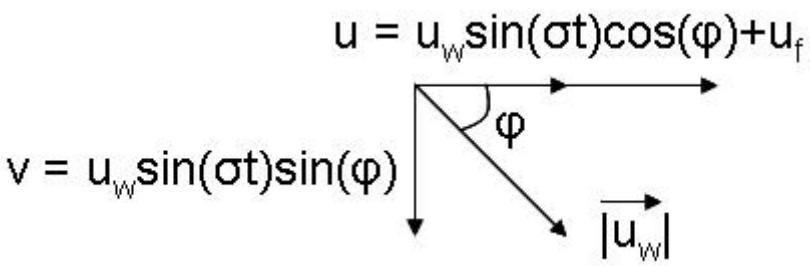

Figure 69. The wave-induced current (u_w) under an angle φ with the tidal current (u_f).

3 Model Input

This Chapter discusses the (general) model input parameters and the data sources from which their values are obtained (section 3.1). In section 0 we explain how the tidal model input is obtained by means of a tidal analysis. Finally, section 0 examines the surface wave data that is used to simulate the effects of surface waves on the sand wave characteristics.

3.1 Input parameters

The general input parameters (independent of the location in the North Sea) for the SWC are listed in Table 11.

Table 11. Overview of general input parameters for the SWC as well as their sources (if any)

Parameter	Symbol	Value	Dimension	Data source
Gravitational acceleration	g	9.81	$m\ s^{-2}$	-
Kinematic viscosity of water	υ	$1.0*10^{-6}$	$g\ m^{-3}$	-
Angular tidal frequency of principal tidal constituent (M_2)	ω	$1.41*10^{-4}$	s^{-1}	-
Ratio sediment and water densities	ρ_s/ρ_w	2.65	-	Sterlini (2009)

The other (site specific) input parameters are listed in Table 12.

Table 12. Overview of site specific input parameters for the SWC as well as their sources

Parameter	Symbol	Value	Dimension	Data source
Constant eddy viscosity	A_v	0.01	$m^2\ s^{-1}$	Sterlini (2009) based on Nemeth (2007)
Slip parameter	S	0.008	$m\ s^{-1}$	Sterlini (2009) based on Nemeth (2007)
Slope factor – (grain weight/area)/(flow shear stress)	λ_1	0.0	-	Sterlini (2009) based on Nemeth (2007)
Slope factor – related to angle of repose	λ_2	1.7	-	Sterlini (2009) based on Nemeth (2007)
Proportionality constant in sediment transport formula	α	0.3	-	Sterlini (2009)
Power of sediment transport	b	0.5	-	Sterlini (2009)
Tidal forcing residual flow component	F_0	Site specific	-	Matroos database www.deltares.nl
Tidal forcing sine flow component	F_s	Site specific	-	Matroos database www.deltares.nl
Tidal forcing cosine flow component	F_c	Site specific	-	Matroos database www.deltares.nl
Mean water depth	h_0	Site specific	M	NLHO data - average of bottom profiles
Mean grain size	D_{50}	Site specific	m	TNO/Deltares D_{50} map

The choice of the parameters A_v, S, λ, α and b is a bit problematic, because their values cannot be measured directly and have to be based on empirical formulae and/or experience (literature). The parameters λ, α and b are usually taken as constants. The parameters A_v and S may differ among locations (Hulscher and Van den Brink, 2001) and are believed to affect the sand wave characteristics considerably (Sterlini, 2009). However, the sensitivity analysis with location specific values for A_v and S (see Chapter 5) shows unrealistic sand-wave

lengths. Therefore, we follow Sterlini (2009) and assume fixed values for these parameters. The parameters F_0, F_s, F_c, h_0 and D_{50} are site specific and are obtained from online databases or field data. The dimensionless parameters F_0, F_s and F_c can be obtained from modelled tidal velocity data from the Matroos database by means of a tidal analysis. The Matroos database, which is run at Deltares and uses data of Rijkswaterstaat, stores realistically modelled x- and y-components of current velocities in the North Sea for the past two years, taking into account both astronomical and wind-drived currents. The tidal analysis is explained in section 3.2. The water depth h_0 and the median grain size D_{50} of the sand fraction are obtained directly from a bathymetric map based on bathymetric data (NLHO) and a TNO/Deltares D_{50} map, respectively.

3.2 Tidal analysis

In order to obtain site-specific values for the tidal forcing parameters F_0, F_s and F_c, we perform an analysis on the modelled tidal data from the Matroos database (see Van Santen, 2009). To account for most of the tidal variations, such as spring-neap tides and seasonal changes, we used depth-averaged tidal velocity data of one year starting from the 1st of July 2008. The magnitudes of the principal tidal component (in our case M_2) and the residual current are determined by a discrete Fourier analysis. Since the SWC works with scaled values for the tidal forcing parameters, a prepared Maple-sheet (Sterlini, personal communication 2010) is used to calculate F_s and F_c. F_0 is scaled directly in the SWC.

In this study, the oscillating flow component and the unidirectional flow component are determined slightly differently than in Sterlini (2009). Where in our analysis the flow components follow directly from the tidal (Fourier) analysis, Sterlini (2009) determines the maximum tidal flow velocities in both directions (flood and ebb) and, consequently, takes the minimum peak flow velocity as the oscillating current U_{osc} and difference between maximum and minimum peak flow velocity as the residual current U_{res}.

3.3 Surface wave data

Location specific surface wave data may be obtained from online databases, such as Waterbase (www.waterbase.nl). However, as this study serves only to explore the possibilities of the SWC, we apply wave data of one fixed location to study the impact of different surface waves on the sand wave characteristics. The surface wave data is taken from Sterlini (2009), who used the wave climate, i.e. different wave heights and periods with different probabilities of exceedance, at the IJmuiden Munition Dump as investigated by De Leeuw (2005). The wave climate data is presented in Table 13.

With model simulations we investigate the effects of the different wave characteristics on the sand wave characteristics. In addition, we investigate the effects of the angle φ between the currents and waves by varying φ between 0° and 180°. In this study we only investigate the effects of continuous storms on the sand wave characteristics, meaning that the surface waves are active over the total simulation period (indicating the extreme scenarios). Note that it is also possible to simulate more realistic surface wave climates with periods of different surface wave characteristics. However, this is beyond the scope of this study.

Table 13. Surface wave characteristics (from Sterlini, 2009).

Probability of exceedance (%)	Surface wave height H_w (m)	Surface wave period T_w (s)
50	1.0	5.3
10	2.4	7.0
1	4.2	8.9
0.1	5.5	10.7

4 Model Results

This Chapter presents the model results for different locations in the North Sea. Firstly, the field locations to be studied are selected (section 3.3.4.1). Consequently, the results of the basic model simulations (without surface waves) are discussed and compared to the measured field data (section 3.3.4.2). Finally, the effects of surface waves on the sand wave characteristics are examined for the selected field locations (section 3.3.4.3).

4.1 Selection of field locations

One time series of the Netherlands Hydrographic Office of the Royal Netherlands Navy, was provided as a test data set and will be referred to as “Navy test area” in the remainder of this report, is one of the selected areas to be studied. This area is also investigated in parallel studies, which allows for comparisons between the studies in a later stage of the project. Furthermore, we use the interpolated sand wave data of Van Santen (2009), containing information of about 30 different locations. From these locations we select four locations, based on the local water depth and tidal current. To cover the range of water depths and tidal currents we roughly take the extreme ends of the water depths and tidal currents. The characteristics of the selected field locations are presented in Table 3.5. The numbers 213, 180, 135 and 222 refer to the areas in Van Santen (2009).

Table 13. Overview of the characteristics of the selected field locations.

Location	x* (m)	y* (m)	H (m)	D_{50} (µm)	U_{osc} (ms^{-1})	U_{res} (ms^{-1})
Navy test area	524142	5754800	30.5	300	0.66	0.02
135	525671	5890409	26.34	269.77	0.46	0.05
180	592918	5823315	17.16	236.35	0.52	0.02
213	489951	5766250	36.87	249.07	0.70	0.03
222	501468	5748168	34.63	343.45	0.69	0.03

* Centre point, in the coordinate system ED50 UTM 31N

4.2 Model results and comparison with field data

The SWC results for the wavelengths L_s corresponding to the fastest growing modes (FGMs) for the five selected locations (section 3.3.4.1) are listed in Table 3.6. Figure 3.27 shows an example of the growth rates for different wavelengths for the Navy test area. The wavelength corresponding to the maximum growth rate corresponds to the FGM (in this case L_s = 200 m). Figure 3.28 shows the results of the long-term calculations for the Navy test area. The upper panel shows the growth of the sand wave crest and trough in time towards their final height H_s and the lower panel shows a side view of the final sand wave shape. In this example the sand waves grow to a more or less stable, saturated state, as expected. However, there are also model runs in which the final sand wave shape is unreliable, as the sand wave does not reach a stable, saturated state (see Figure 3.29 and Figure 3.30).

For both stable and unstable runs the sand wave height H_s is determined by averaging the sand wave height over the last 100 time steps (each time step is 10 weeks), to average possible instabilities. The migration rate M_s is calculated over the last 10-50 time steps of the simulation. In case of stable results, the lengths of these calculation periods do not affect the sand wave height or migration rate (as long as the sand wave has reached its saturated state at the start of the calculation period). However, in case of unstable results, the sand wave height and, especially, the migration rates can be very sensitive to the length of this period. Therefore, the migration rates are checked qualitatively by means of animations of the model results (IJzer, 2010, personal communication) in order to check whether the directions as well as the magnitudes of the migration are reliable relative to the other (stable) model results.

The thus obtained modelled sand wave characteristics are summarized in Table 3.6 and compared to empirical results for all selected field locations.

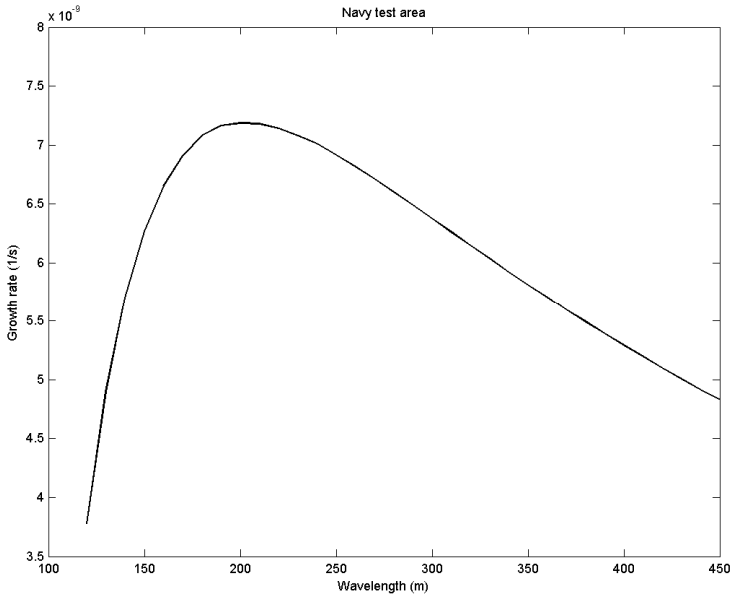

Figure 66. Prediction of the FGM for the Navy test area. The largest growth rate, corresponding to the FGM, is obtained by a wavelength of 200 m.

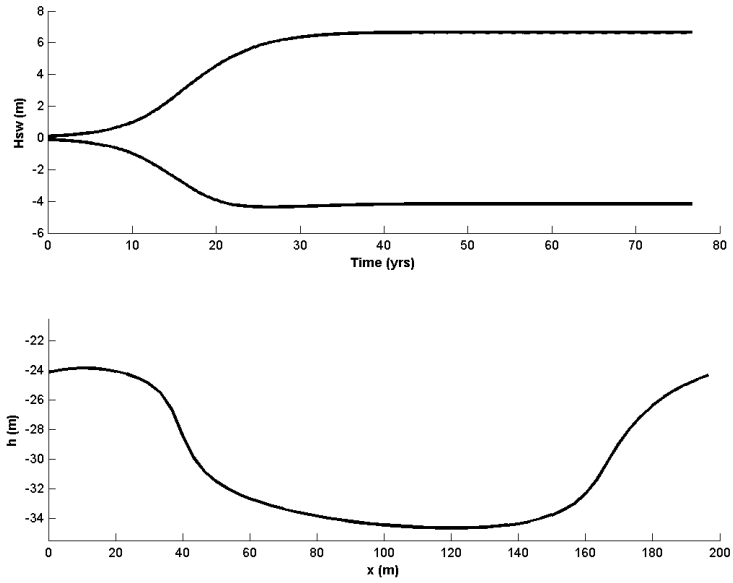

Figure 67. Upper panel: growth of the sand wave crest and trough in time for the FGM for the Navy test area. Lower panel: predicted final sand wave shape.

The results in Table 3.6 show that the modelled sand-wave lengths match the measured wavelengths well for the locations Navy test area, 213 and 222. However, at the other locations the wavelengths are not in agreement with the data. For the locations 135 and 180 the large difference between the observed and modelled sand-wave lengths may partly be explained by the relatively lower U_{osc}, implying that the velocities are relatively closer critical velocity for the initiation of motion. Therefore, at these locations it may not be valid to neglect the critical shear stress in the sediment transport calculations. For the locations with relatively higher U_{osc} the agreement between modelled and observed wavelengths is much better.

Table 14. Overview of observed and modelled sand wave characteristics for all selected field locations.

Location	h_0 (m)	U_{osc} (ms^{-1})	U_{res} (ms^{-1})	L_s (m) [min;mean;max]	H_s (m) [min;mean;max]	M_s (my^{-1}) [min;mean;max]
Navy test area						
Data	30.50	0.66	-	141; 249; 361	1.95; 3.65; 5.89	-5.4; -3.2; 1.2 *(1999-2007)*
Model	30.50	0.66	0.02	200	10.8	2.1
135						
Data	26.34	0.45*	-	1000	0.4	-
Model	26.34	0.46	0.05	150	7.2	5.7
180						
Data	17.16	0.57*	-	730	1.1	-
Model	17.16	0.52	0.02	150	8.4	2.1
213						
Data	36.87	0.76*	-	127; 203; 415	1.3; 3.3; 5.6	-1.6; 0.66; 4.0 *(1995-2003)*
Model	36.87	0.70	0.03	230	7.9#	0.7#
222						
Data	34.63	0.73*	-	149; 299; 445	2.24; 5.12; 9.66	0.64; 3.35; 5.74 *(1990-2003)*
Model	34.63	0.69	0.03	210	9.2#	0.9#

*Note that the tidal currents used in the model differ from the data of Van Santen (2009), because we used a longer dataset

#Unstable model results (see also Figure 3.29 and Figure 3.30), but qualitatively tested

The sand wave height is considerably overestimated for all locations. Although the observations may be hampered by the presence of other bed forms, making it difficult to estimate the sand wave height, the differences between observed and modelled sand wave heights are (unrealistically) large. This suggests that other processes, which are not accounted for in the SWC, may play a role in the sand wave development, such as grain size sorting or suspended sediments, or the above mentioned negligence of the critical shear stress. Additional research is necessary to tackle this problem. Since sand wave height is not

affecting the model results for sand wave migration (Németh, 2007), the model result for migration are trustworthy.

Migration rates show a good agreement with values estimated from empirical analysis. What we can see from Table 3.6 is that the migration rates generally increase for an increasing residual current, except for the areas 213 and 222. However, these two areas show unstable results and, therefore, may be unreliable. To improve the reliability of the model results, we increased the number of (numerical) steps in x-direction Nx from 60 to 120. Figure 3.29 and Figure 3.30 show that the stability does not necessarily improve with a larger Nx, although a positive effect is found for other areas. A disadvantage of increasing Nx is the considerable increase in computation time.

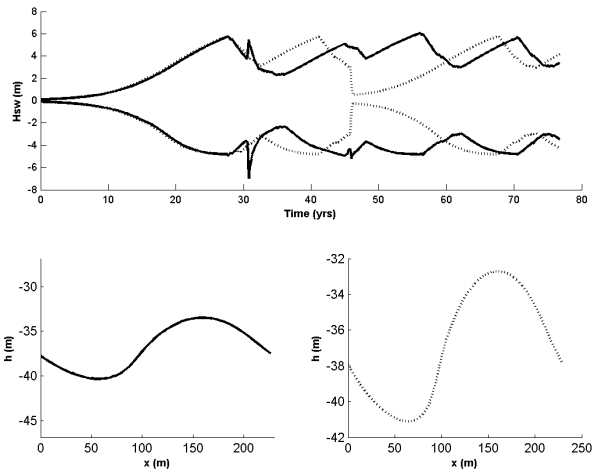

Figure 68. Same as Figure 3.28, but now for area 213. The solid black lines indicate the model results for Nx = 60 and the dotted black lines for Nx = 120.

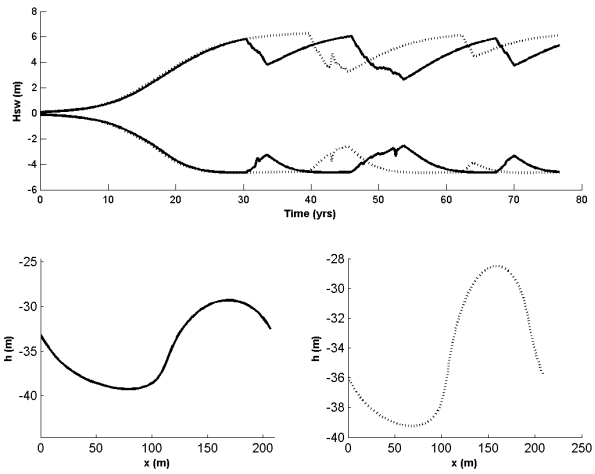

Figure 69. Same as Figure 3.28*, but now for area 222. The solid black lines indicate the model results for Nx = 60 and the dotted black lines for Nx = 120.*

4.3 Effects of surface waves

The surface waves hardly affect the lengths of sand waves, as is also indicated by Sterlini (2009). Therefore, the wavelengths found without surface waves are maintained. The simulation results for the effects of surface waves under variable angle with the currents (φ = 0-180°) on the sand wave heights and migration rates are presented in Figure 3.31 and Figure 3.32, respectively. Note that these figures are partly based on unstable simulation results. Simulations that crashed are omitted from the analysis. Therefore, one should be cautious while interpreting the results quantitatively. Nevertheless, the figures can be useful to compare the sand wave characteristics at the different locations in a qualitative way.

Figure 3.31 shows that the (average) sand wave height generally decreases with increasing surface wave height for the areas Navy, 180, 213 and 222. This is in agreement with the findings of Sterlini (2009). However, for area 135 the sand wave height tends to increase with an increasing surface wave height. It is not exactly clear what explains this behaviour, because there is no clear alternative relation between the sand wave characteristics and the conditions in terms of water depth and tidal currents at this location. Furthermore, we observe that for the locations 213 and 222 the wave angle has a considerable impact on the sand wave heights for smaller surface wave heights relative to the other locations. Since these locations have large water depths, and thus the impact of surface waves is expected to be relatively small, this large impact is probably caused by the severe instabilities in the model results for these locations. Finally, we note that the ranges in sand wave heights due to surface waves under different angles are considerably larger for the locations Navy, 213 and 222 compared to the other locations (also for stable model results). This could indicate that the former locations are more sensitive to changes in surface wave characteristics than the latter ones. The locations Navy, 213 and 222 have in common that (1) the water depths (h_0) are relatively large, which seems to be counter-intuitive as one expects surface waves to have less impact in deeper water, and (2) the tidal currents (U_{osc}) are relatively strong (also found by Sterlini, 2009).

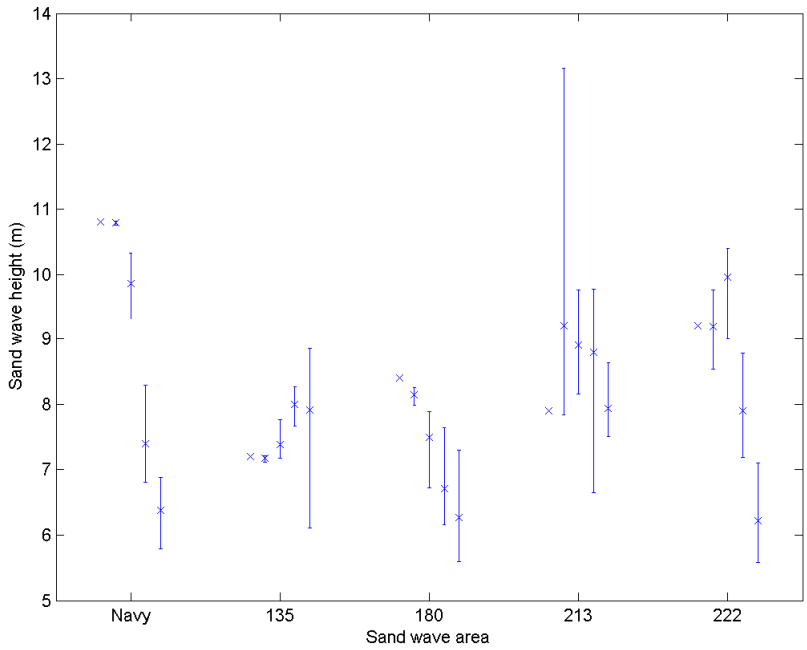

Figure 70. Overview of the effects of surface waves on the sand wave height. For each location the results without surface waves are indicated with the most left cross. Then, from left to right the results of increasing surface wave heights (see Table 3.5) are shown. For each type of surface waves the angle with respect to the tidal current is varied between 0° and 180° resulting in a range of sand wave heights (indicated by the bar). The crosses indicate the mean sand wave height for each type of surface waves.

Figure 3.32 shows that both the average migration rate and the range in the migration rates increase for increasing surface waves under different angles with the currents, as one would expect. In addition, we observe that the locations 135 and 180 generally have larger (absolute) migration rates than the other areas, which may suggest that in these areas the sand waves are (slightly) more dynamic than in the other areas. What these locations have in common is a relatively smaller water depth than the other locations. Although the water depth at location 135 is larger than at location 180, a larger residual current at 135 is probably the cause of the larger (absolute) migration rates at this location. Finally, note that, although we consider rather extreme (continuous) surface wave scenarios, the migration rates are comparable to empirical values. This is rather remarkable, as one would expect much larger migration rates compared to milder storm conditions in the field.
The SWC is capable of simulating realistic wave climates as well, as is shown in Sterlini (2009). Such an analysis could decrease the range of possible sand wave heights and migration rates considerably (i.e. refine the analysis performed above) and, in addition, be useful to obtain insight in the recovery speed of the sand waves after a storm, which is likely to differ spatially.

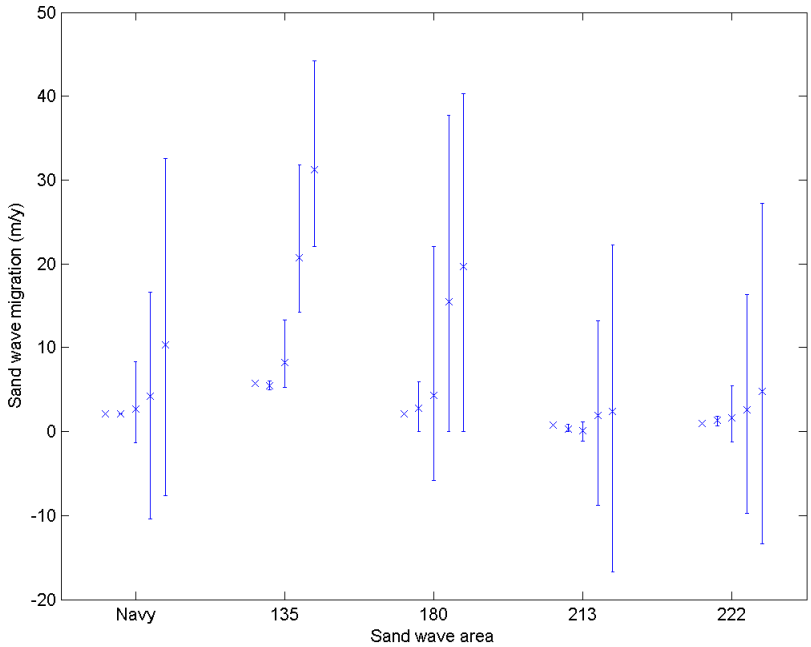

Figure 71. Overview of the effects of surface waves on the sand wave migration rates. For each location the results without surface waves are indicated with the most left cross. Then, from left to right the results of increasing surface wave heights (see Table 3.5) are shown. For each type of surface waves the angle with respect to the tidal current is varied between 0° and 180° resulting in a range of migration rates (indicated by the bar). The crosses indicate the mean sand wave migration rate for each type of surface waves.

5 Model Sensitivities

This Chapter examines some of the sensitivities in the SWC. Firstly, the effects of the parameters related to the turbulence model (i.e. the eddy viscosity A_v and the slip parameter S) and the residual current on the wavelength of the fastest growing mode (FGM) are investigated (section 5.1). Consequently, the effects of numerical parameters on the saturated sand wave characteristics are examined (section 5.1).

5.1 Wavelength fastest growing mode

In this section we firstly discuss the effects of different settings for the eddy viscosity A_v, the slip parameter S and the slope parameters λ_1 and λ_2 on the wavelength of the FGM. Consequently, the sensitivity of the wavelength of the FGM with respect to the residual current U_{res} is investigated.

5.1.1 Sensitivity with respect to A_v, S, λ_1 and λ_2

As indicated in Sterlini (2009) the eddy viscosity A_v, the slip parameter S and the slope parameters λ_1 and λ_2 are difficult to estimate in a physically realistic way. Therefore, we test the sensitivity of the wavelength of the FGM for different sets of A_v, S, λ_1 and λ_2. As a starting point we take the values from Sterlini (2009), i.e. A_v = 0.01, S = 0.008, λ_1 = 0.0 and λ_2 = 1.7 (see Table 12). For the North Sea different sets of these parameter values can be found in the literature (see Table 15). The table shows that the values for A_v differ a factor 6 and for S differ a factor 1.25. The resulting wavelengths for the Navy test area indicate that the choice of these parameter settings can considerably affect the simulation results. The parameter set suggested by Sterlini (2009) seems to work best compared to a wavelength of 200 m found in the field. The settings based on Van den Berg and Van Damme (2006) and Nemeth (2006, 2007) lead to unrealistically large wavelengths. These wavelengths are considerably outside the range for sand waves, which are usually characterized by wavelengths of ca. 100-1000 m.

Table 15. Overview of the parameter settings found in literature and the corresponding wavelengths of the FGM for the Navy test area.

Source	A_v (m^2s^{-1})	S (ms^{-1})	λ_1	λ_2	L_s (m)
Sterlini (2009)	0.01	0.008	0	1.7	200
Van den Berg and Van Damme (2006)	0.03	0.01	0	2.5	>5000
Nemeth et al. (2006)	0.03	0.01	0.002	3.33	>5000
Nemeth et al. (2007)	0.005	0.008	0.006	3.33	>5000

Table 16. Overview of the location specific settings for A_v and S (based on Hulscher and Van den Brink, 2001) and the corresponding wavelengths of the FGM L_{new}. For comparison, also the wavelengths with the initial model settings L_s and the wavelengths in the field L_{fld} are presented.

Location	A_v (m^2s^{-1})	S (ms^{-1})	L_{new} (m)	L_s (m)	L_{fld} (m)
Navy test area	0.178	0.0055	2910	200	249
135	0.108	0.0039	2440	150	1000
180	0.079	0.0044	1630	150	730
213	0.229	0.0059	3460	230	203
222	0.212	0.0058	3270	210	299

Instead of choosing overall settings for the whole North Sea, Hulscher and Van den Brink (2001) give formulas to estimate A_v and S based on location specific parameters such as the water depth h_0 and the oscillating tidal current U_{osc}. This way, location specific sets of A_v and S can be derived. We assume the slope parameters λ_1 and λ_2 to be constant over the whole

North Sea, with the values suggested by Sterlini (2009). Table 16 shows the values for A_v and S and the corresponding wavelength L_{new} of the FGM for all selected field locations. For comparison, also the wavelength with the initial settings of A_v and S L_s and the wavelength in the field L_{fld} are presented in Table 16. Note that for all locations L_{new} is an order of magnitude larger than L_s and does not improve the model results compared to the field observations (L_{fld}).

5.1.2 Sensitivity with respect to residual current

To study the sensitivity of the sand-wave length with respect to the residual current U_{res}, we vary U_{res} from 0 to 0.05 m/s (in steps of 0.01 m/s) for all field locations. In Figure 72 the ranges in the sand-wave length corresponding to the range in U_{res} are presented. Generally the sand-wave length decreases for an increasing U_{res} (as is also found by Sterlini, 2009). The sand-wave lengths at the locations Navy test area, 213 and 222 can change up to 50 m. At the other locations the ranges in sand-wave length are smaller. The changes in wavelength due to changes in U_{res} cannot explain the large differences between the observed and modelled wavelengths at the locations 135 and 180 (see Table 3.6).

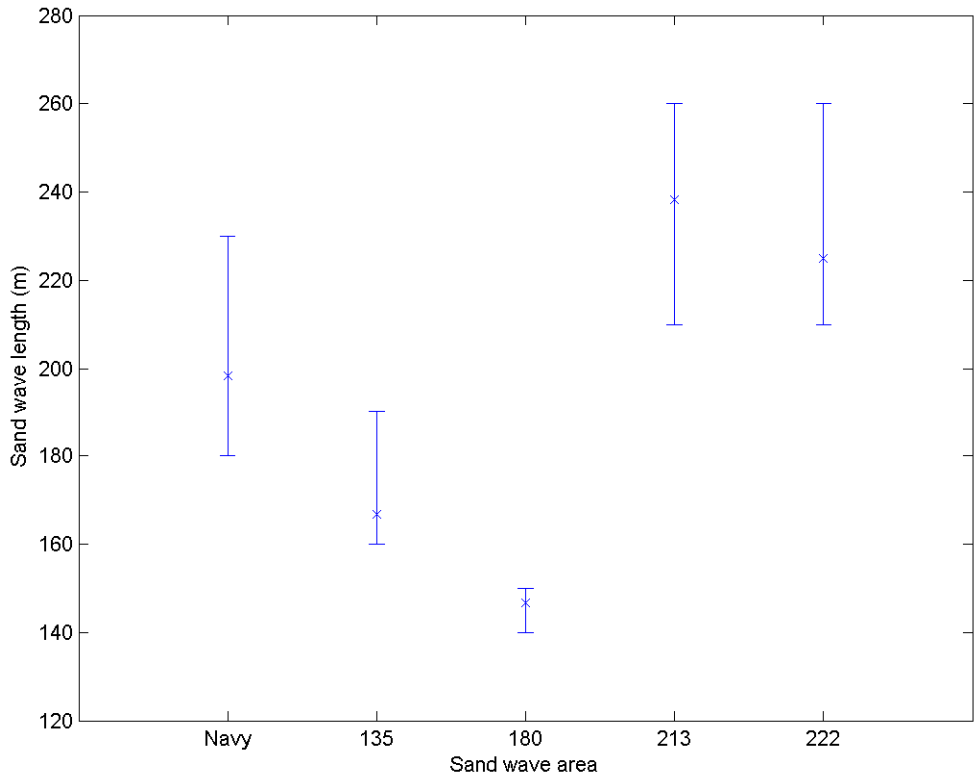

Figure 72. Ranges in the sand-wave length for all field locations for changes in U_{res} from 0 to 0.05 m/s.

5.2 Saturated sand wave shape

As indicated in Chapter 4, the SWC results sometimes show instabilities. In this section we discuss the effects of numerical settings, i.e. the temporal and spatial step size, on the (stability) of the sand wave height and the sand wave shape.

5.2.1 Sensitivity with respect to temporal step size (dt)

Figure 73 presents the model simulation results for different temporal step sizes. The results indicate that a smaller temporal step size does not necessarily increase the stability of the model results. When we choose for the option of a variable time step, i.e. a smart choice of the time step depending on the results of the previous time step, the sand wave tends to reach a stable state, but then the simulation crashes (dotted grey line in Figure 10; no solution is found). Based on these results a fixed time step of dt = 10 weeks seems to be a proper setting for the model simulations. Note that the final sand wave shape varies for the different settings, because of the unstable sand wave height.

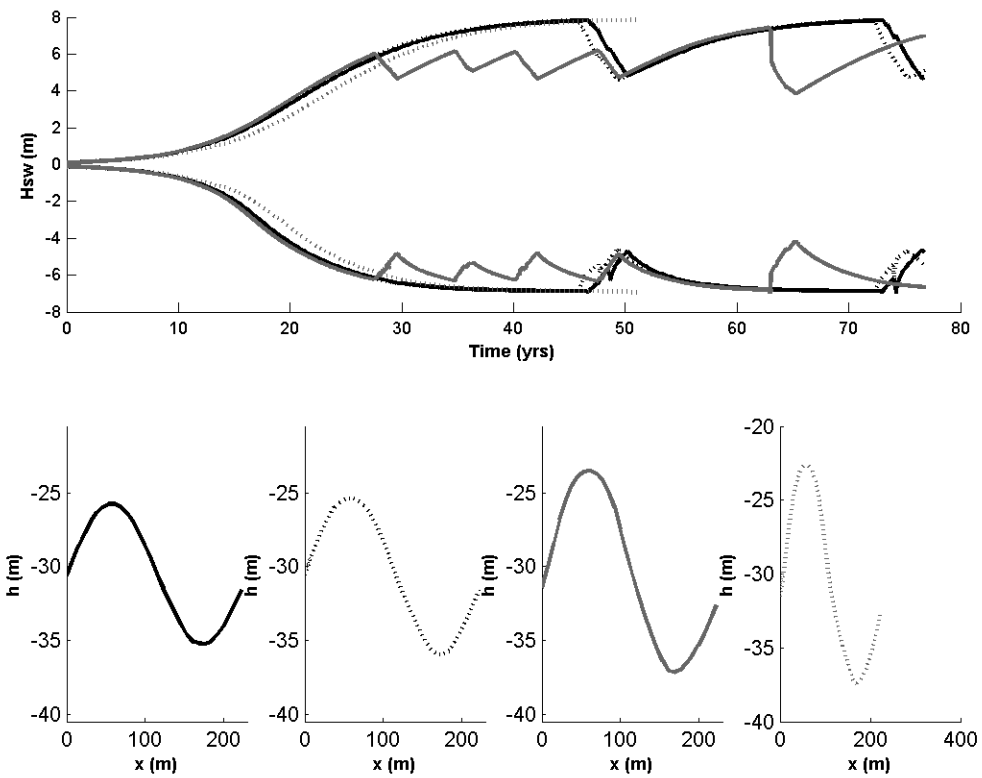

Figure 73. Upper panel: growth of the sand wave crest and trough in time for the FGM for the Navy test area (without residual) current. Lower panel: predicted final sand wave shape. The solid black line shows the results for dt = 10 weeks, the dotted black line for dt = 5 weeks, the solid grey line for dt = 1 week and the dotted grey line for a variable time step.

5.2.2 Sensitivity with respect to spatial step size

Figure 74 presents the model simulation results for different spatial step sizes. The results indicate that a smaller spatial step size may increase the stability of the model results, although this is not true for every sand wave area. Based on the results, Nx = 60 seems to be a proper setting for the model simulations, although this may differ among areas. Note that the final sand wave shape varies for the different settings, because of the unstable sand wave height.

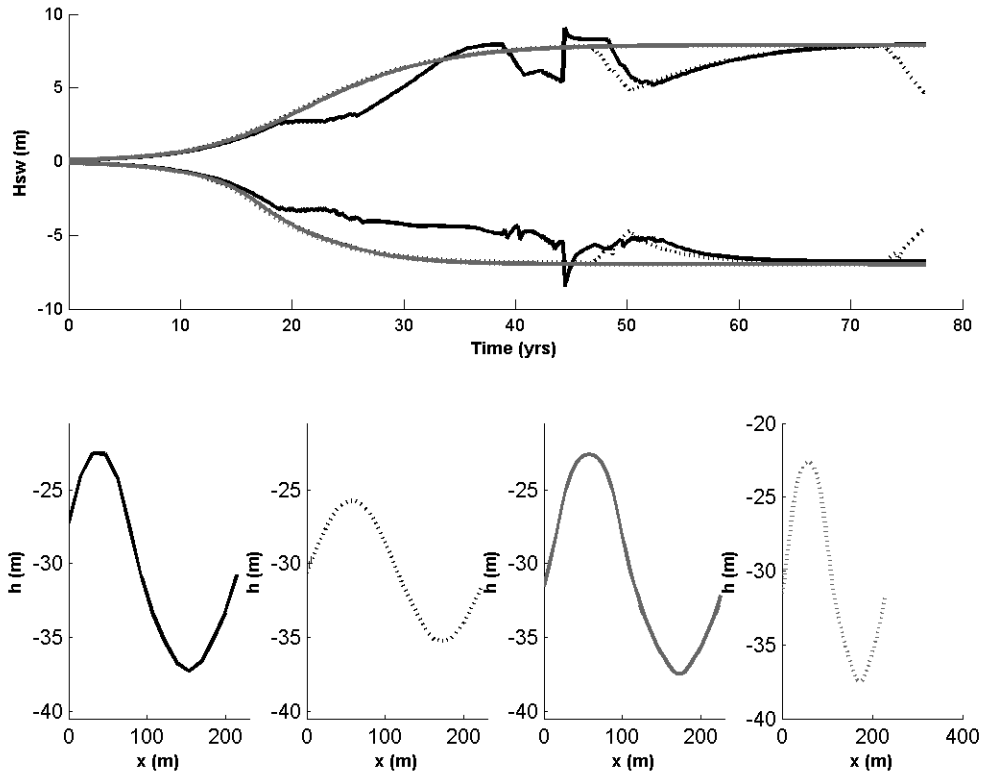

Figure 74. Same as Figure 73, but now for a fixed time step of dt = 10. The solid black line shows the results for Nx = 15, the dotted black line for Nx = 30, the solid grey line for Nx = 60 and the dotted grey line for Nx = 120

6 Conclusions and Recommendations

In this Chapter we present the conclusions (section 3.3.4.4) and recommendations (section 6.2). In the conclusions, we discuss the capabilities of the Sand Wave Code for modelling sand wave dynamics in the North Sea. In the recommendations topics for further research and model improvements are suggested.

6.1 Conclusions

The Sand Wave Code (SWC) is an idealized, process-based, non-linear sand wave model. It is capable of providing information about the sand wave height and shape in all stages of sand wave evolution (Sterlini, 2009), in contrast to sand wave models based on linear stability analysis, which only provide information about the initial stage of sand wave evolution. The SWC is capable of modelling the sand wave characteristics based on physical parameters. Therefore, in contrast to data-based models, it is not dependent on sand wave data from the field and able to simulate the effects of future storm events or human interventions. The SWC shows promising results for the Golden Gate sand waves (Sterlini et al., 2009), both in terms of sand-wave length and sand wave height. However, this study shows that the SWC performs worse for different locations in the North Sea.

In this study, we find that for some locations in the North Sea the sand-wave lengths are modelled reasonably well, but for other locations the sand-wave lengths are considerably underestimated compared to field observations. Sensitivity tests, in which we vary the eddy viscosity, slip parameter, slope factors and residual current, show that the model results can be quite sensitive to parameter variability, but cannot explain the differences between the sand-wave lengths predicted by the SWC and those observed in the field. Especially the locations with small tidal currents show an underestimation of the sand-wave length. This suggests that the exclusion of the critical bed shear stress for initiation of motion may play a role here, i.e. where the currents are small, the critical shear stress is relatively more important for the sediment transport. Furthermore, it is noteworthy that we especially modelled locations with either an extreme value for the water depth h_0 or for the oscillating tidal current U_{osc}. The model seems to give more reasonable sand wavelengths for intermediate conditions, i.e. for the Navy test area, although this has not been tested extensively.

The sand wave heights modelled by the SWC are overestimated for all the selected field locations, independent of the local conditions in terms of water depth and tidal currents. This suggests that other processes, not included in the model, may play a role here, such as grain size sorting (or the presence of a fixed or armoured layer) or interaction between bed load and suspended load sediment transport. Additional research is necessary to tackle this problem. Therefore, in its current form, the SWC is not able to provide (reliable) quantitative information on the sand wave height. Since the sand wave height does not affect the modelled migration rates, the migration results are trustworthy.

The present version of the SWC simulates sand wave migration speeds well. The results of unstable simulations are less reliable in this respect.

Although the SWC may not provide reliable quantitative information on the sand wave heights, it can still be useful to investigate the effects of physical parameters (water depth, residual currents, surface waves) on the sand wave height in a qualitative way (see Sterlini, 2009). This is not possible with a linear stability analysis, as it only provides information about the initial stage of sand wave evolution. Furthermore, the SWC allows for a qualitative investigation of the effects of surface waves on the sand wave characteristics. This is an advantage compared to data-based models, which are only capable of investigating these

effects after a storm. Qualitative model investigations of the sand wave characteristics may identify areas that are more or less dynamic or more or less sensitive to storms, and therewith are a valuable addition to this research.

The model results for five selected locations in the North Sea show that the sand wave height generally decreases for increasing surface wave height. The ranges in the sand wave heights due to variable angles between the surface waves and currents differ among different locations. The average migration rates as well as the ranges in the migration rates increase for increasing surface wave heights for all locations. However, the absolute migration rates differ among areas. The ranges in the sand wave heights and migration rates may be a measure for the potential sand wave dynamics at the different locations.

6.2 Recommendations

The model results indicate that especially the sand wave heights, but at some locations also the sand-wave lengths, are poorly predicted by the SWC. Therefore, further research is necessary to improve the SWC. It may be useful to incorporate the critical shear stress in the sediment transport formulation to improve the model predictions in areas where the tidal currents are relatively low. Furthermore, the model results show considerable deepening of the troughs during the simulations. In reality, a fixed or armoured layer or layering in the subsurface of contrasting sediment composition may hamper this deepening of the troughs and limit the sand wave height. Also the combined effects of bed load and suspended load transport may improve the model predictions (see Sterlini, 2009). All these topics would be interesting for further investigations.

More extensive investigation into the effects of surface waves on the sand wave characteristics may improve model results. In the present version of the SWC, non-linear current-wave interactions (such as wave speed or refraction) and the effects of surface waves on suspended sediments are not included in the model. Furthermore, it would be worthwhile to include more realistic surface wave climates (i.e. variable surface waves from different directions) on the sand wave characteristics, instead of assuming continuous surface waves of specific characteristics. This may narrow the bandwidth of the simulation results.

Literature

Besio, G., Blondeaux, P., Frisina, P. (2003). *A note on tidally generated sand waves*. Journal of Fluid Dynamics 485, 171-190.

Besio, G., Blondeaux, P., Brocchini, M. and Vittori, G. (2004). *On the modeling of sand wave migration*. Journal of Geophysical Research 109, C04018, doi:10.1029/2002JC001622.

Best, J., Kostaschuk, R. and Hardy, R. (2004). The fluid dynamics of low-angle river dunes: results from integrated field monitoring, laboratory experimentation and numerical modeling. In: S. J. M. H. Hulscher, T. Garlan, and D. Idier (Eds.): Marine Sandwave and River Dune Dynamics, University of Twente, Enschede, Netherlands, pp. 17–23.

Borsje, B.W., De Vries, M.B., Bouma, T.J., Besio, G., Hulscher, S.J.M.H., Herman, P.M.J. (2009a). *Modelling bio-geomorphological influences for offshore sand waves*. Continental Shelf Research 29, 1289-1301. Doi: 10.1016/j.csr.2009.02.008.

Borsje, B.W., De Vries, M.B., Hulscher, S.J.M.H., Herman, P.M.J. (2009b). *On the parameterization of biological activity on sandwave and sandbank dynamics*. Ocean Dynamics 59, 659-670. Doi: 10.1007/s10236-009-0199-0.

Borsje, B.W., Buijsman, M.C., Besio, G., De Vries, M.B., Hulscher, S.J.M.H., Herman, P.M.J., Ridderinkhof, H. (2009c). *On the modeling of bio-physical influences on seasonal variation in sandwave characteristics*. Journal of Coastal Research SI56, 698-702.

Buijsman, M.C. and Ridderinkhof, H. (2008). *Long-term evolution of sand waves in the Marsdiep inlet i: High-resolution observations.* Continental Shelf Research, doi:10.1016/j.csr.2007.10.011.

De Leeuw, C.J. (2005). *Model predictions of wave-induced sediment transport on the shoreface.* Msc thesis, University of Twente, The Netherlands, 2005.

Hulscher, S.J.M.H. (1996). *Tidal-induced large-scale regular bed form patterns in a three-dimensional shallow water model*. Journal of Geophysical Research 101, 727-744,1996.

Hulscher, S.J.M.H. and Van den Brink, G.M. (2001). *Comparison between predicted and observed sand waves and sand banks in the North Sea.* Journal of Geophysical Research 106(C5), 9327-9338.

Komarova, N.L. and Hulscher, S.J.M.H. (2000). *Linear instability mechanisms for sand wave formation*. Journal of Fluid Mechanics 413, 219-246.

Mei, C.C. (1999). *The applied dynamics of ocean surface waves, Advanced Series on Ocean Engineering*. Vol. 1, World Scientific Publishing Co Pte Ltd.

Németh, A.A., Hulscher, S.J.M.H., Van Damme, R.M.J. (2006). *Simulating offshore sand waves*. Coastal Engineering 53, 265-275.

Németh, A.A., Hulscher, S.J.M.H., Van Damme, R.M.J. (2007). *Modelling offshore sand wave evolution*. Continental Shelf Research 27, 713-728.

Paarlberg, A.J., Dohmen-Janssen, C.M., Hulscher, S.J.M.H., Van den Berg, J., Termes, P. (2006). *Modelling morphodynamic evolution of river dunes.* In: River Flow 2006, edited by Fereira, Alves, Leal and Cardoso, 969-978, Taylor and Francis Group, London.

Roos, P.C., Hulscher, S.J.M.H., Van der Meer, F.M., Van Dijk, T.A.G.P., Wientjes, I.G.M., and Van den Berg, J. (2007). *Grain size sorting over offshore sand waves: observations and modeling.* In: River, Coastal and Estuarine Morphodynamics: RCEM 2007, Dohmen-Janssen, C.M. and Hulscher, S.J.M.H. (eds.). Taylor & Francis group, London.

Sterlini, F.M. (2009). *Modelling sand wave variation.* PhD-thesis. University of Twente, Enschede.

Sterlini, F., Hulscher, S.J.M.H., Hanes, D.M. (2009). *Simulating and understanding sand wave variation: A case study of the Golden Gates sand waves.* Journal of Geophysical Research 114, F02007, doi:10.1029/2008JF000999.

Van den Berg, J. and Van Damme, D. (2006). *Sand wave simulations on large domains.* In: River, Coastal and Estuarine Morphodynamics: RCEM2005, Urbana, Illinois, USA, 4-7 October 2005, edited by G. Parker and M.H. Garcia, 991-997, Taylor and Francis Group, London.

Van den Berg, J. (2007). *Non-linear sand wave evolution*. PhD-thesis. University of Twente, Enschede.

Van Dijk, T.A.G.P., Lindenbergh, R.C., Egberts, P.J.P. (2008). *Separating bathymetric data representing multiscale rhythmic bed forms: A geostatistical and spectral method compared*. Journal of Geophysical Research, Vol. 113, F04017, doi:10.1029/2007JF000950.

Van Santen, R.B. (2009). *Tidal sand wave in the North Sea, data analysis and modeling*. Master's Thesis, University of Utrecht, Utrecht.

11.3 Difference in bed elevation of stacked data points per node in time

Difference between the maximum and minimum bed elevations per stacked data points per node in time provide the maximum change in absolute bed level (in m) of all surveys available. The value of 217.4 m results from errors in the data sets (water depths of up to 236.74 m are contained in the data). The pattern of elevation differences is still representative.

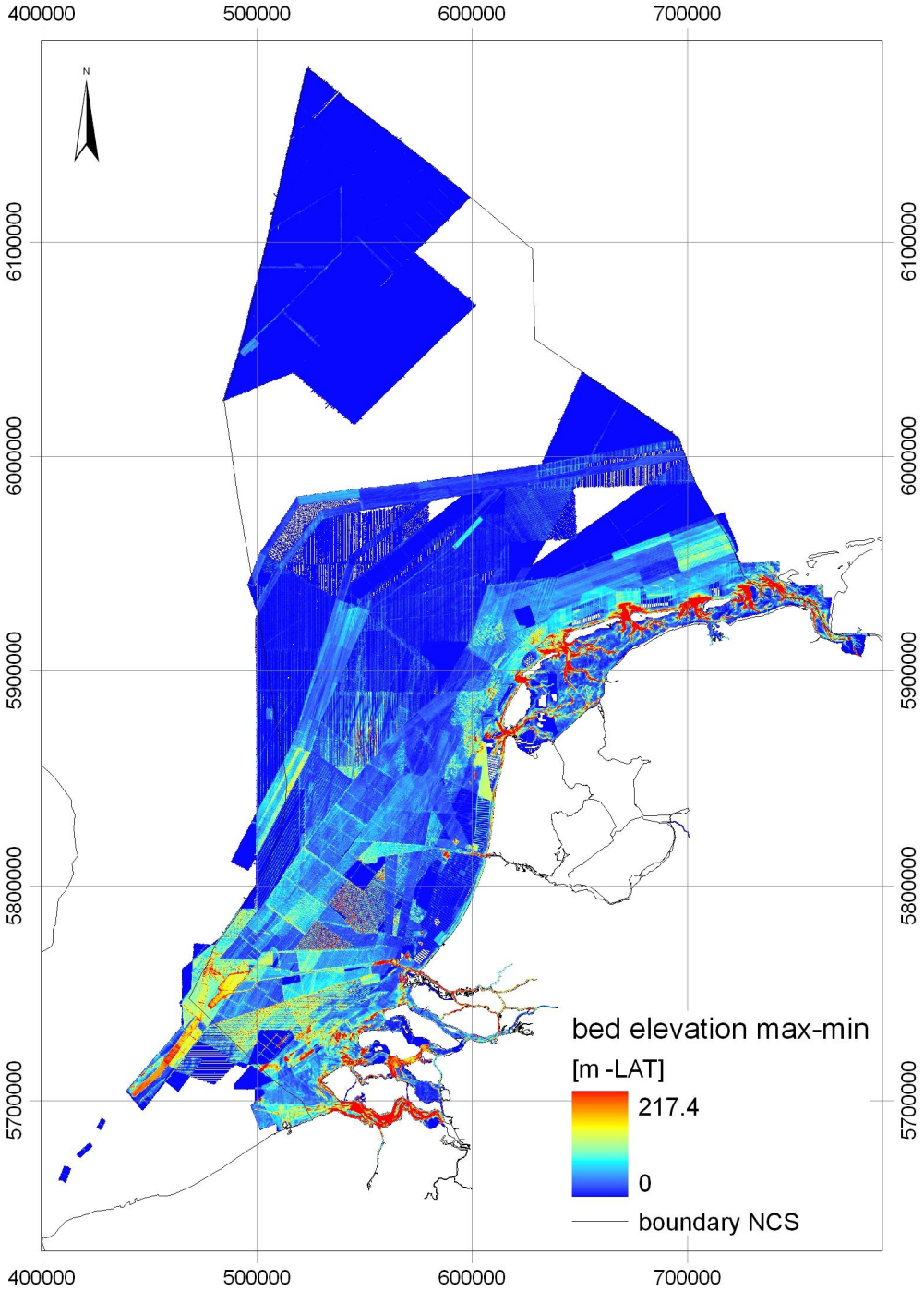

11.4 Number of surveys used in the vertical nodal dynamics map of the NCS

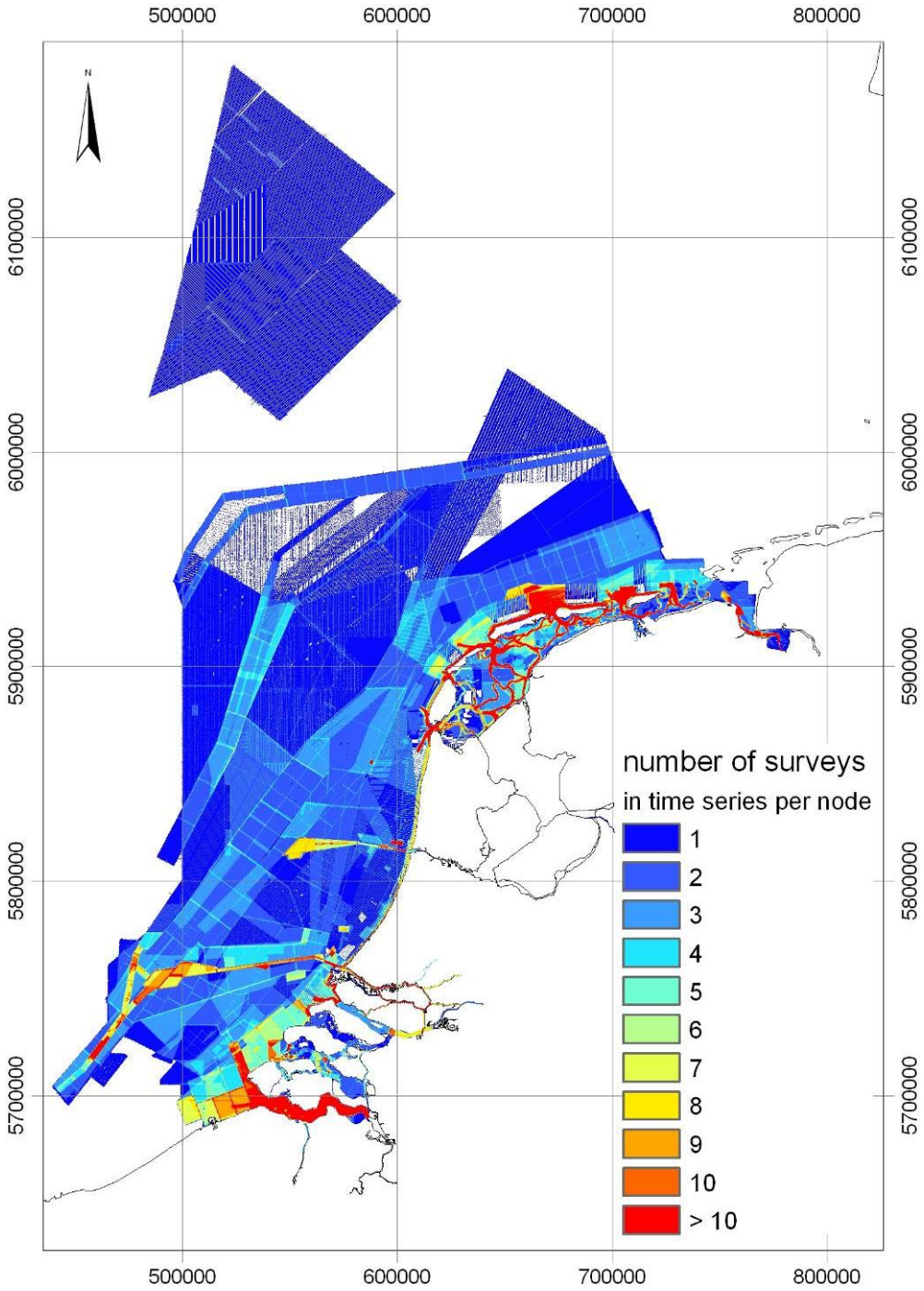

11.5 Goodness of fit (R^2) of the vertical nodal dynamic trend

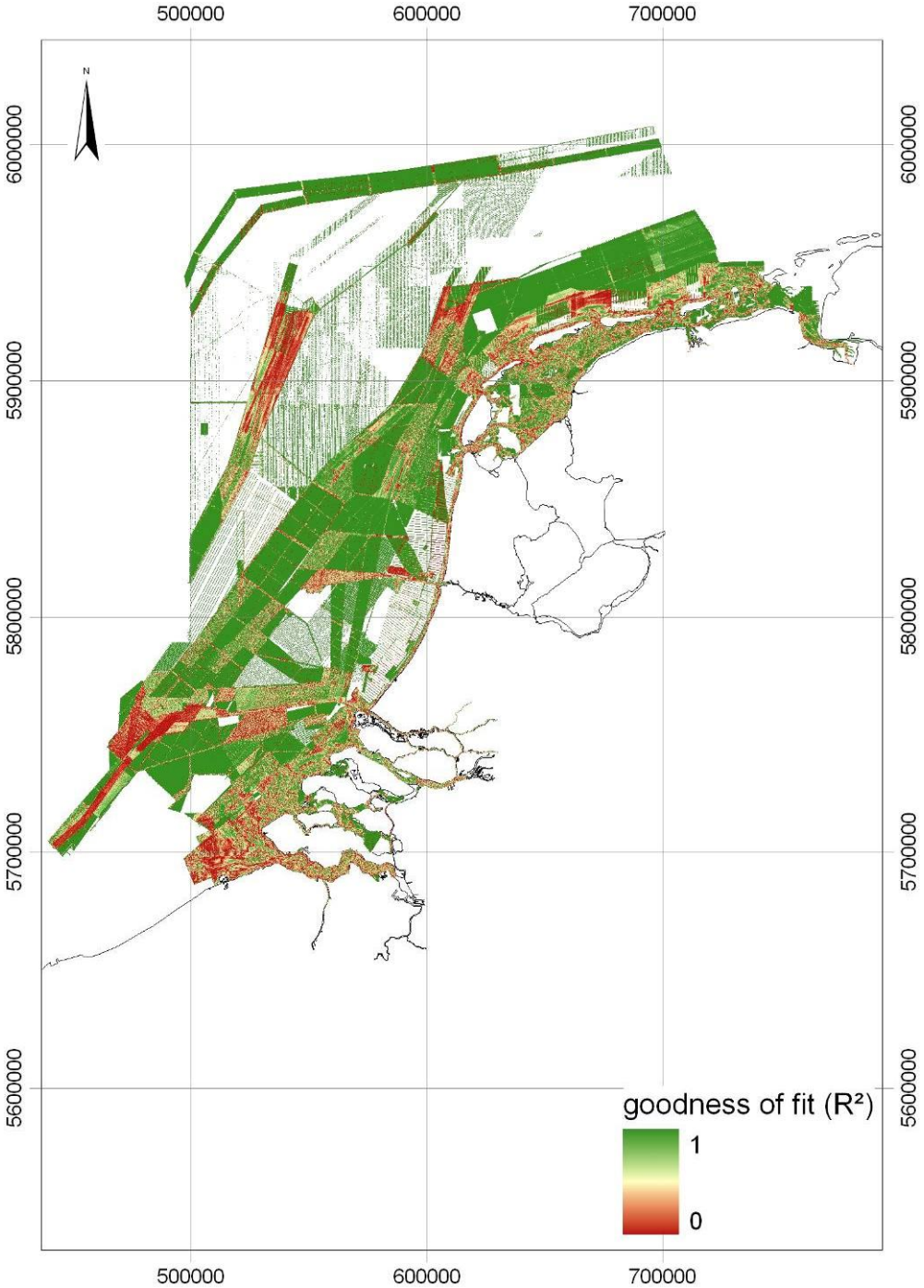

11.6 Marine bedform migration rates collective table

Site	L			H			migr			n
	min	av	max	min	av	max	min	av	max	
--- SANDWAVES ---										
1	141	249	361	1.95	3.65	5.98	-5.4	-3.2	1.2	13
2		1000			0.4		.	.	.	
3		730			1.1		.	.	.	
4	127	203	415	1.3	3.3	5.6	-1.6	0.66	4.0	13
5	149	299	445	2.24	5.12	9.66	0.64	3.35	5.74	10
A1 Texel	100	345	800	0.3	1.4	3.2	5	16-19	34	>20
A2 Texel							12	16-19	37	10
B emd3	171	239	337	1.67	1.99	2.46		1.98		9
C rdam	72	159	288	1.69	3.92	6.85		0.396		8
WIJ12	172	398	688	1.1	2.9	5.8	-2.9	2.2	6	28
TWIN	140	274	382	2.5	4.8	7.3	-4.5	-1.5	0.064	8
WR1A1	136	263	639	1.2	3.2	5.4	-0.09	4.7	8.5	17
WR1A2	121	229	496	0.07	0.88	1.8	.	.	.	37
Wr1n	149	322	434	1.1	3.38	4.6	0.2	3.7	15	19
--- LARGER BEDFORMS ---										
LBW	744	1125	1409	2.7	3.4	4.3	10.5	12.4	18.4	5
Sfcr	4084	4614	5154	2.9	4.3	5.5	-3.9	-1.0	3.6	3
on BNB*								0.6		8
on 1st*								.		.
on 2nd*								5.0		19

* for sand waves on tidal ridges

11.7 Regular grounding danger for ships with margin between -4 and 0 m for mean water depth

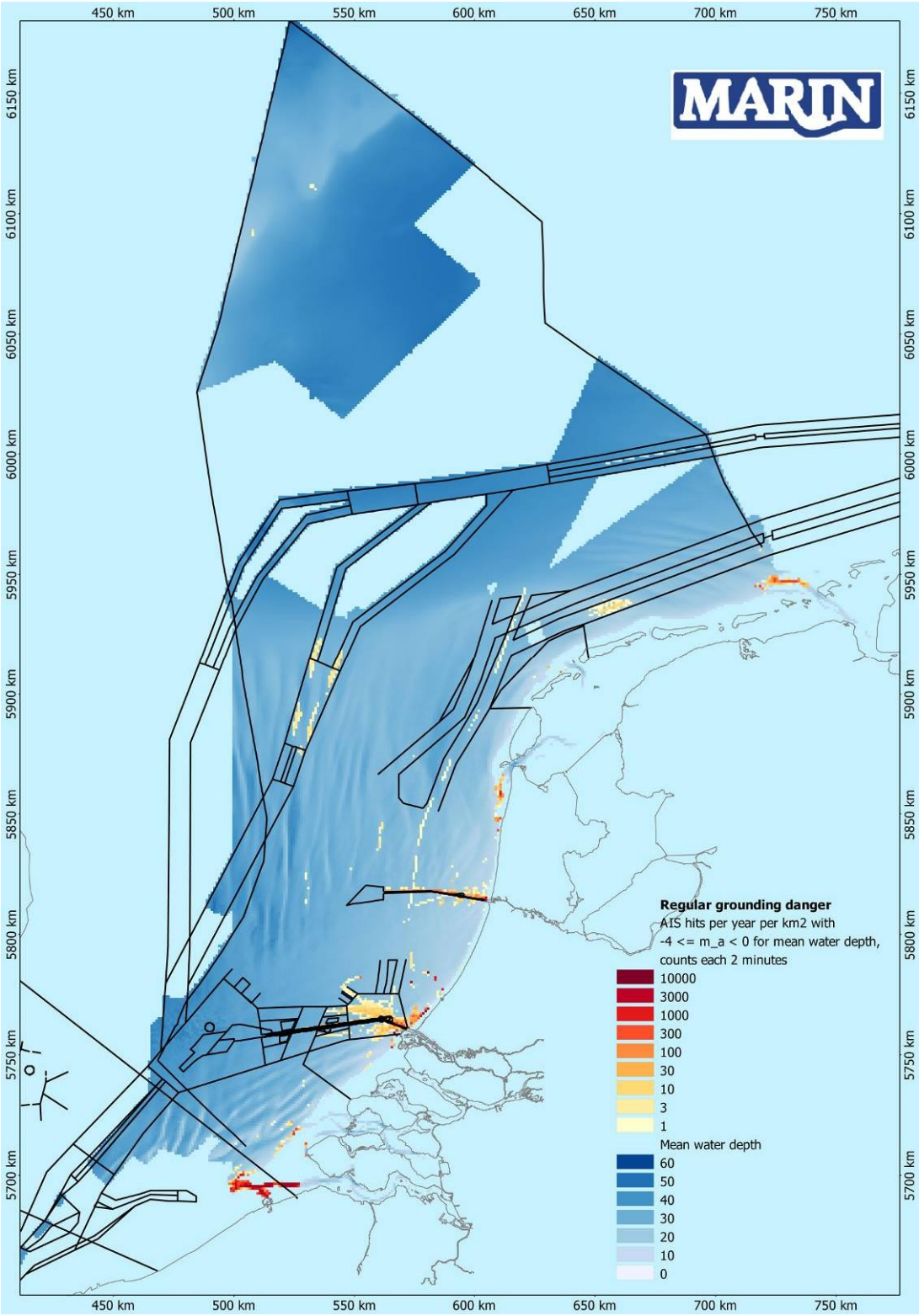

11.8 Regular grounding danger for ships with margin between -8 and -4 m for mean water depth

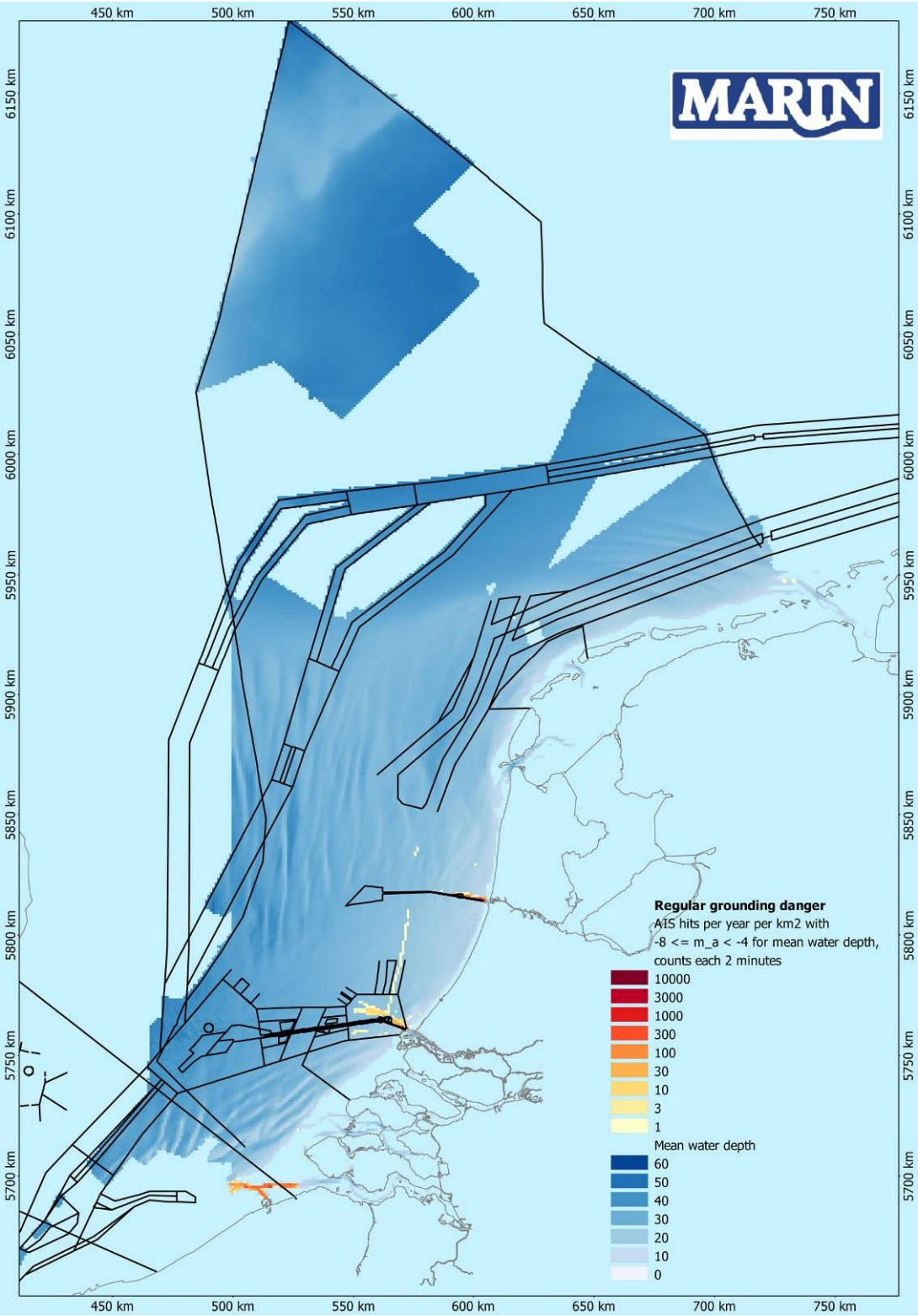

11.9 Regular grounding danger for ships with margin <-8 m for mean water depth

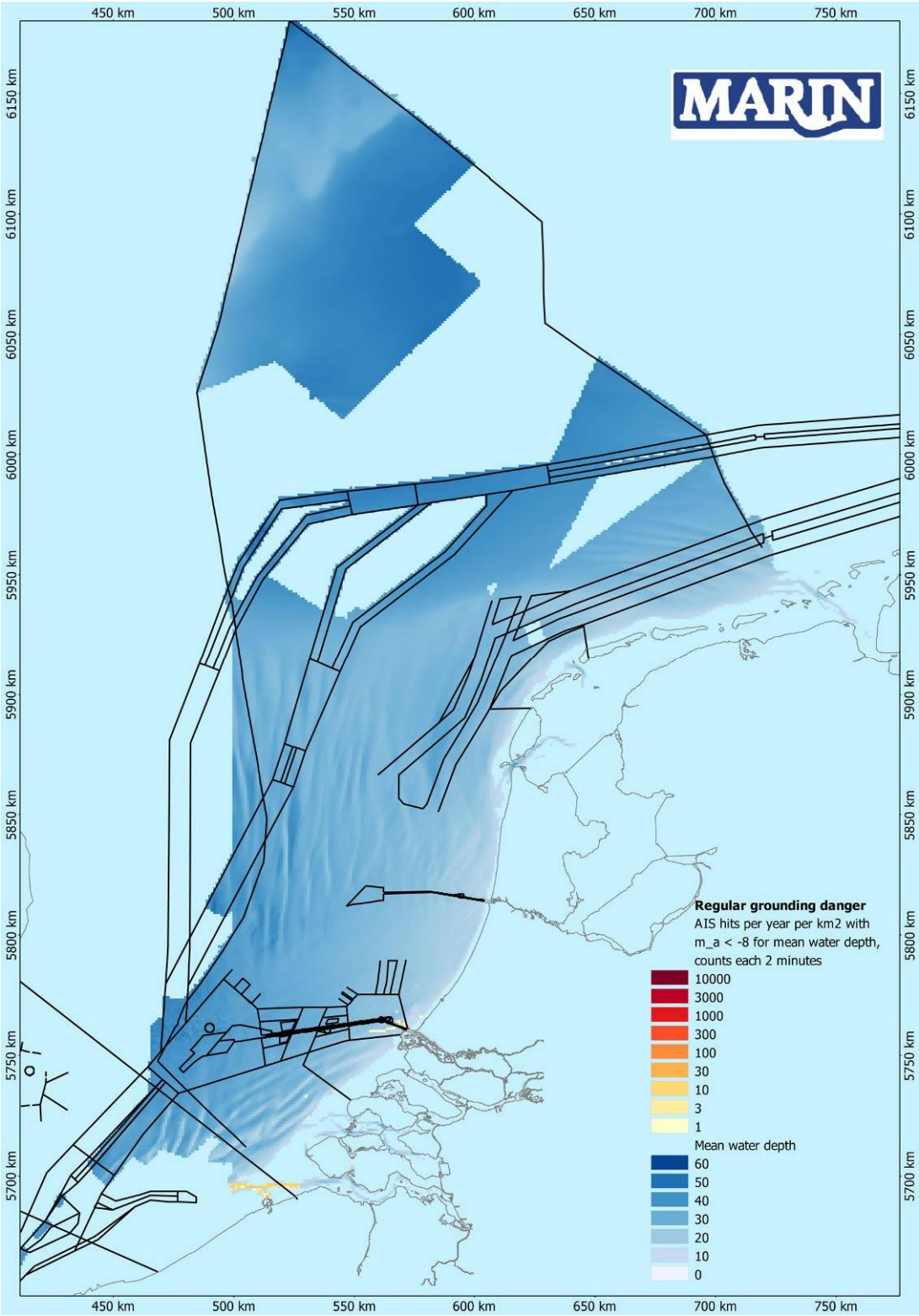

11.10 Object grounding danger with unknown obstructions for mean water depth

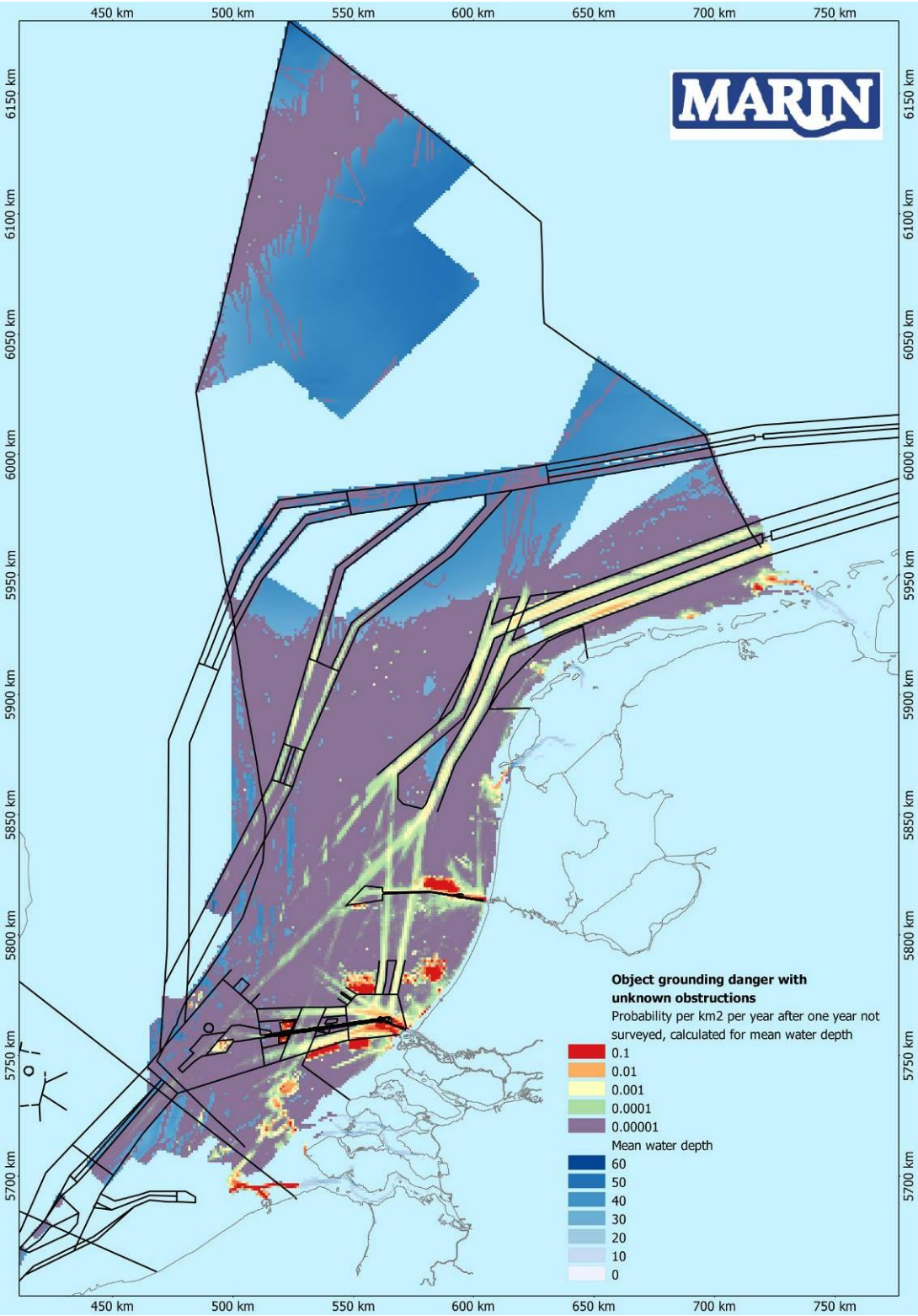

11.11 Object grounding danger with unknown obstructions for maximum water depth

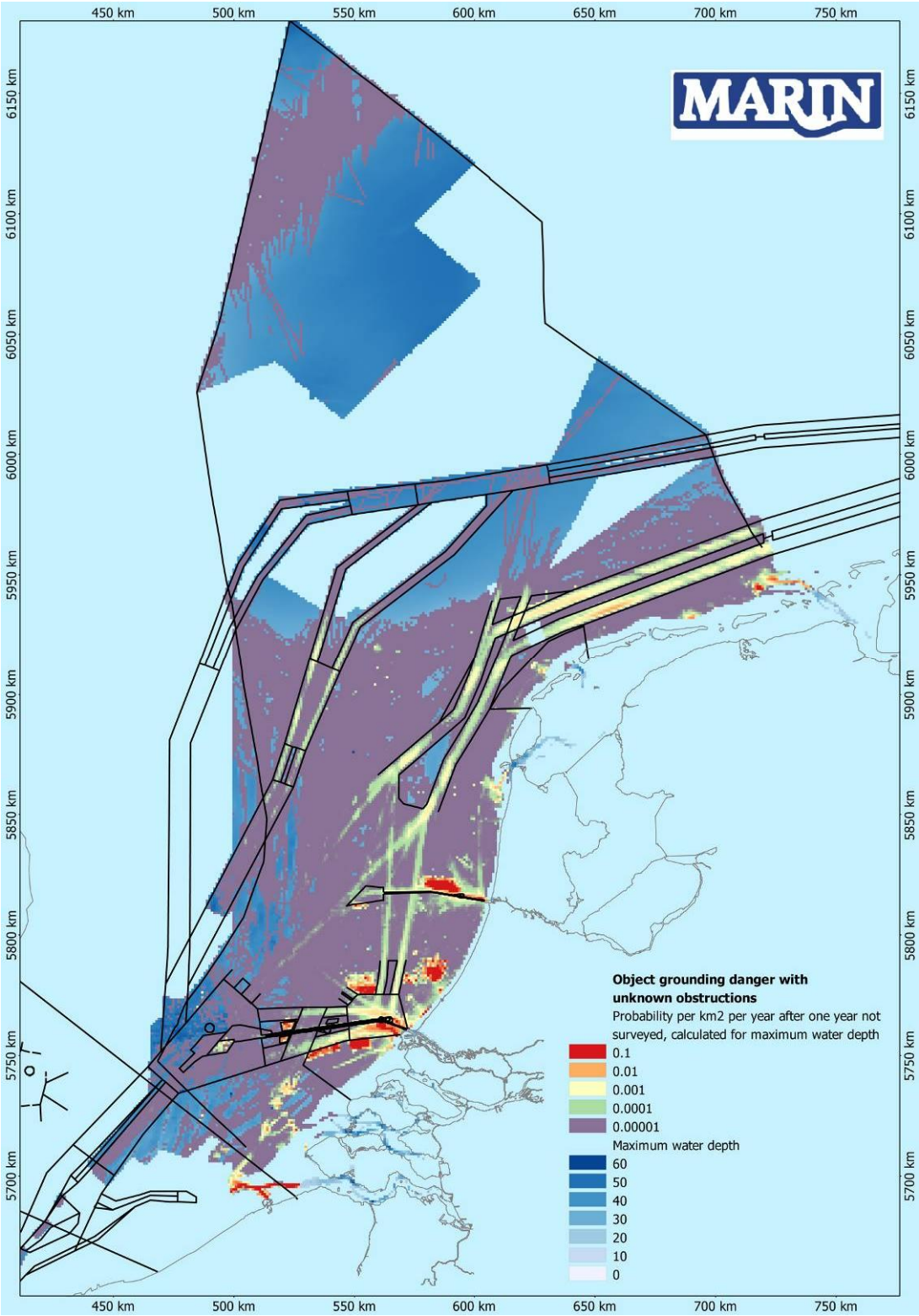

11.12 Regular grounding danger for the predicted water depth for 2015

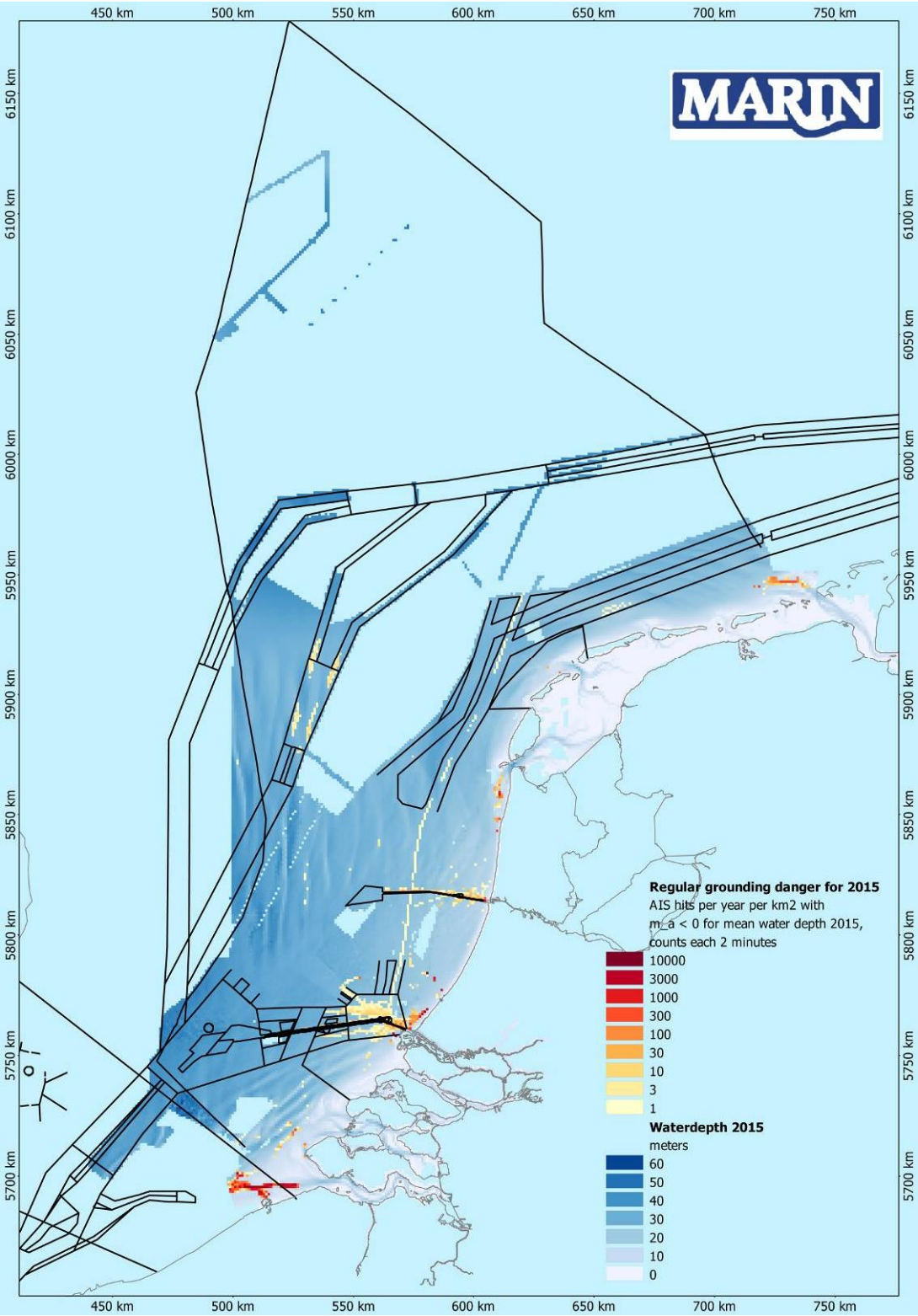

11.13 Regular grounding danger for the predicted water depth for 2020

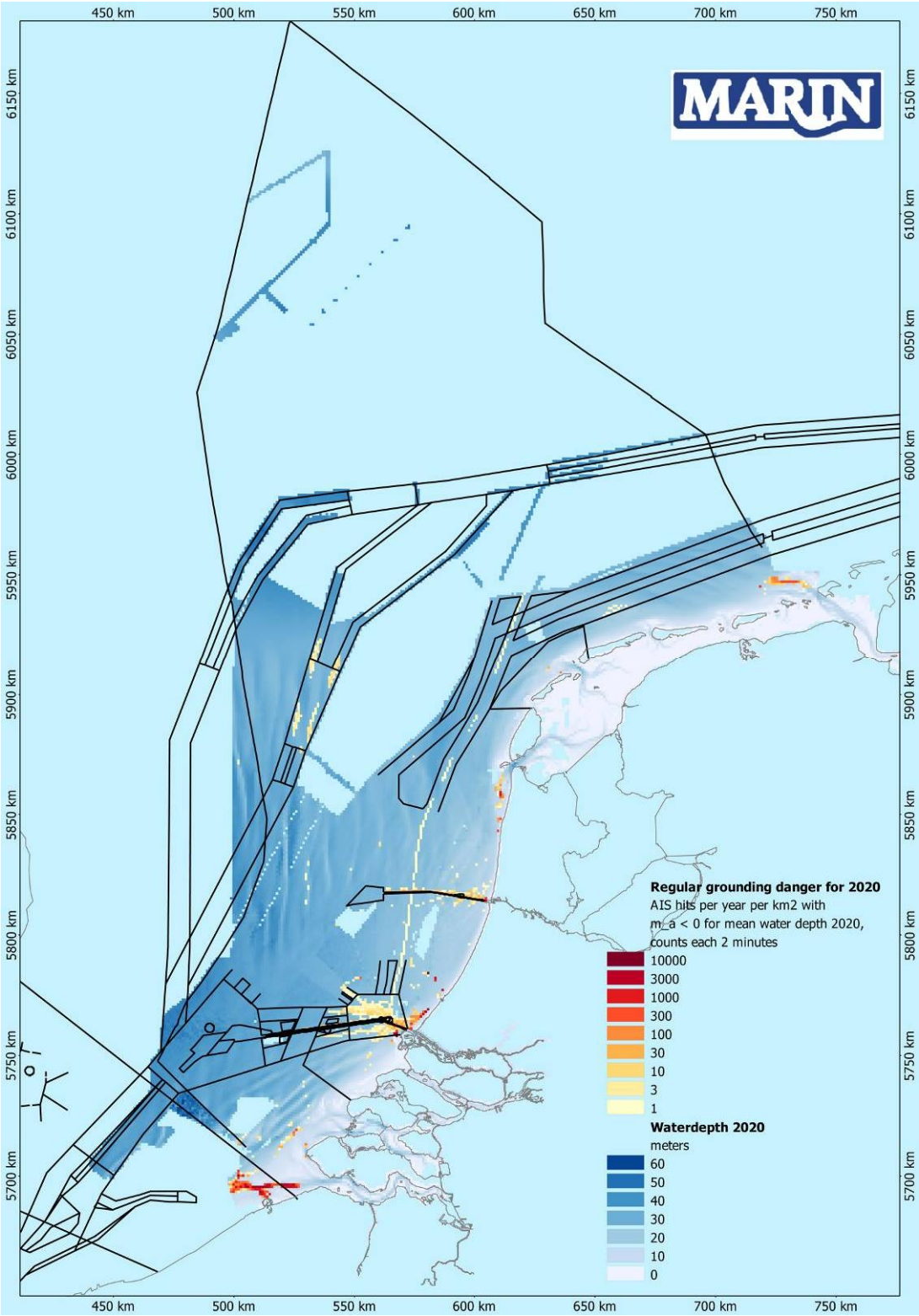

11.14 Object grounding danger for the predicted water depth for 2015

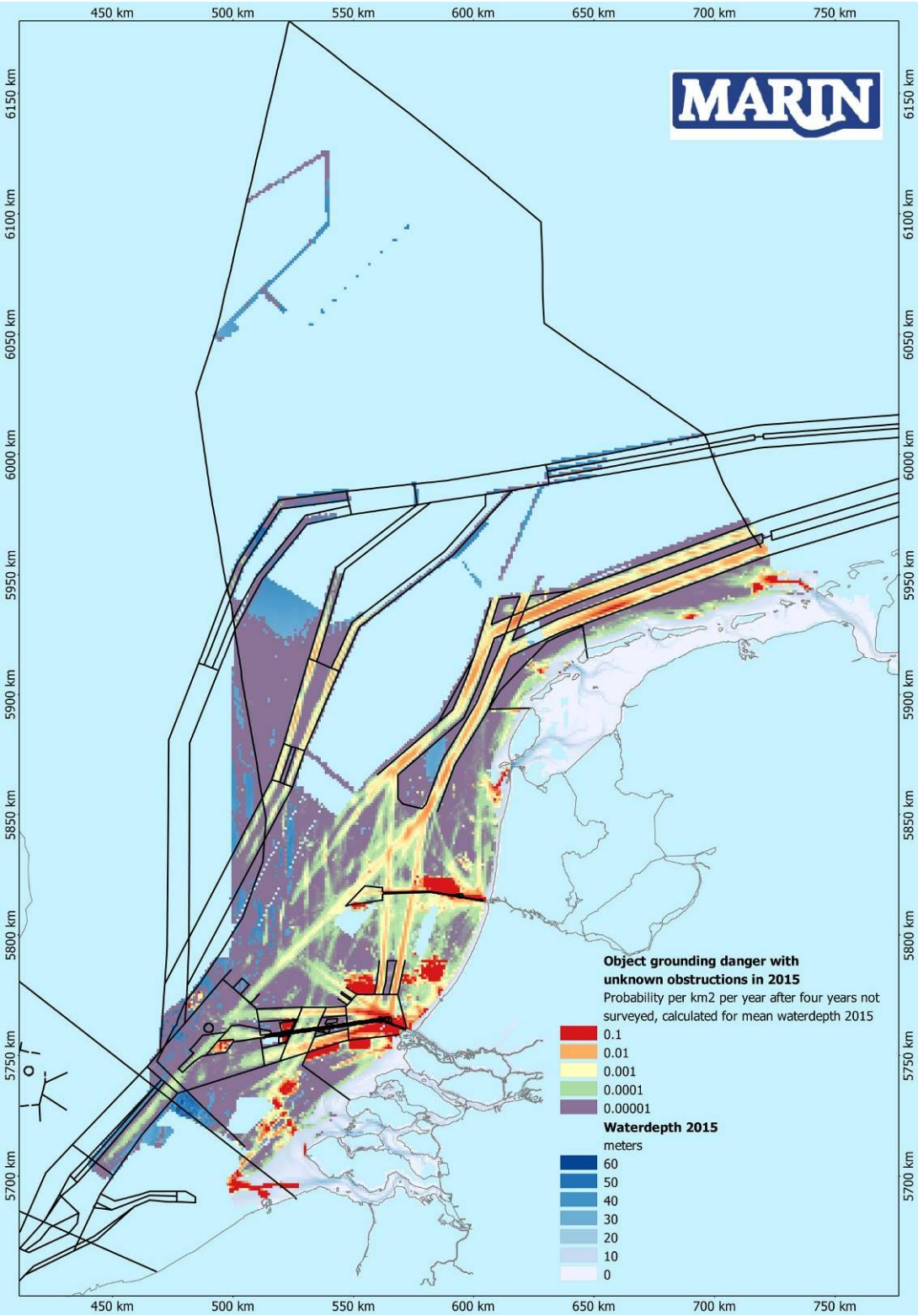

11.15 Object grounding danger for the predicted water depth for 2020

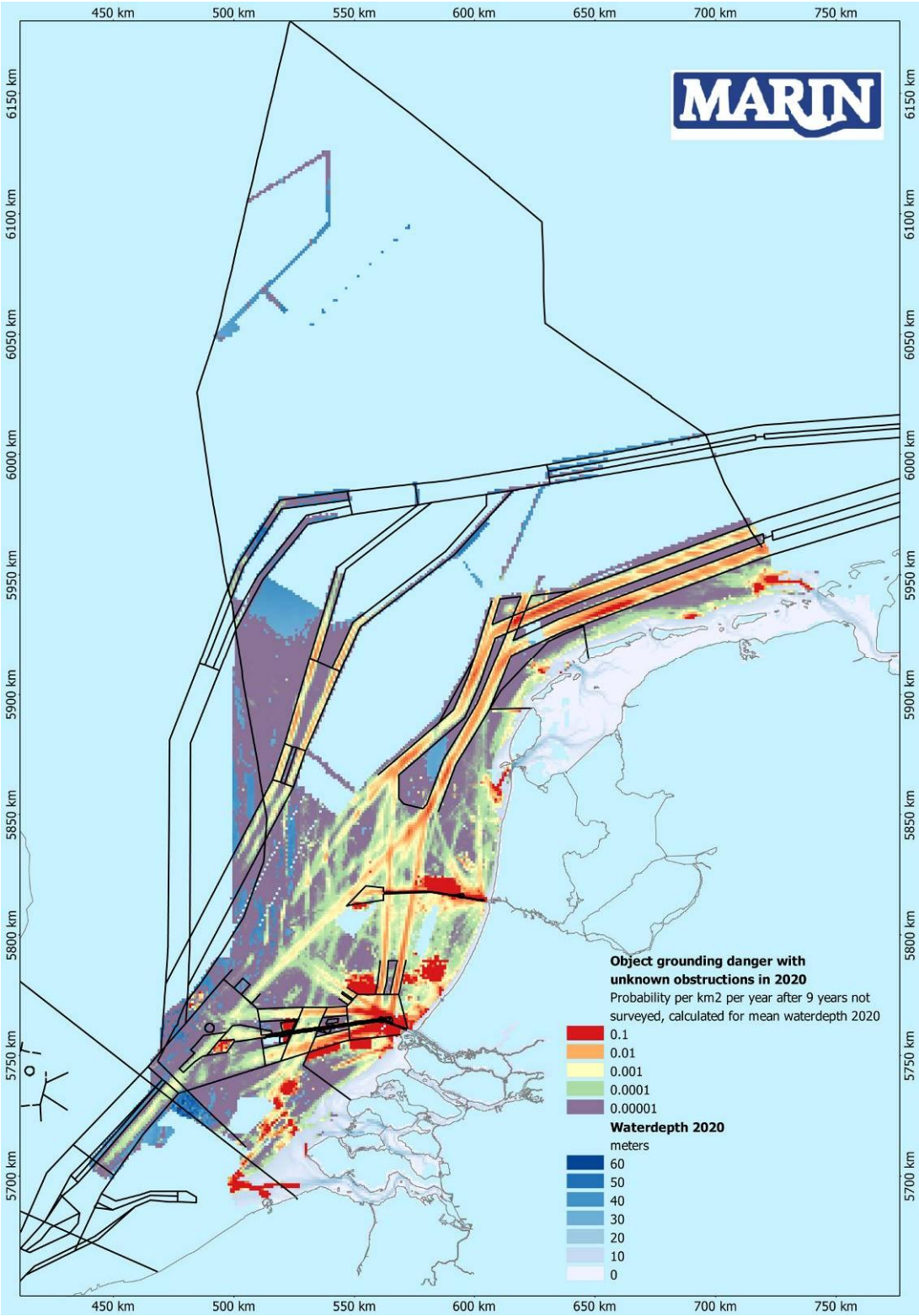

11.16 List of digital products complementing this report

1. DEM 25x25m (most recent bathymetry)
2. dz/dt-map
3. predicted water depths for 2011, 2015, 2020
4. new traffic density map
5. regular grounding danger (mean and different m_a margins: 0, 0 to -4, -4 to -8, <-8 m)
6. object grounding danger (min-mean-max WD)
7. object grounding +3m
8. object grounding 0m height
9. predicted grounding dangers regular and object 2011, 2015, 2020
10. combined grounding danger overlay
11. preliminary new re-survey policy
12. differences in combined grounding danger 2011-2010, 2015-2010, 2020-2010